# Kinetic characterisation of microgram quantities of myosins using a novel flash photolysis apparatus

Dissertation

zur Erlangung des Grades eines

Doktors der Naturwissenschaften

im Fachbereich Chemie

der Universität Dortmund

vorgelegt von

Stefan Weiß

aus Köln

Die vorliegende Arbeit wurde unter Betreung von Herrn Prof. Dr. R. Goody und Herrn Prof. Dr. M.A. Geeves im Zeitraum von Mai 1998 bis Oktober 2001 am Max-Planck-Institut für molekulare Physiologie, Dortmund, und der Universität zu Kent, Canterbury, UK, angefertigt.

1. Gutachter: Prof. Dr. R. Goody

2. Gutachter: Prof Dr. R. Winter

*Für meine Eltern*

## Acknowledgements

I like to express my sincere thanks to PROFESSOR ROGER GOODY in his role as my official supervisor for giving me the opportunity do my Ph.D. at the Max-Planck-Institute in Dortmund and for his continual interest in and support of this work.

I am especially grateful to PROFESSOR MICHAEL A. GEEVES for providing the topic of this thesis and his excellent supervision of my research during all stages of this work at the Max-Planck-Institute in Dortmund and at the University of Kent. It was a great pleasure to work in his research group. His constant support, advice and encouragement was invaluable to me.

I am thankful to PROFESSOR ROLAND WINTER for supporting this thesis as my co-referee at the University of Dortmund and for his interest.

I would like to give my special thanks to DR IGOR CHIZHOV who introduced me to the flash photolysis system and helped me to build a second system for the University of Kent.

I thank PROFESSOR ROBERTO BOTTINELLI and his co-workers, DR ROSETTA ROSSI and DR MARIA-ANTONIETTA PELLERINO, for the successful co-operation on the investigation of skeletal muscle isoform and their provision of pure MHC isoforms. I am also grateful to DR. DOMINIQUE SOLDATI and ANGELIKA HERM for the opportunity to investigate myosin XIV of *Toxoplasma gondii* in co-operation with them. I am thankful to DR ROB CROSS and his co-workers, DR KEVIN ROGERS and DR ISABELLE CREVEL, for being able to work with them on the kinesin-microtubule system. I would also like to thank DR DIETMAR MANSTEIN with whom I had the pleasure of working.

Not least I would like to acknowledge all the members of Professor Geeves' research group who all made it possible for me to perform my research in a great and friendly working environment. Special thanks go to NANCY ADAMEK for her protein preparations and her general help in the lab during my entire work. I thank DR STEPHAN SCHMITZ and DR STEFAN HEIZMANN for their friendly support when I started at the MPI Dortmund. I am grateful that I had the opportunity to work with fine people at the University of Kent including DR MIKLOS NYITRAI, DR CHRISTINE BERGER and SABRINA BOUSSOUF. In addition to that I would like to thank DR ROBIN MAYTUM, DR DAVID PEARSON and RICHARD CLARK for the proof reading and advice on my thesis and RUMIKA SILVA for her hospitality. I am especially grateful to VAL TAYLOR-GEEVES for proof reading my thesis.

Finally I would like to thank all the people I did not mention personally and who I had the pleasure of working with or who I met during the time course of this work. They all helped me to make this an enjoyable and pleasant time.

# 1 Introduction

## *1.1 Motor proteins*

Motility is a fundamental feature of life. Though many processes within a cell can take place simply by diffusion or passive transport, motor molecules are needed to add directionality and are found in all eucaryotic cells. Directed processes in living organisms include for example organelle and membrane transport, cytokinesis, the flow of cytoplasm, fluid movement at the cell surface by cilia or flagella and not least muscle contraction. Directed movement in eucaryotic cells is generated by three distinct families of motor proteins: dyneins, kinesins and myosins. All of these motor proteins convert energy produced by the hydrolysis of ATP to move along a protein filament serving as a track, the polarity of which determines the direction of the movement (Howard, 1997). In the case of dynein and kinesin this filament consists of microtubule and in the case of myosin it is the filamentous actin. Similar filaments have also recently been found in prokaryotic cells (van den Ent et al., 2001; Nogales et al., 1998). A head domain containing a binding site for the filament and an active site capable of ATP hydrolysis is essential to all motor proteins. The sequence of this head domain defines the family the motor protein belongs to. Usually this is followed by a C-terminal tail domain which can be highly variable according to the function of the motor. The current model for how motor proteins generate force is that the motor contains an elastic element, a spring, that becomes strained as a result of one of the transitions between conformational states brought about by the hydrolysis of ATP.

Kinesin is abundant in virtually all cell types, at all stages of development, and in all multi cellular organisms tested. While the majority of kinesins appear to be free in the cytoplasm, some are associated with various membrane bound organelles, including small vesicles and endoplasmic reticulum, and membranes that lie between the ER and Golgi. The usually dimeric kinesin is a processive motor which can take up to several hundred steps before dissociating from the microtubule. The initial idea of kinesin walking on the microtubule in an hand-over-hand model had to be revised after the discovery of a processive single-headed kinesin, KIF1A, and a model of anchoring in a weakly bound state has been suggested (Howard, 1997). A large body of structural, biochemical and biophysical evidence shows that kinesin has just one binding site per tubulin dimer, and that the motor takes 8-nm steps from one tubulin dimer to the adjacent one. Since the isolated motor domain of kinesin can hydrolyse up to 100 ATP molecules per second, it is likely that each step corresponds to one

cycle of the ATPase reaction. Kinesins are generally anterograde motors moving to the plus end of the microtubule filament. Interestingly, other kinesin-like proteins whose motor domains have high sequence homology and nearly identical structure to kinesin move in the opposite direction (Howard, 1997).

Dyneins are also microtubule based motor proteins, but share very little similarities with kinesins (Hirokawa, 1998). They not only play a vital role in intracellular transport but also in the production of the movement of cilia and flagella by active sliding of outer doublet microtubule (Asai and Koonce, 2001). Both dynein and kinesin are involved in the function of spindle and chromosome motility which are essential for cell division (Stearns, 1997; Vernos and Karsenti, 1996).

This work is primarily concerned with myosin, the third motor, which is actin based. Its function and mechanism are explored in more detail as follows.

## *1.2 Myosin*

Myosins are actin binding motor proteins which are most commonly known for their role in muscle contraction. There is a large variety in eukaryotic motility driven by myosin including cell crawling, cytokinesis, phagocytosis, membrane trafficking and signal transduction (Mermall et al., 1998). There is also a large variety of no less than 18 different myosin classes (Berg et al., 2001) named in order of their discovery from myosin class III on.

All myosins are biochemically defined as actin activated $Mg^{2+}$-ATPases. The functionality resides in the ~80 kDa motor domain, which is generally found at the N terminus. This motor domain is highly conserved for all myosins and defines the superfamily (Cope et al., 1996; Sellers et al., 1996). In most myosins the motor domain is connected to a neck domain of various lengths, which is associated with the binding of one or more different light chains. Those calmodulin-like light chains bind to a consensus sequence called the IQ-motif: Ile-Gln-x-x-x-Arg-Gly-x-x-x-Arg. The light chains stabilise the neck domain and can have a regulatory function. The neck domain is followed by a C-terminal tail domain which varies in form and function for the various classes of myosin.

### 1.2.1 Conventional Myosin

The thick filament of muscle consists mainly of myosin II or conventional myosin (see section 1.4.1). Though most commonly known for its role in muscle contraction myosin II also exists as a non-muscle myosin with functions in cell motility or cytokinesis. Myosin II forms a dimer which consists of two identical heavy chains each with a molecular mass of approximately 220 kDa (see Figure 1-1 and Figure 1-2).

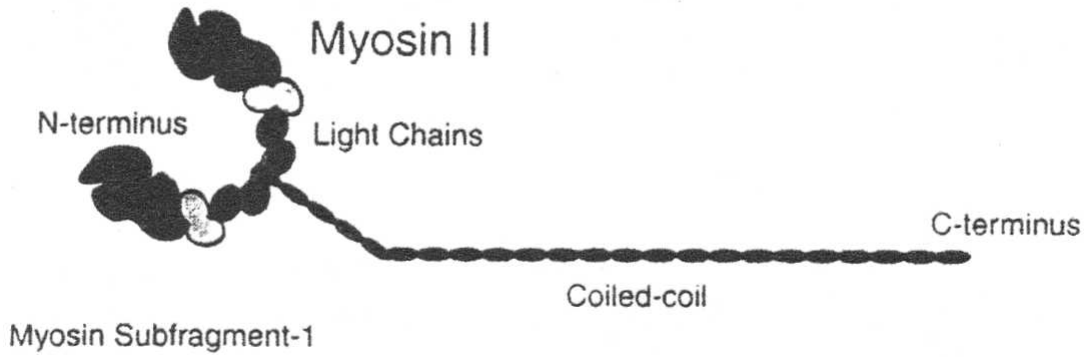


**Figure 1-1:** Schematic picture of myosin II: The dimer features 2 globular heads functioning as the motor domain followed by the neck region with two calmodulin like light chains bound. The C-terminal tail forms a long rod-like superhelical structure dimerising the myosin II (Gulick and Rayment, 1997)

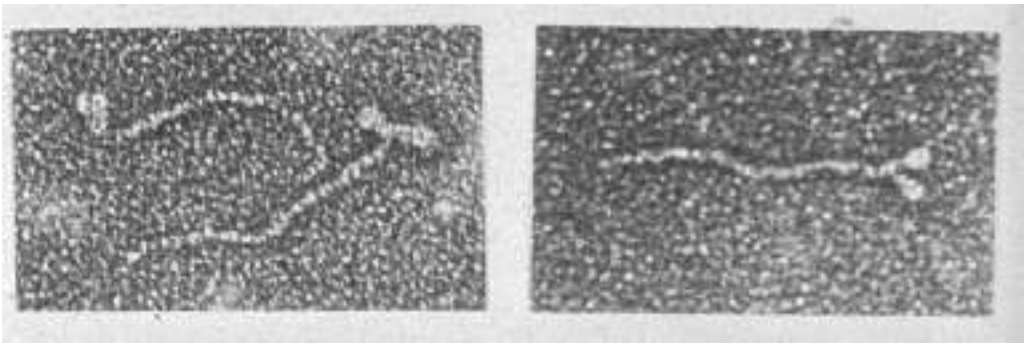

**Figure 1-2:** Dimeric single myosin II molecules in electromicroscopy.

The N-terminal region of the heavy chain forms a globular head which can bind to actin and where the enzymatic ATPase function resides. The head is followed by a neck region binding two different light chains, the essential or A-light chain (ELC) and the regulatory or P-light chain (RLC). The C-terminal region of the heavy chain forms a long α-helical tail. The tail regions of two myosin heavy chains form a superhelical structure, a so-called coiled-coil of approximately 150 nm length resulting in a myosin dimer. This structure is produced by the repeat of 7 amino acids in the α-helical tail (abcdefg) with hydrophobic amino acids in positions a and d. These amino acids form the hydrophobic core of the superhelical structure (see Figure 1-3).

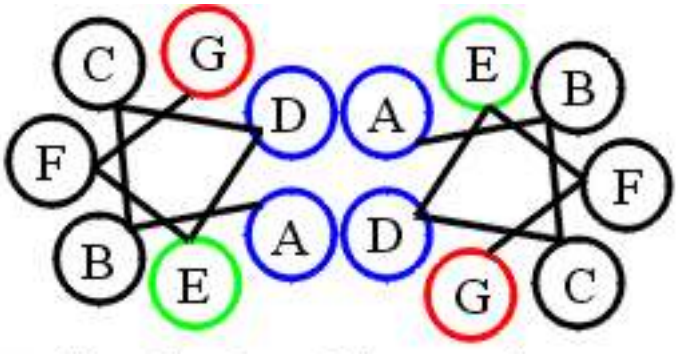


**Figure 1-3:** Schematic view of a coiled-coil structure in cross section: Residues A and D form a hydrophobic core.

The thick filament is a bipolar construct composed of several hundred myosin molecules. The staggered tails form a long smooth filament from which the globular heads extrude.

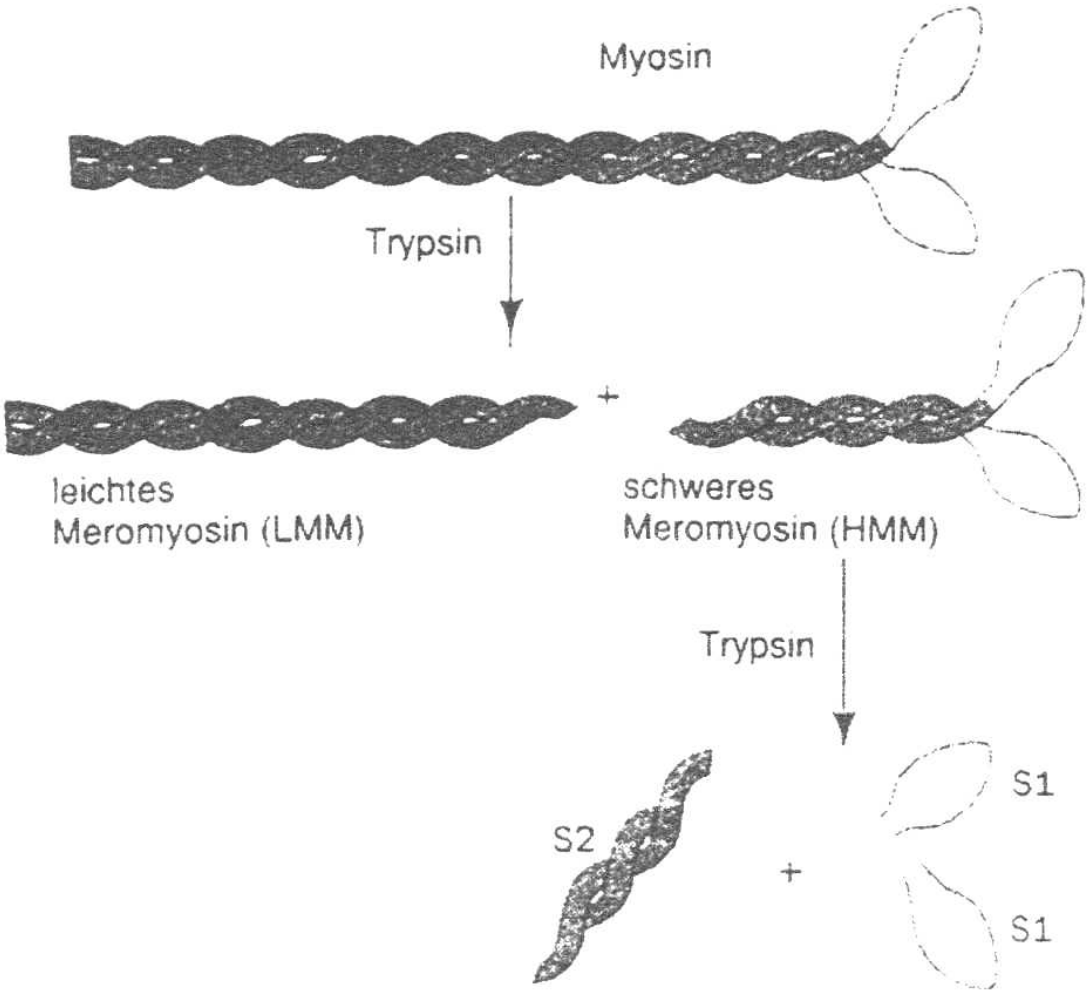


**Figure 1-4:** Enzymatic cleavage of myosin II (Voet and Voet, 1994)

The myosin dimer can be enzymatically cut into functional parts (see Figure 1-4). Chymotrysin splits myosin into light (LMM) and heavy meromyosin (HMM) in the presence of $Mg^{2+}$. The heavy meromyosin is cut in the N-terminal region of the tail domain and therefore contains two globular heads with neck domains and is dimerised in a short tail region. LMM is the long part of the superhelical tail. In the absence of $Mg^{2+}$ the heavy meromyosin is further cut into 2 subfragments: Subfragment 1 (S1) and subfragment 2 (S2) (Weeds and Taylor, 1975). Subfragment 1 is a singular globular head complete with a slightly shortened neck region binding only the essential light chain and retains all motor functions.

The described myosin fragments are often used in solution experiments due to the higher solubility compared to myosin, which aggregates easily under low salt conditions. Despite the shorter neck region S1 shows the same kinetic properties as the native myosin.

Functional domains of the globular head and structure-function relations are explored in more detail in section 1.5.3.

### 1.2.2 Unconventional myosins

The importance of unconventional myosins is stressed by the fact that they constitute about 2/3 of the estimated 40 myosins found in humans. In addition current evidence indicates that typical non-muscle cells only express 1 or 2 conventional myosin genes but upward of 10 unconventional myosins (Berg et al., 2001). Myosins form a large superfamily with a high variety in form and function, but all myosins possess a highly conserved globular head or motor domain with an ATPase and an actin binding function (Sellers et al., 1996; Cope et al., 1996, see Figure 1-5).

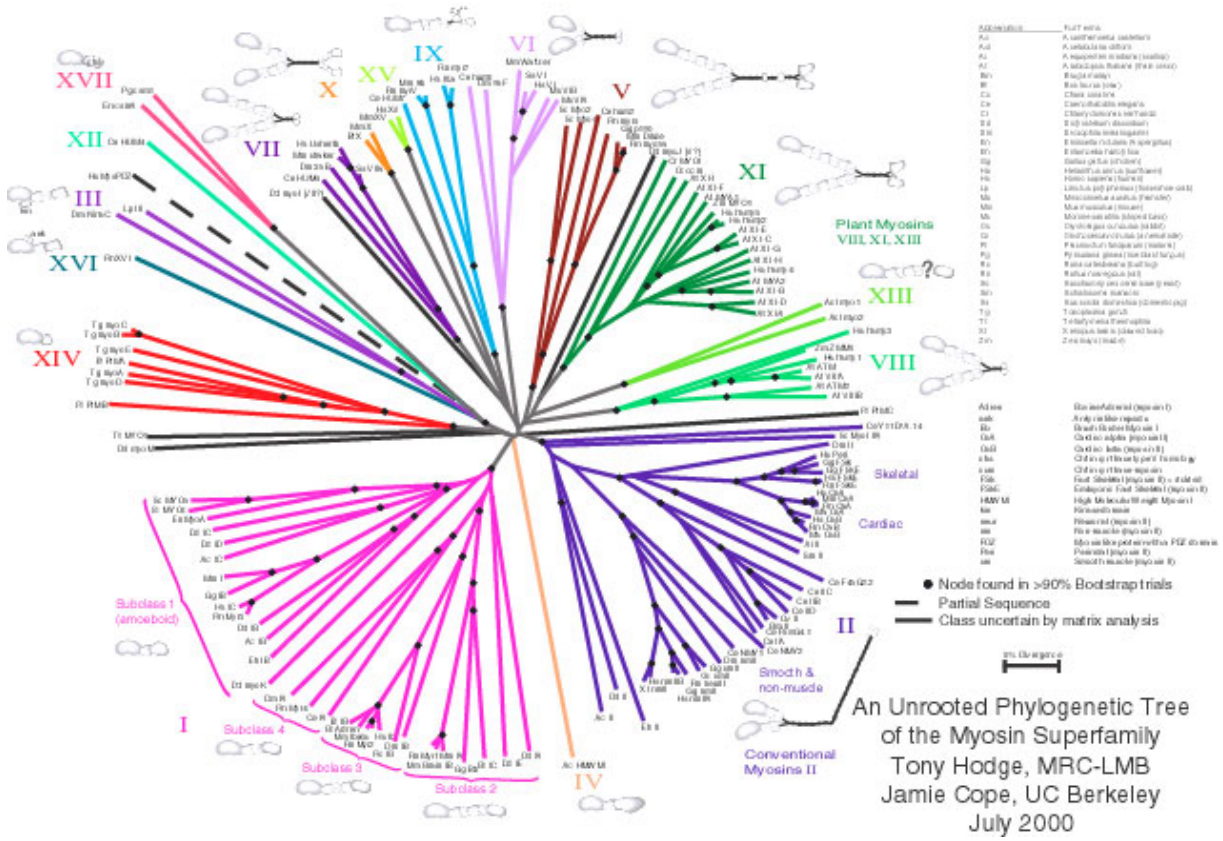


**Figure 1-5:** The myosin superfamily tree (Hodge and Cope, 2000)

The first non-muscle myosin described was found in *Acanthamoeba* in the early 1970s (Pollard and Korn, 1973). Because of its monomeric nature with just one globular head it was named myosin I in contrast to the double headed myosin II. The obvious structural difference to the known muscle myosin made it become the first “unconventional” myosin. The typical motor domain is followed by a neck region with 1-6 light chain binding IQ domains. The C-terminal tail is short compared to myosin II and one of its common functions is binding to the membrane or cytoskeleton. The membrane binding brush border myosins are of this class. Myosin I is associated with supporting cell structure and membrane trafficking.

The high variety of dimeric and monomeric myosins made a distinction in just two classes difficult. Distinct classes of myosins were thereafter named in order of their discovery.

Myosin III is found exclusively in *Drosophila* photoreceptors (Montell and Rubin, 1988). It is a fusion protein with the N-terminal region encoding for a protein kinase and features two light chain binding sites. The comparably poorly conserved myosin III is believed to play a role in the formation of microvilli, the electrophysical response to light and may not have a motor function.

Myosin IV, found in *Acanthamoeba*, has one IQ domain, seems monomeric and appears to have a motor function involved in motility (Horowitz and Hammer, 1990).

The dimer Myosin V has a neck region with 6 light chain binding domains followed by a tail forming partially a coiled-coil with globular ends. It is very likely involved in organelle transport and according to recent results is processive (Mehta et al., 1999; Walker et al., 2000). It takes several steps on the actin filament before dissociation. Because of this walking mechanism it is able to work as a single molecule as opposed to most other myosins which only work efficiently in larger numbers (e.g. in the thick filament).

Myosin VI is another dimeric myosin involved in organelle transport. It features a head domain lacking 28 residues found in conventional myosin and two unusual inserts, one in a surface loop and one before the neck region. Most remarkably it moves actin in the opposite direction (minus-end, Wells et al., 1999). Evidence emerged that no major changes in the myosin sequence are required, but that only a small insert in the converter domain (see 1.5.3) is responsible for this behaviour. Recent experiments with chimeric myosin V and VI in which the converter domain was exchanged, contradict that view however, and suggest the motor core domain is responsible for the directionality (Homma et al., 2001b).

For myosin VII five IQ domains and a coiled-coil forming a dimer are predicted. Mutations in this myosin gene cause Usher's syndrome, a form of deafness and blindness (Redowicz, 1999).

Myosin VIII is found in *Arabidopsis*. With 4 IQ motifs and a short coiled-coil this predicted dimer seems to be only found in plants (Knight and Kendrick-Jones, 1993).

The proposed monomeric myosin IX featuring 4 IQ domains, a $Zn^{2+}$ binding region and a GTPase activating motif (GAP) is most likely involved in signal transduction processes (Reinhard et al., 1995).

Myosin X with 3 IQ motifs and a coiled-coil shows homology with other proteins involved in signal transduction and cytoskeletal targeting (Homma et al., 2001a).

Myosin XI with 6 light chain binding domains shows a high similarity to myosin V though it is only found in plants (Hammer and Jung, 1996).

Myosin XII found in *C.elegans* shows a very high sequence diversity compared with other myosins.

Myosin XIV has no IQ motifs and a very short tail (Heintzelman and Schwartzman, 1997). Expressed only in *Plasmodium, Toxoplasma* and homologues this myosin is involved in the mechanism of host invasion of the parasite. TgM-A of this class is characterised in detail in section 7 of this work.

Little is known about the remaining recently discovered myosins. Much of the information is derived from sequence studies of genomes and these classes are only recognised as myosins by the highly conserved head domain (Berg et al., 2001).

## *1.3 Actin*

Actin plays an important role in the formation of the cytoskeleton even in the absence of myosin and is the predominant part of the thin filament of muscle. It is a highly conserved protein with a molecular mass of 42 kDa. At low concentration and low ionic strength it exists as a globular monomer, G-actin.

At physiological salt conditions and ATP-G-actin concentrations above the critical concentration ($C_c$) globular actin assembles into characteristic actin filaments (F-actin). The polymerisation of actin is a directed process which requires energy from ATP hydrolysis. F-actin is a polar filament and the critical concentration is different for the plus- and the minus end. That can lead to a growth of the filament at the plus end while monomers are lost at the minus end. This process is called treadmilling. The formation and breakdown of actin filaments occurring at different ends of the filament is a highly dynamic process in the cytoplasm. F-actin in the thin filament of muscle is of higher stability.

The structure of G-actin from rabbit skeletal muscle was solved by X-ray crystal structure studies in the presence of DNaseI and nucleotide by Kabsch *et al*. (1990) shown in Figure 1-6. Actin is divided into two similar domains divided by a cleft where ATP or ADP and $Mg^{2+}$ can be reversibly bound. F-actin is a double helix with 36 nm repeats (see Figure 1-7). In X-ray diffraction experiments Holmes *et al*. (1990) and Lorenz *et al*. (1995) found that the basic structure of F-actin monomers remains almost unchanged compared to G-actin. In vitro S1 decorated filaments show an arrowhead-like appearance confirming that all monomers are oriented in the same direction.

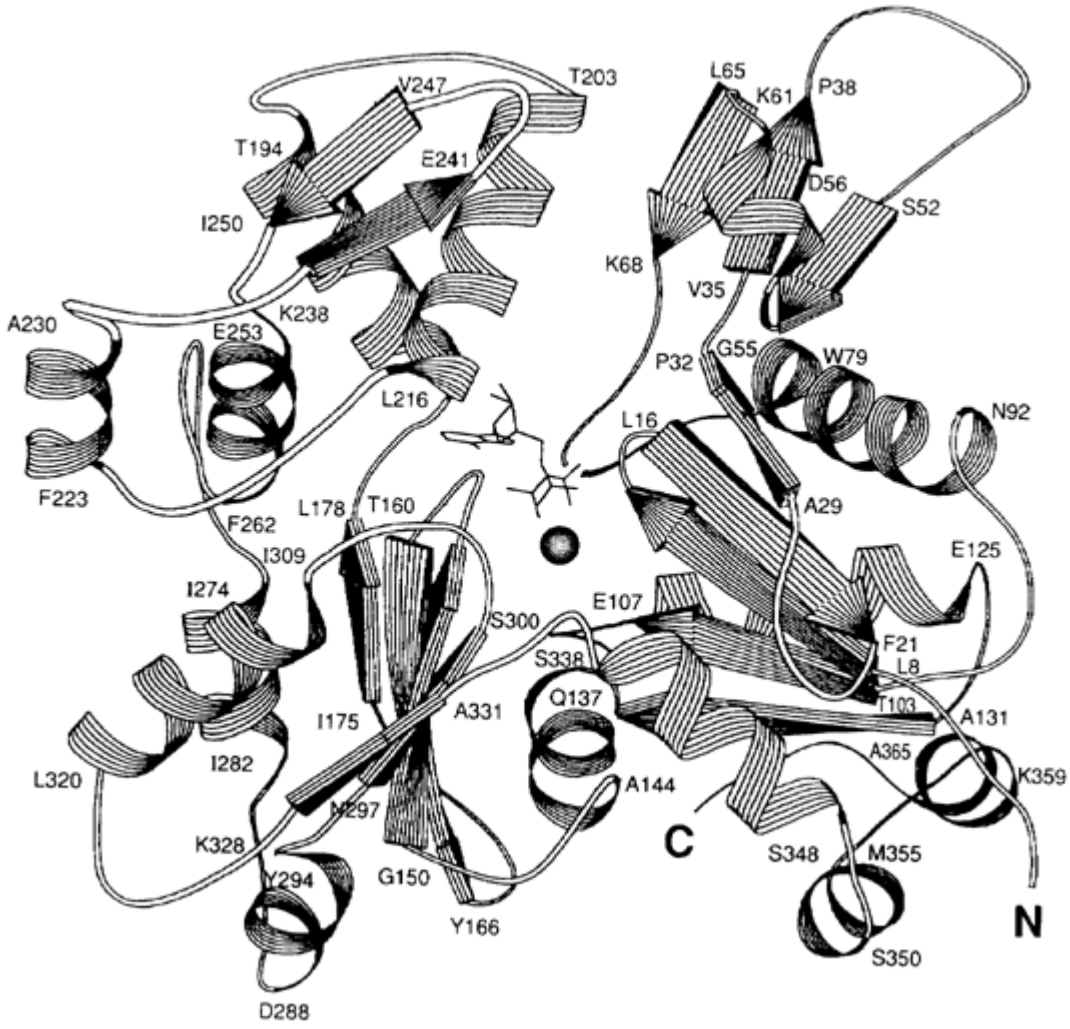


**Figure 1-6:** The crystal structure of G-actin (Kabsch et al., 1990)

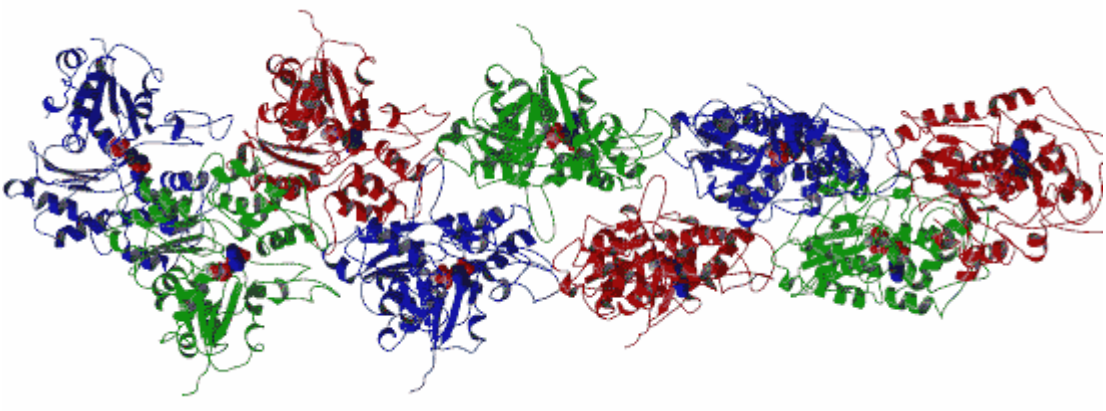

**Figure 1-7:** Atomic model of F-actin constructed from the structure of G-actin: F-actin has 13 actin molecules arranged on 6 left-handed turns repeating every 360Å. The rise per subunit is 27.5Å. The morphology of the actin helix is two intertwined long-pitch right-handed helicies. (Holmes et al., 1990)

## *1.4 Muscle Contraction*

Muscle contraction is the most familiar and best understood form of biological motility. All kinds of movement animals are capable of are the result of muscle contraction. Although a relatively late evolutionary development this highly specialised system was an obvious target of interest. For 40 years the process of muscle contraction has been the subject of research and the system serves as a model for all myosin actin interactions which are all believed to work in a similar manner. Though major advances have been made to elucidate the mechanism of acto.myosin based motility many questions remain on exactly how movement in muscle is generated.

### 1.4.1 Anatomy of the muscle

We have to distinguish between two different types of muscle, striated muscle and smooth muscle. The two types are easily distinguished under a light microscope, where striated muscles show a periodic structure (see Figure 1-8), while a similarly ordered structure in smooth muscle is absent. Vertebrate skeletal and cardiac muscle as well as insect flight muscle are examples of striated muscle while muscles contracting organs, like gizzard or intestines, are of the smooth type. Because of the highly organised structure and the ready availability vertebrate skeletal muscle was the most common target of study.

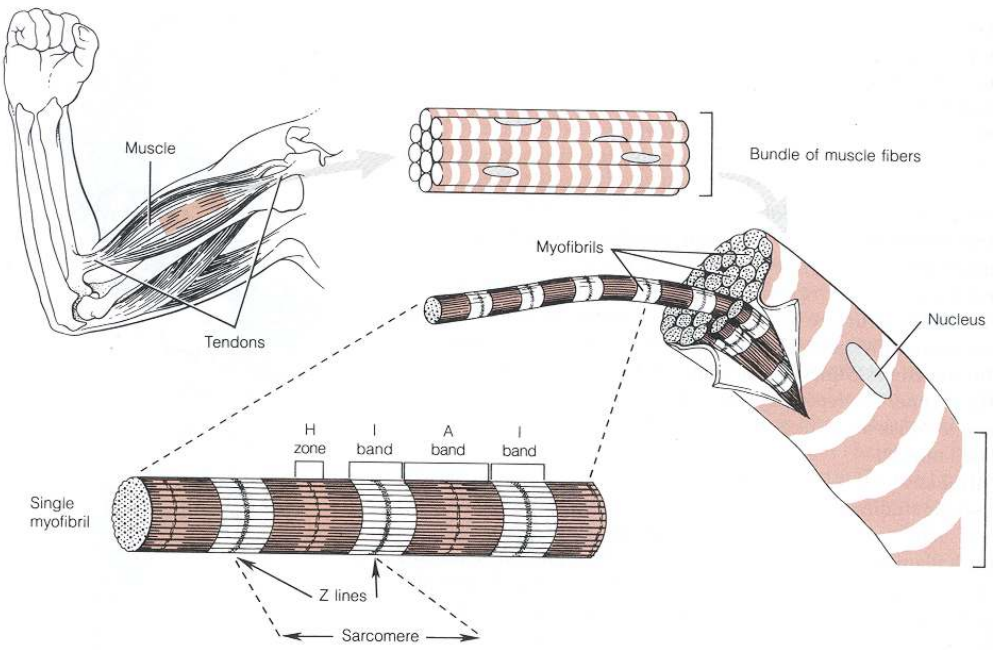


**Figure 1-8:** Anatomy of the muscle: The skeletal muscle is a bundle of fibres. Each fibre is a single cell with multiple nuclei and consists of a bundle of myofibrils which contain a row of sarcomeres (Mathews et al., 2000)

Under the microscope the organisation of striated muscle into long parallel bundles, muscle fibres, with a diameter of 20 – 100 µm becomes apparent. The length of these bundles can equal the length of the entire muscle. Each muscle fibre is a single cell with multiple nuclei formed during development from many separate cells. The bulk of the muscle fibres themselves are again made up from parallel bundles of myofibrils which are about 1 – 2 µm in diameter and can be as long as the fibre. The myofibrils consist of a chain of tiny contractile units, the sarcomeres, each about 2.2 µm long (see Figure 1-9).

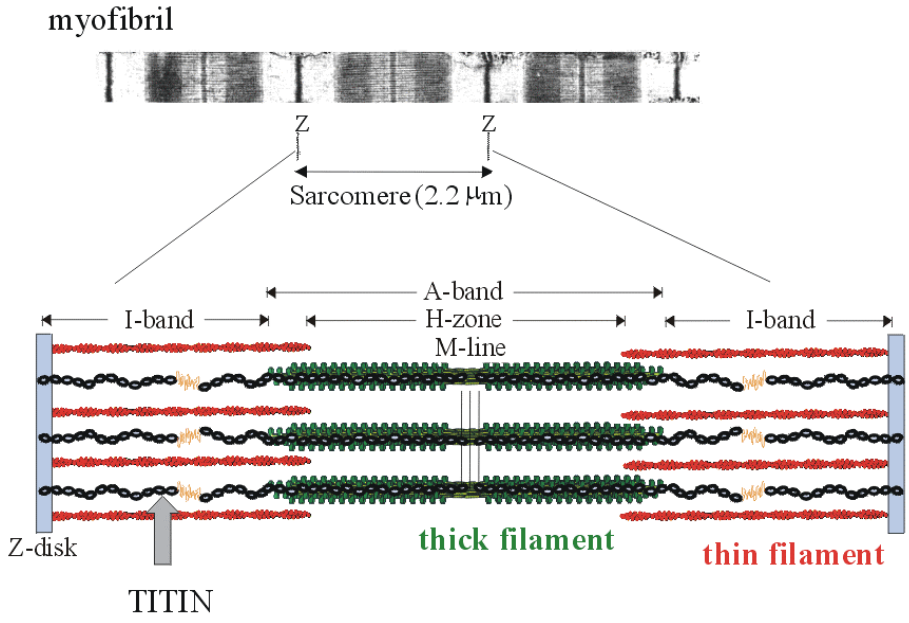


**Figure 1-9:** The sarcomere: The electronmicrograph of a myofibril clearly shows the various bands causing the striation of the muscle (top). The schematic picture of the sarcomere shows how this correlates to the sarcomeric structure of the most important filaments within the sarcomere (courtesy of H. Granzier).

At high magnification broad dark and light bands, the A-band and the I-band respectively, can be seen in the myofibrils with a dark line, the Z-disk, separating the sarcomeres in the light band area. At even higher magnification the electron microscope reveals filaments spanning the sarcomere. In the middle of the A-band a dark M-line can be seen from which the thick filaments extend. The A-band appears dark because of the density of the thick filaments. The thin filaments extend from the Z-disk into the lighter area of the sarcomere and overlap with the thick filament in a very dark area of the A-band in contrast to the lighter H-zone around the M-line. Since the A-bands and I-bands of the myofibrils are all on the same length the entire fibre appears striated (Voet and Voet, 1994; Bagshaw, 1982).

Electron microscopy pictures of a cross section of the myofibril show the two kinds of filaments in more detail. The thick filaments of the A-band are about 1.5 µm long and 15 nm in diameter. The thin filaments are about 1µm long and 7 nm in diameter and extend from the Z-disk into the overlap area of the A-band. In this area the filaments are organised in a hexagonal array where each thick filament is surrounded by 6 thin filaments while the each thin filament has 3 thick filaments next to it.

### 1.4.2 Muscle proteins

#### *1.4.2.1 Myosin*

The thick filament of the muscle is mainly made up of myosin class II. Myosin in general or conventional class II myosin in particular has been described in detail in section 1.2

#### *1.4.2.2 Actin*

Actin makes up the major part of the thin filament and is described in detail in section 1.3

#### *1.4.2.3 Control proteins*

In vertebrate skeletal muscle the F-actin of the thin filament binds the so-called control proteins, troponin and tropomyosin, which regulate calcium dependent contraction of the sarcomere (see Figure 1-10). Tropomyosin is a long filamentous α-helical protein forming a dimer in a coiled-coil structure (as described for the tail of conventional myosin in section 1.2.1). It has two isoforms, α and β, which show very little difference in sequence. The dimer exists in either an αα or an αβ form. Tropomyosin binds to the cleft formed by the actin double helix binding 7 G-actin molecules. Tropomyosin overlaps at its ends with neighbouring tropomyosins spanning the entire thin filament. The binding of tropomyosin to actin is stabilised by ionic interactions (Lehrer and Geeves, 1998).

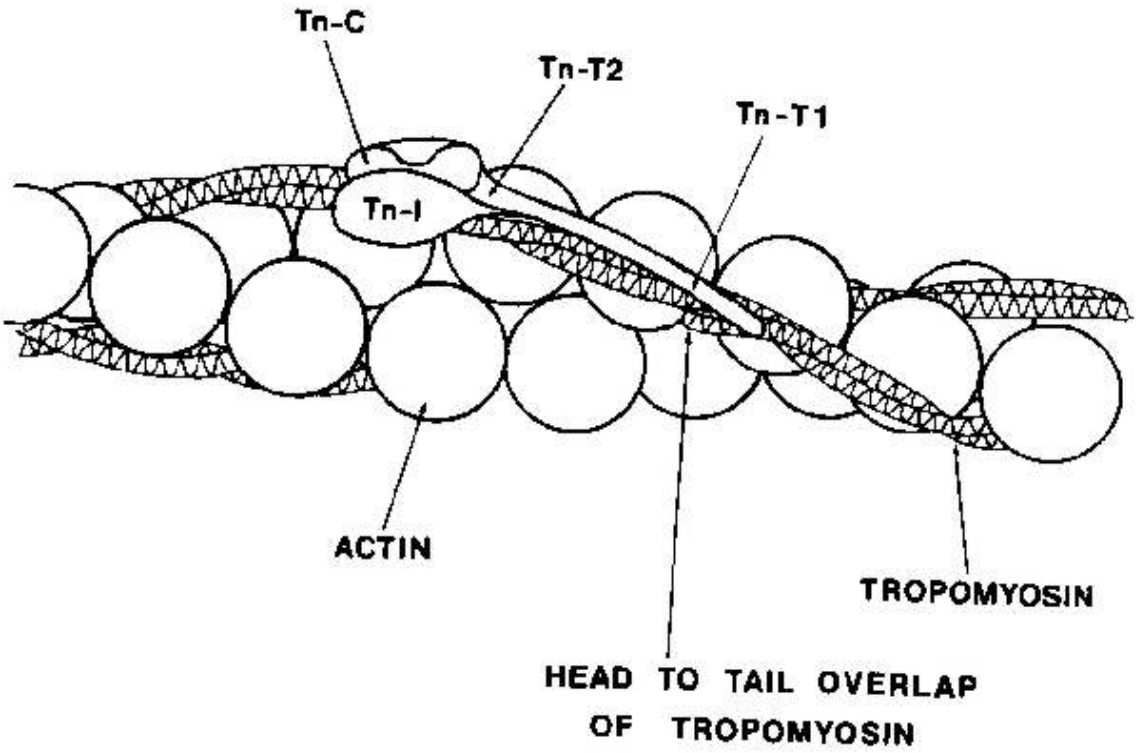


**Figure 1-10:** Schematic picture of actin with the troponin tropomyosin complex bound (Heeley et al., 1987)

Troponin, which is made up from the subunits TnI, TnC and TnT (Greaser and Gergely, 1973), binds to tropomyosin in a 1:1 ratio. The calcium binding TnC shows a high homology with the regulatory calmodulin. The two domains of TnC connected by a helix bind $Ca^{2+}$-ions in a so-called EF-hand motif. The carboxy-terminal domain has a higher affinity for $Ca^{2+}$-ions ($K_d$ = 0.1 µM) than the amino-terminal domain ($K_d$ = 10 µM).

The inhibitory unit TnI binds to actin, TnC and TnT which connects the troponin complex with the tropomyosin. TnT's tail-like region binds to the region where the tropomyosins overlap. This suggests a stabilisation of the tropomyosin-tropomyosin binding in the overlap region. (Ishii and Lehrer, 1991; Morris and Lehrer, 1984; Heeley et al., 1987).

At low calcium concentrations (<10 µM) only the domains of TnC with a high affinity bind $Ca^{2+}$-ions. The increase of calcium concentration by release of calcium from the sarcoplasmatic reticulum causes binding of $Ca^{2+}$-ions to the TnC domains of lower affinity. This triggers a conformational change which is transferred to the tropomyosin, changing its position on the actin. This switch allows binding of myosin to actin (Hill et al., 1980). McKillop and Geeves (1991) more recently proposed that the regulation of TmTn containing thin filaments can be interpreted in terms of a rapid $Ca^{2+}$ dependent equilibrium between 3 states of the thin filament: blocked, closed and open. A steric blocking model of thin filament

regulation has been proposed (Figure 1-11) which shows the relationship between the three states of the thin filament and the binding of myosin to actin. This model is also supported by evidence from electromicroscopy in which the 3 states become visible (Vibert et al., 1997).

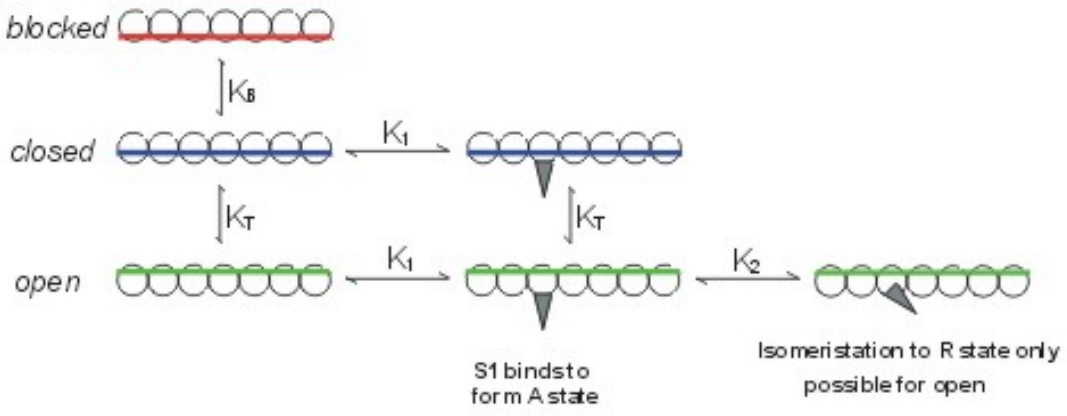


**Figure 1-11:** Three state model of regulation of acto.myosin binding by tropomyosin. In contrast to the BLOCKED state the CLOSED state allows weak binding of myosin to actin, but the isomerisation to the strongly binding rigor state of acto.myosin can only occur in the OPEN state. (McKillop and Geeves, 1991)

#### *1.4.2.4 Other Proteins*

Though actin and myosin play the predominant role of proteins involved in muscle contraction other proteins are necessary to ensure the structural integrity of the sarcomere. These proteins are not well characterised since they do not show enzymatic activity. Some of those structural proteins are mentioned here.

α-actinin anchors the thin filaments to the Z-disk. They also ensure a proper sterical distribution.

Titin, one of the largest proteins known, extends from the Z-disk to the thick filament and is believed to stabilise the position of the thick filament in the sarcomere acting like a spring.

Nebulin is a long repetition of an actin binding motif of 35 amino acids. It spans the distance between the thin filaments and is believed to regulate the polymerisation of actin and therefore regulate the length of the thin filament during muscle development.

Various intermediate filaments and proteins e.g. desmin and dystrophin connect myofibrils or anchor them to the membrane of the muscle fibre.

### 1.4.3 Fast and slow sarcomeric muscle types and their isoforms

Striated muscles perform a wide variety of functions in animals including maintaining posture, moving the body in space, chewing food and pumping blood. The requirements to perform these various actions are different in terms of mechanical power and animals developed different types of muscles to cater for these requirements. Compared to a faster muscle type a slower muscle is more energy efficient under isometric conditions, i.e. bearing a load without shortening. A slow muscle types thus is better suited for maintaining posture while a faster muscle type is preferable for fast contractile movements such as used in running. Larger sized species generally develop slower type muscles compared to smaller species (Schiaffino and Reggiani, 1996).

The composition of the isoforms of muscle proteins is typical for the type of muscle. It is now clear that the myosin heavy chain isoform is the major determinant for mechanical properties of the muscle fibre (Pette and Staron, 1990; Schiaffino and Reggiani, 1996). While in bulk mammalian muscle a mixture of isoforms is always expressed, single muscle fibres often express a single myosin heavy chain isoform. Measurements with single fibres expressing different pure MHC isoforms showed distinct differences in the values for shortening velocity, ATPase activity and power output which define the mechanical properties of the fibre (see section 6; Bottinelli et al., 1994a; Bottinelli et al., 1994b; Greaser et al., 1988; Mabuchi and Sreter, 1980; Sweeney et al., 1988). For fibres containing faster MHC isoforms the type of essential light chain bound also seems to be influential for the speed of shortening, but not the ATPase activity. However the MLC isoform appears to influence the shortening velocity less compared with the MHC isoform (Bottinelli et al., 1994a; Bottinelli et al., 1994b; Canepari et al., 2000; Wagner, 1981).

Currently 8 MHC isoforms are known to be expressed in mammalian sarcomeric muscle (Weiss et al., 1999; Schiaffino and Reggiani, 1996). MHC-α and MHC-β/slow are the major cardiac isoforms expressed in the heart. MHC-emb (embryonic) and MHC-neo (neonatal) are the predominant isoforms in developing skeletal muscle and are replaced by the slow MHC-I and the fast MHCs IIA, IIX and IIB in adult muscle. The slow skeletal isoform MHC-I is identical to the cardiac MHC-β/slow. MHC-eo (extraocular) is restricted to the exraocular and laryngeal muscle. Likewise a ninth isoform, MHC-m (mandibular), is only expressed in the masseter muscles of carnivores (Rowlerson et al., 1983). The fast skeletal muscle isoforms IIX and IIB are rarely or not expressed at all in larger animals.

All these myosin II heavy chain isoforms are well conserved in the motor domain and most of the sequence changes are found in the two surface loops 1 and 2 and the secondary actin binding loop (see section 1.5.3.2) which are believed to play a role in the structure function relation of myosin. Sequence comparisons showed that orthologous isoforms (corresponding isoforms in different species) are more conserved than paralogous isoforms (different isoforms within the same species, Weiss et al., 1999).

There are 2 essential light chain isoforms MLC-1sa and MLC-1sb which can bind to the slow adult skeletal muscle isoform MHC-I and 2 further essential light chain isoforms, MLC-1f and MLC-3f, which can bind to the fast skeletal muscle MHCs IIA, IIX and IIB. Fast and slow type skeletal muscle isoforms bind one regulatory light chain isoform each, MLC-2f and MLC-2s respectively.

Single fibre studies have elucidated many of the mechanical properties of muscle fibres expressing specific isoforms. In muscle fibres the conversion of chemical energy into mechanical energy is defined by the chemical energy ($\Delta G$) generated by the hydrolysis of ATP (~ 50 kJ/mol) and the work generated by the fibre, which is a product of the force and movement. The power output equals the product of force developed and the velocity of shortening. The maximum shortening velocity ($V_0$) is the shortening velocity at zero load which is generally faster in fast fibres than in slow ones. The rate of ATPase activity under these conditions is correlated to the maximum shortening velocity and thus higher for fast isoforms than for slow isoforms (Barany, 1967). Under isometric conditions, where tension against a load is maintained but no contraction occurs, ATP consumption is also higher in fast fibres, while the force developed is similar compared to slow fibres. Thus slow fibres are more energy efficient in bearing tension (Reggiani et al., 1997). It is therefore not surprising that a higher ratio of slow fibres is found in muscles designed to bear tension (e.g. maintaining posture) and a higher ratio of fast fibres in muscles which are designed to generate fast movement.

### 1.4.4 Other muscle

The description of muscle so far was based on vertebrate skeletal muscle, a typical striated muscle system. All types of muscle are based on a universal contractile system involving actin and myosin II. Cardiac muscle is another striated system showing a similar organisation as skeletal muscle. It is also a troponin-tropomyosin regulated system. In contrast to skeletal

muscle heart muscle cells are not syncytial but are cells with a single nucleus, which are joined together by special structures called intercalated discs.

Smooth muscle has no striations and is composed of sheets of elongated spindle shaped cells with single nuclei. Furthermore the thin filament is not strictly organised but is only roughly aligned with the long axis of the cell. This allows slow but long ranged contraction without a skeletal bone acting as a lever to amplify the motion. Vertebrate smooth muscle is also regulated differently by phosphorylation of the regulatory light chain, without the need of a actin based regulation system (Chacko et al., 1977; Sobieszek and Small, 1977). In non-vertebrate muscle systems different forms of regulation occur, e.g. $Ca^{2+}$ regulation of scallop muscle thick filament.

## *1.5 Models of muscle contraction and acto.myosin interaction*

The fundamental question left to answer is: How does the interaction of myosin and actin generate movement? Muscle motility as a model has been studied for more than 40 years and though a general mechanism has been elucidated many important details remain unanswered. There have been several major findings which led to a better understanding of acto.myosin motility, starting with the development of the sliding filament model for sarcomere shortening (see 1.5.1.1). This was followed by the cross bridge model explaining motility on a molecular level for the first time. This model was constantly refined and combined with biochemical knowledge. The next big step was the incorporation of structural results into this model since the X-ray crystal structures of S1 and actin were solved (see section 1.5.3). More recently, single molecule experiments, including measuring the step size by the use of optical tweezers, provided a way of addressing the remaining questions.

### 1.5.1 Mechanical models

#### *1.5.1.1 Model of the sliding filaments*

A closer look at the sarcomere revealed that the filaments did not change their length during sarcomere shortening. The width of the A-band as well as the distance between Z-disk and the near end of the H-zone remain the same during contraction. In contrast both the I-band and the H-zone decrease in width. This led to the model of sliding filaments developed by Huxley and Hanson (1954) as well as Huxley and Niedergerke (1954).

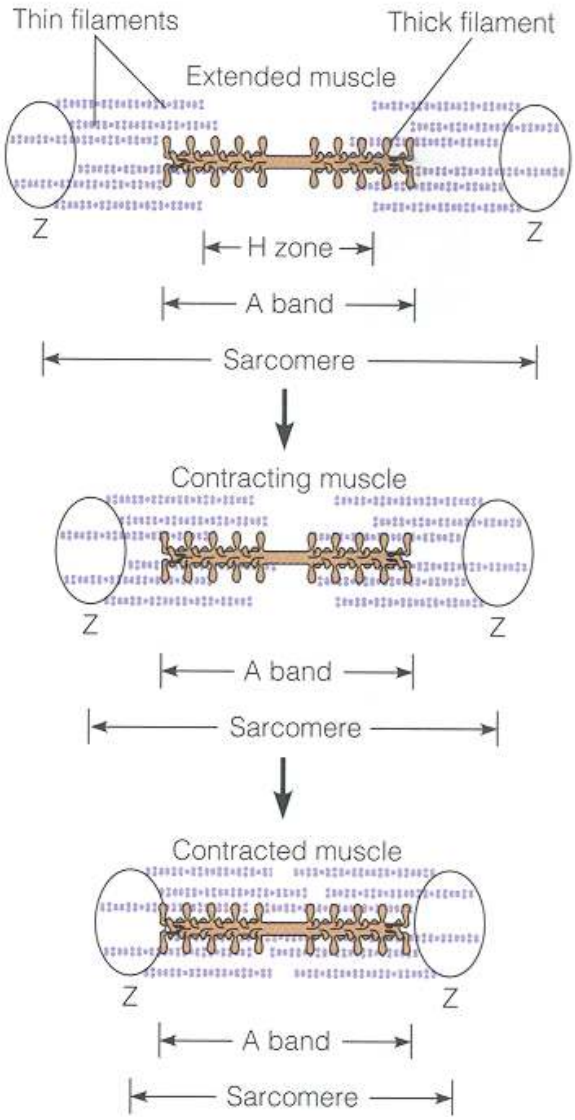


**Figure 1-12:** Sarcomere shortening by sliding filaments: (Mathews et al., 2000)

In this model contraction is caused by the thin and the thick filament sliding past each other driving the thin filament and therefore the attached Z-disk closer to the M-line, the centre of the sarcomere (see Figure 1-12). The myosin seemed to be the driving force in this process with consumption of ATP.

### *1.5.1.2 Cross bridge model*

The cross bridge model proposed how the movement of the fibres was generated by the proteins. The current opinion on how acto.myosin motility is generated is still based on a much refined cross bridge model (see Figure 1-21 for an updated model of the cross bridge cycle)

A.F. Huxley proposed two states. One where the myosin is attached to actin and another one where it is detached. In both states myosin undergoes a conformational change. While it is attached this drives the actin or thin filament past the thick filament.

The first refinement was proposed by A.F. Huxley himself in collaboration with R.M. Simmons (Huxley and Simmons, 1971) as well as Huxley and Kress (1985) in the form of the swinging cross bridge cycle model. The later models already take the biochemical models (see section 1.5.2) into account. In these models actin and myosin dissociate upon the binding of ATP. ATP is hydrolysed and myosin can bind actin again, after which the hydrolysis products ADP and Pi are released. While attached to actin myosin changes conformation in a way that the myosin head bound to actin in a 90° angle shifts to a 45° angle thereby driving the thin filament. This conformational change was named the power stroke. Structural evidence later lead to the development of the lever arm hypothesis which leaves the angle of the myosin binding to actin unchanged (see section 1.5.3.1).

### 1.5.2 Biochemical models

The mechanical swinging cross bridge model alone was not able to explain adequately the role of ATPase function for the generation of movement. Biochemical models were needed for a better understanding of the interaction of myosin, actin and nucleotides. The results needed for those models were obtained in steady-state and transient kinetic experiments.

The mechanism of ATP hydrolysis in the absence of actin was elucidated in the 1970s (Trentham et al., 1976, see Scheme 1-1).

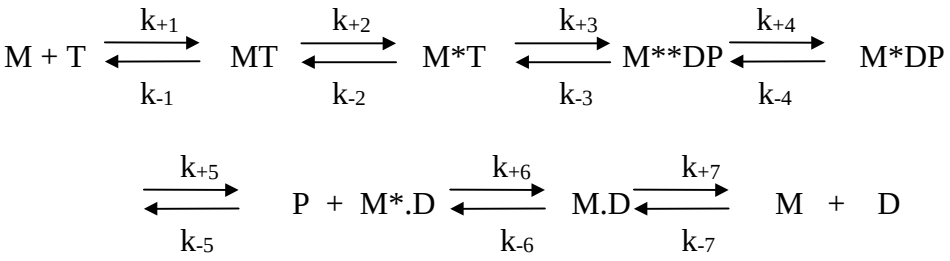


**Scheme 1-1:** The myosin ATPase. M = myosin; A = actin; T = ATP; D = ADP; P = phosphate. The stars mark conformations with enhanced tryptophan fluorescence.

Myosin and ATP form a binary collision complex (MT) which isomerises fast and irreversibly to a myosin.ATP complex with an enhanced intrinsic fluorescence (M*T). This is followed by reversible hydrolysis of ATP during which the intrinsic fluorescence is enhanced further. Recent evidence suggests that the correlation between the fluorescence change and the hydrolysis step is not that simple (see section 3.2.1). Pi is released in the rate limiting step followed by ADP release. Both Pi and ADP release are two-step processes with an isomerisation step and a dissociation step. During each isomerisation step a loss of intrinsic fluorescence can be observed. The change in fluorescence is associated with a conformational change.

This mechanism of myosin ATPase does not incorporate the binding of actin and is therefore not sufficient to describe the biochemistry in the cross bridge cycle. Furthermore in the presence of actin the ATPase function is greatly enhanced. This indicates that in the presence of actin the kinetics of the described mechanism are likely to change significantly.

#### *1.5.2.1 Lymn Taylor Model*

Lymn and Taylor developed the first model which tried to explain the role of ATP hydrolysis in the cross bridge cycle (Lymn and Taylor, 1971). They found that ATP reduced the tight binding ($K_A \cong 10^7\ M^{-1}$) of myosin to actin to cause dissociation. In the presence of actin the steady-state ATP hydrolysis for myosin is much faster. This indicates that a rebinding of actin takes place which increases the speed of the release of the hydrolysis products allowing rebinding of ATP. This model proposes a cyclic interaction of myosin and actin during which one ATP is hydrolysed. The model can easily be combined with the mechanical cross bridge model (see Figure 1-13).

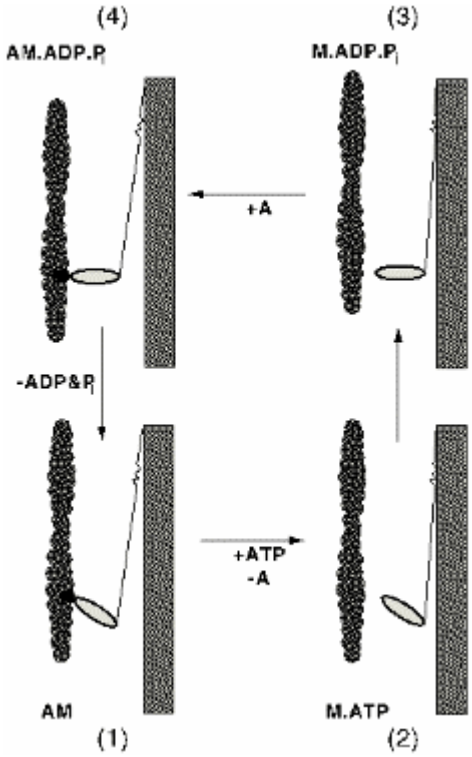


**Figure 1-13:** Lymn-Taylor-Model: The figure combines the mechanic and the kinetic model initially proposed by Lymn and Taylor (1971) (http://lala.mpimf-heidelberg.mpg.de/~holmes/muscle/muscle1.html)

The acto.myosin complex without a nucleotide bound is seen as the initial configuration. Binding of ATP dissociates actin and myosin followed by hydrolysis. Myosin rebinds to actin after which the hydrolysis products Pi and ADP are released. The power stroke, the conformational change producing motility, is linked to the release of the hydrolysis products. For the power stroke to occur at some stage of the cycle a reverse conformational change must happen resulting in a pre-power stroke conformation. Lymn and Taylor associated this step with the hydrolysis step which is controversially discussed and is a central question in all following models.

### *1.5.2.2 Eisenberg Greene model*

Eisenberg and Greene based their model (Greene and Eisenberg, 1980, see Figure 1-14) on results of Stein *et al*. (1979) who showed that the reduction of affinity of myosin for actin (by more than 1000 fold) is not necessarily accompanied by acto.myosin dissociation followed by hydrolysis. At very high protein concentrations hydrolysis can occur without dissociation of the acto.myosin complex.

Looking at the interaction of actin and myosin in equilibrium Eisenberg and Greene proposed two states of binding for myosin or the myosin nucleotide complex for actin: the weak binding state with a $K_A<10^5\ M^{-1}$ and the strong binding state with $K_A>10^5\ M^{-1}$. The myosin.ATP complex and the myosin.ADP.Pi complex are associated with the weak binding state. The nucleotide free myosin and the myosin.ADP complex are associated with the strong binding state.

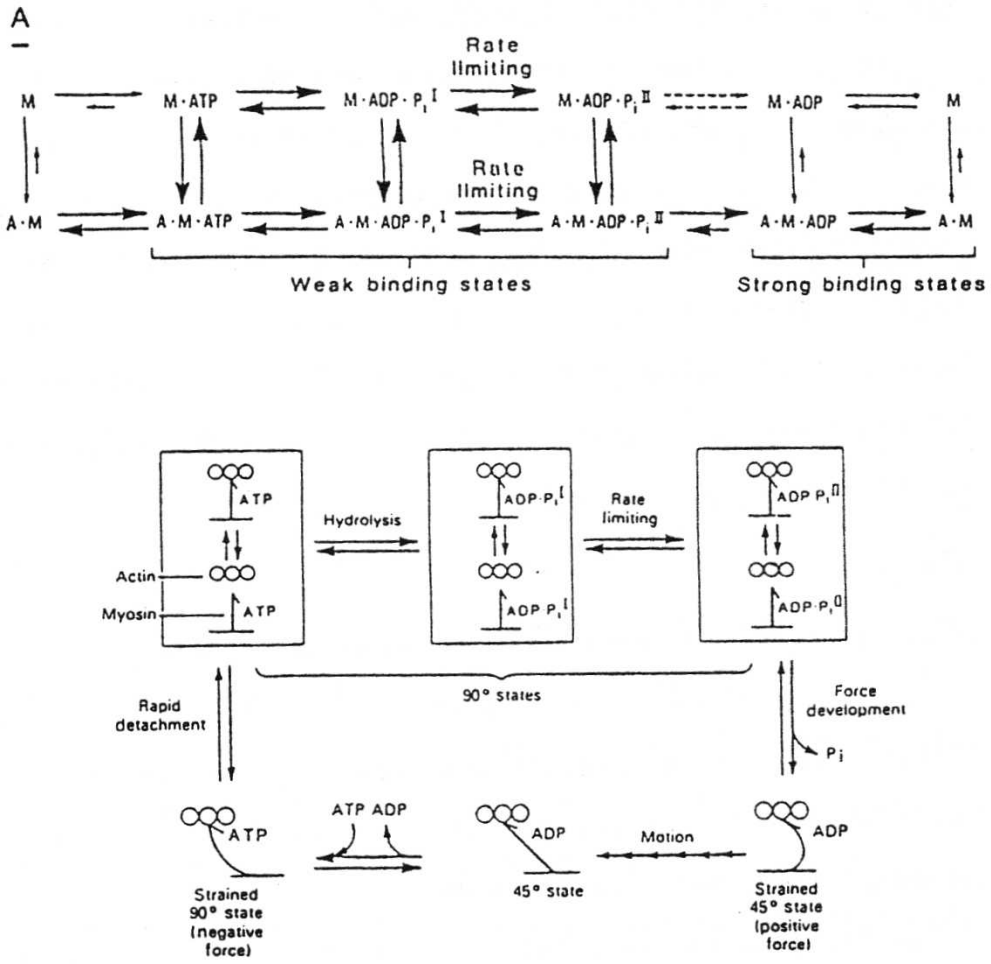


**Figure 1-14:** The Eisenberg-Greene model: On the top a kinetic scheme of the acto.myosin ATPase is shown. The dotted arrows indicate the rate limiting step. On the bottom a mechanical model of the cross bridge cycle is shown. The transition of weak to strong binding is associated with the change of angle of myosin bound to actin. (Greene and Eisenberg, 1980)

In contrast to the strong binding state in the weak binding state association and dissociation of myosin and actin are in fast equilibrium. It is essential for this model that the two binding states are linked with two different conformations: the weak binding state with a pre-power stroke conformation and the strong binding state with a post-power stroke conformation. This means that the inversion of the power stroke must occur before dissociation can take place.

The force in the opposite direction this step would impose can be neglected because of the immediate dissociation of the complex after reaching this conformation.

### *1.5.2.3 3G model (Geeves, Goody and Gutfreund)*

In 1983 Goody and Holmes described the interaction of myosin, actin and nucleotide as a competitive binding system in which tighter binding of the nucleotide or an analogue to myosin results in a weaker binding of actin and vice versa (Goody and Holmes, 1983). According to them myosin.nucleotide complexes can be classified as a continuum between those in a weak and those in a strong binding state. A model was suggested in which actin is bound weakly in an initial "attached" state (or A-state) which is in rapid equilibrium with free actin. This complex can reversibly isomerise to the rigor state (or R-state). In the R-state actin is more tightly bound while the affinity for the nucleotide is reduced and the nucleotide is able to dissociate at low concentrations. These relations are summarised in Scheme 1-2.

$$A+M.N \underset{}{\overset{K_I}{\rightleftharpoons}} \underset{\text{A-state}}{A\text{-}M.N} \overset{K_{II}}{\rightleftharpoons} \underset{\text{R-state}}{A.M.N} \overset{K_N}{\rightleftharpoons} A.M+N$$

**Scheme 1-2:** The two step binding model (Goody and Holmes, 1983). M = myosin: A = actin; N = nucleotide.

Kinetic evidence for more than one acto.myosin complex in the presence of nucleotides or analogues supported this idea (Konrad and Goody, 1982; Sleep and Hutton, 1980; Geeves and Gutfreund, 1982; Millar and Geeves, 1983). From this evidence Geeves, Goody and Gutfreund proposed a model which became known as the 3G model (Geeves et al., 1984, see Figure 1-15). It includes the isomerisation of the A-state (A-M.N) to the R-state (A.M.N) in a two step reaction. The A-state represents the weak binding state proposed by Eisenberg and Greene while the strong binding state is represented by the R-state.

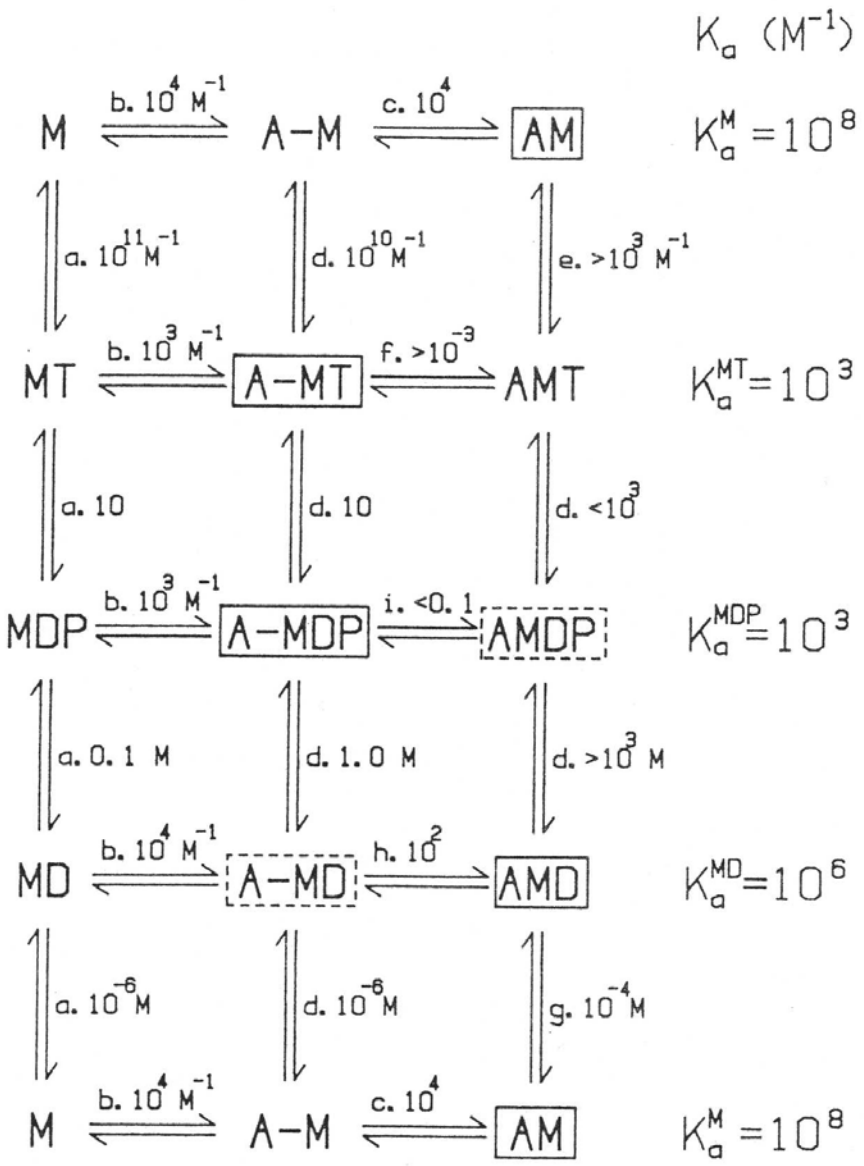


**Figure 1-15:** The 3G model shows the implications of the two step binding model on the kinetic scheme of the myosin nucleotide complex binding to actin. The equilibrium constant for the transition of the detached to the attached state is independent of the nucleotide while the equilibrium constant for the transition to the R-state depends on the nucleotide bound to myosin. Preferred states are marked with frames. (Geeves et al., 1984)

In this model all states (detached state, A-state and R-state) are in equilibrium (as shown in Figure 1-15) and weak or strong binding of a specific myosin.nucleotide complex is defined by the equilibrium constant $K_{II}$ (Scheme 1-2). If $K_{II} > 1$ the R-state predominates and if $K_{II} < 1$ the A-state does. It was proposed that the value of $K_I$ is relatively independent of the binding of nucleotides and of the order of $10^3$-$10^4$ $M^{-1}$. Because of the large changes of $K_{II}$ depending on the binding of a specific nucleotide the predominant state alternates between strongly bound R-state and weakly bound A-state during the ATP hydrolysis cycle. In the absence of a nucleotide ($K_{II} = 200$) the R-state predominates. Binding of ATP reduces the $K_{II}$

to less than $10^{-2}$ and results in predomination of the A-state. The myosin.nucleotide complex and therefore the value of $K_{II}$ changes during the process of ATP hydrolysis and the subsequent release of the products. Later in experiments with the nucleotides and analogues the values for $K_{II}$ could be estimated (Geeves and Jeffries, 1988; Coates et al., 1985). During hydrolysis the acto.myosin progresses back to the R-state. In agreement with the model by Eisenberg and Greene this model also suggests the force generating step to be a conformational change in the transition from the weakly bound A-state to the strongly bound R-state. Unlike in Eisenberg and Greene`s model this transition is not immediately connected to a specific myosin.nucleotide complex but the result of a system in equilibrium. The implications of this model for the cross bridge cycle are illustrated in Figure 1-16.

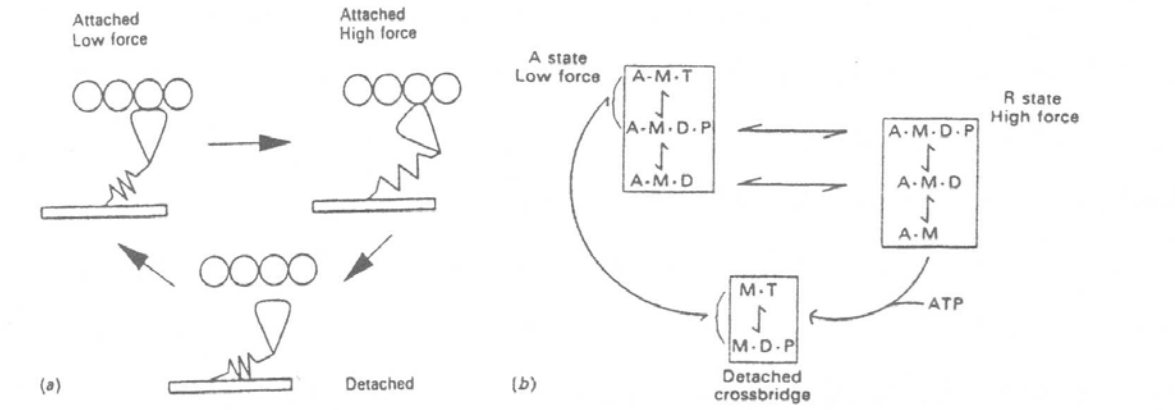


**Figure 1-16:** A mechanical cross bridge cycle model based on the biochemical 3G model.
A) The cross bridge binds fast and reversibly to actin in a weak binding state. The transition to a strong binding state is associated with a change in conformation causing a strain on an elastic element. The binding of ATP leads to dissociation of the complex.
B) A correlation of the mechanical and the biochemical model. Only the states with high probability are featured for each conformation.

### 1.5.3 Structural models

Biochemical evidence led to models which explain how ATP hydrolysis and movement by swinging cross bridges are linked. In such models a conformational change as a force generating step, the power stroke, was always proposed. However only structural evidence could help to understand how this conformational change produces movement and which parts of the molecule play vital roles in that.

Because of the long filament forming rods myosin is difficult to crystallise. In contrast S1 forms crystals which can be analysed by X-ray diffraction experiments as Rayment *et al.* showed in 1993 (Rayment et al., 1993b, see Figure 1-17). Their measurements resulted in the first high resolution structure of chicken skeletal S1.

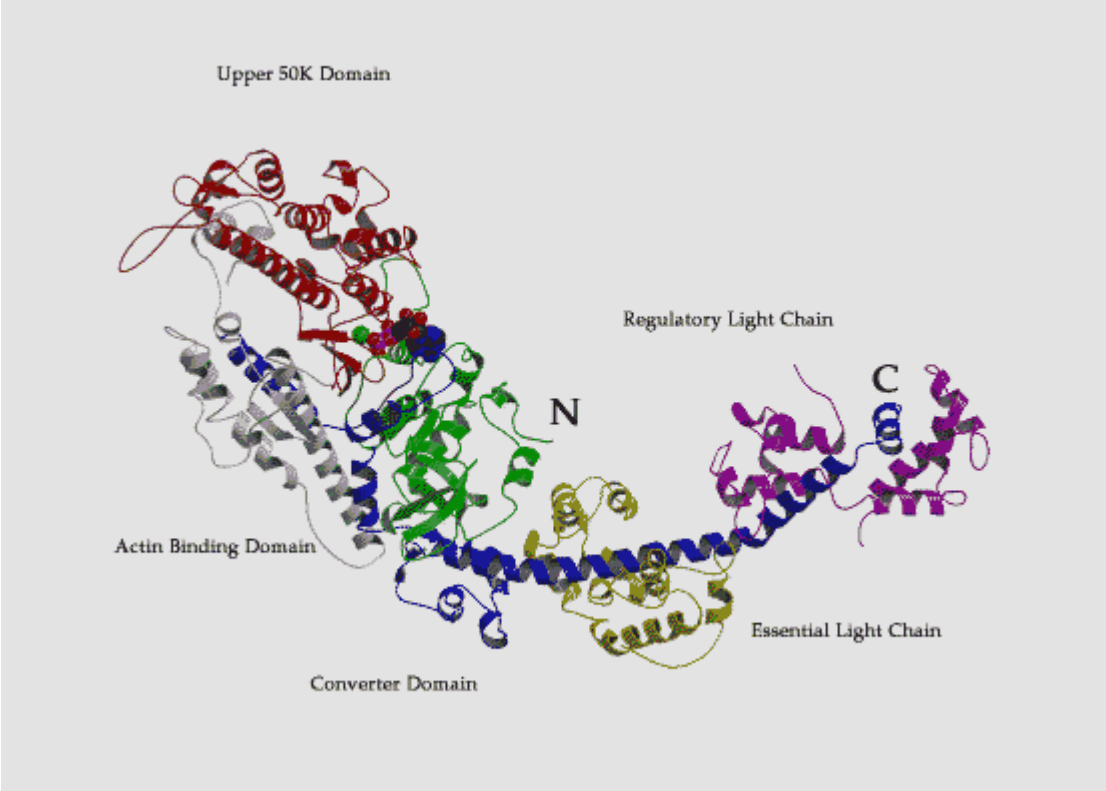


**Figure 1-17:** The structure of myosin S1 from chicken skeletal muscle (Rayment et al., 1993b). S1 has an elongated globular head consisting of a 7-stranded β-sheet. The C-terminal α-helical neck domain carries two calmodulin-like light chains, the regular light chain (magenta) and the essential light chain (yellow). The proteolytic fragments are colour coded: 25K in green, 50K in red and 20K in blue. The 50K fragment spans two domains: the upper 50K domain and the lower 50K domain containing the actin binding site coloured in grey (Geeves and Holmes, 1999).

The sequence of the chicken skeletal S1 used by Rayment comprises 843 residues of the heavy chain plus two light chains. Further limited proteolysis breaks S1 up into three fragments named after their apparent molecular weights: 25 K (N-terminal), 50 K (middle) and 20 K (C-terminal) (Mornet et al., 1979). Rather than being functional subdomains all three domains which are connected by surface loops contribute to a 7-stranded β-sheet surrounded by several α-helices. Those α-helices form a deep cleft extending from the nucleotide binding site near the 25-50 K fragment boundary to the actin binding site. The N-terminus lies near the start of the neck and the first 80 amino acids form a protruding β-barrel called the SH3 domain. The 50 K fragment spans two domains, separated by the cleft called the 50 K upper domain (81-486) and the 50 K lower domain (487-600). While the 50 K upper domain together with the 25 K domain constitute most of the β-sheet and the bulk of the head domain,. the 50 K lower domain constitutes the major part of the actin binding site. The first part of the 20K domain is an integral part of the 25-50K domain followed by a compact so-called “converter” domain and a long α-helix.

#### *1.5.3.1 The lever arm hypothesis*

The most remarkable feature Rayment found for his structure of S1 is that it consists not only of the globular head domain with the actin and the nucleotide binding site but also a long α-helical neck domain at the C-terminal end of the 20K domain. This long neck domain contained two binding sites for calmodulin-like light chains which could stabilise the structure. In combination with structural evidence from cryoelectromicroscopy of S1 decorated actin (see Figure 1-18) this region was proposed to act as a lever arm for the force generating step (Rayment et al., 1993a). This meant that during the conformational change of the power stroke the angle of the globular head remains essentially the same while small changes in the catalytic domain of the protein produce a much larger change by tilting the lever arm. In experiments with genetically modified light chains to which a fluorescent label was attached the lever arm swings through angles of 30-40 degrees (Corrie et al., 1999). This is in good agreement with molecular models and recent further evidence for the lever arm hypothesis in which the native myosin neck domain was replaced with a rigid α-actinin repeat of variable length (Kliche et al., 2001). The speed in *in vitro* motility assays increased linearly with the increase of the length in the artificial lever arm (Anson et al., 1996). Likewise the step size increased which could be measured by a novel method of force measurements utilising optical tweezers and special microneedles (Ruff et al., 2001). Image processed high resolution electronmicrographs show the lever arms of myosin V dimers attached to actin emerge from the heads in two positions (Walker et al., 2000). The position of the myosin heads remains unchanged in these pictures which correlate well with structural models of myosin binding to actin.

Unfortunately there is no crystal structure of myosin bound to actin since crystallisation of the complex proved too difficult. Atomic models of the acto.S1 complex were a result of fitting the crystal structures of S1 and actin to cryoelectronmicroscope reconstructions of decorated actin (Schroder et al., 1993; Rayment et al., 1993a).

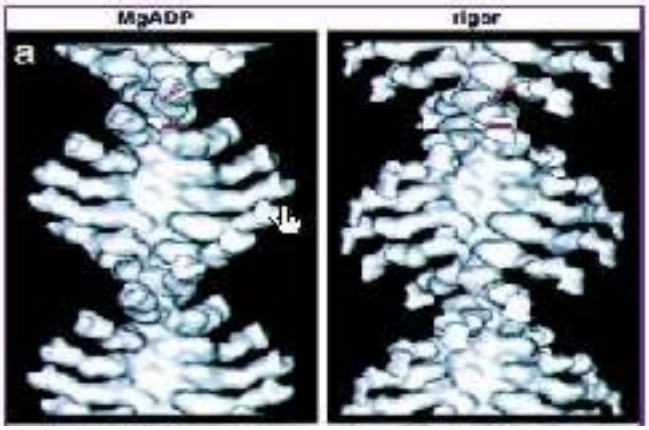


**Figure 1-18:** Cryoelectromicroscopy of the conformational change of acto.myosin (Jontes and Milligan, 1997)

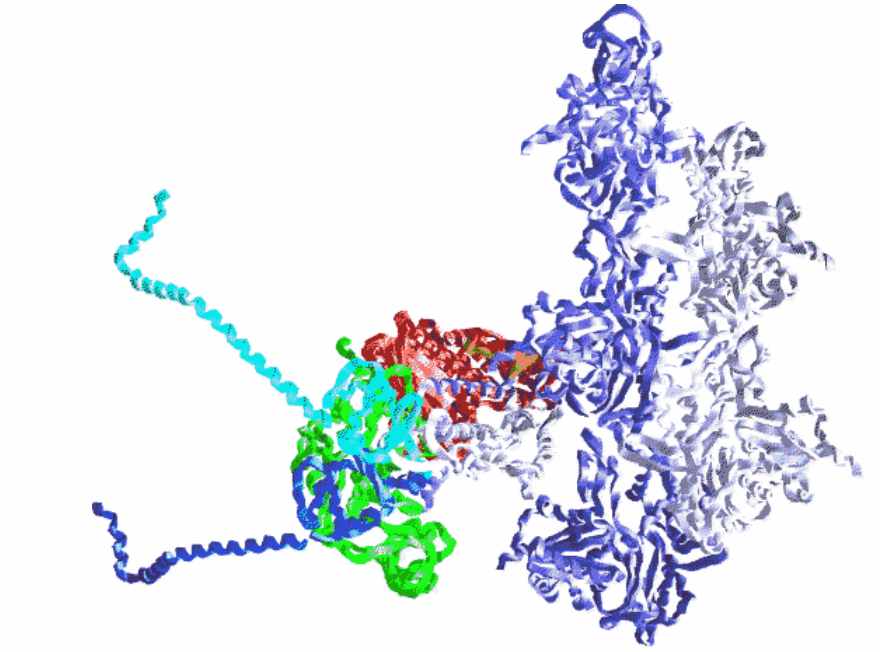

**Figure 1-19:** Overlay of structural models of the pre-power stroke state and the post-power stroke state of S1. The pre-power stroke state shows a reconstruction of a *Dictyostelium* construct truncated at residue 759 complexed with ADP•Vanadate (Smith and Rayment, 1996). The post-power stroke state shows the same construct complexed with ADP•$BeF_x$ (Fisher et al., 1995). In both cases the missing lever arm has been modelled from chicken S1 data by superimposing the converter domains. The overlay shows a 60° rotation and a distance of 11 nm at the end of the lever arm between the two states (Holmes and Geeves, 2000).

The Rayment structure without nucleotide is believed to be in a conformation in which the lever arm is in an orientation similar to a post-power stroke rigor conformation. Structures in a proposed pre-power stroke conformation could be obtained by co-crystallisation with nucleotide analogues (see Figure 1-19). Dominguez *et al*. (1998) solved a pre-power stroke structure of chicken smooth muscle complexed with ADP•$AlF_4$ or ADP•$BeF_3$ which includes the essential light chain binding domain of the neck region. The post-power stroke conformation binds nucleotides with high affinity and features an open γ-phosphate binding

pocket to permit Pi release. It is called the OPEN conformation. The pre-power stroke conformation binds both nucleotides and Pi with high affinity and the γ-phosphate binding pocket is closed. It is called the CLOSED conformation.

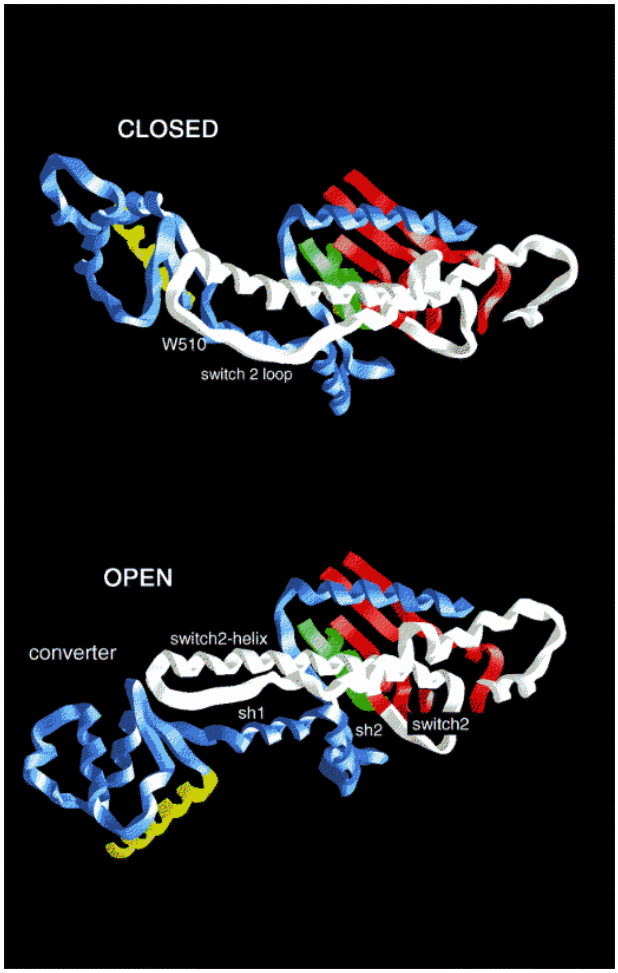


**Figure 1-20:** The figure shows the conformational change the switch 2 helix undergoes in the transition from CLOSED to OPEN state. This results in a large change in the orientation of the converter domain. The inward movement of the switch 2 element in a bending and twisting of the switch 2 helix and the associated switch 2 loop which carries the highly conserved W510. W510 is mainly responsible for the change of intrinsic fluorescence during the ATP hydrolysis cycle of myosin.(Geeves and Holmes, 1999)

It appears that closing of the pocket is essential for hydrolysis of ATP. Transition between the two conformations is accompanied by a reorganisation of parts of the active site which appear to work as a switch (SWII-helix 475-519, see Figure 1-20). The switch communicates with a the SH1-SH2 helix in the converter domain containing a hinge (G499). This causes a rotational movement of the converter of about 60° moving the emerging lever arm. The small change in the active site (5• ) results in a significant movement at the end of the lever arm (11 nm). The changes caused by the hydrolysis of ATP represent the reversal of the power stroke

requiring a change from the OPEN to the CLOSED conformation. The power stroke itself is then associated with the opening of the γ-phosphate binding pocket, the release of Pi and a conformational change in the opposite direction.

According to acto.myosin solution kinetics, both the OPEN and the CLOSED conformation bind actin weakly, suggesting that the structure of myosin in the strongly binding R-state is still missing. The isomerisation to the R-state would cause stronger actin binding and a decrease in nucleotide affinity. In slow myosins a further step associated with a conformational rearrangement was observed on ADP release (Collucio and Geeves, 1999). ATP binding might then reverse the R-state to A-state transition in terms of actin binding but without the conformational change from OPEN to CLOSED.

#### *1.5.3.2 The myosin sequence*

The crystal structure of myosin can be correlated to the amino acid sequence which is highly conserved in the head domain for various myosins. Studying the variation in this sequence provides a wealth of information about which parts of the molecule are essential for function, thereby elucidating structure function relations in general. As discussed in section 1.5.3 the 25K, 50K and 20K domains do not form functional subunits. However they are connected to each other by surface loops which are poorly conserved compared to the rest of the motor domain. This led to the idea that these variations in the loops modulate the biochemical properties of the molecule. Spudich (1994) proposed that loop 2 in proximity to the actin binding site influences interaction between actin and myosin and therefore indirectly actin activated ATPase while loop 1 in proximity of the nucleotide binding site plays a role in controlling nucleotide affinity and ADP release. Sweeney *et al*. (1998) and Uyeda *et al*. (1994) provided more experimental evidence working with chimeric myosins of chicken smooth muscle which showed variations in loop 1. Though both changes in charge and flexibility of the loop influenced ADP release a simple correlation is not obvious. Overall a reduction in flexibility seems to cause an inhibition in ADP release. This idea was supported by work with catch and striated muscle from scallop (Kurzawa-Goertz *et al*., 1998) which also suggests an influence on Pi release. Mutational studies of *Dictyostelium* myosin with a series of changes to loop 2 showed no effect on nucleotide binding properties. However the increase in positive charge in that loop increased the affinity of the nucleotide-free head for actin 100-fold (Furch et al., 1998). Despite evidence that variation in these loops influences protein

behaviour no simple solution on how this behaviour is influenced is available (Goodson et al., 1999). This seems especially true since major changes in mechanical properties can occur without changes in either of the two loops (Canepari et al., 2000). For these myosins, however, differences in a third loop, the secondary actin binding loop or loop 3, exist. This loop apparently binds to the neighbouring actin monomer (Bonafe and Chaussepied, 1995; Andreeva et al., 1993) and seems to be specific for skeletal muscle myosins. This contact was not observed with smooth muscle or *Dictyostelium* myosin (Marianne-Pepin *et al*., 1985). Studies in which this loop has been inserted into *Dictyostelium* myosin show that this loop can influence binding and dissociation from actin, however, changes in ATPase activity were not observed (Van Dijk et al., 1999).

Of further interest is the cardiomyopathy surface loop (Geisterfer-Lowrance *et al*., 1990), which contains the highly conserved TEDS-site. The TEDS-site is found in a position 16 residues upstream of the DALAK consensus sequence and generally carries an acidic (E or D) or a phosphorylatable (T or S) residue. Only a few myosins are known to have exceptions to this rule (Vargas et al., 1997, see section 7.6). It has been proposed that a negative charge at the TEDS-site facilitates actin binding and Pi release and thus might influence the coupling of actin binding and ATP hydrolysis (Ostap and Pollard, 1996; Bement and Mooseker, 1995). This hypothesis is supported in recent studies of myosin VI, in which a point mutation at this site not only influenced the release of Pi, the ATPase activity and the actin affinity, but also the ADP affinity in the presence and absence of actin (De La Cruz et al., 2001).

The idea of a lever arm mechanism naturally led to the attempt to locate the fulcrum point for the lever arm. Crystal structures and dependence of velocity on the length of the lever arm in in vitro motility assays indicated this fulcrum point close to two short helices(Sk691-714) carrying reactive cysteins (SH1 at Sk697 and SH2 at Sk707). This region contains three glycines often used as hinge points in proteins. Mutational studies of this region, in particular the replacement of the glycines with bulkier residues, predicted SkG699 as the most probable residue functioning as a hinge (Batra et al., 1999; Kinose et al., 1996).

### 1.5.4 The acto.myosin cross bridge cycle: A summary

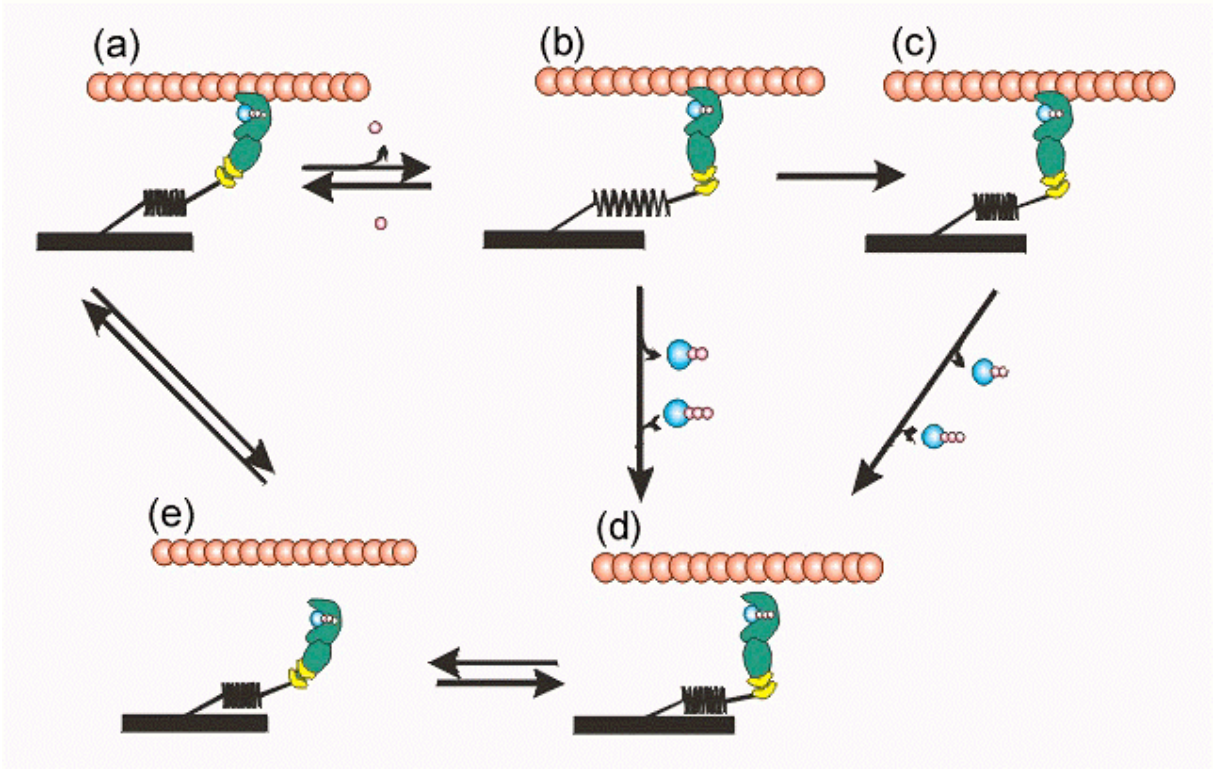


**Figure 1-21:** A model for the cross bridge cycle taking the 3G model and the lever arm hypothesis into account. The myosin head and neck domain are shown in green, the tail domain with the elastic element in black, actin in orange and the nucleotide in blue with magenta phosphates.

The acto.myosin system generates motility by a cyclic interaction of myosin cross bridges with actin driven by hydrolysis of ATP. The efficient conversion of biochemical energy requires a precise temporal coupling between the biochemical and mechanical events. In Figure 1-21 a current view of how the cross bridge cycle works is depicted based on the acto.myosin system of fast skeletal muscle, which is the most thoroughly studied. The essential mechanochemical steps are shown lettered (**a**) to (**e**). The basic cycle is believed to be the same for all myosins but to differ in the rates of the biochemical steps for each individual myosin to account for different physiological requirements.

ATP binding to either a rest length myosin head (**c**) or to a head bearing a load (**b**) causes a rapid almost irreversible dissociation of the myosin head from actin (**d**). This is followed by fast and reversible hydrolysis of ATP. The hydrolysis is accompanied by a major conformational change which represents the reversal or a repriming of the power stroke. It has been proposed that the conformational change is between an OPEN and a CLOSED conformation (d and e; see section 1.5.3.1) and that a switch to the CLOSED conformation must take place for hydrolysis to occur. The affinity of the resulting M.ADP.Pi complex for

actin is significantly higher than that of M.ATP and the myosin head can bind rapidly and reversibly to an actin site within reach. The majority of myosin heads within a contracting muscle are likely to be in equilibrium between states **a**, **d** and **e**.

After binding of the myosin head the interaction with actin can promote a major change in conformation (**a** and **b**), the power stroke, which is believed to be from a CLOSED to an OPEN conformation and the OPEN conformation is proposed to be required for Pi to be released. The reversible Pi release and the conformational change of the power stroke seem to be closely connected. Crystal structures suggest that the power stroke consists of a rotation of a part of the myosin head including the converter domain and the light chain-binding region, the lever arm. This results in the displacement of the distal tip of the lever arm by up to 11 nm (depending of the length of the lever arm and the angle of rotation). The structural changes in the actin-myosin interface that produces the power stroke are believed to be the conformational change between OPEN and CLOSED inducing the rotation of the lever arm mediated via the switch 2 region (see section 1.5.3.1). Under load the power stroke results in the distortion of an elastic element (**b**). The location and nature of the elastic element is unknown but may represent a distortion in the myosin head or of the lever arm. For simplicity the elastic element is drawn here as part of the connection between the myosin head and the thick filament.

After the reversible release of Pi, ADP is released from the cross bridge and under physiological conditions irreversibly replaced by ATP which dissociates the acto.myosin complex and completes the cycle. It has been proposed that the rate of release of ADP is inhibited by a strain on the elastic element. Thus ADP release from **b** is much slower than from **c**. Therefore a sliding motion of the actin relative to the myosin filament which takes strain off the elastic element is likely to occur before ADP release and under isometric conditions where no sliding can occur ADP release is slow. The mechanism of the strain limited ADP release appears to be a key event which differs between myosins designed for efficient fast shortening vs. efficient bearing of load and rates release of ADP seem to be generally faster in myosins designed for fast shortening. The structural changes observed on binding ADP to complexes of actin with smooth muscle myosin and rat liver myosin I (myr 1) might reflect this strain sensing mechanism (Collucio and Geeves, 1999).

# 2 Aims of the project

Traditional methods of measuring transient kinetics have made major contributions to the elucidation of the molecular basis of motor function (Trentham et al., 1976; Taylor, 1979; Geeves, 1991). These methods are primarily based on a stopped flow or a quenched flow apparatus which mixes two or more reactant solutions. To achieve proper mixing relatively large volumes and therefore amounts of material are required. This was not a serious limitation when the proteins could be obtained in relatively pure form from the large skeletal muscles of mammals or similar animals. However in many instances the quantity of material required has proven a serious limitation and the development of methods which can use smaller quantities will have wide uses. For example pure mammalian myosin heavy chain isoforms can only be extracted from single fibres, as bulk muscle tissue contains a mixture of isoforms and an expression system for mammalian muscle isoforms is currently not available. This is not only of use for characterisation of a system of very closely related myosins but may also prove useful diagnostically for identifying disease states that result in altered muscle activity. Most members of the recently discovered myosin superfamily are only available in very small amounts and remain to be fully characterised (Cope et al., 1996). Likewise a highly efficient expression system is missing for most myosins which makes the expression of large quantities of genetically engineered protein difficult. Structure-function relationships in the myosin superfamily can be elucidated by characterisation of the naturally occurring variants of myosin and variations introduced by site-directed mutagenesis. The *Drosophila* system, to which mutations can be introduced easily, is also an attractive system for correlating structure and function in muscle myosins, but again the quantities available are limited to micrograms of material.

For these reasons a flash photolysis apparatus for use with sub-microgram quantities of material was developed. The release of a chemical compound acting as one of the reactants makes the need for large volumes to achieve proper mixing redundant.

This work evaluates this system by determination of accuracy compared to traditional methods, dead time, sensitivity and therefore ultimately minimum requirements of protein amounts for the model system of rabbit acto.myosin or acto.S1. This includes not only the evaluation but also the improvement of the system.

The aim of this thesis is also to apply the system for experiments which were previously impossible. This includes the kinetic characterisation of all four skeletal muscle myosin heavy

chain isoforms of adult rat as well as two human isoforms, thereby helping to understand the correlation of mechanical and biochemical properties of muscle and elucidating structure function relationships in a highly conserved system.

The flash photolysis method was also used in conjunction with traditional stopped flow methods to kinetically characterise TgM-A, a member of recently discovered class XIV myosins. This protein is found in the parasite *Toxoplasma gondii* which is closely related to *Plasmodium* organisms causing malaria and it is believed to play an essential role in the host invasion of the parasite. This myosin is furthermore of high interest due to its remarkable differences in sequence compared to all other known myosins.

# 3 Background theory

## *3.1 Observable parameters*

Many results of this work were obtained from spectroscopic measurements. The parameters observed in those measurements were: Absorbance, fluorescence and light scattering.

### 3.1.1 Absorbance

Chemical substances or biochemical macromolecules in solution absorb light at certain wavelengths. This is because the light of specific energy and therefore wavelength can shift electrons to higher energetic states. The absorbance is equal to the negative logarithm of the ratio of the absorbed light to the initial light intensity $A = -\log \Delta I/I_0$. The amount of light absorbed at those certain wavelengths is specific for a substance. Hence each substance has a specific extinction coefficient at a given wavelength. From the absorbance the concentration (c) of the substance in solution can be calculated according to the law of Lambert-Beer: $A=\varepsilon \cdot c \cdot d$ with values for absorbance (A), the molar extinction coefficient (ε) and the distance (d) the light travels through the solution. By measuring the time resolved change in absorbance the formation and decay of a substance can be monitored.

### 3.1.2 Fluorescence

The state of lowest energy is the preferred state for molecules. A molecule which is put into an energetically higher energy electron state by absorption of light can return to its preferred state either by transition with emission of light, fluorescence and phosphorescence, or without the emission of light by diverting the energy to vibrations and rotations of the molecule. In contrast to phosphorescence, fluorescence does not disrupt the spin coupling. According to the Franck-Condon principle light emitted by fluorescence is red shifted from the absorbed light. When light is absorbed there is a transition from the lowest vibrational state of the lower electron state to a higher vibrational state of the higher electron state. Before the light is emitted the molecule has already lost part of the energy by going to an energetically lower vibrational state within the higher electron state. After the emission of light of longer wavelength the molecule returns to the lower electron state but in a higher vibrational state as shown in Figure 3-1.

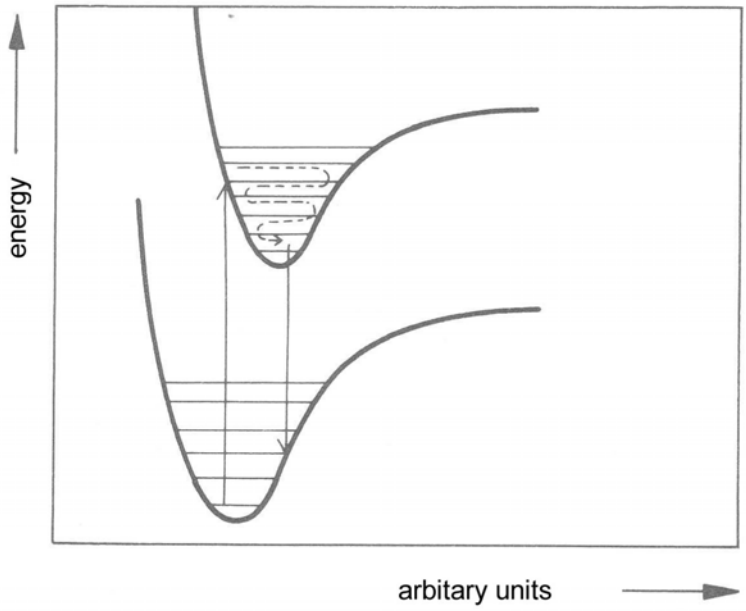


**Figure 3-1:** Energetic diagram illustrating the effect of the Franck-Condon principle resulting in fluorescence. (Barrow, 1984)

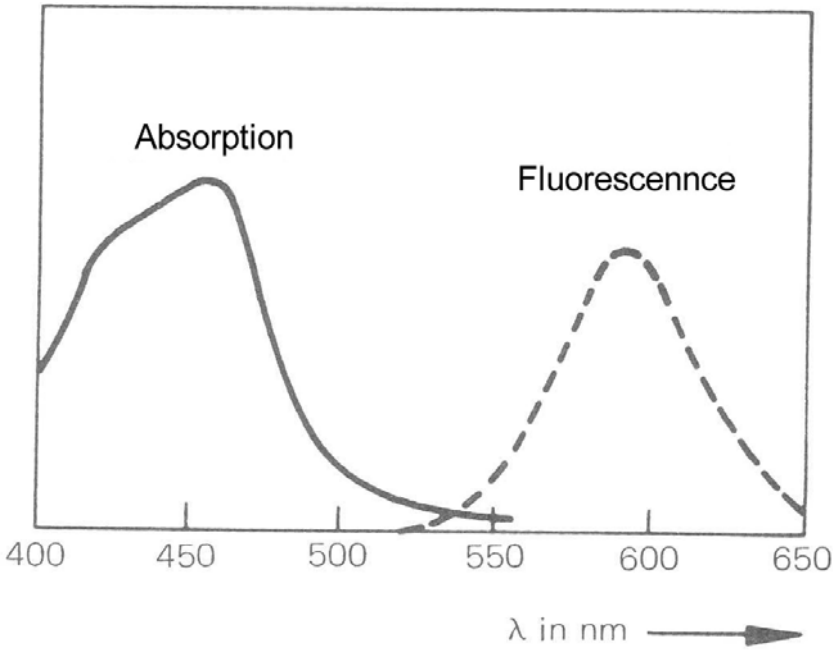


**Figure 3-2:** Overlay of an absorption- and a fluorescence spectrum (of $Ru(bipy)_3^{2+}(aq)$). The red-shift for the fluorescence spectrum is clearly visible. (Barrow, 1984)

For the investigation of biological molecules we have to distinguish between two kinds of fluorescence:

- Intrinsic fluorescence stems from natural fluorescent groups within the molecule.
- Extrinsic fluorescence stems from external fluorophores which have been artificially attached to the biomolecule.

#### *3.1.2.1 Intrinsic Fluorescence*

There are 3 amino acids acting as natural fluorophores in proteins: tryptophan (trp), tyrosine (tyr) and phenylalanine (phe) (Lakowicz, 1983).

Because of the low quantum efficiency of phenylalanine and tyrosine the intrinsic fluorescence is dominated by tryptophan fluorescence. Denaturing a protein causes the emission maxima to shift to red resulting in a similarity of the emission maxima of all proteins (Friefelder, 1982). Tryptophan fluorescence reacts to changes in the polarity of the close environment and the exposure to the aqueous phase. Therefore it can report on conformational changes in the immediate environment (see section 3.2.1). Tryptophan fluorescence is excited at 295 nm and the flourescence emission is measured above 320 nm through a 320 nm cut-off filter.

#### *3.1.2.2 Extrinsic Fluorescence*

An external fluorophore can be covalently or non-colvalently attached to a protein to give it an extrinsic fluorescence. The following conditions have to be met for the fluorophore to be suitable for structure function studies of the protein:

- The fluorophore needs to be stably attached to a specific location of the protein
- Changes in the immediate environment must be reported by fluorescence changes of the fluorphore
- The fluorophore should not alter the properties of the protein.

Therefore only fluorophores which react with strong changes in fluorescence on polarity changes in the environment are used to study biochemical processes like nucleotide-protein interaction, protein-protein interaction or protein conformation changes. Most fluorophores used are covalently bound since fluorophores binding non-covalently are not binding as specifically and are therefore not as suitable for the investigation of specific reactions and the resulting conformational changes.

Used fluorophores usually are chromophores with a reactive group which is able to form a bond with reactive groups of the protein. These include the SH-group of cysteine and the free $NH_2$-group of lysine. It is important that the introduction of the fluorescent group does not modify the activity of the protein. Actin can for example be selectively labelled at the cysteine 374 with the pyrene fluorophore. Pyrene fluorescence can be excited at 365 nm and has an emission maximum at 405 nm. It is quenched by 70% upon binding of actin to myosin.

Often the selective binding of a fluorophore to a specific location where it does not interfere with protein activity proves to be difficult because of the large number of active groups. In these cases it can be favourable to label the substrate instead of the protein.

ATP and ADP can be labelled with the mant fluorophore: N-methylanthraniloyl derivates (Hiratsuka, 1983). They can be esters of N-methylanthraniloyl acid and either ribonucleotides or desoxyribonucleotides. The resulting mant ATP or mant ADP is a mixture of 2 isomeres (35% 2'-isomer, 65% 3'-isomer) which are in equilibrium with each other and can therefore not be isolated (Cremo et al., 1990).

The mant fluorophore can be either excited directly at 366 nm or by energy transfer from tryptophan fluorescence (295 nm). The emission maximum is at 450 nm.

### 3.1.3 Light scattering

Incoming light can be scattered in all direction from the surface of particles or macromolecules in solution which are larger or of similar size as the wavelength of the monitoring light. For molecules the amount of light scattering increases with the molecular weight. The light scattering changes according to the increase of the molecular weight of the filamentous actin with or without myosin or S1 attached (Cantor and Schimmel, 1980). In the case of actin and myosin the acto.myosin complex scatters the light much more than the separate proteins. Therefore the change of light scattering can be used to monitor dissociation or association of myosin or S1 from actin.

Light scattering is best measured in 90° from the incident light source and at a wavelength which does not interfere with possible fluorescence emission.

## *3.2 Transient kinetics*

Kinetic studies of proteins include steady-state and transient kinetics. In contrast to steady-state kinetics transient kinetics characterise how the steady-state is reached from non-steady-state starting conditions. Enzymatic reactions typically take place in less than a second. A single cycle of interaction between myosin and actin for example is driven by the hydrolysis of one ATP molecule per myosin head and can be completed in less than 50 ms. To understand the chemomechanical coupling of ATP hydrolysis and motor activity requires methods of studying the dynamic interaction of actin and myosin (or its subfragments) on the millisecond time scale. Stopped flow and quenched flow methods are commonly used to study such kinetics (see section 4.3.3). Further methods use the disruption of the equilibrium state by pressure or temperature jump and monitoring how a new equilibrium is reached by relaxation. The flash photolysis method for small protein quantities described in this work makes a further addition to methods determining transient kinetics.

### 3.2.1 ATPase function of myosin

Transient kinetic analysis of the ATPase function of myosin goes back to Bagshaw and Trentham (1974) who elucidated the ATPase cycle of rabbit skeletal S1 by monitoring the changes in intrinsic fluorescence. The suggested mechanism was shown previously in Scheme 1-1. Only recently this scheme was modified by Malnasi-Csizmadia *et al.* (2001) as shown in Scheme 3-1. They used a mutant *Dictyostelium* myosin in which all but one tryptophan residue (W501) have been replaced. In contrast to the earlier scheme the hydrolysis step and the event causing the increase in fluorescence, the transition from OPEN to CLOSED conformation, are regarded as separate events.The mechanism can be described as follows:

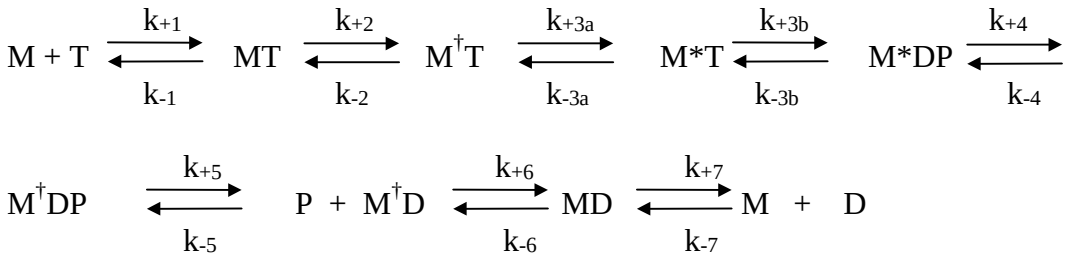


**Scheme 3-1:** The myosin ATPase (Malnasi-Csizmadia et al., 2001). M = myosin; A = actin; T = ATP; D = ADP; Pi = phosphate. The star marks conformations with enhanced tryptophan fluorescence while the cross indicates a decrease in fluorescence.

ATP binds to S1 in two steps. First a collision complex is formed which then quickly and irreversibly isomerises to the $M^{\dagger}T$ complex binding the nucleotide tightly. When ATP is first bound in the $M^{\dagger}T$ complex, with myosin in an OPEN conformation, the intrinsic fluorescence is decreased. However this conformation is in rapid equilibrium with the CLOSED conformation which is accompanied by a fluorescence enhancement. Therefore binding of ATP appears as single step with an overall fluorescence enhancement. This is followed by the reversible hydrolysis of ATP and the preceding equilibrium (see step 3a in Scheme 3-1) is shifted towards the CLOSED conformation giving a further enhancement in fluorescence. Then the rate limiting release of the reaction products Pi and ADP occurs. Both the release of Pi and the release of ADP are two-step processes with an isomerisation step preceding the dissociation step. In Scheme 3-1conformational changes which result in an increase in intrinsic fluorescence are marked with a star while a decrease is marked with a cross.

Use of the stopped flow method allows fast mixing of the reactants and the time resolved monitoring of fluorescence changes. S1 is mixed with various concentrations of ATP. The concentrations of ATP are always in large excess over S1 to achieve pseudo first order conditions. This results in a single exponential progress of the reaction and therefore the monitored change of fluorescence. The formation and dissociation of the collision complex is in fast equilibrium with an equilibrium association constant of $K_1$ preceding the isomerisation step associated with the fluorescence change with a rate of $k_{+2}$. The isomerisation can be regarded as irreversible with a value of $k_{-2}$ of about 0. Fitting of the exponential curve gives the observable rate constant $k_{obs}$. For small ATP concentrations, with $K_1 \bullet [ATP] << 1$, $k_{obs}$ and the ATP concentration show a linear relation which can be expressed as follows:

**Equation 3-1:** $\mathbf{k_{obs} = K_1 k_{+2} \bullet [ATP] + k_{-2} \quad with\ k_{-2} \approx 0}$

At very high ATP concentrations the rate reaches a plateau value. This value defines the hydrolysis step, $k_{+3}+k_{-3}$, and is independent of the ATP concentration. Very fast reactions (>300 $s^{-1}$) are difficult to measure with stopped flow since a large amount of the amplitude is lost in the dead time of the apparatus (ca. 2 ms).

Binding of ADP also changes the intrinsic fluorescence. The rate of ADP dissociation from S1 is defined by $k_{-D} = k_{+6}$ while the rate of ADP binding is defined by $k_{+D} = k_{-6}/K_7$ (Equation 3-2). ADP binding can be measured analogous to ATP binding experiments and also shows a linear relation to the concentration of ADP at small concentrations. The affinity of ADP for S1 can then be calculated to be $K_D = 1/K_6K_7$.

### 3.2.2 Nucleotide interaction with the acto.myosin complex

Transient kinetic studies of ATP binding to the acto.myosin or acto.S1 complex revealed that the kinetics followed a similar pattern to the binding of ATP to S1 under pseudo first order conditions. Millar and Geeves developed the following model:

$$AM + T \underset{}{\overset{K_1}{\rightleftharpoons}} A.M.T \xrightarrow{k_{+2}} A\text{-}M.T \longrightarrow A + MT$$

**Scheme 3-2:** Scheme of the dissociation of the acto.myosin complex by ATP (Millar and Geeves, 1983). M = myosin; A = actin; T = ATP.

The formation of the collision complex A.M.T results in a fast equilibrium with the equilibrium constant $K_1$. The rate of the following isomerisation to a ternary complex ($k_{+2}$) determines the rate of the dissociation which is described by the following equation:

**Equation 3-3:** $$\mathbf{k_{obs}=K_1k_{+2}\bullet[ATP]/(1+K_1\bullet[ATP]) + k_{-2} \quad with\ k_{-2} \approx 0}$$

Dissociation can be monitored by either light scattering or the fluorescence change of pyrene-labelled actin. At small ATP concentrations ($K_1$•[ATP]<<1) the observed rate constant increases linearly with the ATP concentration which simplifies Equation 3-3 to

**Equation 3-4:** $$\mathbf{k_{obs} = K_1k_{+2}\bullet[ATP]}$$

The slope of a plot of $k_{obs}$ versus [ATP] is the apparent second order rate constant ($K_1k_{+2}$). At higher ATP concentrations the plot shows a hyperbolical progression which reaches a plateau at the rate of $k_{max}$. $k_{max}$ corresponds to $k_{+2}$ and $K_{0.5} = 1/K_1$ (see Figure 3-3).

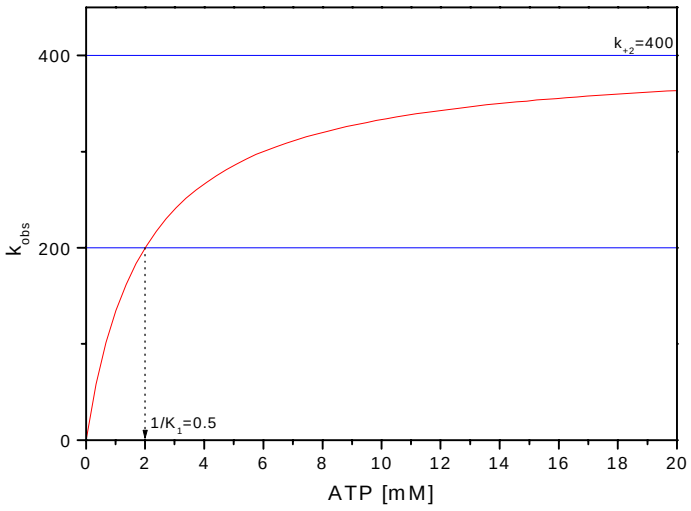


**Figure 3-3:** Plot of $k_{obs}$ versus [ATP]. The plot simulates an experiment of ATP-induced dissociation of acto.myosin with high ATP concentrations. For this simulation $k_{+2}$ is set to 400 $s^{-1}$ and $K_1$ to 500 $M^{-1}$

It is important to note that although the equations for the binding of ATP to the acto.S1 complex follow the same format as the binding of ATP to S1 the equilibrium and rate constants describe different processes.

In the presence of ADP both nucleotides compete for the binding to acto.S1. At low ATP concentrations the overall rate of ATP induced dissociation of acto.S1 ($K_1k_{+2}$) is sufficiently slow for the binding and dissociation of ADP to be a preceding fast equilibrium with the constant $K_{AD}$.

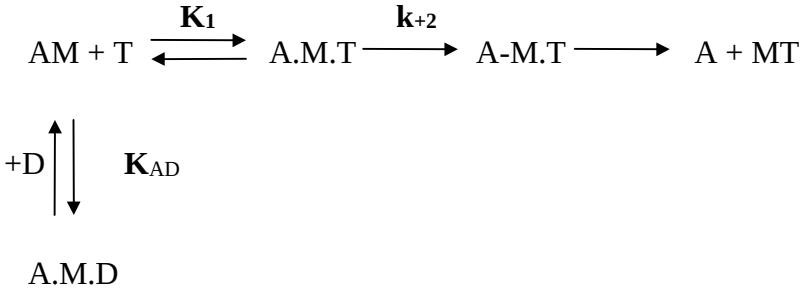


**Scheme 3-3:** Scheme of ATP induced dissociation of the acto.myosin complex in the presence of ADP (Siemankowski and White, 1984) M = myosin; A = actin; T = ATP; D = ADP.

Under those conditions the presence of ADP inhibits the rate of ATP induced dissociation of acto.S1. This relation can be expressed in the following equation:

**Equation 3-5: $k_{obs} = K_1 k_{+2} \cdot [ATP]/(1+[ADP]/K_{AD})$**

The dissociation equilibrium constant $K_{AD}$ defines the affinity of ADP for the acto.S1 complex.

Binding of a nucleotide to myosin or S1 reduces the affinity for actin and binding of actin reduces the affinity for the nucleotides. This relation can be expressed in the following scheme.

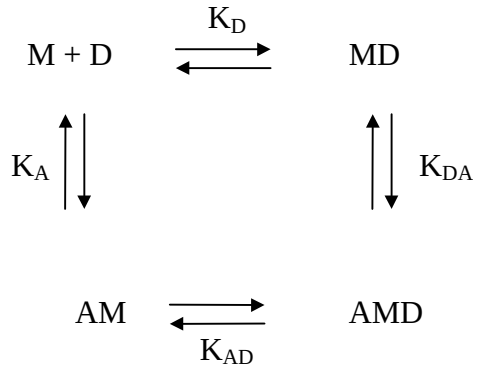


**Scheme 3-4:** Scheme of the coupling between the dissociation constants of actin and ADP binding to myosin. M = myosin; A = actin; T = ATP; D = ADP

In Scheme 3-1 $K_D$ is defined by $1/K_6K_7$. $K_A$ describes the affinity of myosin for actin. Binding of ADP to the complex reduces the affinity of myosin for actin which is represented by the constant $K_{DA}$. Likewise the formation of a ternary complex by binding of actin to a myosin.ADP complex reduces the affinity for the nucleotide ($K_{AD}$). For such a system the following equation must prove valid:

**Equation 3-6: $K_D \cdot K_{DA} = K_A \cdot K_{AD}$**

### 3.2.3 Actin activated ATPase

In the presence of a large excess of ATP myosin hydrolyses ATP under steady-state conditions. This ATPase activity is greatly enhanced in the presence of actin. The reactions follow the rules first described in 1913 by Michaelis and Menten. The relation expressed in Equation 3-7 describes a two step reaction, which includes the reversible formation of an enzyme substrate complex and a following irreversible reaction under the release of the enzyme and the product.

**Equation 3-7: $v = V_{max} \cdot [ATP] / (K_{M(ATP)} + [ATP])$**

$K_M$ is the Michaelis-Menten constant and $V_{max}$ the maximum rate of the reaction. $K_M$ is an equilibrium dissociation constant of the enzyme substrate complex and $V_{max}$ the rate of the reaction if the enzyme is totally saturated by the substrate. A special case for reactions following Michaelis-Menten kinetics is when $v = V_{max}/2$, then the substrate concentration is equal to $K_M$. Although the hydrolysis of ATP by myosin is a more complicated reaction it follows Michaelis-Menten kinetics. However then the constants $K_M$ and $V_{max}$ are more complex and include various rate constants of the previous steps. In the absence of actin the release of Pi has been proposed to be the rate limiting step. The catalytic activity under saturation with ATP can be described by the first order reaction rate $k_{ATP}$ which equals the maximum rate of the Michaelis-Menten reaction divided by the concentration of myosin heads: $k_{ATP} = V_{max} / [M]$. This so-called turnover number is the number of ATP molecules hydrolysed by a myosin head per second.

In the presence of actin the release of the hydrolysis products is greatly enhanced and the release of ADP from the cross bridge has been proposed to be the rate limiting step (Siemankowski et al., 1985). To enter into this fast actin activated cross bridge cycle the myosin nucleotide complex, which according to the biochemical model is M.ADP.Pi, has to form a collision complex with actin. The formation and dissociation of this complex forms a preceding equilibrium to the rest of the cross bridge cycle. Under a large excess of ATP the reaction is described by Scheme 3-5 and Equation 3-8 and also follows a typical Michaelis-Menten kinetic.

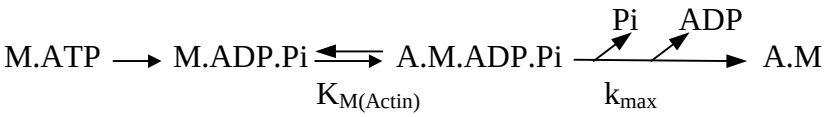


**Scheme 3-5:** Simplified reaction scheme of the actin activated ATPase function of myosin. (M=myosin, A = actin, Pi = phosphate, $K_M$ = Michaelis-Menten constant, $k_{max}$ = rate limiting step of the cross bridge cycle)

**Equation 3-8: $k_{ATP} = k_{max} \cdot [Actin] / (K_{M(Actin)} + [Actin])$**

The ATPase activity, $k_{ATP}$, is then determined by the kinetic parameters $k_{max}$ which is rate limiting for the cross bridge cycle and the Michaelis-Menten constant $K_{M(Actin)}$, which is a complex constant which heavily depends on the dissociation constant of the myosin.ADP.Pi complex and actin. At saturation levels of actin, [actin] >> $K_{M(Actin)}$, $k_{ATP}$ equals $k_{max}$. For most myosins however the affinity of the nucleotide.myosin complex for actin is low and therefore a direct measurement of $k_{max}$ by measuring the ATPase activity is difficult, because of the very high actin concentrations necessary for saturation. If the concentration of actin is much smaller than $K_{M(Actin)}$ Equation 3-8 be described by the simpler Equation 3-9.

**Equation 3-9: $k_{ATP} = (k_{max}/K_{M(Actin)}) \cdot [Actin]$**

Under these conditions the expression ($k_{max}/K_{M(Actin)}$) is a second order rate constant for the apparent binding to actin.

# 4 Materials and Methods

## *4.1 Chemicals*

All chemicals not specifically mentioned below were purchased from Sigma-Aldritch, BDH or Merck.

| | |
|---|---|
| Acrylodan | Mobitec, Germany |
| ATP | Boehringer Mannheim, Germany |
| ADP | Boehringer Mannheim, Germany |

## *4.2 Buffers and stock solutions*

### 4.2.1 Kinetic studies

Experimental buffer: 2 – 500 mM KCl
20 mM MOPS
5 mM $MgCl_2$
pH 7.0

The ionic strength of the buffer was varied for different experiments by varying the concentration of KCl. The pH of the buffer was adjusted to 7.0 by addition of KOH at 20 °C.

The small intrinsic fluorescence of the buffer components ensure minimal interference for measurements monitoring fluorescence changes of reactions.

Addition of 5 mM $MgCl_2$ provides $Mg^{2+}$ ions to build the Mg-nucleotide complex. Only in this complex can the nucleotide be bound by myosin. For flash photolysis experiments DTT was added to a final concentration of 10 mM to remove nitroacetophenone, a by-product of the photolytic reaction of cagedATP, from the solution.

### 4.2.2 SDS-PAGE

| | |
|---|---|
| Acrylamide solution: | 30% Acrylamide |
| | 0.8% N,N-methylenbisacrylamide |
| SDS solution: | 10% SDS |
| APS solution | 1.5% APS |
| Resolving gel buffer | 11.36 g Tris-HCl ad 50 ml $H_2O$; pH 8.8 |
| Stacking Gel buffer | 7.56 g Tris-HCl ad 50 ml $H_2O$; pH 6.8 |
| Sample buffer: | 2.5 ml stacking gel buffer |
| | 1 g SDS |
| | 2.5 ml 2-mercaptoethanol |
| | 5.8 ml glycerol |
| | 5 mg brome phenol blue |
| | ad 50 ml $H_2O$ |
| Running buffer: | 72.1 g glycerol |
| | 15.2 g Tris |
| | 5 g SDS |
| | ad 500 ml $H_2O$ |
| Coomassie solution | 5 g Coomassie G250 |
| | 0.5 g Coomassie R250 |
| | solved in 50 ml methanol |
| | ad 1 l $H_2O$; filtered |
| Staining solution: | 50 ml 0.55% Coomassie solution |
| | 100 ml acetic acid |
| | 250 ml isopropanol |
| | 600 ml $H_2O$ |
| Destaining solution: | 70 ml acetic acid |
| | 250 ml methanol |
| | ad 1 l $H_2O$ |

### 4.2.3 Buffers for protein preparation

The buffers for protein preparation are described together with the protein preparations themselves in section 4.4.

## *4.3 Hardware*

### 4.3.1 Flash photolysis apparatus

| | |
|---|---|
| Nd YAG Laser | Surelite I-10, Continuum, USA |
| Energy at 355 nm | 70 mJ |
| Pulse duration | 5 ns |

| | |
|---|---|
| Ruby Laser | QSR2/6, Lumonics LTD, Warwickshire, England |
| Energy at 347 nm | 300 mJ |
| Pulse duration of | 20ns |

| | |
|---|---|
| Cuvette (1.5 x 1.5 x 20 mm) | Hellma-Worldwide, Germany |
| Optical bench | Spindler & Hoyer, Germany |
| 100 W halogen lamp | Xenophot HLX 12V, OSRAM, Germany |
| 100 W Xe/Hg lamp | Hamamatsu Photonics, Japan |
| Xe/Hg lamp casing and power supply | A1020S, LPS0210-U, AMKO, Germany |
| Monochromator | Bausch and Lomb, USA |
| Filters | SCHOTT, Germany |
| Photomultipliers | R376, Hamamatsu Photonics, Japan |
| Digital oscilloscope | Lecroy 9310C, Lecroy, USA |
| Datacollection board GPIB | National Instruments, USA |
| Joulemeter | EM500, Molelectron, USA |
| Shuttersystem | JML Optical Industries, USA |

### 4.3.2 UV-spectrometer

| | |
|---|---|
| Cary 50 Bio | Varian, Germany |
| Quartz cuvettes | Varian, Germany |

### 4.3.3 Stopped flow

| | |
|---|---|
| Tech Scientific SF-61 DX2 | Hi-Tech Scientific, Salisbury, UK |
| Filters | SCHOTT, Germany |
| Water bath temperature control | K20, Haake, Germany |

### 4.3.4 FPLC/HPLC

| | |
|---|---|
| ÄKTA Basic 10 | amersham pharmacia biotech, Sweden |
| ODS-Hypersil column | Jones Chromatography, UK |
| Resource Q (1 ml) column | amersham pharmacia biotech, Sweden |

### 4.3.5 Other systems

| | |
|---|---|
| Centrifuges | Microcentrifuge, DenverInstrument, USA |
| | 5415C, Eppendorf; Germany |
| | J2-21, Beckman; USA |
| Ultracentrifuges | Optima MAX, Beckman, USA |
| Scales | AB104, Mettler, Switzerland |
| | PB302, Mettler, Switzerland |
| pH-meter | Hydrus 300, Orion Research, USA |
| Gel electrophoresis system | Mini Protean II, Biorad, USA |
| Microscope | SM2-2B, Nikon, Japan |
| Pipettes | Gilson, USA |

## *4.4 Protein preparation*

### 4.4.1 Rabbit muscle proteins

The proteins were prepared from freshly killed white New Zealand rabbits. Two rabbits were used in each preparation. Immediately after the slaughter the muscles from the back and the legs were dissected and kept on ice. The meat ( ~ 1 kg) was minced in a normal mincer and transferred into 3 l of Guba-Straub solution (0.3 M KCl, 0.1 M $KH_2PO_4$, 0.05 M $K_2HPO_4$, pH 6.6). The mix was stirred for 15 min and then centrifuged at 5000 rpm for 30 min. The supernatant was used for the myosin preparation and the pellet for the preparation of actin and control proteins.

### 4.4.2 Rabbit myosin preparation

The myosin preparation is based on Margossian and Lowey (1982). The supernatant from the rabbit protein preparation (4.4.1) was filtered through a 1 cm layer of homogenised Whatman paper (3 mm CHr). The remaining solution was transferred under stirring into 30 l of cold distilled water. A white aggregate formed and settled overnight. After careful removal of most of the water the remaining mix was centrifuged for 45 min at 5000 rpm and 4 °C.

The pellet was re-dissolved in 1 l 0.5 M KCl. For further purification the solution is transferred into 10 l of distilled water again where the aggregate forms overnight. The next day after removal of the water and centrifugation for 15 min at 12000 rpm and 4 °C the resulting pellet was re-dissolved in 500 ml of a high salt buffer (10 mM KPi, 1 mM DTT, 0.5 M KCl, pH 6.5). After mixing with 500 ml glycerol the myosin solution can be stored at –20 °C for at least 5 years.

For use in experiments 2 ml of this stock solution were dissolved in 50 ml of distilled water and centrifuged for 15 min at 12000 rpm at 4 °C. The pellet was re-dissolved in 3 ml 0.5 M KCl, then 50 ml of distilled water were added and the centrifugation step repeated. Then the pellet was dissolved in 3 ml of experimental buffer (500 mM KCl, 20 mM MOPS, 5 mM $MgCl_2$, pH 7.0)

#### *4.4.2.1 Preparation of S1*

About 10 g myosin was dissolved in 42 ml 3 M KCl. Then 10 ml 1 M KPi (pH 6.5), 10 ml 200 mM EDTA and 300 mg DTT were added. Water was added to a final volume of 1 l. Then 1 ml of 0.1 mg/ml Chymotrypsin was added. After 10 min of stirring the solution at room temperature the reaction was stopped with 0.85 mg PMSF in 5ml Ethanol. This solution was dialysed 12 h against 5 mM KPi pH 6.5 and then centrifuged at 12000 rpm and 4°C for 1 h. The concentration of S1 in the solution was determined to be 100-200 mg/g myosin on average.

The supernatant was loaded on a DEAE-Sephacel column (17 cm, 2.5 cm), which was washed with 100 ml 50 mM Imidazol pH 7.0 and the protein was eluted. 15 ml fractions were collected while monitoring the protein concentration by the absorbance at 280 nm. Two peaks were observed belonging to 2 isoforms differing in the content of the light chains. The fractions with high protein concentrations were dialysed against 10 mM KPi pH 7.5. The concentration was determined by UV spectroscopy. To store the S1 an equal amount of sucrose was added and the protein was freeze dried. In this state it can be stored for several months. For usage in experiment it was dissolved in the desired buffer and dialysed against 10 volumes of the same buffer to remove sucrose and phosphate. The S1 solution is stable at 4°C for several days.

#### *4.4.2.2 Fluorescein (IAF) labelled S1*

The preparation was performed according to Aguirre *et al*. (1986). S1 was labelled with 5-(iodoacetamido)fluorescein (IAF) in a buffer containing 60 mM KCl, 30 mM HEPES, 2 mM $MgCl_2$ pH 7.5. S1 and a solution of 1 mM IAF in DMF was mixed in a molar ratio of 6:5. The solution is stirred for 12 h in the absence of light and then centrifuged for 2 min at 1000 rpm. The supernatant is dialysed twice against 60 mM KCl, 30 mM HEPES, 0.5 mM DTT, 2 mM $MgCl_2$ pH 7.5.

The concentration can be determined from the absorbance at 496 nm ($\varepsilon_{496}$=7.7 $M^{-1}m^{-1}$) in a buffer containing 5 M Urea, 60 mM KCl, 30 mM HEPES, 2 mM $MgCl_2$ pH 7.5.

### 4.4.3 Actin preparation

#### *4.4.3.1 Acetone powder*

The pellet from section 4.4.1 was stirred into 5 l of buffer containing 4 % $NaHCO_3$ and 0.1 mM $CaCl_2$ and left stirring for 30 min at 4°C. The mix is filtered through cotton cloth and the residue stirred into 1 l of buffer containing 10 mM $NaHCO_3$. 10 mM $Na_2CO_3$ and 0.1 mM $CaCl_2$ for 10 min at 4°C. Then 10 l of distilled water (20°C) were added and the mix filtered again through cotton cloth. The residue was stirred into 2.5 l acetone, filtered through cotton cloth and stirred into acetone again. The residue was dried out on Whatman paper in the fume cupboards for 2 days. The resulting powder was sifted through a mesh to remove unwanted tissue residues. The powder can be stored at –20°C for several months.

#### *4.4.3.2 Preparation of F-actin*

The preparation of F-actin is based on a method by Lehrer and Kerwar (1972). 5 g acetone powder (4.4.3.1) was stirred into 200 ml of 0°C cold buffer (10 mM Tris, 0.5 mM ATP, .2 mM $CaCl_2$, 1 mM DTT pH 8.0). After 30 min of stirring on ice the mix was filtered through cotton cloth under vacuum. The residue can be used to prepare the control proteins troponin and tropomyosin. The filtrate was centrifuged at 30000 rpm and 4°C for 1h. To polymerise the actin 3 M KCl and 1 M $MgCl_2$ were added to the supernatant to give a final concentration of 100 mM KCl and 2 mM $MgCl_2$. After 1 h of stirring the solution is centrifuged for 3 h at 30000 rpm and 4°C. The pellet of filamentous actin is picked up in depolymerising buffer (5 mM Tris, 0.2 mM $CaCl_2$, 0.2 ATP, 1 mM $NaN_3$, pH 7.5) and homogenised in a homogeniser. The solution is dialysed overnight against depolymerising buffer and centrifuged for 1 h at 8000 rpm and 4°C. The actin concentration of the supernatant is determined by UV-spectroscopy then depolymerising buffer is added to a final actin concentration of 1 mg/ml. 3 M KCl and 1 M $MgCl_2$ were added to a final concentration of 100 mM KCl and 2 mM $MgCl_2$ to polymerise the actin again after 1 h of stirring. After this step the actin can be labelled with a fluorescent dye as described in sections 4.4.3.3 and 4.4.3.4. To obtain unlabelled actin the solution was centrifuged at 30000 rpm and 4°C for 3 h. The pellet is taken up in the appropriate experimental buffer (2 – 500 mM KCl, 20 mM MOPS, 5 mM $MgCl_2$, pH 7.0), homogenised and dialysed overnight against the same buffer. Addition of 0.5 mM DTT and $NaN_3$ prevents oxidation of the sulfhydryl groups and possible growth of bacteria. The final concentration of actin should be approximately 100-200 µM. The F-actin can be stored in this form for at least 2 weeks at 4°C.

#### *4.4.3.3 Pyrene labelled actin*

The preparation of pyrene actin is based on a method by Criddle *et al*. (1985). N-(1-pyrenyl)iodoacetamide (pyrene) (5 mg/ml solved in DMF) was added stepwise with stirring to a solution of 1 mg/ml F-actin (see section 4.4.3.2) to a final concentration of 0.8 %. The solution was stirred overnight in the absence of light and then centrifuged for 1 h at 8000 rpm and 4°C to remove residual pyrene. The solution was centrifuged for 3h at 30000 rpm and 4°C. The pellet was taken up in the appropriate experimental buffer (2 – 500 mM KCl, 20 mM MOPS, 5 mM $MgCl_2$, pH 7.0), homogenised and dialysed overnight against the same buffer. Addition of 0.5 mM DTT and $NaN_3$ prevents oxidation of the sulfhydryl groups and possible growth of bacteria. The final concentration of actin should be approximately 100-200 µM and the efficiency of labelling 90-100 %.

#### *4.4.3.4 Acrylodan labelled actin*

Labelling actin with acrylodan (6-acrylodyl-2-dimethylaminonaphthalene, Molecular Probes, Leiden, Netherlands), a thiol reactive adduct of prodan (Prendergast et al., 1983) was based on a method of Marriott *et al*. (1988). A solution of fresh polymerised actin (1mg/ml) (see section 4.4.3.2) was used in a buffer containing 5mM Tris, 0.2 mM $CaCl_2$, 1 mM $NaN_3$, 100 mM KCl and 2 mM $MgCl_2$ at pH 7.5. 2 µl acrylodan label (25 mM in DMF) per ml of actin solution was added at a rate of 1 µl every 2 min. The reaction was left at 4°C for 3h. Residual label was removed by centrifugation at 10000 rpm. Actin was pelleted by centrifugation at 100000 rpm for 45 min and homogenised in a smaller volume of buffer containing 30 mM KCl, 20 mM MOPS, 2 mM $MgCl_2$ and 1mM $NaN_3$ at pH 7.0. The labelling ratio was determined by using the extinction coefficient for actin at 290 nm of $2.6 \cdot 10^4$ $M^{-1}cm^{-1}$ (Gordon et al., 1976) and for acrylodan at 375 nm of $1.85 \cdot 10^4$ $M^{-1}cm^{-1}$ (Weber and Farris, 1979). The protein concentration for the fluorescent conjugate was calculated after correction of the absorbance of acrylodan at 290 nm ($\varepsilon^{1\%}=1.85 \cdot 10^4$ $M^{-1}cm^{-1}$). Labelling ratios were 30 – 40 %.

#### *4.4.3.5 Phalloidin stabilised actin*

To keep actin in the filamentous form at concentrations of less than 1 µM, phalloidin is added to a 10 µM F-actin solution in an equimolar amount. The solution is incubated overnight at 4°C (Kurzawa and Geeves, 1996).

### 4.4.4 Rat proteins

#### *4.4.4.1 Myosin from bulk muscle preparations*

The Edl and soleus muscle from both legs of a freshly killed medium sized rat was dissected and weighed. After removing all connective tissue, ligaments and fat, the muscles were cut up finely and minced using a scalpel carefully avoiding contamination between the two muscle types. The minced muscles were transferred into cooled glass homogenisers (3-5ml) and 2ml of cooled Guba-Straub buffer (0.3 M KCl, 0.1 M $KH_2PO_4$, 0.05 M $K_2HPO_4$, pH 6.6) were added to each. After the mixture was thoroughly homogenised and left on ice for 30 min under occasional stirring, it was centrifuged at 5000 rpm for 10 min in 2ml eppendorf tubes. The supernatant was transferred to cooled 35ml centrifuge tubes and the tubes filled with cold distilled water. The myosin was precipitated and centrifuged for 15 min at 12000 rpm at 4 °C. The pellet was re-dissolved in 3 ml 0.5 M KCl, then cold distilled water was added filling the tubes and the centrifugation step repeated. Then the pellet was dissolved in 3 ml of experimental buffer (500 mM KCl, 20 mM MOPS, 5 mM $MgCl_2$, pH 7.0). The myosin could be stored at 4°C for several days.

#### *4.4.4.2 S1 from bulk muscle preparations*

The myosin pellet of the second precipitation step from bulk muscle preparation (see section 4.4.4.1) was dissolved in 5 ml of digestion buffer (125 mM KCl, 10 mM KPi, 2 mM EDTA, 2 mM DTT, pH 6.5). 0.1 mg/ml chymotrypsin was added and the mix incubated under stirring for 10 min at room temperature. The reaction was quenched by adding 0.5 mM PMSF (in ethanol). The solution was dialysed overnight against a low salt experimental buffer (30 mM KCl, 20 mM MOPS, 5 mM $MgCl_2$, pH 7.0). After centrifugation for 30 min at 12000 rpm and 4°C to remove myosin rods and undigested myosin the supernatant was ready for usage. It could be stored at 4°C for several days.

#### *4.4.4.3 Glycerol muscle preparation*

The Edl and soleus muscles from the legs of a freshly killed medium sized rat were dissected and tied to a toothpick. The construct was equilibrated for 6 h on ice in 25 ml of fibre preparation buffer (6 mM Imidazole, 8 mM Mg-acetate, 70mM propionate, 5 mM EGTA, 7 mM ATP, 1 mM Na-azide, pH 7.0) changing the buffer every 2 h. Then it equilibrated in fibre preparation buffer + 0,5 % Brij 58 for another 2 h skinning the fibres. For storage the

construct was transferred to fibre preparation buffer + 50 % glycerol equilibrated at 4°C over night and then stored at -18 °C.

#### *4.4.4.4 Myosin from single muscle fibres*

The myosin used in these measurements was extracted from 15 mm long single muscle fibres dissected from bundles of fresh soleus and psoas rat. The fibres were manually dissected, chemically skinned (according to Bottinelli et al., 1994a) and cut into two segments The smaller segment (ca. 2 mm) was dissolved in 20 µl Lämmli solution and used for MHC isoform identification by SDS-PAGE. Alternatively muscles from a glycerol muscle preparation can be used (see section 4.4.4.3).

The major part of the fibre (ca 13 mm)was incubated in 30 µl of myosin extraction buffer (100 mM $KH_2PO_4$: 50 mM $K_2HPO_4$; 0.3 M KCl) for 3h on ice after which the fibre was removed and discarded The myosin solution was dialysed twice in a microdialysis system developed with Dr J Sparrow (University of York) against 0.5 ml of experimental buffer containing 500 mM KCl, 20 mM MOPS and 5 mM $MgCl_2$ at pH 7.0 and used without further purification.

### 4.4.5 Myosin XIV from *Toxoplasma gondii*

Transgenic *T. gondii* parasites expressing the constructs pS•TgMyoAΔtail and pS•TgMyoA were used as a source of recombinant proteins (Hettmann et al., 2000). *T. gondii* tachyzoites were grown in Vero cells in tissue culture flasks.

TgMyoA was purified as described by Hettmann *et al*. (2000). Freshly lysed transgenic parasites were lysed under native conditions by freezing and thawing 3 times followed by sonification. In the case of full length TgMyoA sonification took place in a buffer with detergent (2 % Triton X-100, 4 mM ATP, 2 mM $MgCl_2$, 0.5 mM DTT, pH 7.6 and 1x of Complete protease inhibitor cocktail (Roche)). The sample was centrifuged at 65000 rpm and 4°C and the supernatant applied to a Ni-NTA resin column and eluted according to the manufacturer's instructions (QIAexpressionist) An average yield of 30 µg of TgMyoA and 250 µg of TgMyoA Δtail were obtained per gram of parasites. Active forms of TgMyoAΔtail and TgMyoA were further purified by co-precipitation with F-actin (Anson, 1992).

## *4.5 Preparation of cagedATP*

According to Walker *et al*. (1988)

### 4.5.1 Synthesis of 2-nitroacetophenone hydrazone (VII)

8.26 g 2-nitroacetophenone, 5.62 g hydrazine hydrate and 3.2 ml acetic acid were heated for 3h under reflux. Ethanol was distilled off under vacuum. The orange residue was washed with $CHCl_3/H_2O$ and the aqueous phase discarded. $CHCl_3$ was distilled off under vacuum. The product was collected from a high vacuum distillation at 140°C and 1.6 mbar.

### 4.5.2 Synthesis of 1(2-nitrophenyl)diazomethane (VII)

5 g 2-nitroacetophenone hydrazone (VII) were stirred for 5 min with 20 g $MnO_2$ in $CHCl_3$ in the dark at room temperature. After filtration the solution was washed with 0.1 M $NaHCO_3$. $MgSO_4$ was added and the solution filtered again.

### 4.5.3 Synthesis of Adenosine 5'-triphosphate (1-(2-nitrophenyl)ethyl ester)

ATP in 350 ml of an aqueous NaOH solution (pH 4) was added to the filtrate (see section 4.5.2) in an estimated molar ratio of 1:10 of the 1(2-nitrophenyl)diazomethane (VII) product. The solution was stirred vigorously for 20 h in the dark. The aqueous phase was separated and washed with $CHCl_3$. Residual CHCl3 was removed by distillation and the volume of the aqueous solution was reduced by distillation.

The product was purified by FPLC with a Pharmacia Q-sepharose fast flow column (40x3 cm). The product was eluted using a linear gradient of 50 mM – 0.5M of triethylammonium hydrogen carbonate over 3600 ml with a flow rate of 3 ml/min.

## *4.6 Methods*

### 4.6.1 Photometric Estimation of protein concentrations

Protein concentrations can be determined by measuring the absorbance of the solution at 280 nm. The aromatic amino acids Phe, Tyr and Trp absorb light of this wavelength. According to the law of Lambert-Beer: $A=\varepsilon \cdot c \cdot d$ the concentration (c) can be calculated in mol/l from the absorbance (A), the molar extinction coefficient (ε) and the length of the light path (d).

#### *4.6.1.1 Myosin*

The concentration was determined at 0.5 M KCl to ensure that myosin is completely dissolved. Because of the strong light scattering caused by myosin a base line correction for the linear increase of light scattering/absorbance with decreasing wavelength (270 nm – 400 nm) is necessary .

#### *4.6.1.2 S1*

The extinction coefficient for S1 is $\varepsilon^{1\%} = 7.9\ cm^{-1}$. The approximated molecular weight of S1 from myosin II is 115 kDa (Margossian and Lowey, 1982). Because of the strong light scattering caused by S1 a base line correction for the linear increase of light scattering/absorbance with decreasing wavelength (270 nm – 400 nm) is necessary.

#### *4.6.1.3 Actin*

The extinction coefficient of a 1% actin solution is $\varepsilon^{1\%} = 11.1\ cm^{-1}$ (West et al., 1967) The approximated molecular weight of monomeric G-actin is 42 kDa.

#### *4.6.1.4 Pyrene actin*

For the determination of pyrene actin concentration the absorbance of pyrene at 280 nm needs to be taken into account. Therefore the concentration of pyrene label is determined first with an extinction coefficient of $\varepsilon = 2.33 \cdot 10^4\ M^{-1}cm^{-1}$ at 344 nm. With the molar extinction coefficient for pyrene at 280 nm $\varepsilon = 2.33 \cdot 10^4\ M^{-1}cm^{-1}$ the absorbance of pyrene at this wavelength can be calculated. The concentration of actin can be determined as in section 4.6.1.3 from the absorbance at 280 nm which is equal to the total absorbance minus the pyrene absorbance at this wavelength. Labelling ratios were 70 – 100 %.

#### *4.6.1.5 Acrylodan actin*

The labelling ratio was determined by using the extinction coefficient for actin at 290 nm of $2.6 \cdot 10^4$ $M^{-1}cm^{-1}$ (Gordon et al., 1976) and for acrylodan at 375 nm of $1.85 \bullet 10^4$ $M^{-1}cm^{-1}$ (Weber and Farris, 1979). The protein concentration for the fluorescent conjugate was calculated after correction for the absorbance of acrylodan at 290 nm ($\varepsilon=1.85 \cdot 10^4$ $M^{-1}cm^{-1}$) similar to the procedure used for pyrene actin. Labelling ratios were 30 – 40 %.

#### *4.6.1.6 Nucleotides*

The absorbance of ADP or ATP nucleotides is measured at 259 nm. The extinction coefficient for both nucleotides is $\varepsilon = 1.54 \bullet 10^4$ $M^{-1}cm^{-1}$.

### 4.6.2 Bradford assay

To determine the protein concentration according to Bradford (1976) a calibration curve needs to be made by mixing the Bradford reagent with known concentrations of BSA (10 mg/ml = 6.6 $OD_{280}$) and the protein solution of unknown concentration. After 15 min the absorbance is measured at 595 nm. The protein concentration can be determined with the BSA calibration curve.

### 4.6.3 SDS-Page

#### *4.6.3.1 Standard SDS-PAGE*

To check the quality of proteins after purification and roughly estimate their concentration a standard gel electrophoresis with 12.5 % SDS-PAGE gels according to Laemmli (1970) was carried out using the MiniProtean II system (Biorad).

A freshly prepared resolving gel solution was poured in between 2 glass plates. A layer of isopropanole was added to obtain a smooth upper border. After polymerisation of the gel (10-15 min) isopropanol was removed and a freshly prepared stacking gel solution was poured on top of the resolving gel filling up the space between the glass plates. A comb was inserted to create pockets for the samples. It was carefully removed after the stacking gel polymerised. The gels were transferred to the electrophoresis chamber and covered with running buffer. Sample buffer was added to the samples in a 1:5 ratio. The samples were

denatured for 5 min at 95°C and inserted into the gel pockets. The electrophoresis was run for 45 min at 50 A after which the glass plates were removed from the gel and the gel transferred into staining solution for 1 h. To visualise the protein bands the gel was destained in destaining solution for 1h.

12.5 % resolving gel: 6.25 ml acrylamide solution
5.55 ml water
3 ml resolving gel buffer
150 µl SDS solution
15 µl TEMED
100 µl APS

4.8 ml stacking gel: 0.8 ml acrylamide solution
3.6 ml water
0.5 ml stacking gel buffer
50 µl SDS solution
10 µl TEMED
34 µl APS

#### *4.6.3.2 SDS-PAGE for identification of MHC isoforms*

A small segment of a dissected single muscle fibre (ca. 2 mm) was dissolved in 20 µl sample buffer and used for MHC isoform identification by SDS-PAGE on 8% polyacrylamide gels prepared according to Talmadge *et al*. (1993). Electrophoresis was run for 24h at 250 V. Gels were silver-stained.

### 4.6.4 Stopped flow

Enzymatic reactions usually take place on the millisecond time scale. A single cycle of acto.myosin interaction driven by the hydrolysis of one ATP molecule per myosin head can be completed in less than 50 ms. Those reactions are too fast to monitor transiently with conventional spectrometers or fluorimeters. The stopped flow apparatus is essentially a spectrometer/fluorimeter designed to monitor these fast reactions in a mixing chamber. Figure 4-1shows the schematic design of a stopped flow apparatus.

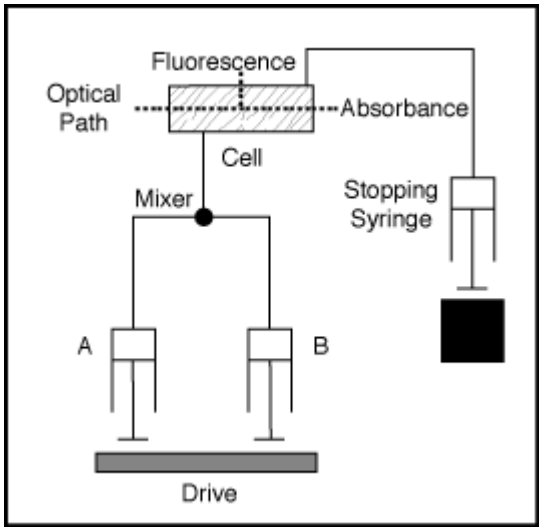


**Figure 4-1:** Schematic set up of a stopped flow apparatus (taken from http://www.hi-techsci.co.uk/scientific/stoppedflow.html)

Two syringes contain the reactant solutions. The flow into or from the syringes is controlled by 3 way Teflon valves allowing loading of the syringes or flow into the mixing chamber. Reactant solutions are pushed from the syringes into the mixing chamber by a pneumatic drive using air pressure. The flow continues from the mixing chamber to a stop syringe where the flow is stopped. This triggers the spectroscopic time resolved monitoring of the reaction in the mixing chamber. The apparatus can be set up for either absorbance measurements or fluorescence/light scattering measurements (see section 3.1).

For this work a Hi-Tech Scientific SF-61 DX2 stopped flow apparatus was used. The dead time of 1.5-2 s allows the measurement of rate constants of up to 500 $s^{-1}$. The system is temperature controlled using an external water bath.

The light from a 100 W Hg/Xe lamp illuminating the mixing chamber is selected to a single wavelength by a monochromator. Light scattering or fluorescence is measured at 90° from the incoming light by a photomultiplier. In the case of fluorescence, scattered light of the same wavelength as the excitation light is cut off by a filter allowing only the fluorescent light to pass. A 320 nm cut-off filter was used for trp fluorescence, a 389 nm cut-off filter for pyrene fluorescence and a 455 nm cut-off filter for acrylodan fluorescence. Light scattering measurements can be done at any wavelength (250 – 700 nm) with a high light intensity from the Xe/Hg lamp.

The signal is transferred to a data collection board of a PC, where the data is visualised and analysed by the KinetAsyst 2.0 software provided by Hi-Tech Scientific.

Each measurement needs about 80 µl of each of the 2 reactant solutions to achieve proper mixing. To improve the signal to noise ratio at least 3 consistent measurements were taken and averaged for each reaction. The data of the first shot of a series of measurements of the same reaction was discarded due to possible contamination of mixing chamber and tubing with the previous reaction mix. Depending on the reactions the system was washed with buffer in between series of measurements for the same reason.

### 4.6.5 FPLC/HPLC

#### *4.6.5.1 ATP turnover reaction*

The ATP turnover reaction for a defined concentration of protein was measured by assaying the ATP/ADP ratio as a function of incubation time using HPLC analysis. 50 µl samples in experimental buffer with 30 mM KCl were quenched at various times by the addition of 50 µl 6.25 % TCA. The sample was centrifuged for 10 min at 12000 rpm to remove precipitated protein. The 80 µl of supernatant was neutralised with 4 µl 1M NaOH and diluted 10 fold with running buffer. 100 µl of sample were applied to an ODS-Hypersil column and analysed using an isocratic flow of 125 mM KPi pH 5.5 at a flow rate of 1 ml/min over 15 ml.

#### *4.6.5.2 Analysis of nucleotides used in flash photolysis*

40µl ethanol were added to 20 µl of sample used in flash photolysis. After centrifugation for 3 min at 14000 rpm to remove precipitated protein the sample was diluted in 500 µl of 10 mM KPi, pH 8. 100 µl of sample were applied to a ResourceQ column and analysed using a linear gradient of 10 mM KPi pH 8 to 50 mM KPi, 250 mM NaCl pH 8 at a flow rate of 1 ml/min over 12 ml.

#### *4.6.5.3 FPLC/HPLC data analysis*

An elution profile was recorded for each run measuring the absorbance at 254 nm. Different nucleotides were eluted from the column at different times. Integration of the peak areas of the elution profile gave a measure of the relative amounts of nucleotides in the sample. By comparison of the peak areas of the elution profiles with those of a calibration curve, measured with samples of known nucleotide concentration, the amounts of nucleotides in the sample could be determined.

# 5 A flash photolysis apparatus for measuring transient kinetics of sub microgram quantities of acto.myosin

## *5.1 Introduction*

The interaction of myosin with actin forms the molecular basis of muscle contraction and of motility of non-muscle myosin motors. A single cycle of interaction is driven by the hydrolysis of one ATP molecule per myosin head and can be completed in less than 50 ms. To understand the chemomechanical coupling of ATP hydrolysis and motor activity requires methods of studying the dynamic interaction of actin and myosin (or its subfragments) on the millisecond time scale. Traditional fast reaction methods (stopped flow or quenched flow) using purified solutions of proteins have required relatively large amounts of material. This was not a serious limitation when the proteins could be obtained in relatively pure form from the large vertebrate skeletal muscles. These methods have made major contributions to the elucidation of the molecular basis of motor function (Taylor, 1979; Trentham et al., 1976; Geeves, 1991). However in many instances the quantity of material required has proven a serious limitation and the development of methods which can use smaller quantities will have wide uses. Firstly myosin isoforms expressed in mammalian muscle can often only be purified in very small amounts. In the ideal case the proteins isolated from a single muscle fibre characterised mechanically and for isoform content should be analysed (see section 6.3.2; Canepari et al., 1999). Protein amounts extracted from single fibres are too small to be measured by stopped flow while they would be sufficient for flash photolysis measurements. Secondly, most members of the recently discovered myosin superfamily are only available in very small amounts and remain to be fully characterised (Cope *et al*., 1996). Detailed mechanistic analysis of the members of the myosin family will complement site directed mutagenesis of specific myosins for the understanding of the structure-function relationships in myosins. However a highly efficient expression system does not exist for most myosins and the amounts available remain low. Thirdly, the *Drosophila* system is an attractive system for correlating structure and function in muscle myosins but again the quantities available are limited to µg of material. For these reasons we have been investigating fast reaction methods which use smaller quantities of protein than the traditional fast reaction methods.

The use of fluorescently labelled actin (or myosin subfragment 1, S1) which has been stabilised by phalloidin allows the interaction of actin, S1 and ATP to be studied at acto.S1 concentrations of less than 50 nM (Kurzawa and Geeves, 1996). This allows many studies to

be made with a few μg of protein in commercially available stopped flow equipment. Further reductions in concentration cannot be achieved simply without significant loss of signal sensitivity. The amounts of material used in the stopped flow is dictated by the need for relatively large volumes (2 x 80 μl per shot) to ensure adequate rapid mixing of the two solutions and efficient washout of samples between shots. Specialist equipment has been built which can use smaller volumes but the speed of the apparatus or optical efficiency is usually compromised (Eccleston et al., 1993).

In this work the use of flash photolysis of an inert precursor of ATP to initiate the dissociation of acto.S1 and acto.myosin and the subsequent ATP turnover reaction was investigated as first described by Walker *et al*. (1988). Using a sample volume of 10 μl and highly efficient usage of sample by multiflash experiments a significant amount of information on the properties of the system can be obtained using less than 100 ng of actin or S1 and less than 250 ng of myosin. Therefore, measurements of myosin extracted from single mammalian fibres are possible. Indeed one of the key findings was that much of the information can be obtained using light scattering signals, removing the necessity to fluorescently label one of the proteins used.

### 5.2 The experimental set-up of the flash photolysis apparatus

This thesis is based on data which was collected on two flash photolysis systems. The first system was designed and built by Dr. Chizhov at the MPI for molecular physiology in Dortmund. The bulk of the results on the properties of the flash photolysis apparatus presented in this chapter were obtained from this first system. Various improvements to the system have been made by Dr. Chizhov and myself and based on this experience a second very similar system was designed and built with Dr. Chizhov for my continued work at the University of Kent. The flash photolysis results for the rat and human skeletal myosin isoforms, the myosin XIV TgM-A and kinesin were collected on the second system. The experimental set-up of the first system is described here followed by the changes made for the second system.

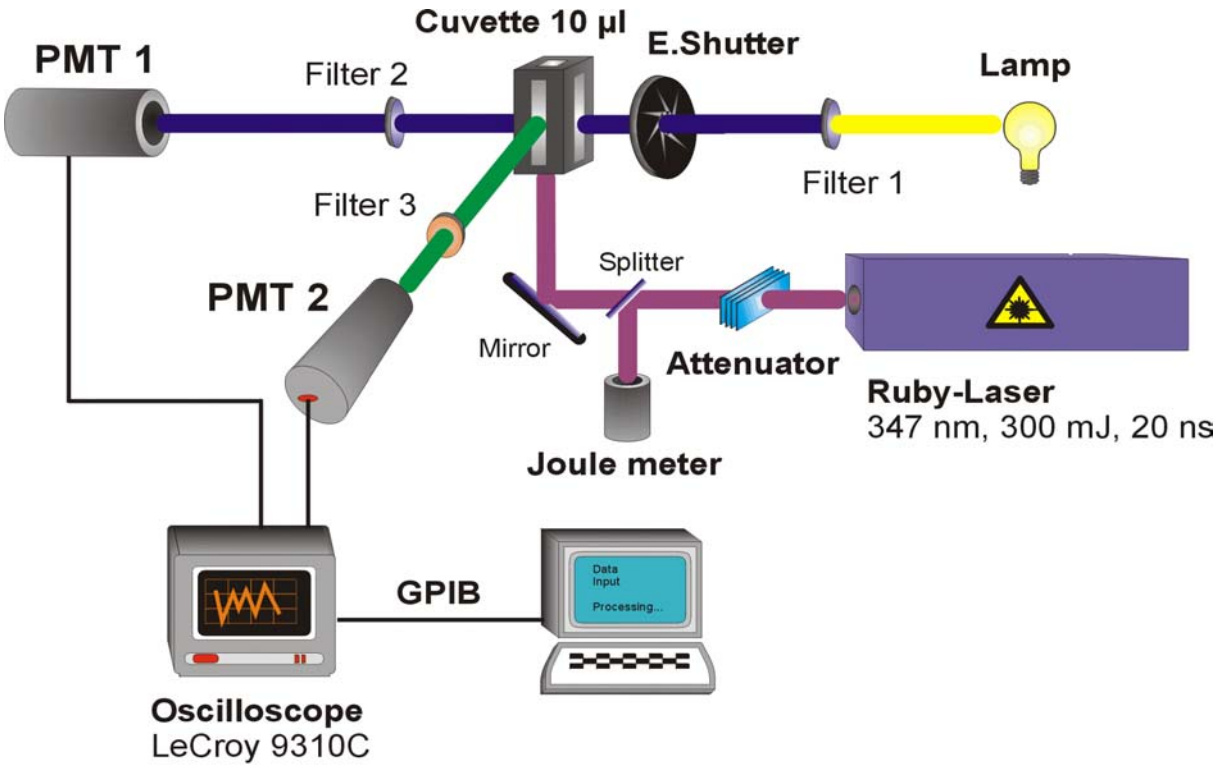


**Figure 5-1:** Schematic set-up of the flash laser photolysis system. The sample is held in a quartz cuvette and requires a minimal sample volume of 10 µl. A ruby laser is used to release the cATP into the solution. The optical bench allows simultaneous time resolved detection of transmission changes and of fluorescence or light scattering changes in the cuvette using a single monitoring light source and two photomultipliers, one in line with the excitation beam (PMT1) and the other at 90° (PMT2). The figure shows the set-up of the first system. Changes to the set-up for the second system at the University of Kent are described in the text.

Figure 5-1 shows the experimental set-up of the flash photolysis apparatus. The quartz cuvette (1.5 x 1.5 x 20 mm ) in the core of the optical system operates with a minimal sample volume

of 10 µl. A Ruby Laser (QSR2/6, Lumonics LTD, Warwickshire, England) with a wavelength of 347 nm, a beam diameter of 6 mm, a pulse duration of 20 ns, a pulse energy of up to 300 mJ and a maximum repetition rate of 0.1 Hz provides the source of the photolysis light for the release of ATP from the caged compound. The beam was focussed on the bottom window of the cuvette (ca. 2 mm diameter) with a quartz lens (F = 50 mm). Matching the beam diameter to the size of the cuvette is very important, too small a beam diameter produces inhomogeneous illumination and ATP release. This can result in non exponential curves for the transients. Too large a beam diameter decreases the efficiency of the photolysis and can increase the reflection and scattering of the laser beam from the cuvette surfaces, which can then overload the photomultipliers during the flash. The optical bench was designed for simultaneous time resolved detection of transmission changes and either fluorescence or light scattering changes. For detection of light scattering changes a 100 W halogen lamp (Xenophot HLX 12V, OSRAM, Germany) was used. The sample was exposed to white light of wavelengths > 389 nm (KV 389 filter, SCHOTT, Germany, at position 1 of Figure 5-1 to prevent photolysis of cATP by light of shorter wavelength) and transmission changes were recorded at 405 nm via a monochromator (Bausch&Lomb, Rochester, NY) at position 2. Light scattering changes were monitored via a photomultiplier (R376, Hamamatsu Photonics, Japan) at 90° to the incident light. To collect the maximal scattered light a glass rod with reflecting walls (diameter: ca. 5 mm, length: ca. 5 cm) was attached between the side wall of the cuvette and the photomultiplier. No release of cATP by the monitoring light was detected using the halogen lamp (4.8 mW at cuvette).

For detection of transmission at 405 nm and acrylodan fluorescence a 100 W Xe/Hg-lamp (L2422-02, Hamamatsu Photonics, Japan) was used with a 405 nm interference filter (SCHOTT, Germany) in position 1 and a 455 nm cut-off filter in position 3. In fluorescence mode the electronic shutter was only opened during the time of data collection to prevent release of cATP by light from the Xe/Hg-lamp.

The detection electronics include two photomultipliers, a digital oscilloscope (LeCroy 9310C, LeCroy, Chestnut Ridge, NY) connected to a PC by a GPIB interface. 50,000 data points were collected per transient, then compressed to 560 data points on quasi logarithmic time scale for computer analysis (Chizhov et al., 1996).

The operation of the flash photolysis apparatus, data collection and transfer from the oscilloscope to the PC was driven by program written in C++ by Dr. Chizhov. Analysis and presentation of flash photolysis data were carried out with Microcal Origin 4.1.

In the second system a Nd-YAG Laser (Surelite I-10, Continuum, USA) with a pulse energy of 70 mJ at a wavelength of 355 nm, a pulse duration of 5 ns and a beam diameter of 6 mm was used. The monitoring light was projected onto the cuvette through a light guide (Hi-Tech Scientific, UK) instead of using direct optics. Transmission changes were recorded through a 405 nm interference filter (SCHOTT, Germany) in position 2 by a photodiode. In fluorescence mode the wavelength of the light source (100 W Xe/Hg-lamp, L2422-02, Hamamatsu Photonics, Japan) was limited by a monochromator (Bausch&Lomb, Rochester, NY) in position 1. The flash photolysis data was analysed and presented with Microcal Origin 6.0 Professional.

### *5.3 General sample preparation*

Standard samples were made up to a final volume of 200 µl of which 20 µl were added to the cuvette. An example of such a standard sample from the stock solutions is:

| | |
|---|---|
| 1 µM S1 | e.g. 2 µl of a 100 µM S1 stock solution |
| 1 µM actin | 20 µl of a 10 µM actin/phalloidin stock solution |
| ca. 0.5 mM cATP | 10 µl of a ca. 10 mM cATP stock solution |
| 10 mM DTT | 2 µl of a 1 M DTT stock solution |
| Optional: | |
| 10 µg/ml apyrase | 2µl of a 1 mg/ml apyrase stock solution |
| or | |
| 0.03 u/µl hexakinase | 6 µl of a 1unit/µl hexakinase stock solution |
| 1 mM glucose | 2 µl of a 100 mM glucose stock solution |
| 100 µM Ap5A | 2 µl of a 1 mM Ap5A stock solution |

The sample was made up to a final volume of 200 µl by addition of experimental buffer (100 mM KCl, 20 mM MOPS and 5 mM $MgCl_2$, pH 7.0). If myosin was used instead of S1 an experimental buffer of higher ionic strength was needed (500 mM KCl, 20 mM MOPS and 5 mM $MgCl_2$ at pH 7.0) because myosin with the long C-terminal α-helical tail tends to aggregate at lower salt concentrations. The concentration of the cATP stock solution was estimated and varies slightly from batch to batch. DTT was added in excess to remove the breakdown product of the cATP after photolysis. Apyrase could be added to speed up hydrolysis of ATP and to remove ADP. Hexakinase in conjunction with glucose also hydrolyses ATP quickly but without breakdown of ADP. The nucleotide analogue Ap5A is an

inhibitor of myokinase which often contaminates myosin samples and converts ADP to ATP and AMP.

The set-up of flash photolysis apparatus is currently capable of working with a minimal sample volume of 10 µl. However working with 20 µl sample was often preferred. It improved the loading of the sample to the cuvette and the precision of working with small volumes in sample preparation.

For myosins which were only available in small amounts and small concentrations the sample was prepared in a different way to minimise the loss of protein. A sample mix was prepared containing 4 times the concentrations of all components except myosin compared to the desired concentration for the sample used in the experiment. 5 µl of this sample mix were added to 15 µl of myosin sample to make up a final sample volume of 20 µl.

Before loading the sample into the cuvette it was centrifuged in a table top centrifuge at 5000 rpm for 1 min. This procedure removed small air bubbles or microparticles from the sample which might interfere with light scattering measurements.

The sample itself was loaded to the cuvette with a pipette using microtips (Greiner, Germany).

Between experiments the cuvette was washed, first with ethanol and then several times with water using a dental brush. The removal of particles and residual proteins from the inner cuvette walls is important because it prevents the formation of air bubbles during the loading of the cuvette.

Sample and washing solution were removed from the cuvette with microtips and tubing connected to a vacuum pump.

## 5.4 The photochemical reaction

The cATP was prepared by selective alkylation of ATP with 1(2-nitrophenyl)ethyl ester as described by Walker *et al*. (1988) (see section 4.5).

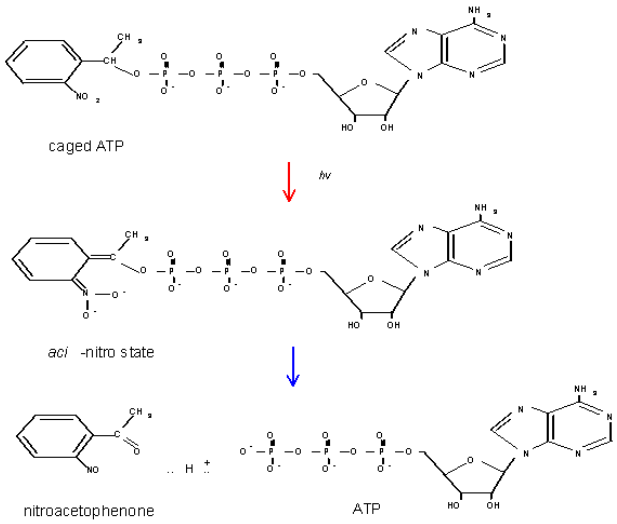


**Figure 5-2:** The photochemical reaction.

A flash of laser UV light was used to excite the cATP and the formation of the exited aci-nitro state, on a very fast time scale (≤ µs), results in an increased absorbance at 405 nm ($\varepsilon$=9.1*$10^3$ $M^{-1}cm^{-1}$; Walker *et al*., 1988). As shown in Figure 5-2 the aci-nitro state decays to free ATP and nitroacetophenone in a proton catalysed reaction at a rate of 1.25 • $10^9$ • $[H^+]$ $s^{-1}$ giving a $k_{obs}$ at pH 7.0 of about 125 $s^{-1}$. The rate of release of ATP is also dependent on the $Mg^{+2}$ concentration, which stabilises the aci-nitro intermediate and therefore slows down the rate of ATP release. The chemically reactive and water insoluble breakdown product 2-nitroacetophenone is removed from the solution by a large excess of the hydrophilic thiol DTT. Figure 5-3 shows the time scale of the formation and decay of the aci-nitro intermediate from the absorbance changes at 405 nm.

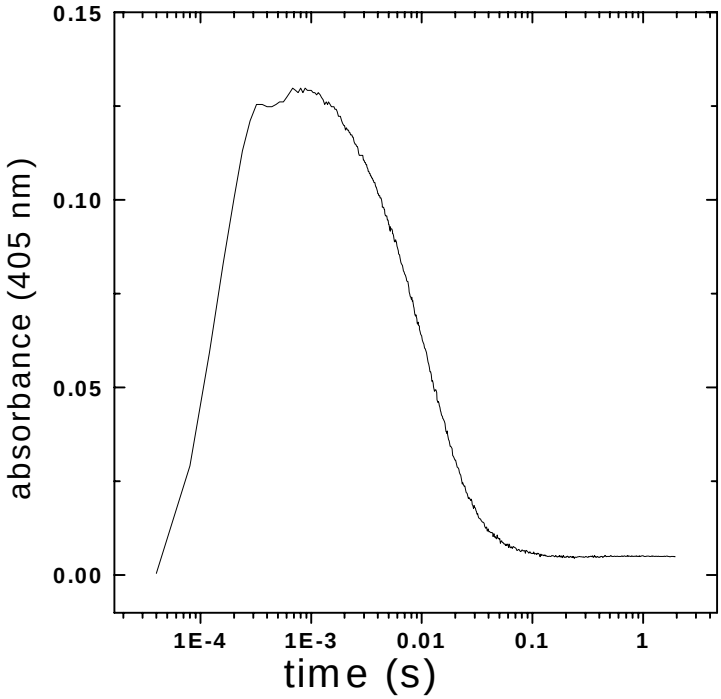


**Figure 5-3:** Monitoring the formation and decay of the aci-nitro intermediate in the photochemical reaction of release of ATP from cATP by monitoring the absorbance at 405 nm. The formation of the intermediate happens on a very fast time scale (≤ µs) and is therefore not well resolved.

## *5.5 Monitoring ATP release*

The amount of ATP released per laser flash is simply characterised in situ by measuring the amplitude of the 405 nm absorbance changes, which monitors the formation and decay of the aci-nitro intermediate. This gives a direct measure of the amount of cATP broken down in each flash and an example is shown in Figure 5-4A. The concentration in µM of ATP released can be calculated according to Lambert-Beer: $c = A \cdot 10^6/(\varepsilon \cdot d) = A \cdot 733$. The absorbance (A) is equal to the amplitude of the absorbance change at 405 nm, the extinction coefficient (ε) of the intermediate at 405 nm is $9.1*10^3$ $M^{-1}cm^{-1}$, the path length of the cuvette (d) is 0.15 cm.

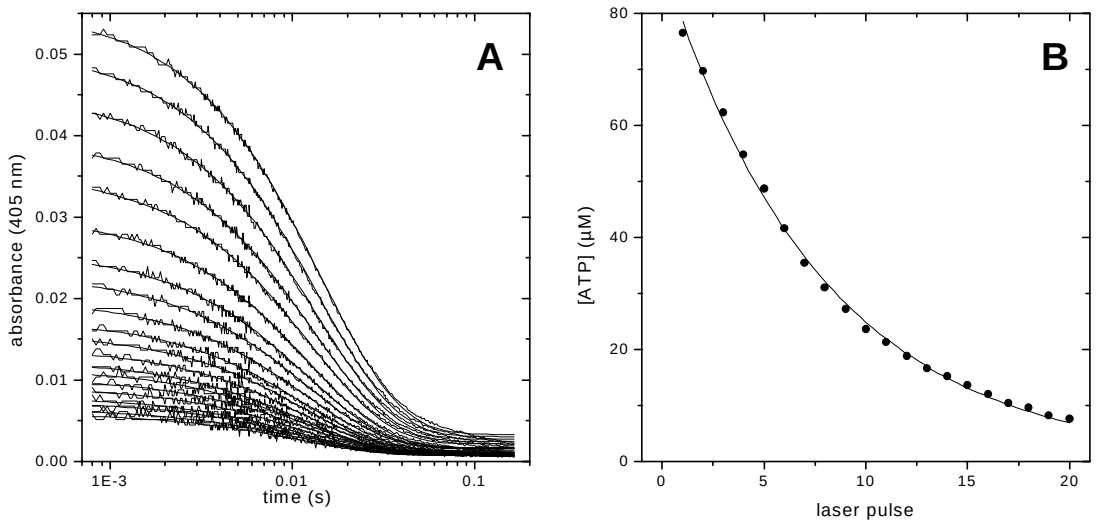


**Figure 5-4:** Calibration of the amount of ATP released from cATP by monitoring the absorbance change of the decay of the aci-nitro intermediate at 405 nm.

A) The sample (20 µl) containing 1 mM cATP solution was irradiated by series of 20 consecutive laser pulses (ca 15 mJ) and the absorbance changes at 405 nm were monitored. The best fit to a single exponential decay of the absorbance decrease is shown superimposed with $k_{obs}$ = 90 $s^{-1}$ in each case.

B) The dependence of the fitted amplitude of the aci-nitro decay reaction on the flash number is shown fitted to a single exponential function. The fitted parameters give the amount of cATP released per flash as 13% of the cATP present at the constant level of flash illumination.

The sample (10 µl) containing about 1 mM cATP was irradiated by a series of 20 identical laser pulses (ca 15 mJ) and the absorbance changes at 405 nm were monitored. The experiment was carried out in standard experimental buffer containing 100 mM KCl, 20 mM MOPS and 5 mM $MgCl_2$ at pH 7.0 and at 22°C. The formation of the aci-nitro intermediate ($k > 10^5$ $s^{-1}$) was too fast to follow completely within our time resolution but the decay was well resolved. The best fit of a single exponential to the decay curve showed the rate of decay to be identical in each case (90 $s^{-1}$). The rate constant is therefore smaller than the 125 $s^{-1}$ reported by Walker *et al*. (measured in absence of $Mg^{2+}$), but the value is in agreement with their observation that the rate of the decay decreases in presence of $Mg^{2+}$.

The amplitude of the reaction declined with each subsequent flash. For a constant laser intensity the amount of ATP released is expected to be directly proportional to the amount of cATP present in solution at the time of the flash. The overall concentration of cATP decreases in each flash by an amount equal to the ATP released. Therefore in a series of identical laser flashes the amplitude should follow an exponential decay law as shown in Figure 5-4B. The fit of an exponential function to the data gave the efficiency of photolysis as 13% of the cATP present for this particular laser energy (15 mJ). This means that the first flash produced a free ATP concentration of 77 µM and the 20th flash released a further 7.5 µM. This indicates that the initial concentration of cATP was 590 µM. The actual initial concentration of cATP can

vary depending on the batch of the stock solution used. The amount of ATP released from a specific concentration of cATP is dependent on the intensity of the laser flash with higher intensities releasing more ATP. Use of flash intensities above 25 mJ were not used because the energy can be absorbed by micro-particles or air bubbles in the sample solution causing the formation, growth and bursting of further micro air bubbles which disturb the measurement. At a flash intensity of 25 mJ approximately 120 µM ATP are released from 1 mM cATP.

The amount of ATP released per flash was calibrated using HPLC analysis of the solution. In this experiment the peak area of a sample of known ATP concentration was compared to a flash photolysis sample after one flash for which the ATP concentration was calculated as described above. While this calibration was in agreement with the calculated amounts of ATP of the first flash photolysis system, for the second flash photolysis system the amounts of ATP released were calculated to be about 2 times lower than the actual amounts of ATP determined by HPLC (Figure 5-5). This result was observed both in light scattering and fluorescence mode of the flash photolysis. In fluorescence mode the incoming light was limited to a wavelength of 405 nm by a monochromator in position 1. This indicated that the 2 fold difference was not due to the replacement of a filter in place of a monochromator in position 2. Considering that the light intensities (measured by an optometer; model 268R, UDTinstruments, Baltimore, USA) reaching the photodiode and recording the absorbance changes are different in light scattering (2 µW) and fluorescence (10,5 µW) mode, while the change by a factor of about 2 is evident with little difference for both modes, the problem is most likely to be software related rather than a result of using a photodiode instead of a photomultiplier. For all of the following results obtained with the second flash photolysis system a correction factor of 1.76 was applied to the amounts of ATP calculated from the absorbance changes. This correction factor was confirmed in various HPLC experiments over a wide range of ATP concentrations released for both modes of the flash photolysis system.

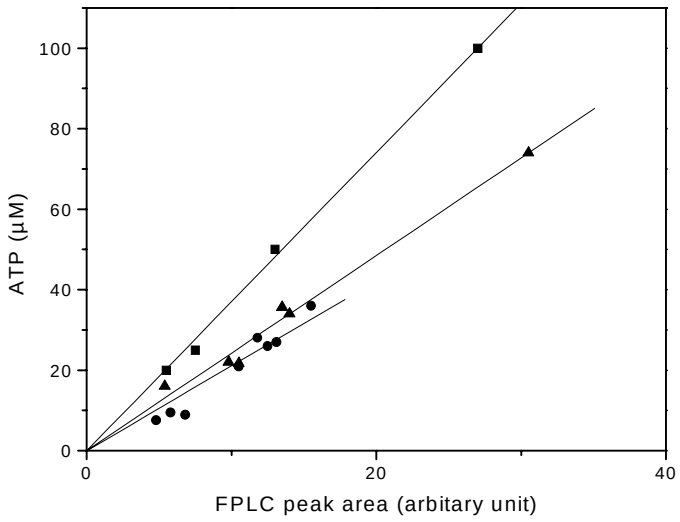


**Figure 5-5:** Calibration of ATP content of flash photolysis samples by HPLC. The figure shows a plot of various known ATP concentrations vs. the corresponding peak area of the ATP peak from HPLC experiments with 20 µl samples (■). It also shows plots of calculated ATP concentrations of 20 µl flash photolysis samples from light scattering (●) and fluorescence (▲) experiments vs. the corresponding ATP peak areas of these samples in HPLC experiments. A linear fit is superimposed in each case giving a slope of 3.7 µM/area, 2.1 µM/area and 2.4 µM/area for the known ATP concentrations, ATP concentrations calculated from a light scattering experiments and ATP concentrations calculated from a fluorescence experiments respectively. This indicated that a correction factor of 1.76 needed to be applied.

## *5.6 ATP induced dissociation of acto.myosin*

Binding of ATP to the myosin causes fast and irreversible dissociation of the acto.myosin or acto.S1 complex and the complex is restored after all of the ATP is hydrolysed. In the following measurements acto.S1 of rabbit skeletal muscle is used as an example to illustrate the capabilities of the system unless stated otherwise. The dissociation of the acto.S1 complex after laser induced release of ATP from cATP was monitored by changes in light scattering as shown in Figure 5-6. The decrease in light scattering can report the kinetics of the dissociation reaction as the undecorated actin filament and the single myosin molecule scatter light far less than a myosin-decorated actin filament. The light scattering signal is therefore a direct measure of the amount of actin and myosin associated at any given time. The samples (20 µl) containing 1 µM rabbit S1, 1 µM actin and 0.5 mM cATP were irradiated by a series of laser pulses of different intensities which released a range of ATP concentrations. The absorbance at 405 nm was monitored simultaneously with the scattering signal to define the amount of ATP released in each flash.

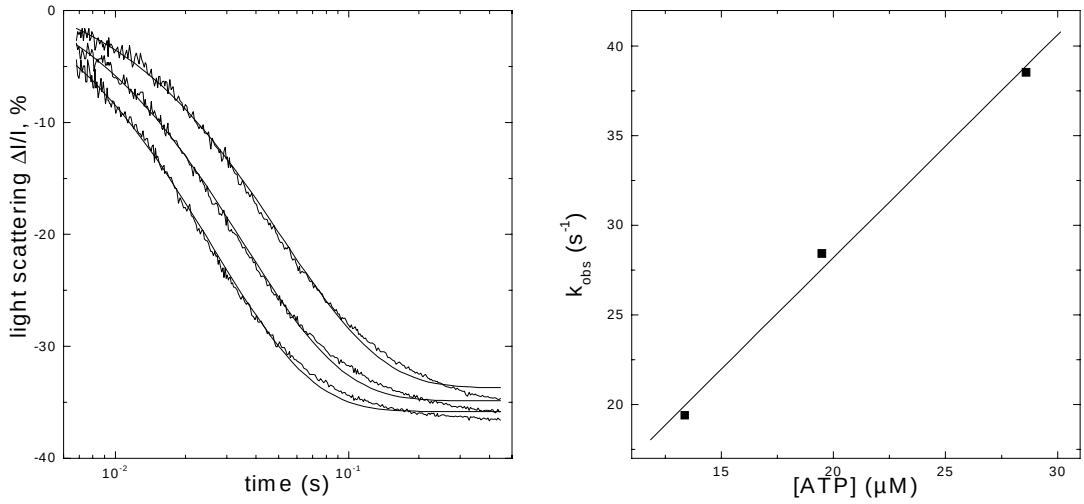


**Figure 5-6:** ATP induced dissociation of acto.S1
A) Light scattering changes 1μM rabbit actin and 1 μM rabbit S1 after laser induced release of different amounts of ATP from cATP. The best fit to a single exponential decay of the light scattering decrease is shown superimposed.
B) A plot of $k_{obs}$ vs. [ATP] for the dissociation reaction. Best fit to a straight line gives a slope of $1.2 \pm 0.1$ $\mu M^{-1}s^{-1}$ and an intercept of $3.3 \pm 2.2$ $s^{-1}$.
Other conditions: buffer 100 mM KCl, 20 mM MOPS, , 5 mM $MgCl_2$, 10 mM DTT, 0.5 mM cATP, pH 7.0.

At ATP concentrations much larger than the protein concentrations the dissociation of acto.myosin is a pseudo first order reaction in which the concentration of the ATP remains approximately constant. The decrease in scattering can therefore be described by a single exponential. The best fit to a single exponential gives the observed rate constant ($k_{obs}$) of each reaction. In the case of rabbit skeletal S1, $k_{obs}$ shows a linear dependency upon the concentration of ATP up to rate constants of 60 $s^{-1}$ (Figure 5-6). For faster reactions measuring the kinetics of the reaction is compromised by the kinetics of cATP release and a different fitting procedure must be used as explained in section 5.12. The slope of the plot of $k_{obs}$ vs. [ATP] defined the apparent second order rate constant of the ATP induced dissociation reaction, $K_1k_{+2} = 1.3 \pm 0.2$ $s^{-1}\mu M^{-1}$ (see Equation 3-4 and Scheme 3-2). Stopped flow experiments proved that the presence of 1 mM cATP slowed down the $k_{obs}$ by less than 5% due to the competition of cATP with ATP for the nucleotide binding site. Flash photolysis transients usually fit less well to single exponentials compared to transients from stopped flow experiments. Two effects contribute to this behaviour. Firstly the release of cATP throughout the sample is not totally homogenous which causes a diffusion effect. This effect can be greatly reduced by aligning the laser beam properly to the cuvette. The focus should be underneath the centre of the cuvette producing a beam which fits the dimensions of the

cuvette to illuminate the sample as homogenously as possible. Too large a beam diameter decreases the efficiency of the photolysis and can increase the reflection and scattering of the laser beam from the cuvette surfaces. Secondly, due to the absence of turbulence in the system, cross-linking of filaments may occur due to the gelation of the proteins. Breakage of the cross linking due to either the laser flash or the acto.myosin dissociation reaction changes the light scattering signal and shows as either a second reaction kinetic or might influence the dissociation reaction directly. This effect is more commonly observed with the larger myosin than with S1 and varies with each protein preparation. It is also more common at high protein concentrations (>2 µM) or the large excess of one protein over the other. The bulk of the results including better and worse fits to single exponentials shows that these deviations in most cases have no significant effect on the result of $k_{obs}$.

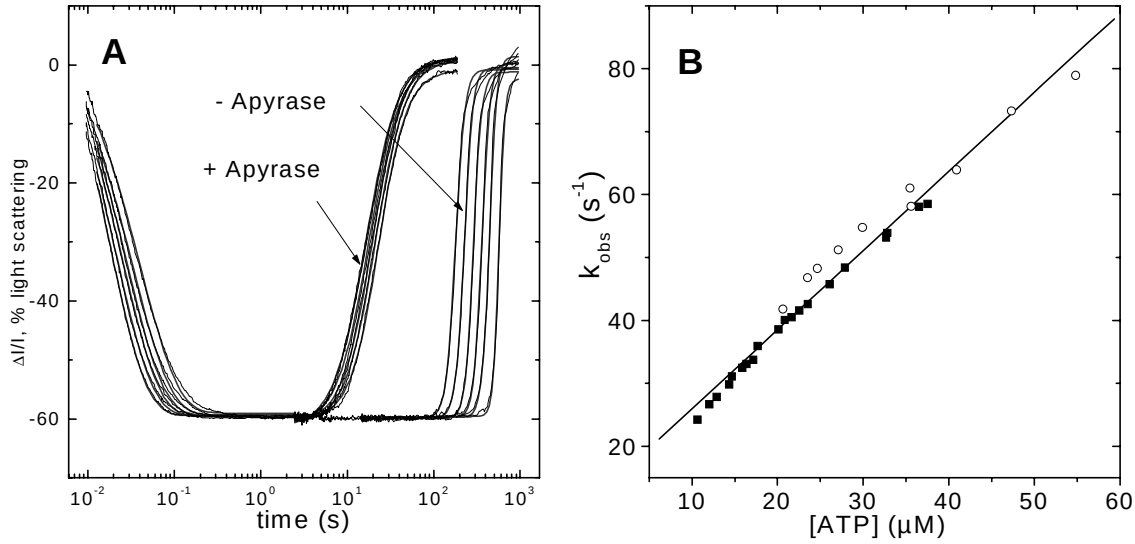


**Figure 5-7:** Dissociation and re-association of acto.S1 after ATP release and hydrolysis.
A) Light scattering signals from two 10 µl samples of 1 µM actin and 1 µM S1 with 0.5 mM cATP in multiple flash photolysis measurements one with and one without 10 µg/ml apyrase. The best fit to a single exponential decay of the light scattering decrease is shown superimposed.
B) A plot of $k_{obs}$ vs. [ATP] for the light scattering decay reaction. Best fit to a straight line gives a slope of 1.3 ± 0.2 $\mu M^{-1}s^{-1}$. (○ = without apyrase; ■ = with apyrase)

The experiment was performed with two different protocols. In one a fresh sample was used for each transient i.e. the sample was exposed to only a single laser flash. A greater efficiency of sample usage is possible if, after the release of ATP, the sample is left to hydrolyse all of the ATP and the actin and myosin re-associate before the next flash is used to reinitiate the reaction. In this case after the fast dissociation of actin and myosin the reaction enters a steady-state phase of up to ten minutes under the condition described above and at 60 µM ATP. During the steady-state phase the ATP is hydrolysed showing a constantly low light

scattering signal while the overall amount of ATP is high enough for actin and myosin not to re-associate. This is followed by a phase during which ATP is still hydrolysed but the concentrations are low enough for the acto.myosin to re-associate eventually reaching the point where no ATP is left in solution, all of the acto.myosin is re-associated and the light scattering signal therefore reaches its initial level.

Identical results for $k_{obs}$ were obtained using the two protocols and the second approach was used in Figure 5-7. This suggests that the activity of the proteins is not affected by the laser flash at the intensities used. This is expected since the absorbance of proteins at the wavelength of the laser (355 or 365 nm) is low. The result furthermore suggests that the products of both the photochemical breakdown and the ATPase reaction do not interfere with the measurements. This is not surprising in the case of Pi where the affinity is very low (>1 mM). It also shows that the breakdown product is efficiently removed by the excess of DTT. A decrease in the observed rate constant due to the presence of ADP however is expected. For this particular experiment using the fast type rabbit skeletal S1 the affinity of ADP for acto.S1 is relatively weak (100-200 μM) so the inhibitory effect would be large only after several flashes. For slower type myosins with a higher affinity for ADP a stronger effect is expected. This effect can be avoided all together by adding the enzyme apyrase which quickly removes both ATP and ADP by hydrolysis to AMP and Pi. This not only eliminates the effect of ADP but also allows for more rapid data collection for the dissociation reaction due to the increased steady-state rate of removal of ATP. With the addition of 10 μg/ml apyrase about 60 μM free ATP is completely removed in less than 2 minutes. In Figure 5-7 complete reaction profiles including re-association are shown for both cases, with and without apyrase, to make a direct comparison of the length of the steady-state phase possible. In the case of most experiments the dissociation reaction happens on a time scale during which the loss of ATP due to apyrase is not significant enough to influence the reaction. However when either the dissociation reaction is very slow or the amounts of ATP released are very low the removal of ATP by apyrase can be fast enough to influence the reaction. This is indicated by re-association of acto.myosin immediately after the dissociation without an apparent steady-state phase. This might lead to a loss of amplitude if re-association starts before the dissociation reaction is complete. In these cases the concentration of apyrase needs to be reduced accordingly.

### *5.7 Steady-state ATPase*

Analysis of the complete reaction profile including re-association gives information on the rate of the ATP induced dissociation reaction and the time taken to hydrolyse all of the ATP.

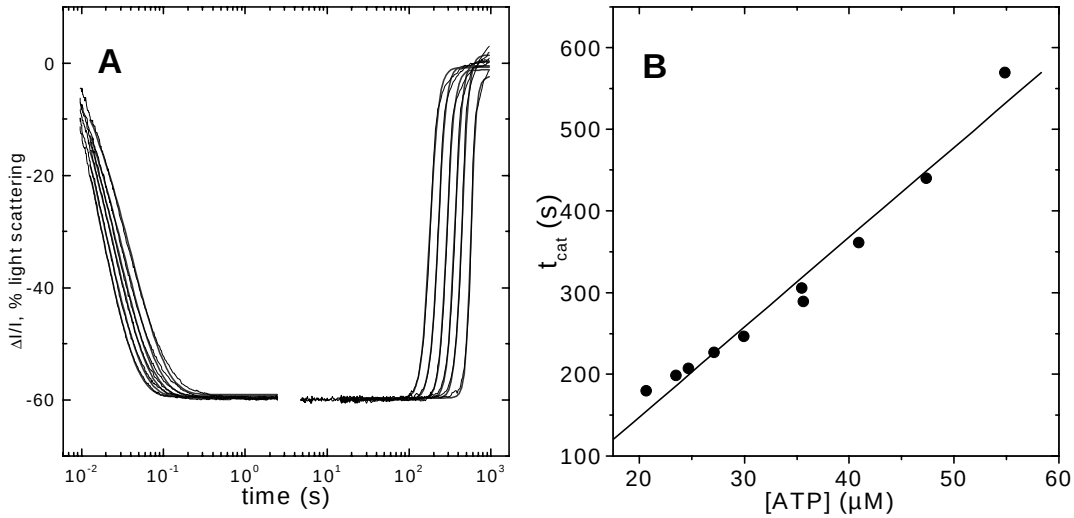


**Figure 5-8:** Estimation of the steady-state ATPase activity from the time taken by acto.myosin to hydrolyse ATP before re-association occurs.

A) Light scattering signals from two 10 µl samples of 1 µM actin and 1 µM S1 with 0.5 mM cATP in multiple flash photolysis measurements The best fit to a single exponential decay of the light scattering decrease is shown superimposed.

B) The time, $t_{cat}$, taken to hydrolyse all of the ATP thereby reforming acto.S1 is plotted against [ATP] The slope of the best-fit line was used to estimate the $k_{cat}$ =0.11 ± 0.01 $s^{-1}$ for the reaction.

The time taken to hydrolyse all of the ATP ($t_{cat}$) was estimated from the time at which the dissociation reaction was 50% complete ($t_{diss}$) to the time for 50% recovery of light scattering ($t_{ass}$). This time period ($t_{cat}$) was linearly dependent upon the amount of ATP released (Figure 5-8). The steady-state rate of ATP hydrolysis was estimated as follows, steady-state rate = $[ATP]/t_{cat}$ = 0.11 ± 0.01 µM $s^{-1}$. From the steady-state rate the catalytic activity can be calculated under consideration of the protein concentration as $k_{cat}$ = steady-state rate/[S1] = 0.11 ± 0.01 $s^{-1}$.

When trying to determine the steady-state ATPase it is essential to remove any residual apyrase from the cuvette as apyrase contributes to the fast removal of ATP. This is best accomplished by thoroughly cleaning the cuvette with ethanol and a small brush. This measurement ideally needs a signal amplitude of more than 10% and a very stable baseline. Especially in light scattering measurements, changes in the baseline can occur when micro air bubbles in the sample grow bigger or proteins crosslink. The changes in the baseline complicate finding the point where 50% of the complex is restored especially at small

amplitudes of dissociation. The point of 50% restored light scattering signal is used since it is the easiest to define in the re-association curve and the concentration of ATP dropped below the concentration of the acto.myosin complex. With concentrations of released ATP which are much larger than the concentration of the acto.myosin complex this indicates that most of the ATP has been hydrolysed.

In many cases myosin preparations are contaminated with the enzyme myokinase which converts ADP to ATP and AMP. The nucleotide analogue Ap5A (100 µM) which disables myokinase was therefore generally added for this experiment.

### *5.8 ADP affinity*

ADP competes with the ATP binding site on myosin but does not induce significant dissociation of the acto.S1 complex with the concentrations used. At the ATP concentrations used in our experiments (<50 µM) the overall rate of ATP induced dissociation of acto.S1 ($K_1k_{+2}$) is sufficiently slow for the binding and dissociation of ADP to be a preceding fast equilibrium with the constant $K_{AD}$ which inhibits the rate of ATP induced dissociation of acto.S1. This relation is expressed in Equation 3-5 according to Scheme 3-3. The competition between ADP and ATP can therefore be used to determine the affinity of ADP for the acto.myosin complex which is reciprocal to $K_{AD}$ (Siemankowski et al., 1985).

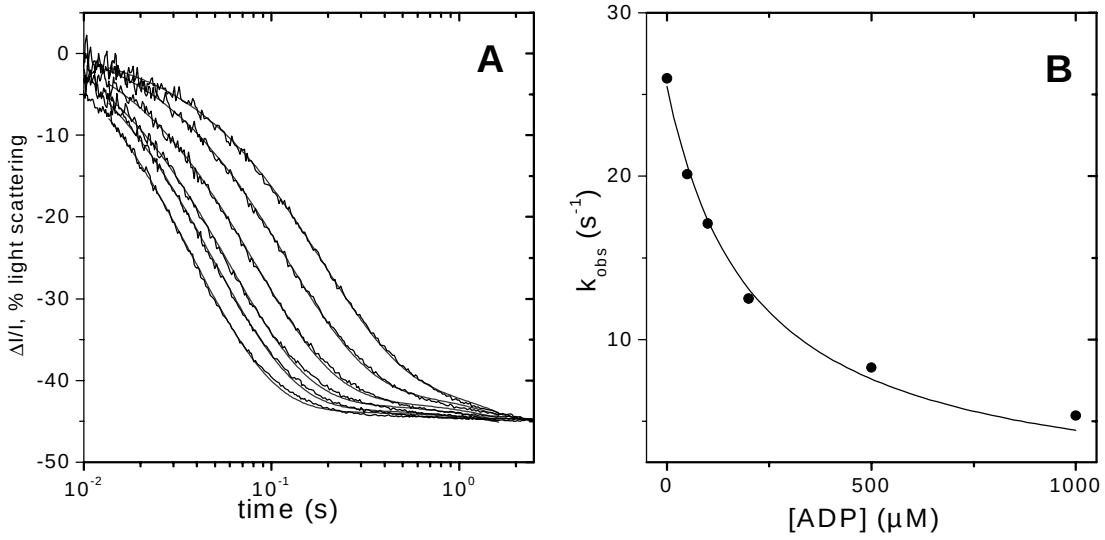


**Figure 5-9:** Determination of ADP affinity for acto.myosin
A) Light scattering signals from 6 samples of 1µM actin and 2 µM S1 with different concentrations of ADP following laser flash induced release of 25 µM free ATP were recorded. The best fit to a single exponential decay of the light scattering decrease is shown superimposed.
B) The plot shows the [ADP] dependence of $k_{obs}$. The data were fitted to the model of Scheme 3-3 and gave a value of $K_{AD}$=210 ± 20 µM.

The light scattering changes for samples containing identical amounts of cATP and other components differing only in the concentration of ADP were monitored after single laser flashes of constant intensity released the same amounts of ATP. The dissociation reaction appeared similar to that without ADP except that the observed rate constant was reduced with increasing concentrations of ADP. Figure 5-9A shows an example of six samples containing 1µM actin, 2µM S1 and different amounts of ADP. The light scattering changes were monitored after a single laser flash for each transient induced release of 25 µM ATP. The plot

of $k_{obs}$ vs. [ADP] was fitted to the Equation 3-5 (Figure 5-9B) and gave a value of $K_{AD}$=210 ± 20 µM. This value is in good agreement with that obtained by stopped flow measurements (Geeves et al., 1980).

To prevent conversion of ADP to ATP and AMP by myokinase contamination the use of the nucleotide analogue Ap5A (100 µM) which disables myokinase is recommended. In addition hexakinase (0.03 units/µl) in conjunction with glucose (1 mM) which removes ATP should be used for this experiment to avoid partial dissociation of acto.myosin by residual ATP.

Often the energy of the laser flash was not identical for each measurement of a series, and as a result, slightly different concentrations of ATP were released in each flash. The values for $k_{obs}$ of the series were corrected for a common value of ATP according to the linear dependency of $k_{obs}$ on the concentration of ATP (see Equation 3-4).

To achieve a more efficient sample usage in the case of limited protein availability a variation of the multi-flash experiment can be attempted. After the dissociation reaction and the hydrolysis of ATP the sample could be recovered from the cuvette. For this variation the use of hexakinase and glucose was essential to remove ATP quickly and effectively. A desired amount of additional ADP as well as cATP to make up for the loss of cATP from the previous flash and the volume change were added to the sample in a minimal volume (1-2 µl). The final ADP concentration for each measurement of the series was calculated by adding up the amount of ADP present at the beginning of the previous measurement, the amount of ADP generated by the hydrolysis of the ATP released in the previous measurement and the amount of ADP added. The sum was divided by the final volume. The sample was centrifuged and added to the cuvette again for the measurement.

### *5.9 Sensitivity of light scattering experiments*

The sensitivity of the optical methods was assessed by repeating the standard dissociation reaction at lower concentrations of protein. Using light scattering a sample containing 1 µM S1 and 1 µM actin gave a signal change of about 60% (Fig. 3A). The affinity of S1 for actin under the conditions used here is ca 50 nM (Kurzawa and Geeves, 1996). Therefore keeping the S1 concentration constant at 1 µM and decreasing the actin concentration is expected to result in a proportional decrease in the concentration of the acto.S1 complex. In Fig. 5A about 30 µM ATP was used to dissociate 0.2, 0.1 and 0.05 µM actin from 1 µM S1.

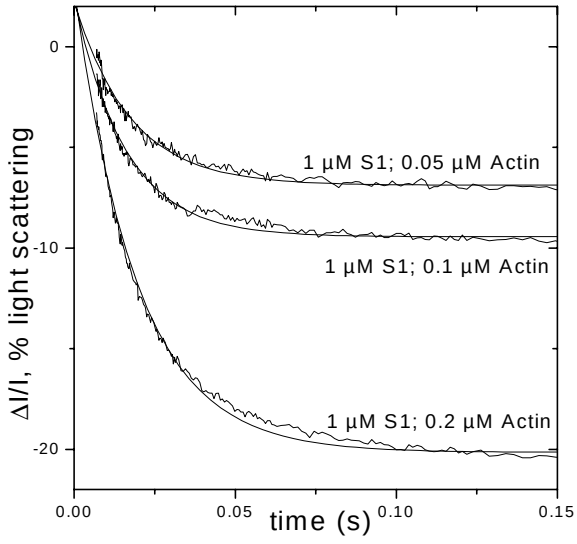


**Figure 5-10:** Sensitivity of flash photolysis measurements in light scattering mode
Light scattering signals from 3 samples with constant rabbit S1 concentration of 1 µM and decreasing actin concentration (0.2 µM, 0.1 µM, 0.05 µM) ([ATP]: ca. 20 µM)
The best fit to a single exponential decay of the light scattering decrease is shown superimposed. A loss of amplitude occurs on decrease of either actin or S1, but no change in $K_1k_{+2}$.

While the rate of dissociation was unchanged ($k_{obs} \approx 45\ s^{-1}$) the amplitudes of the light scattering signal changes were 20, 9.5 and 7 % (Figure 5-10). The decrease in amplitude is approximately proportional to the complex concentration as expected. With our current sensitivity 50 nM acto.S1 complex is the lowest concentration we can use to give a reasonable ratio of signal to noise with the noise being up to about 10 % of the signal amplitude. The measurement was repeated with constant actin concentration (1 µM) and varying S1 concentration but the presence of excess actin led to large scattering artefacts attributed to actin-actin aggregation/gelation.

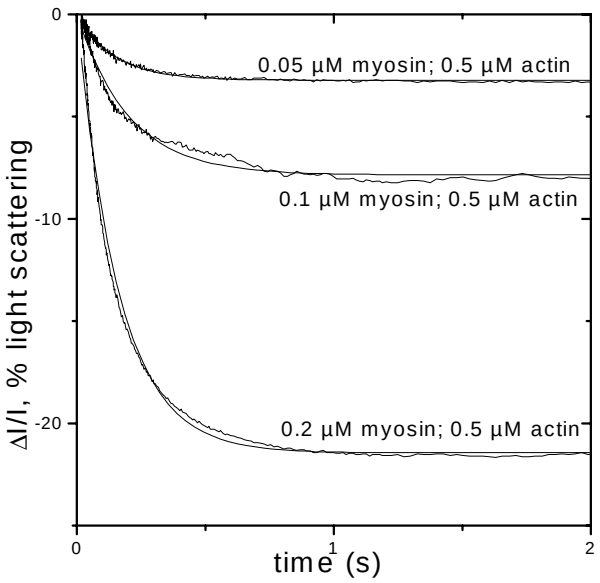


**Figure 5-11:** Sensitivity of flash photolysis measurements in light scattering mode
Light scattering signals after laser induced release of ATP (ca. 30 µM) from 3 samples with constant actin concentration of 0.5 µM and decreasing myosin concentration (0.2 µM, 0.1 µM, 0.05 µM).
The best fit to a single exponential decay of the light scattering decrease is shown superimposed. A loss of amplitude occurs on decrease of myosin, but no change in $K_1k_{+2}$.

Myosin can be used in place of S1 at higher ionic strength (0.5 M KCl) and under these conditions myosin has an affinity for actin of < 50 nM. In this case 20 µM ATP was used to dissociate 0.2, 0.1 and 0.05 µM myosin from 0.5 µM actin (Figure 5-11). This resulted in amplitudes of 21.5, 8 and 3 % with an invariant $k_{obs}$ of 7 $s^{-1}$. The acto.myosin complex had a stronger initial light scattering signal than the acto.S1 complex. Because of this overall improved signal to noise ratio the smaller amplitude of 3% could still be analysed. This suggests that for both, myosin and S1, the limit of resolution is at about 50 nM of the acto.myosin or acto.S1 complex.

### *5.10 Fluorescence experiments*

The presence of a fluorescent label on one of the two proteins could provide a way to increase the sensitivity of the measurement. Initial experiments evaluated the use of fluorescein labelled S1 (IAF-S1) and the pyrene labelled actin which is commonly used in stopped flow measurements. IAF fluorescence is exited at 436 nm and recorded above 530 nm. A fluorescence decrease of up to 25% was measured upon ATP induced dissociation of samples with 1µM actin and 1 µM IAF-S1. The average second order rate constant for the dissociation reaction was 1.3 $s^{-1}\mu M^{-1}$ and is in good agreement with light scattering measurements (Figure 5-12). The fluorescent label however was photobleached by the laser flash causing a decrease in amplitude for each measurement of a series in a multiflash experiment. The monitoring light (436 nm) did not release ATP from cATP.

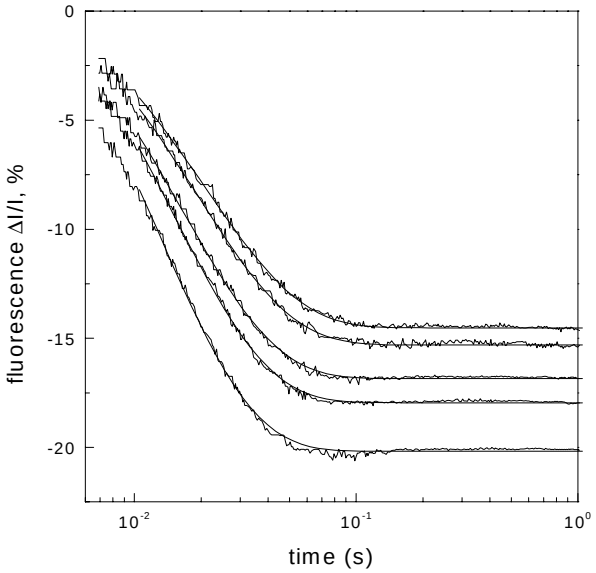


**Figure 5-12**: Measurements with fluorecein labelled S1
Fluorescence changes 1 µM rabbit actin and 2 µM fluorescein labelled rabbit S1 after laser induced release of different amounts of ATP from the cATP. The best fit to a single exponential decay of the fluorescence decrease is shown superimposed.
Other conditions: buffer 100 mM KCl, 20 mM MOPS, , 5 mM $MgCl_2$, 10 mM DTT, 0.5 mM cATP, pH 7.0.

In contrast pyrene labelled actin proved not suitable for fluorescence measurement in flash photolysis since the excitation wavelength (365 nm) is too close to the action spectrum of the cATP reaction. This has two consequences; firstly the fluorescence excitation light causes a constant background level of cATP breakdown. At a power output of 123 µW light of a

wavelength of 365 nm illuminating the cuvette released enough ATP from cATP within 5 seconds to completely dissociate the acto.myosin complex (Figure 5-13). Secondly, the laser flash can cause disruption of the fluorescence signal due to fluorescence bleaching.

Measurements of intrinsic fluorescence are not suitable for the flash photolysis system either since the energetic light at a wavelength of 295 nm releases ATP from cATP very quickly.

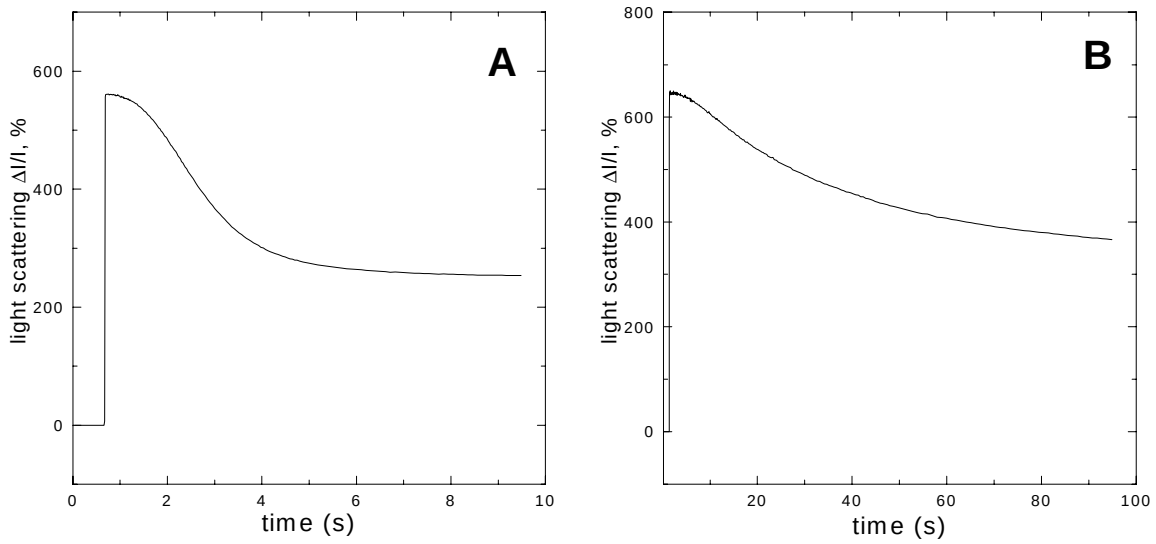


**Figure 5-13:** ATP release from cATP by energetic light. The light scattering changes of the dissociation of 1µM acto.myosin complex by ATP give an estimate of how fast the monitoring light of the Xe/Hg-lamp releases ATP from cATP. The sharp increase in light scattering marks the opening of the shutter for the monitoring light.

A) At a power output of 123 µW light of a wavelength of 365 nm illuminating the cuvette released enough ATP from cATP within 5 seconds to completely dissociate the acto.myosin complex.

B) At a power output of 67 µW light of a wavelength of 405 nm released enough ATP within 100 seconds to completely dissociate the acto.myosin complex.

Therefore the use of actin labelled at cys 374 with acrylodan (see section 4.4.3.4) was investigated which is excited at 405 nm and the excitation light produces little photolysis of cATP. At a power output of 67 µW light of a wavelength of 405 nm released enough ATP within 100 seconds to completely dissociate the acto.myosin complex (Figure 5-13). To prevent ATP release prior to the laser flash the electronic shutter was opened only during the time of data collection of the dissociation transient. When the shutter was opened shortly before or simultaneously with the laser flash the amount of ATP released by the monitoring light was insignificantly small compared to the release of ATP by the laser flash and did not influence the measurement.

In both stopped flow and flash photolysis measurements, dissociation of 1 µM actin and 2 µM S1 resulted in up to a 30 % increase in acrylodan fluorescence (Figure 5-14). The average second order rate constant for the dissociation reaction was 1.2 $s^{-1}\mu M^{-1}$. The label reduced the affinity of actin for S1 to ca. 180 nM limiting its usefulness (measured by N. Adamek within the group by stopped flow).

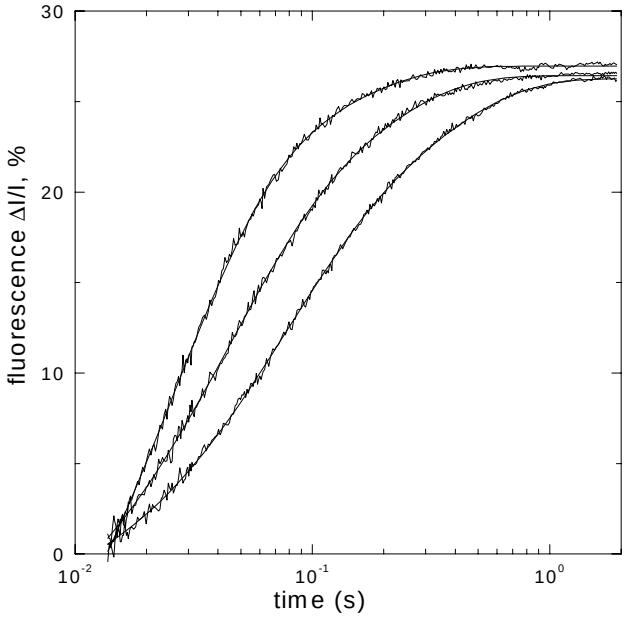


**Figure 5-14:** Measurements with acrylodan labelled actin
Fluorescence changes 1µM acrylodan labelled rabbit actin and 2 µM rabbit S1 after laser induced release of different amounts of ATP from the cATP. The best fit to a exponential association of the fluorescence increase is shown superimposed.
Other conditions: buffer 100 mM KCl, 20 mM MOPS, , 5 mM $MgCl_2$, 10 mM DTT, 0.5 mM cATP, pH 7.0.

### *5.11 Sensitivity of fluorescence experiments*

Since this work concentrates on measuring small amounts of myosin the sensitivity of fluorescence measurements with labelled actin is of interest. Reducing the S1 concentration from 2 µM to 0.8 µM at a constant acrylodan actin concentration of 0.1 µM results in a reduction in amplitude of the fluorescence change from 26% to 17% (Figure 5-15).

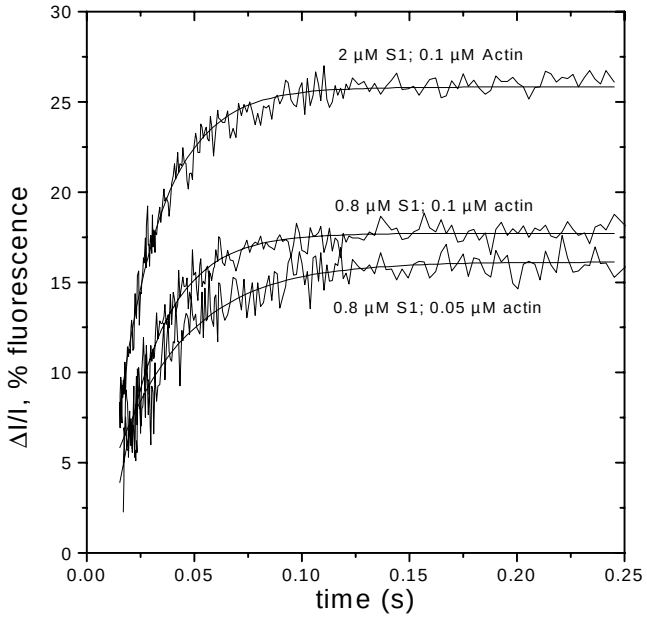


**Figure 5-15:** Sensitivity of flash photolysis measurements in fluorescence mode
Fluorescence signals from 2 samples with constant actin concentration of 0.1 µM and decreasing S1 concentrations (2 µM, 0.8 µM) and a sample containing 0.05 µM actin and 0.8 µM S1. (ATP: ca 70 µM) The best fit to a single exponential decay of the fluorescence increase is shown superimposed. A loss of amplitude occurs on decrease of either actin or S1, but no change in $K_1k_{+2}$.

Decreasing the acrylodan actin concentration from 0.1 µM to 0.05 µM at a fixed excess S1 concentration of 0.8 µM has almost no effect on the amplitude of the signal change, but the noise on the signal is increased at low concentrations of fluorophore (see Figure 5-15). However at 0.05 µM acrylodan actin concentration the signal amplitude drops further to 4% when reducing the S1 concentration to 0.2 µM (see Figure 5-16). This loss of amplitude is due to the low affinity of acrylodan actin for S1. A lower ionic strength can compensate for low affinities between the proteins allowing measurements at lower total protein concentration (see Figure 5-16). Measurements at lower ionic strength result in faster dissociation rates.

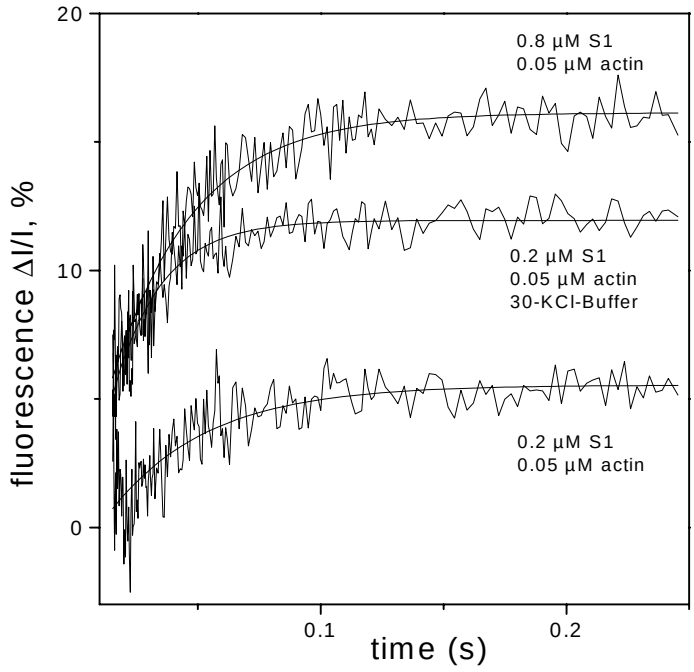


**Figure 5-16:** Increase of affinity of S1 and acrylodan actin at lower salt concentration
Fluorescence signals from 2 samples with constant actin concentration of 0.05 µM and decreasing S1 concentrations (0.8 µM, 0.2 µM) in an experimental buffer containing 100 mM KCl and a sample the same low protein concentration 0.05 µM actin and 0.2 µM S1 at a low salt experimental buffer containing 30 mM KCl. (ATP: ca 70 µM, other buffer conditions: 20 mM MOPS, 5 mM $MgCl_2$, pH 7.0)

The acrylodan actin can also be used with myosin and reducing myosin concentration from 0.3 µM to 0.075 µM at a constant concentration of acrylodan labelled actin of 0.5 µM results in an amplitude change from 17% to 3% (Figure 5-17). Note that amplitudes as low as 4% are sufficient to give data from which rate constants may be calculated. The changes in protein concentrations shown in Figure 5-17 leave the rate constants unchanged.

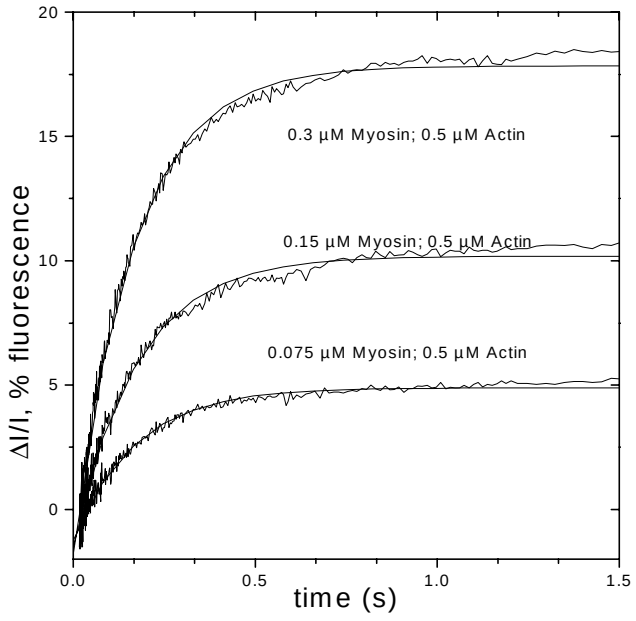


**Figure 5-17:** Sensitivity of flash photolysis measurements in fluorescence mode
Fluorescence signals of acrylodan labelled actin after laser induced release of ATP (ca. 80 µM ATP) from 3 samples with constant actin concentration of 0.5 µM and decreasing myosin concentration (0.3 µM, 0.15 µM, 0.075 µM).

In addition to the limit of signal sensitivity the use of low concentrations requires high photomultiplier sensitivity which emphasises the laser artefact and can decrease the time resolution for the measurements. Under the lowest concentrations of acrylodan actin used in Figure 5-15 the dead time was of the order of 15 ms.

## *5.12 Kinetic evaluation of the system*

The dead time of the flash photolysis apparatus is difficult to determine exactly. The rates of reactions which are possible to measure depend on how much the reaction is influenced by the rate of release of ATP from cATP. The release rate was generally $100 \pm 10\ s^{-1}$ in a buffer of 30-500 KCl, 20 mM MOPS, 5 mM KCl at pH 7.0 and was dependent on both the pH and the $Mg^{2+}$ concentration. In particular small changes in the pH can change the rate significantly. The ATP release rate needs to be much faster than the rate of the induced dissociation reaction or the kinetics of the dissociation reaction deviate from the single exponential decay describing a reaction of pseudo first order.

Simulations with the software KSIM 2.0 by Neil C. Millar were used to determine the error of single exponential fitting of acto.S1 dissociation reactions at various concentrations of released ATP.

The reaction scheme was as follows:

$$cATP \xrightarrow{k_r} ATP$$

$$ATP + A.M \xrightarrow{K_1 k_{+2}} ATP.M + A$$

The release rate of ATP ($k_r$)was set to a value at the lower error margin at 90 $s^{-1}$. The second order rate constant of acto.S1 dissociation was set according to stopped flow measurements to 2 $s^{-1}\mu M^{-1}$. The concentration of acto.myosin complex was set to 1 µM. The amount of ATP released was varied. The decrease of acto.myosin complex A.M was simulated which would correspond to the change of the light scattering of fluorescence signal in an actual experiment.

The release of ATP creates a lag phase at the beginning of the acto.myosin dissociation reaction. In flash photolysis experiments the lag phase is usually too short to be recorded. Even at high ATP concentrations (>80 µM) the simulated data could be fitted well with a single exponential if the initial lag phase was not included in the fit. However at these high ATP concentrations the rate determined by the exponential fit differed significantly from the simulated rate. At 80 µM ATP the simulated rate for the dissociation was 160 $s^{-1}$ while the rate of the fitted exponential was 120 $s^{-1}$. At lower ATP concentrations the simulation and the fit agreed better (see Figure 5-18). At ATP concentrations of 30 µM and lower, corresponding to reaction rate constants of up to 60 $s^{-1}$, the error of fitting the dissociation transients exponentially was then less than 15% (see Table 5-1).

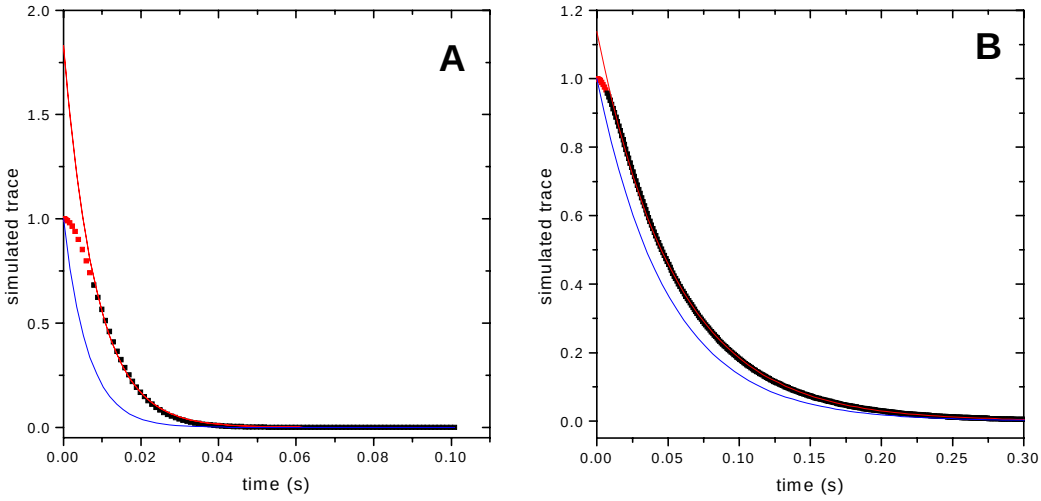


**Figure 5-18:** Simulation of thedecrease of acto.myosin complex in ATP induced dissociation reactions of acto.S1 after the release of 80 µM (A) and 10 µM (B) of ATP from cATP. The data of the simulated reaction is in black dots with the red dots being the lag phase which is not recorded in flash photolysis measurements. Two single exponential fits are superimposed, one fitting the entire reaction kinetic (blue) the other excluding the lag phase from the fit (red). The parameters used for the simulations are described in the text.

| [ATP] (µM) | $k_{sim}$ ($s^{-1}$) | $k_{fit}$ ($s^{-1}$) | Error (%) |
|---|---|---|---|
| 5 | 10 | 8.8 | 12 |
| 10 | 20 | 18.2 | 9 |
| 20 | 40 | 35.5 | 11 |
| 30 | 60 | 51.4 | 14 |
| 50 | 100 | 80.2 | 20 |
| 80 | 160 | 120 | 25 |

**Table 5-1:** Comparison of the rates constants of simulated acto.S1 dissociation reactions with rates of single exponential fits to the reaction kinetics.
The table shows the ATP concentration [ATP], the rate of the simulated dissociation reaction ($k_{sim}$), the rate of the single exponential fit to the reaction kinetic ($k_{fit}$) and the error of the rate of the fit compared to the simulated rate in percent.

The transients for the acto.myosin dissociation reaction recorded by the flash photolysis apparatus can also be fitted with the software program Scientist from MicroMath, USA (see section 10.2) using the full reaction kinetics including the ATP release reaction, the exact rate of which can be determined from monitoring the decay of the aci-nitro intermediate at 405 nm (see section 5.5). Figure 5-19 shows that a dissociation reaction, where 68 µM ATP were released at a rate of 98 $s^{-1}$, gave a $k_{obs}$ of 123 $s^{-1}$ calculated with this method which compares to a $k_{obs}$ of 89 $s^{-1}$ calculated from a single exponential fit. Using this fitting procedure values of $k_{obs}$ can be correctly determined which are more than double the rate of ATP release. Then the rate of the reaction which can be measured is more limited by the amount of ATP the system is able to release (see section 5.5) than by the speed of the reaction.

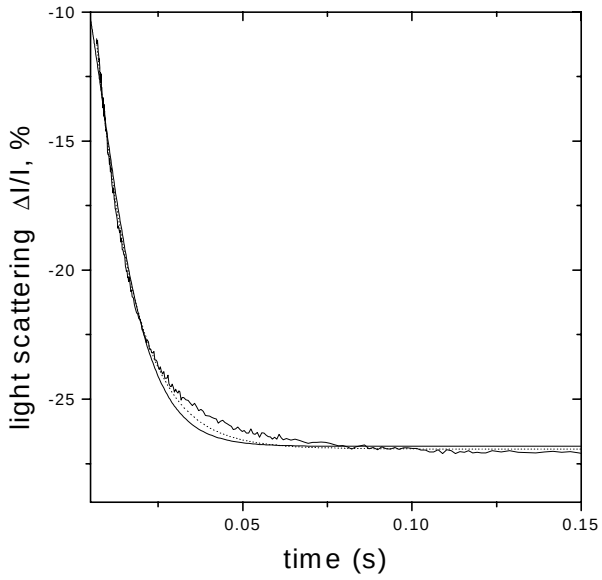


**Figure 5-19:** Comparison between a single exponential fit to a fast reaction transient of ATP induced acto.S1 dissociation to a fit using the correct kinetic model. According to the absorbance of the aci-nitro intermediate at 405 nm a concentration of 68.2 µM ATP has been released from cATP at a rate of 98 $s^{-1}$. A single exponential fit (solid) to the light scattering transient monitoring the ATP induced dissociation of acto.S1 gave an apparent rate constant, $k_{obs}$, of 88.7 $s^{-1}$. A fit with the program scientist (dotted) using the correct kinetic model for the entire reaction gave a $k_{obs}$ of 123 $s^{-1}$.

## *5.13 Experiments with the Kinesin-Microtubule system*

Though the flash photolysis apparatus was primarily designed to measure the reaction kinetics of actin and myosin in small amounts, it can potentially be used for measuring the reaction kinetics of other proteins which can be activated by a caged compound and can be monitored by spectroscopic changes. In the case of the kinesin.microtubule system the flash photolysis method seems to be better suited to perform light scattering measurements of reaction kinetics than the stopped flow system. Light scattering measurements with the kinesin.microtubule complex proved difficult with stopped flow because the large microtubule filaments produced major mixing artefacts (Ma and Taylor, 1997). In flash photolysis, in contrast, no turbulence is induced in the sample, hence no mixing artefacts occur. A range of experiments with kinesins and microtubule were performed in collaboration with Dr. Rob Cross' lab at the Marie-Curie Institute, Oxted, UK (Rogers et al., 2001). Proteins were provided by Dr. Kevin Rogers and Dr. Isabelle Crevel. Both ATP and ADP (using cADP) induced dissociation of the kinesin.microtubule complex resulted in a decrease in light scattering which could be monitored by the flash photolysis system.

The samples (20 µl) were irradiated by a series of laser pulses of different intensities which released a range of ATP or ADP concentrations in multiflash experiments with apyrase

(see Figure 5-20 for an example of ADP induced dissociation). The light scattering transients of the kinesin.microtubule dissociation could be fitted by single exponentials indicating a pseudo first order reaction. Because the large microtubule filaments created a strong light scattering background the reaction amplitudes were smaller than for similar concentrations of acto.myosin.

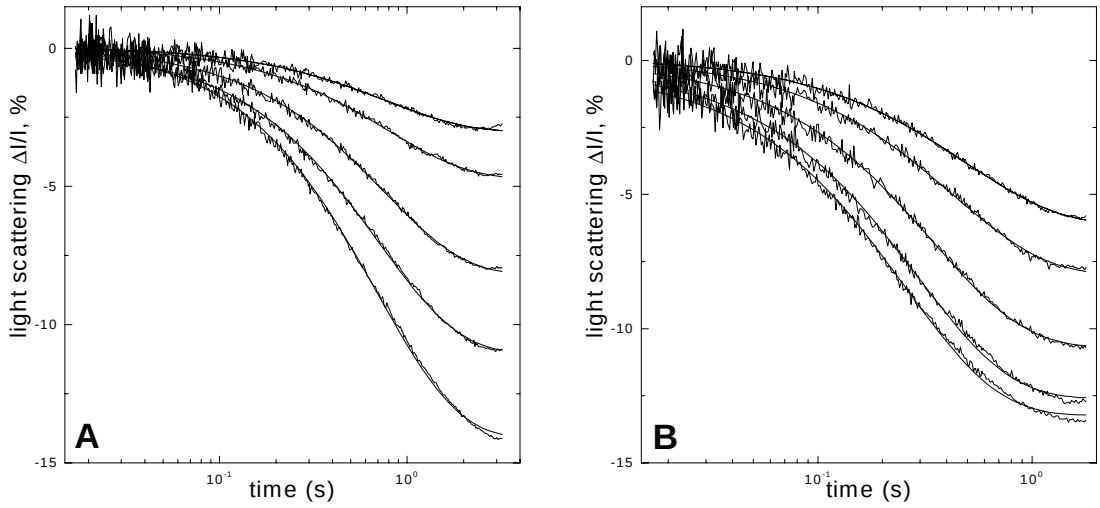


**Figure 5-20:** ADP induced dissociation of the kinesin.microtubule complex.
A) Light scattering changes observed with 0.45 µM microtubule (MT) site and 0.8 µM double headed rat kinesin construct K430 after laser induced release of different amounts of ADP from cADP. The best fit to a single exponential decay of the light scattering decrease is shown superimposed.
B) Light scattering changes observed with 0.45 µM microtubule (MT) site and 0.4 µM single headed rat kinesin construct K340 after laser induced release of different amounts of ADP from cADP. The best fit to a single exponential decay of the light scattering decrease is shown superimposed.
Other conditions: buffer 20mM MOPS , 20µM paclitaxel, 1mM DTT, 5mM MgCl2 at pH 7.2 and 22°C.

## *5.14 Discussion*

The data presented show that the flash photolysis system is capable of measuring acto.myosin dissociation and re-association using significantly lower quantities of protein than stopped flow measurements. Also the ability to use multiple flashes on a single sample by applying the next flash after complete ATP hydrolysis greatly increases the efficiency of sample usage.

Using light scattering we have shown that transients can be recorded with just 50 nM acto.myosin or acto.S1 complex. The total quantity of protein required depends upon the affinity of actin for myosin or S1. Under standard conditions (0.1 M KCl, pH 7, 20 C) the affinity of actin for S1 is of the order of 50 nM and therefore 50 nM acto.S1 complex requires significantly higher concentrations of at least one of the two proteins. Working at equimolar protein concentration data can be collected at 200 nM concentrations. Lowering the ionic

strength increases the affinity and should allow measurements at 50 nM of both actin and S1. The solubility of myosin limits the standard conditions to 0.5 M KCl. However the double headed interaction between myosin and actin results in a similar affinity to actin as for S1 at 0.1 M KCl. Thus the limits of sensitivity are similar for both S1 and myosin. Using excess actin in a volume of 10 µl would then require only 250 ng of myosin or 62 ng of S1 per assay. With excess S1 only 25 ng of actin is required. This compares to the 1.5 µg of actin, 2.5 µg of S1 or 10µg of myosin required for a 0.5 ml solution of 30 nM which is our standard stopped flow requirement.

Even with these low concentrations of protein, the measured rates of ATP induced dissociation of the complex are in good agreement with data from parallel stopped flow measurements. Using flash photolysis the second order rate constant $K_1k_{+2}$ is lower than in the related stopped flow experiments but generally by less than a factor of 2. Some inhibition of the rate of dissociation by the cATP present is expected based on the $K_I$ previously reported (Sleep et al., 1994). However, measurements of the effect of 1 mM cATP on the rate of ATP induced dissociation in the stopped flow under our experimental conditions showed a reduction of less than 5%. Furthermore fitting the dissociation reaction transients in flash photolysis with a single exponential results in rates which are slightly lower than the actual reaction rates as discussed in more detail below. Using the multiple flash approach, $K_1k_{+2}$ can be elucidated in several measurements at various ATP concentrations using a single 10 µl sample. In the absence of apyrase $k_{cat}$ can be estimated in the same experiment.

The measurements of $K_{AD}$ agree with estimates from stopped flow studies (Siemankowski et al., 1985; Geeves, 1989). Though ideally a freshly prepared sample is used for determination of each $k_{obs}$, the affinity of ADP for acto.S1 can also be obtained in a multiflash experiment, either in the absence of apyrase or by using hexakinase and glucose to accelerate the turnover of ATP to ADP. In practice it could be of use for myosins with a high affinity for ADP such as smooth muscle myosin (Cremo and Geeves, 1998) or myosin I (Coluccio and Geeves, 1999) to determine the $K_{AD}$ in a simple multi flash approach. For fast muscle myosins, however, the affinity of ADP is too weak to make such an approach feasible and ADP needs to be added to the sample between flashes. The rate of ADP dissociation from acto.S1 can also be measured for some myosins where the value lies within the resolution of the method (50 $s^{-1}$); for example smooth muscle S1.

The method is in principle also capable of measuring the affinity of actin for S1 ($K_A$) from the concentration dependence of the amplitude of the dissociation reaction (Kurzawa and Geeves,

1996). However the amplitudes of the light scattering signals are less reproducible than fluorescence measurements.

The light scattering signal is subject to disturbance by background scattering, air bubbles or dust and these become worse as the signal amplitude is reduced. Fluorescence measurements should gain an advantage at very low protein concentrations but the ideal fluorescent label has yet to be discovered. The fluorophore of choice for stopped flow measurements is pyrene labelled actin but the wavelength for pyrene excitation (344 or 365 nm) overlaps the action spectrum for the release of cATP. Thus, excitation of pyrene fluorescence results in continuous low level release of ATP and the laser flash can bleach the pyrene fluorescence. An electronic shutter can be used to limit this artefact when the amount of ATP released by the laser over the reaction time of the dissociation is much larger than the amount released by the monitoring light. Advanced programming of the shutter to open at exactly the same time as the laser flash occurs might be a feasible approach of working with the pyrene label for fast dissociation reactions. The use of mant nucleotides faces the same problems as pyrene-fluorescence, because it is excited at approximately the same wavelength as the pyrene label.

Measurements with fluorescein labelled S1 work well in flash photolysis although the label is bleached by the laser flash. However most experiments are aimed at measuring myosins in low quantities. For these experiments the fluorescent label is required on the more readily available actin since attempts to label myosin or S1 lead to a further loss of protein. Therefore the sensitivity of measurements with fluorescein labelled S1 have not been investigated further.

The acrylodan label is the best label we have found to date. Binding of acrylodan actin to S1 gives a maximum fluorescence change of about 30% compared to 70% with the pyrene label. Labelling actin with acrylodan reduces the affinity to S1 about 4 fold to give a $K_A$ of 180 nM. This effect can be countered by working in low salt buffers which also increases the observed rate constants. To date, the sensitivity using the fluorescence signals gives no advantage over the light scattering signals. However the independence of the fluorescence signal of commonly occurring air bubbles in the flash photolysis sample allows a higher reliability in measuring amplitude changes. Furthermore, the lower signal intensity in fluorescent measurements using small amounts of acrylodan actin involves higher photomultiplier sensitivity resulting in a more significant laser flash artefact. The resulting increase in dead time could be reduced by the use of gated photomultipliers and faster optical shutters. Further

improvements to the optical set-up are still possible and raise the possibility of measurements using even smaller amounts of protein.

The recent discovery of coumarin-labelled nucleotides (Webb and Corrie, 2001) presents the exciting possibility of increasing the number of experiments possible with the flash photolysis method. In contrast to the mant-label, coumarin is excited at a higher wavelength (405-445 nm), which interferes less with the action spectrum of the cATP. Furthermore it does not share the problem of the mant-label that the fluorescence change decreases to almost 0 in the presence of actin. Therefore experiments should be possible in which the ADP release can be measured directly by chasing off coumarin-labelled ADP from acto.myosin with ATP released from cATP. For many myosins however the ADP release rate is very fast (see section 6) and a faster release of ATP from a caged compound would be needed (see discussion below).

In general the dead time depends on the rate of release of the cATP which is about 100 $s^{-1}$ with the caged compound used and under the conditions currently used. The dead time can be decreased by using alternative caged compounds with a much faster release rate developed recently (Sokolov et al., 1998). However, these compounds generally have a lower quantum efficiency and do not allow the simple monitoring of the photoreaction by absorbance, which is a major advantage of the 1(2-nitrophenyl)ethyl ester cATP. The relatively slow release of ATP from the cATP used here limits simple analysis of the $k_{obs}$ to values of 50-70 $s^{-1}$ before significant corrections need to be applied to the estimated single exponential fits. Rates of exponential fits to faster reaction transients are more than 15% slower than the actual reaction rate. For the acto.S1 dissociation reaction this results in a deviation from the linear fit of the plot of $k_{obs}$ vs. [ATP]. Using a complete kinetic model to perform a non-linear fit to the data (Using the Scientist program, MicroMath, Utah, USA) allows analysis of faster reactions which are limited only by the maximum amount of ATP release possible using the current laser set up. The availability of the 405 nm signal to give a precise estimate of the rate and quantity of ATP liberation gives confidence to such an analysis. Using this approach, however, makes the analysis of experimental data more time consuming and complicated as each transient has to be fitted individually with carefully chosen fitting parameters. The simple method using single exponential fits is therefore preferred for reactions with a rate of up to 50 $s^{-1}$ for which the error is small.

At this stage of development, light scattering measurements are the method of choice for monitoring the kinetics of acto.myosin reactions with flash photolysis allowing measurements

using 50 nM acto.myosin or acto.S1 complex at a reasonable signal/noise ratio. While at the moment no higher sensitivity can be reached by recording fluorescence changes of acrylodan labelled actin, experiments with stopped flow have shown fluorescence measurements with pyrene actin to be possible with concentrations as low as 25 nM (Kurzawa and Geeves, 1996).

The low protein quantities required make flash photolysis the method of choice for analysing actins or myosins available only in very small amounts. The approach therefore allows kinetic characterisation of muscle myosin isoforms as shown in the next chapter (see section 6). The method should also allow kinetic characterisation of muscle proteins from micro biopsies allowing diagnose with small amounts of tissue, thus minimising patient distress.

The quantities of protein required are of the same order as that which can be prepared from a single flight muscle of *Drosophila melanogaster* (about 1 µg, Razzaq, 1995; Swank et al., 1998). This will enable parallel biochemical and mechanical experiments on actin or myosin mutants expressed in *Drosophila.* Other examples of myosin only available in small quantities are proteins which are difficult to overexpress or which are unstable (expected yields ≤ 1µg). Indeed the quantities used are of the order of those available from *in vitro* expression systems opening up the possibility of using this method for rapid screening of myosin mutants before scaling up expression in baculovirus or *Drosophila*. The methodology presented allows a much wider characterisation of myosin isoforms and mutants of myosin than has previously been possible.

In addition to being a suitable instrument for measuring the kinetics of acto.myosin, which it was initially designed for, the flash photolysis apparatus opens up the possibility of measuring reactions with any other protein or enzyme, in small amounts, which can be activated by the photolysis of a caged compound with an observable optical change. Furthermore the lack of a mixing turbulence can make flash photolysis preferable to the stopped flow method as it was shown here for the kinesin.microtubule system.

In the following two chapters (sections 6 and 7) the flash photolysis method is used to obtain biologically relevant results which could not have been obtained by traditional transient kinetic methods because the protein amounts available for these experiments would have been too small. In section 6 pure skeletal muscle MHC isoforms of human and rat, which were extracted from single muscle fibres, have been characterised. In section 7 the use of the flash photolysis method was essential to confirm that the kinetic properties of a rare full length myosin XIV agree with the characterisation of the more readily available truncated form of the myosin by stopped flow measurements.

### 5.15 Summary

Transient kinetic methods such as stopped flow and quenched flow have been used to elucidate many of the fundamental features of the molecular interactions which underlie muscle contraction. However, these methods traditionally require relatively large amounts of protein (> 0.1 mg) and so have been limited to proteins purified from bulk muscle tissue of large animals or where the proteins can be expressed in large amounts.

This work investigates the use of flash photolysis of an inert precursor of ATP (cATP) to initiate the dissociation of acto.S1 and acto.myosin and the subsequent ATP turnover reaction. Using a sample volume of 10 μl a significant amount of information on the transient and steady state kinetics of the system can be obtained, including the determination of the second order rate constant of ATP induced dissociation, the ADP affinity and the catalytic ATPase activity. The sensitivity of the method allows measurements with samples containing just 50 nM of acto.myosin or acto.S1 complex in solution. With one protein in excess the measurements require only 250 ng myosin, 62 ng S1 or 25 ng actin. This is therefore the method of choice for kinetic analysis of acto.myosins which are only available in microgram quantities. Furthermore the potential usefulness of this method for measuring proteins other than acto.myosin is shown in the example of the kinesin.microtubule system.

# 6 Biochemical characterisation of fast and slow type skeletal muscle myosin isoforms

## *6.1 Introduction*

Striated muscles perform a wide variety of functions in animals. To meet differing requirements animals developed a variety of muscle types with distinct mechanical properties (see section 1.4.3). The composition of muscle protein isoforms is typical for a specific type of muscle. Mammalian skeletal muscle fibres, which often express pure myosin isoforms, show characteristic mechanical properties including shortening velocity, power output (Bottinelli et al., 1994a; Bottinelli et al., 1994b; Greaser et al., 1988; Sweeney et al., 1988) and ATPase activity (Mabuchi and Sreter, 1980; Bottinelli et al., 1994b). It is now clear that all of these properties are to a large extent determined by the isoform of the myosin heavy chains expressed in individual muscle cells (Pette and Staron, 1990; Schiaffino and Reggiani, 1996). Light chain isoforms seem to play a minor role in determination of these properties as myosins with different light chains display primarily the properties of the myosin heavy chain isoform (Wagner, 1981; Canepari et al., 2000). Biochemical and structure-function studies have attempted to define the underlying molecular basis of the differing mechanochemical properties of myosins within the skeletal muscle myosins and in the wider family of myosins.

Muscle contraction results from a cyclical interaction of myosin cross bridges with actin driven by ATP hydrolysis. It is generally accepted that the sequence of events in the acto.myosin cross bridge cycle is essentially the same for all muscle myosins. The different properties can therefore be attributed to modulation of the rates and equilibrium constants (and hence free energy changes) of individual molecular events by changes in myosin sequence. Early studies suggested a correlation between the maximum shortening velocity of a muscle fibre (i.e the velocity in the absence of any mechanical load) and the overall ATPase rate for a range of muscle types since both reflect the underlying speed of the cross bridge cycle (Barany, 1967).

Detailed biochemical kinetic studies of myosin isoforms were pioneered in 1980 by Marston and Taylor (1980) using myosins from 4 different muscle types of the chicken. They found that the relative rates of most of the steps in the ATPase cycle varied with myosin isoform, but that most events were too fast to be rate limiting for ATP hydrolysis and thus the overall rate of energy transduction. For example, the rate of the ATP cleavage step was too fast to limit the overall cycling rate. They proposed that the rate limiting step in the ATPase cycle was

associated with the overall rate of reattachment of actin to the myosin products complex (M.ADP.Pi) and the product (Pi & ADP) release. In a paper of great insight Siemankowski *et al.* (1985) estimated the rate of release of ADP from the acto.myosin complex for a series of myosins isolated from different muscle types. This study used a wide range of muscle types (smooth, cardiac, skeletal) of different species (rabbit, rat, chicken). They were able to correlate the rates of ADP release (15 – 600 $s^{-1}$) with the unloaded shortening velocities over a 40-fold range and therefore proposed that the ADP release rate for a myosin was a major contributor to defining the maximum shortening velocity of a muscle expressing that myosin. However only two values of ADP release above 200 $s^{-1}$ were determined in this study and these were the least well defined. Therefore the question if the hypothesis held true for faster myosins and over a smaller range of values for ADP release remained.

Since this work the focus of attention has largely switched to studies of myosins of defined sequence and 3-D structure. Such studies have examined naturally occurring variants of myosin to look for structure-function relationships. The over-expression of modified versions of myosin have allowed the investigation of chimeric myosins and myosins carrying specific mutations (e.g. cardiac myopathy point mutations) to pinpoint the parts of myosin responsible for particular properties (Sweeney et al., 1998; Spudich, 1994; Rovner et al., 1997; Geeves and Holmes, 1999).

In a series of recent studies the mechanochemical properties of single muscle fibres and the myosin isoforms isolated from such fibres were compared (Bottinelli et al., 1994a; Bottinelli et al., 1994b; Canepari et al., 1999; Canepari et al., 2000). In particular these works by Canepari *et al.* (2000) showed that significant changes in shortening velocity could occur for minimal changes in myosin sequence. For example the β-isoforms of rat and human myosin heavy chain (β-MHC or MHC-I) are >95% identical in the myosin motor domain, with only 14 non-conservative residue changes throughout the 860 amino acid sequence, yet they differ by a factor of more than 2 in velocity assays (Canepari et al., 2000).

A study of the biochemical kinetic properties of the mammalian myosin isoforms may therefore prove of interest in testing the hypothesis of Siemankowski *et al*. (1985) on a series of closely related myosins whose contractile and energetic properties are well characterised. The 4 myosin heavy chain isoforms expressed in adult rat skeletal muscle (MHCs I, IIA, IIX and IIB) used here represent such a system in that they are paralogous isoforms of the same species and the rates of ADP release, as estimated in this chapter, were fast (ca. 600 – 2220 $s^{-1}$) and varied over a smaller range (ca. 4-fold). To complement this data 2 myosin heavy

chain isoforms of human skeletal muscle were measured (MHC-I and MHC-IIA). This data was used to see if the trends which were observed for the 4 paralogous isoforms of rat could be confirmed for the corresponding isoforms in another species of different size. It is also very interesting to see how these properties can be attributed to the differences in sequence found in orthologous and parologous isoforms, especially since the measurements included the isoform MHC-I of both rat and human, for which only 14 non-conservative residue changes are reported (Canepari *et al*., 2000).

While there have been many studies of the mechanical properties of mammalian muscle fibres (both intact and skinned), biochemical characterisation of mammalian striated MHC isoforms has been limited because of the difficulty of isolating pure heavy chain isoforms. There is no effective overexpression system for mammalian striated muscle myosin isoforms. Isolation of myosin from bulk muscle (as used by Siemankowski *et al.* (1984)) results in a preparation containing mixed isoforms. In contrast, single isolated muscle fibres often contain a single MHC isoform (Staron and Pette, 1987).

The amount of myosin which can be isolated from a single 2 cm long muscle fibre of rat is sufficient to characterise the ATP induced dissociation reaction and the affinity of ADP for acto.myosin using the flash photolysis apparatus developed for use with small protein amounts (see section 5).

This work undertakes the first kinetic characterisation of all 4 MHC skeletal isoforms (MHC-I, IIA, IIB and IIX) expressed in adult rat muscle and of 2 human skeletal isoforms MHC-I and IIA. It will be discussed how both the rate of ATP induced dissociation of acto.myosin and the affinity of ADP for acto.myosin can influence the maximum shortening velocity of muscles expressing specific MHC isoforms.

## *6.2 Biochemical characterisation of myosin extracted from slow type (soleus) and fast type (Edl) whole rat muscles*

Flash photolysis experiments with myosin extractions from bulk rat muscles were performed prior to experiments with pure myosin isoforms extracted from single fibres (see sections 6.3 and 6.4). Extractions from bulk muscle tissue yields enough myosin to be analysed by stopped flow. This makes a direct comparison of the results obtained from stopped flow and flash photolysis possible. The fast type Edl muscle and the slow type soleus muscle of rat were chosen for extractions. Rat Edl muscle contains mostly MHC-IIX and MHC-IIB isoforms (Ranatunga, 1984) while rat soleus muscle contains mostly MHC-I and MHC-IIA isoforms (see section 6.3.2). Measuring the kinetic values of these extracts containing a mixture of isoforms gave an idea of the values which would be obtained with pure isoforms. The agreement of the values determined with both the stopped flow data for the same extracts and those subsequently determined for pure isoforms increases the confidence in the reliability of the single fibre experiments.

### 6.2.1 ATP induced dissociation

Both the Edl and soleus muscles were dissected from freshly killed rats. The muscles were separately minced and the myosin extracted in Guba-Straub solution as described in section 4.4.4.1. For flash photolysis experiments 200 µl samples were prepared containing 1 µM myosin, 1 µM phalloidin stabilised actin and 0.5 mM cATP, 10 mM DTT, 10 µg/ml apyrase. In contrast to experiments with S1, a high salt buffer (500 mM KCl; 20 mM MOPS; 5 mM $MgCl_2$; pH 7.0) was used to prevent aggregation of the full length myosin. 20 µl samples were added to the cuvette. The ATP dissociation was measured in multiflash experiments as described in section 5.6. The binding of ATP to acto.myosin causes fast and irreversible dissociation of the complex and when all the ATP is hydrolysed the complex reforms. The rate of breakdown of ATP by acto.myosin under these conditions is relatively slow, so apyrase was added to the samples to allow a faster elimination of ATP and ADP. This procedure allows the same sample to be reused a number of times with different flash intensities to vary the ATP concentration released.

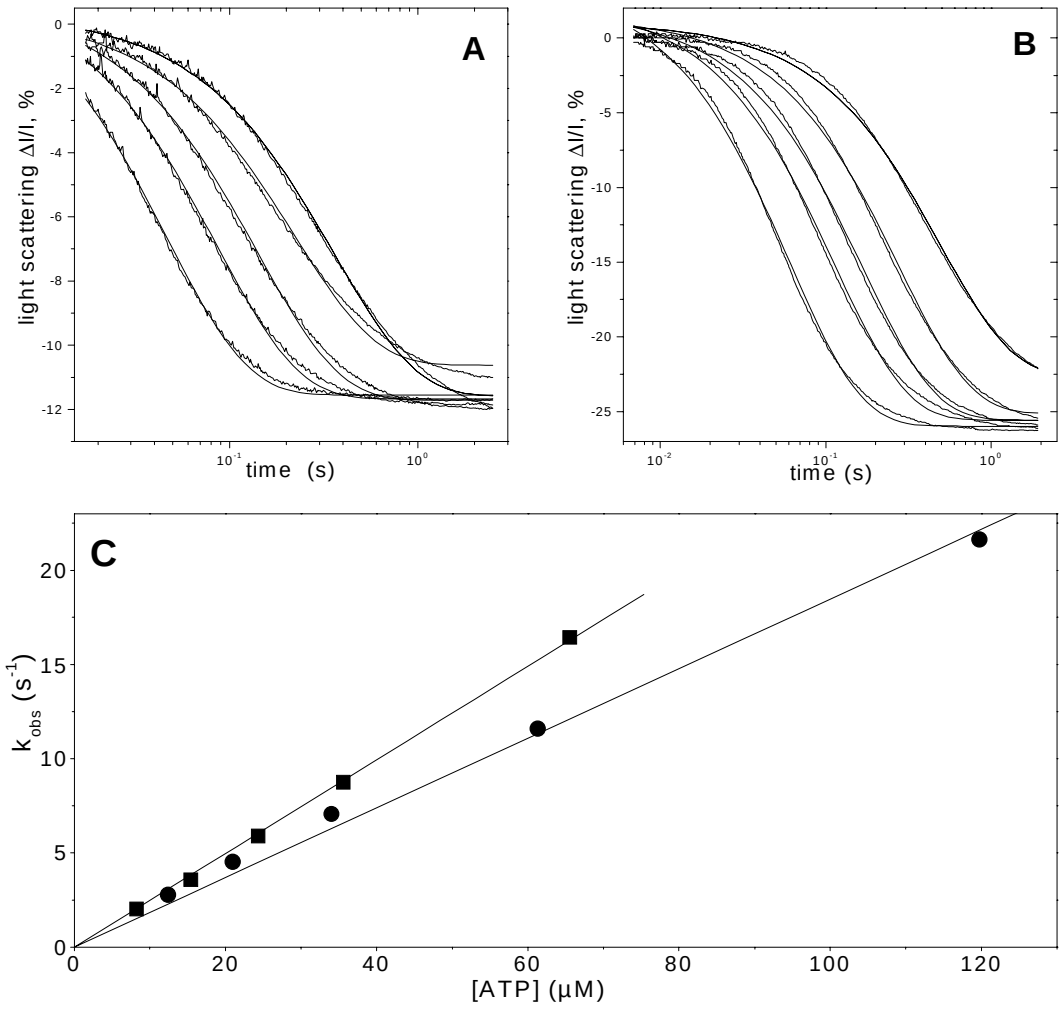


**Figure 6-1:** ATP induced dissociation of actin and myosin extracted from rat Edl and soleus muscle

A) Light scattering signals from a 20 µl sample containing 0.5 µM actin, 1 µM Edl-myosin, 0.5 mM cATP and apyrase in a multiple flash experiment. The best fit to a single exponential decay of the light scattering decrease is shown superimposed.

B) Light scattering signals from a 20 µl sample containing 0.5 µM actin, 1 µM soleus-myosin, 0.5 mM cATP and apyrase in a multiple flash experiment. The best fit to a single exponential decay of the light scattering decrease is shown superimposed.

C) The apparent rate constants of dissociation $k_{obs}$ for Edl (■) and soleus (●) are plotted versus the concentration of ATP released. The slope of a linear fit through the origin to the dataset for each isoform gives the second order rate constants ($K_1k_{+2}$), 0.253±0.003 $\mu M^{-1}s^{-1}$ and 0.185±0.002 $\mu M^{-1}s^{-1}$ for Edl and soleus respectively.

Other conditions: experimental buffer containing 500 mM KCl, 20 mM MOPS, 5 mM $MgCl_2$ and 10 mM fresh DTT at pH 7.0 and 22°C.

Figure 6-1A shows the light scattering changes due to ATP induced dissociation of the acto.myosin complex with myosin extracted from the Edl muscle while Figure 6-1B shows the light scattering transients for myosin extracted from soleus. The concentration of ATP liberated in each flash was estimated from the decay of the absorbance of 405 nm which

monitors the formation and decay of the aci-nitro photolysis intermediate (see section 5.5). The same sample was used for all the transients shown in Figure 6-6A or B. After each transient was recorded the sample was left for 3 min to allow complete ATP hydrolysis before the next flash. The decrease in light scattering is described by a single exponential and the best fit to a single exponential is superimposed in each case. The observed rate constant ($k_{obs}$) for each reaction was linearly dependent upon the concentration of ATP. Figure 6-6C shows the dependence of $k_{obs}$ on the concentration of ATP for both Edl and soleus myosin. For both cases a linear relationship was observed and the slope of the fitted line defined the apparent second order rate constant of the ATP induced dissociation reaction (see Equation 3-4 and Scheme 3-2). The plot of $k_{obs}$ vs. [ATP] results in different slopes for Edl and soleus myosin. The apparent second order rate constants were 0.25 $\mu M^{-1}s^{-1}$ and 0.185 $\mu M^{-1}s^{-1}$ for myosin extracted from Edl and soleus respectively.

The magnitude of these values was confirmed by stopped flow measurements of the ATP induced dissociation of actin and myosin from bulk muscle preparations of Edl and soleus. The experiments were carried out within the group by N. Adamek at the University of Kent and resulted in second order rate constants of 0.38 $\mu M^{-1}s^{-1}$ and 0.25 for myosin extracted from Edl and soleus respectively. As with experiments with rabbit S1, the second order rate constant appeared up to a factor of 2 smaller in flash photolysis than in stopped flow experiments (see section 5).

Experiments with S1 prepared from Edl and soleus carried out within the group by Dr. O. Nikolaeva and N. Adamek showed that the ATP induced dissociation of Edl-S1 from actin was slightly faster than that of soleus-S1 even if the difference was less pronounced than in myosin. The second order rate constants determined were 2 $\mu M^{-1}s^{-1}$ and 1.8 $\mu M^{-1}s^{-1}$ for Edl-S1 and soleus-S1 respectively. These experiments were carried out in an experimental buffer containing 100 mM KCl; 20 mM MOPS; 5 mM $MgCl_2$ at pH 7.0 and 22°C. The higher rate constants compared with myosin were a result of working at a lower salt concentration.

### 6.2.2 ADP affinity for the acto.myosin complex

ADP binds to the same binding site as ATP. At the low ATP concentrations used in these experiments (<100 µM) the overall rate of ATP induced dissociation of acto.S1 ($K_1k_{+2}$) for fast myosins is sufficiently slow for the binding and dissociation of ADP to be a preceding fast equilibrium defined by the constant $K_{AD}$. The competition between ADP and ATP for the myosin nucleotide site results in an inhibition of the rate of ATP induced dissociation. The dependency of this inhibition on the concentration of ADP can be used to determine $K_{AD}$ which is a measure for the affinity of ADP for the acto.myosin complex (Siemankowski and White, 1984). The samples contained hexakinase and glucose to remove ATP, but leave ADP present. Additionally the myokinase inhibitor $Ap_5A$ was added as a precaution against interconversion of ADP and ATP by myokinase.

Figure 6-2 show typical experiments for the inhibition of the ATP induced dissociation by ADP for the case of Edl (A) and soleus (B). A separate sample was used for each measurement. For each sample 15 µl of the extracted myosin solution in experimental buffer were mixed with 5 µl of reaction mix to give a final volume of 20 µl containing 1 µM myosin, 1 µM phalloidin stabilised actin and 1 mM cATP, 10 mM DTT, 0.03 units/µl Hexakinase, 1 mM Glucose, and 100 µM Ap5A and the desired concentration of ADP. Single exponential light scattering transients were observed in each measurement with both the $k_{obs}$ and the amplitude of the reaction decreasing as ADP concentration increased. The decrease in $k_{obs}$ is predicted from Scheme 3-3 and Equation 3-5. The values of $k_{obs}$ were then plotted against the ADP concentration as shown in Figure 6-2C and D for each myosin isoform. The data were fitted to the Equation 3-5. The affinity of ADP for acto.myosin is tighter for soleus ($K_{AD}$ = 308 µM) than for Edl ($K_{AD}$ = 901 µM). ADP reduces the affinity of myosin for actin which results in partial dissociation of the acto.myosin complex and therefore a loss of signal amplitude notable at higher ADP concentrations (see Figure 6-2A and B).

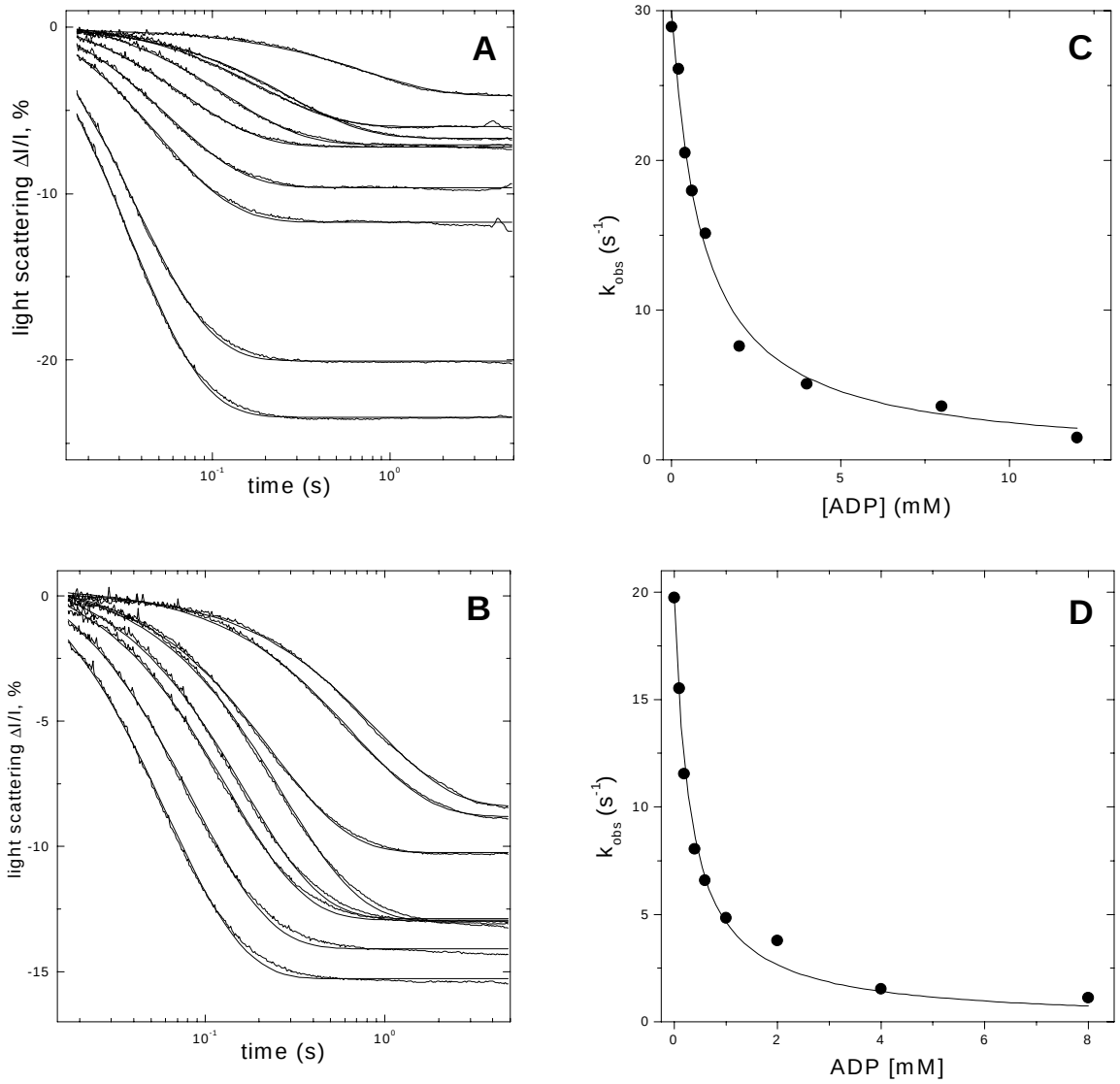


**Figure 6-2:** Inhibition of the ATP induced rate constant by ADP for the complex of actin and Edl-myosin or soleus-myosin

A + B (A) Light scattering signals from 9 20 µl samples containing 1 µM actin, 1 µM Edl-myosin, 1 mM cATP, hexakinase, Ap5A and Glucose and (B) light scattering signals from 8 20 µl samples containing 1 µM actin, 1 µM soleus-myosin, 1 mM cATP, hexakinase, Ap5A and Glucose. Each sample contained a different amount of ADP and the samples were irradiated with the same laser intensity releasing an identical concentration of 80 µM ATP from cATP. The amplitude of the light scattering changes decreased with increasing ADP concentration. The best fit to a single exponential decay of the light scattering decrease is shown superimposed.

C + D) The plots show the ADP dependence of $k_{obs}$ for Edl (C) and soleus (D) myosin, respectively. The data were fitted to the model of Scheme 3-3 and gave a value of $K_{AD}$ of 901±91 µM for Edl and a value of $K_{AD}$ of 308±25 µM for soleus

Other conditions: experimental buffer containing 500 mM KCl, 20 mM MOPS, 5 mM $MgCl_2$ and 10 mM fresh DTT at pH 7.0 and 22°C.

These results were confirmed by stopped flow experiments. For these experiments solutions containing 1 µM myosin (Edl or soleus) and 1 µM pyrene-labelled actin in experimental buffer (500 mM KCl; 20 mM MOPS; 5 mM $MgCl_2$; pH 7.0) were mixed with solutions of 50 µM ATP and various amounts of ADP. The increase in pyrene fluorescence reported the ATP induced dissociation of the acto.myosin complex and the rate constant was determined by a single exponential fit to that increase. As in the flash photolysis experiments the rate constant decreased with increasing amounts of ADP and the $K_{AD}$ could be determined by fitting the hyperbolic decrease to Equation 3-5. Figure 6-3 shows the stopped flow results which were very similar to those obtained by flash photolysis, giving values for $K_{AD}$ of 926 µM and 417 µM for Edl and soleus respectively.

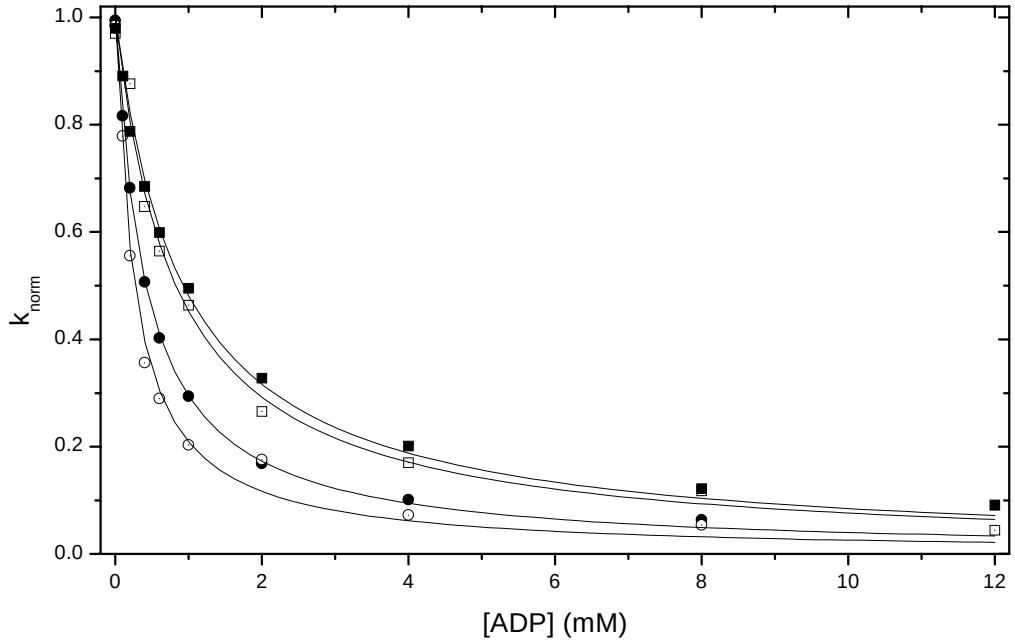


**Figure 6-3:** ADP affinity for Edl or soleus acto.myosin in flash photolysis and stopped flow.
$k_{norm}$ is plotted versus the concentration of ADP for Edl (■) and soleus (●) in flash photolysis measurements and for Edl (□) and soleus (○) in stopped flow measurements. For easier comparison of the hyperbolic decrease defining $K_{AD}$ between the 4 curves the initial value at 0 [ADP] for $k_{norm}$ in each case has been set to 1, to which all measurements within a series at higher ADP concentrations are referenced. For each series of measurements a fit to Equation 3-5 (with $K_1k_{+2}$ [ATP] = 1) is superimposed giving $K_{AD}$ values of 901±91 µM for Edl and 308±25 µM for soleus in stopped flow measurements and $K_{AD}$ values of 926±33 µM for Edl and 417±6 µM for soleus in flash photolysis measurements.

## *6.3 Biochemical characterisation of the 4 major myosin heavy chain isoforms of rat skeletal muscle*

### 6.3.1 Flash photolysis measurements of myosin extractions from single muscle fibres

In section 5 it was shown that the amount of myosin a single muscle fibre of 2 cm length contains (about 4-6 µg) is sufficient to be analysed in flash photolysis light scattering experiments. Such an experiment was attempted with extracted myosin from a 2 cm long glycerinated rabbit psoas muscle fibre using micro incubation and dialysis methods. This method was adapted for the use of single fibre extractions from a method used at the University of York for preparing myosin from single *Drosophila* muscles and is described in section 4.4.4.4. The extracted myosin appears as a single heavy chain band on a SDS-PAGE gel indicating little contamination with actin or other proteins. The light chain bands were not readily visible under these conditions. The amount of myosin extracted was estimated by comparison with myosin standards (Figure 6-4A) which indicated that an average of up to 5 µg of myosin was extracted from each fibre in a volume of less than 50 µl. 15 µl of the extracted myosin solution was mixed with 5 µl of reaction mix to give a final volume of 20 µl containing ca. 300 nM single fibre myosin, 500 nM phalloidin stabilised actin, 0.5 mM cATP, 10 mM DTT and 10 µg/ml apyrase in experimental buffer. In a light scattering (4-flash) experiment various amounts of ATP were released and produced the transients shown in Figure 6-4B. Analysis showed amplitudes of about 13 % which could be fitted by single exponentials. This proved further experiments with myosin extractions from single fibres would be possible.

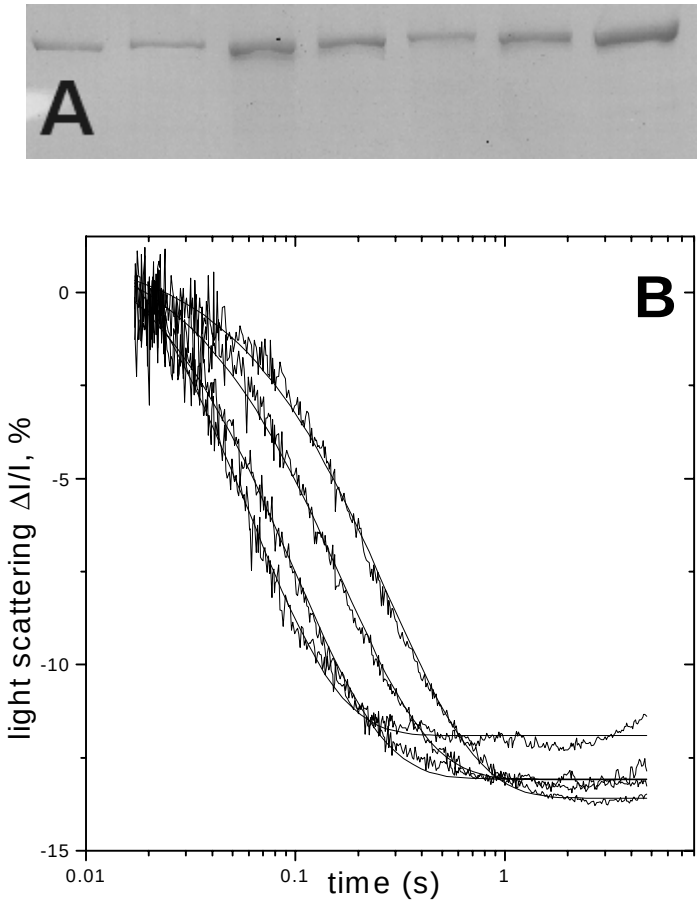


**Figure 6-4:** ATP induced dissociation of actin and myosin extracted from a single muscle fibre
A) SDS-PAGE: Rows 1-5: 5µl of the myosin extractions of 2 cm lengths of different single psoas rabbit muscle fibres. The total volume of each extraction after micro incubation of the fibre and dialysis was about 30 µl. Row 6-7: 1 µg and 2 µg of purified rabbit skeletal myosin respectively.
B) Light scattering signals from a 20 µl sample of 0.5 µM actin and about 0.3 µM myosin extracted from a single muscle fibre in a multi flash experiment releasing 4 different concentrations of ATP from 0.5 mM cATP in the presence of apyrase. The best fit to a single exponential decay of the light scattering decrease is shown superimposed.

### 6.3.2 Myosin extraction from single fibres and the identification of MHC isoforms

Single fibres of ca. 15 mm length were dissected from fresh preparations of soleus and psoas rat muscles. A small part of the fibre (~2 mm) was used to identify the content of myosin as described in section 4.6.3.2 (Talmadge and Roy, 1993). Four bands were separated corresponding to the four MHC isoforms (Figure 6-5A). The remaining part was used to isolate pure myosin isoforms according to the method used in section 6.3.1. Single soleus fibres yielded myosin preparations of pure isoforms of MHC-I (38%), MHC-IIA (32%) and preparations containing mixed isoforms (30%). For psoas fibres the preparations gave isolated isoforms of 47% pure MHC-IIB and 49% pure MHC-IIX. Mixed isoforms were found in 4%

of the psoas fibres. Muscle fibres which did not contain a pure isoform were discarded and pure myosin isoforms were extracted from the remaining fibres into a final volume of less than 50µl using micro incubation and dialysis methods. Figure 6-5B shows that the extraction method provides yields of approximately 2 µg myosin with little contamination with actin or other proteins. More than 2/3 of the total myosin content of the fibre was extracted using this method. The experiments in this and in the following sections 6.3.2 - 6.4.3 were done in collaboration with Professor R. Bottinelli's lab in Pavia, Italy. Single fibres were dissected and the myosin extracted by R. Rossi. The isoforms were determined by M.A. Pellegrino. All kinetic experiments were done at the University of Kent by myself.

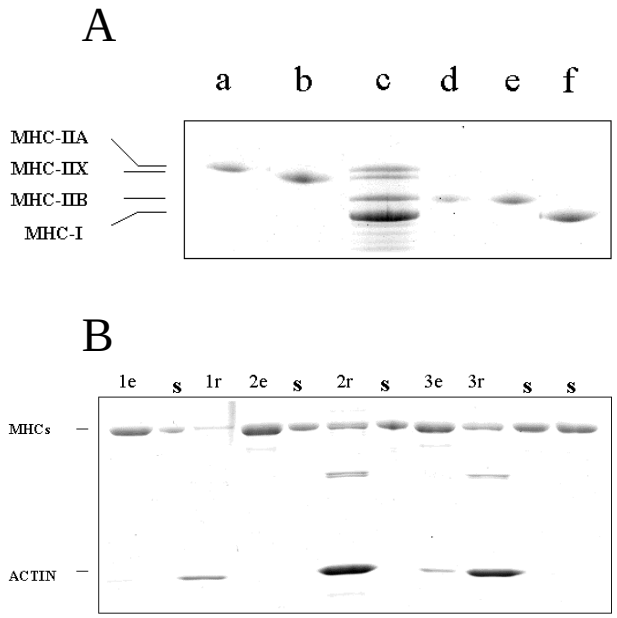


**Figure 6-5:** Electrophoretic separation of rat MHC isoforms.

A) Electrophoretic separation of rat MHC isoforms. Area of migration of the four MHC isoforms is indicated on the left. Single muscle fibres were loaded in lanes a, b, d-f; a sample of a mixture of slow and fast rat muscles to show all four MHC isoforms was loaded in lane c. Lane a: single muscle fibre containing MHC-IIA; lane b: single fibre containing MHC-IIX; lane d and e: single fibres containing MHC-IIB; lane f: single fibre containing MHC-I. The gel is a 8% polyacrylamide gel; silver staining was used.

B) Example of gels used for electrophoretic determination of the amount of myosin extracted from single fibres and of the remainder amount of myosin left in the fibre after myosin extraction. Lanes in which known amounts of myosin, to be used as standards, were loaded are indicated with S; from left to right the amounts loaded were 1, 2, 2.5, 3 and 3.5 µg. 1e: lane in which myosin extracted from fibre #1 was loaded; 1r: lane in which the remainder amount of myosin left in the same fibre after myosin extraction and extracted by standard buffer (Laemmli, 1970) was loaded. The same applies to lanes 2e and 2r for fibre #2 and to lanes 3e and 3r for fibre #3. Gel is a 10-20% gradient polyacrylamide gel; comassie staining was used.

### 6.3.3 ATP induced dissociation

The ATP dissociation was measured in multiflash experiments as described in section 5.6 allowing a sample to be reused. Upon binding of ATP to acto.myosin, fast and irreversible dissociation is followed by hydrolysis of ATP and reformation of the complex. Experiments were carried out in presence of apyrase to allow a faster elimination of ATP and ADP.

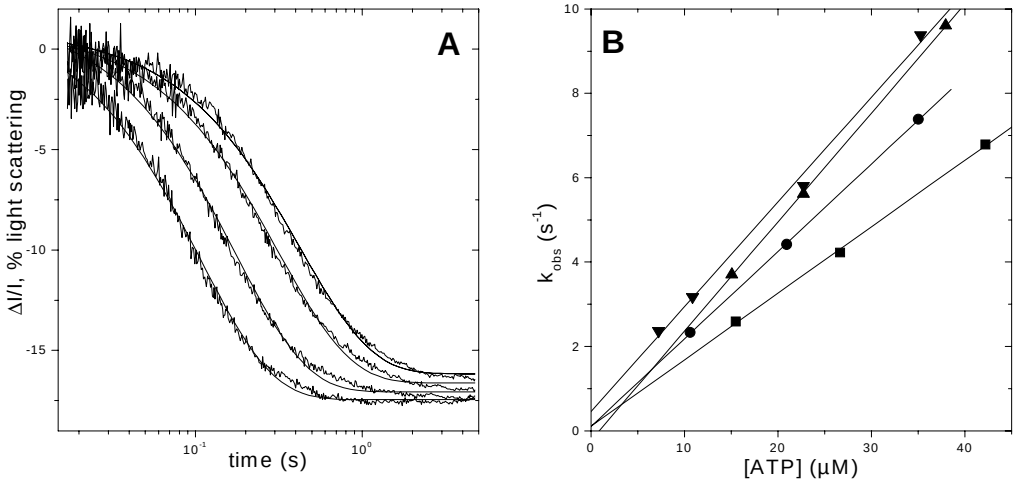


**Figure 6-6:** ATP induced dissociation of myosin and actin

A) Light scattering signals from a 20 µl sample containing 0.5 µM actin, approx. 0.15 µM myosin (MHC-IIB), 0.5 mM cATP and apyrase in a multiple flash experiment. The best fit to a single exponential decay of the light scattering decrease is shown superimposed. Other conditions: experimental buffer containing 500 mM KCl, 20 mM MOPS, 5 mM $MgCl_2$ and 10 mM fresh DTT at pH 7.0 and 22°C.

B) The apparent rate constants of dissociation $k_{obs}$ for 4 different MHC-isoforms are plotted versus the amount of ATP released. The slope of a linear fit to each set of data from one isoform gives the second order rate constants ($K_1k_{+2}$) (• :MHC-IIX, 0.258 ± 0.005 $\mu M^{-1}s^{-1}$; • :MHC-IIB, 0.25 ± 0.011 $\mu M^{-1}s^{-1}$; • :MHC-IIA, 0.21 ± 0.02 $\mu M^{-1}s^{-1}$; • :MHC-I, 0.168 ± 0.009 $\mu M^{-1}s^{-1}$)

15 µl of the extracted myosin solutions in experimental buffer were mixed with 5 µl of reaction mix to give a final volume of 20 µl containing ca. 0.15 µM myosin, 0.5 µM phalloidin stabilised actin and 0.5 mM cATP, 10 mM DTT, 10 µg/ml apyrase. As shown in Figure 6-6A for a sample of MHC-IIB, irradiation by a series of laser pulses of different intensities released a range of ATP concentrations. The same sample was used for all the transients shown in Figure 6-6A. After each transient was recorded the sample was left for 3 min for all the ATP to be hydrolysed before the next flash. The decrease in light scattering was described by a single exponential and the best fit to a single exponential is superimposed in each case. The observed rate constant ($k_{obs}$) of each reaction was linearly dependent upon the concentration of ATP. Figure 6-6B shows the dependence of $k_{obs}$ on the concentration of ATP calculated from the absorbance at 405nm (see section 5.5) for each of the four MHC

isoforms isolated. In each case a linear relationship was observed and the slope of the fitted line defined the apparent second order rate constant of the ATP induced dissociation reaction (see Equation 3-4and Scheme 3-2). The plots show different slopes for each isoform except for IIB and IIX, which were very similar. The pooled data from a series of measurements using at least 6 individual fibres for each myosin isoform are given in Table 6-1. These show that the difference between isoforms IIX and IIB is not statistically significant whereas all other differences are significant. According to Equation 3-4 the intercept of the linear fit defining the second order rate constant should be 0. As seen in Figure 6-6B the linear fits of the experimental data often deviate slightly from an intercept of 0. The fitting procedure was therefore repeated with linear fits through the origin. This changed the mean value for the second order rate constant for each isoform by less than 0.05 $\mu M^{-1}s^{-1}$.

### 6.3.4 ADP affinity for the acto.myosin complex

The competition between ADP and ATP for the myosin nucleotide site provides a method to determine the affinity of ADP for the acto.myosin complex (see section 5.8). At higher concentrations ADP will reduce the affinity of myosin for actin and at the low protein concentrations used here this results in a loss of signal amplitude (see Figure 6-7A). To counteract this loss of amplitude the protein concentrations were increased to 1 μM actin and 0.75 μM myosin. In order to have sufficient myosin for these experiments 5 fibres of the same isoform content were pooled for the extraction procedure. The samples contained hexakinase and glucose to remove ATP, but leave ADP present and additionally the myokinase inhibitor $Ap_5A$ was added as a precaution against interconversion of ADP and ATP.

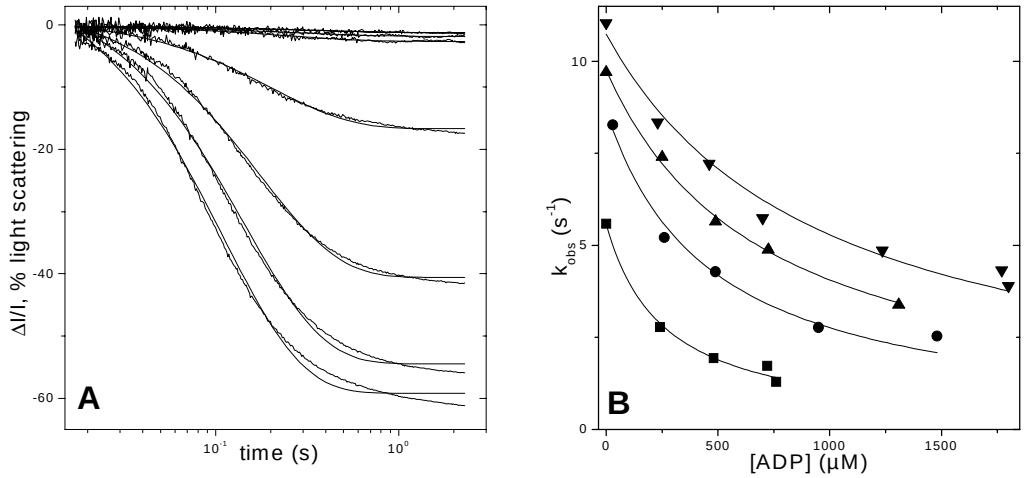


**Figure 6-7:** Determination of ADP-affinity for acto.myosin with different myosin MHC isoforms

A) Light scattering signals from a 20 µl sample containing 1 µM actin, approx. 0.75 µM myosin (MHC-IIB), 1 mM cATP, hexakinase, Ap5A and Glucose. During the multiple flash experiment the laser energy was kept constant to ensure a constant release of ATP (ca. 40 µM). A defined amount of ADP as well as a calculated amount of cATP to counteract the loss from the previous flash was added to the sample between flashes. The amplitude of the light scattering changes decreased with increasing ADP concentration. The best fit to a single exponential decay of the light scattering decrease is shown superimposed. Other conditions: experimental buffer containing 500 mM KCl, 20 mM MOPS, 5 mM $MgCl_2$ and 10 mM fresh DTT at pH 7.0 and 22°C.

B) The plot shows the ADP dependence of $k_{obs}$ for each set of data from the 4 different MHC isoforms examined. The data were fitted to the model of Scheme 3-3 and gave values of $K_{AD}$ of 970 ± 97 µM for MHC-IIB (• ), 713 ± 31 µM for MHC-IIX (• ), 469 ± 63 µM for MHC-IIA (• ) and 257 ± 23 for MHC-I (• ).

Because of the limited amount of myosin, a multiflash approach was used for each series of measurements. A typical experiment is shown in Figure 6-7A for MHC-IIB. The initial sample of each series contained 1 µM actin, approx. 0.75 µM myosin, 1 mM cATP, 0.03 units/µl Hexakinase, 1 mM Glucose, and 100 µM Ap5A in 500 mM KCl experimental buffer. The first flash, in the absence of ADP, shows a single exponential decay of scattering as in Figure 6-6A. The amount of ATP released in each flash was calculated by analysis of the transmission changes at 405 nm as before (see section 5.5). After allowing 5 minutes for the elimination of the ATP, ADP was added to the sample (maximum added volume 2µl) along with a small amount of cATP to replenish that used in the previous flash. The procedure was repeated for a series of 4-6 ADP concentrations. Single exponential light scattering transients were observed in each measurement with both the $k_{obs}$ and the amplitude of the reaction decreasing as ADP concentration increased. The decrease in $k_{obs}$ is predicted from Scheme 3-3 and Equation 3-5. The decrease in amplitude was due to the dilution effect and the weaker affinity of actin for the myosin.ADP complex. The ADP concentration in each case was calculated as the sum of the ADP added and the ADP which built up through the hydrolysis of

the ATP released in each previous flash. This procedure has been validated using the well characterised rabbit muscle myosin S1. The values of $k_{obs}$ were corrected according to Equation 3-4 for the small variations in the amount of ATP released in each flash and then plotted against the ADP concentration as shown in Figure 6-7B for each myosin isoform. The data was fitted to the Equation 3-5. Each MHC isoform gave a distinct value of $K_{AD}$ and pooled data from 3 different experiments shows the differences to be significant (Table 6-1).

| | $V_0$ ($L\ s^{-1}$) | $K_1k_{+2}$ ($\mu M^{-1}s^{-1}$) | $K_{AD}$ ($\mu M$) |
|---|---|---|---|
| rat MHC-I | 1.05±0.37 | 0.172±0.019 (9) | 250±17 |
| rat MHC-IIA | 2.33±0.29 | 0.21±0.027 (6) | 483±30 |
| rat MHC-IIX | 3.07±0.7 | 0.27±0.032 (5) | 753±52 |
| rat MHC-IIB | 3.69±1.01 | 0.255±0.019 (6) | 934±39 |
| human MHC-I | 1.15±0.36 | 0.18±0.02 (5) | 163±11 |
| human MHC-IIA | 2.37±0.34 | 0.26±0.02 (4) | 237±17 |

**Table 6-1:** Comparison of the experimental values for the 4 MHC isoforms of rat skeletal muscle
The values for $V_0$ were taken from Bottinelli *et al.* (1994a) for rat fibres measured at 12°C and He *et al*. (2000) for human fibres measured at 20°C. $K_1k_{+2}$ and $K_{AD}$ were measured at 22°C in experimental buffer containing 500 mM KCl, 20 mM MOPS, 5 mM $MgCl_2$ and 10 mM fresh DTT at pH 7.0. All $K_1k_{+2}$ values are quoted as the mean value with the standard deviation and the number of observations in brackets. A similar format is used for $K_{AD}$ values except the number of observations was 3 in each case for rat and 4 in each case for human.

Thermodynamic coupling between actin and ADP binding to myosin (Siemankowski and White, 1984; Ritchie et al., 1993) predicts that the weaker the affinity of acto.myosin for ADP the weaker the affinity of myosin.ADP for actin. Light scattering measurements are not very reliable for amplitude data due to factors like micro air bubbles and dust particles. However there was a clear trend for the MHC isoforms IIX and IIB to show a greater amplitude loss at comparable ADP concentrations than isoforms I and IIA consistent with weaker affinity for actin for isoforms IIX and IIB.

## *6.4 Biochemical characterisation of a fast (MHC-IIA) and a slow (MHC-I) myosin heavy chain isoform of human skeletal muscle*

To complement the data collected on rat isoforms, 2 myosin heavy chain isoforms of human skeletal muscle were measured (MHC-I and MHC-IIA). The sequences for all 4 MHCs of human are known. However only the isoforms MHC-I and MHC-IIA are expressed as pure isoforms in skeletal muscle fibres. In addition the human samples represent a much larger species than rat for which the shortening velocities of fibres expressing pure isoforms are known to be slower than for the corresponding (orthologous) isoforms of rat. It is therefore interesting if the trends which were observed for the 4 paralogous isoforms of rat could be confirmed for the human isoforms. Furthermore an attempt can be made to attribute differing properties between the species to differences in sequence found in orthologous and parologous isoforms, especially since the measurements include the isoform MHC-I for both rat and human, for which only 14 non-conservative residue changes are reported.

### 6.4.1 Myosin extraction from single fibres and the identification of MHC isoforms

Single fibres of ca. 15 mm length were dissected from biopsies of human vastus lateralus muscles. Human biopsies were taken by R. Bottinelli's group in Pavia, Italy, in accordance with the ethical regulations for handling human tissue. Analogous to single fibre dissections from rat muscle a small part of the fibre (2mm) was used to identify the MHC isoform (see sections 6.3.2 and 4.6.3.2) and myosin was extracted from the rest of the fibre as described in sections 6.3.2 and 4.4.4.4. Single fibres yielded preparations of pure isoforms of MHC-I (28 %), MHC-IIA (42 %), MHC-IIX (3 %) and mixed isoforms (26 %). Fibres which did not contain a pure isoform were discarded. Since the fibres containing the pure MHC-IIX isoform were very rare in human the isoform was not considered for further investigation. The myosin yields from human fibres were similar to those from rat fibres.

### 6.4.2 ATP induced dissociation

The ATP dissociation measurement described in section 6.3.3 for rat isoforms was repeated for the two human isoforms (see Figure 6-8) and gave average values for $K_1k_{+2}$ of 0.18±0.02 $\mu M^{-1}s^{-1}$ and 0.26±0.02 $\mu M^{-1}s^{-1}$ for the isoforms MHC-I and MHC-IIA respectively (see Table 6-1). The averages were calculated from a series of measurements using at least 4 individual fibres for both myosin isoforms and the difference between the two is statistically significant.

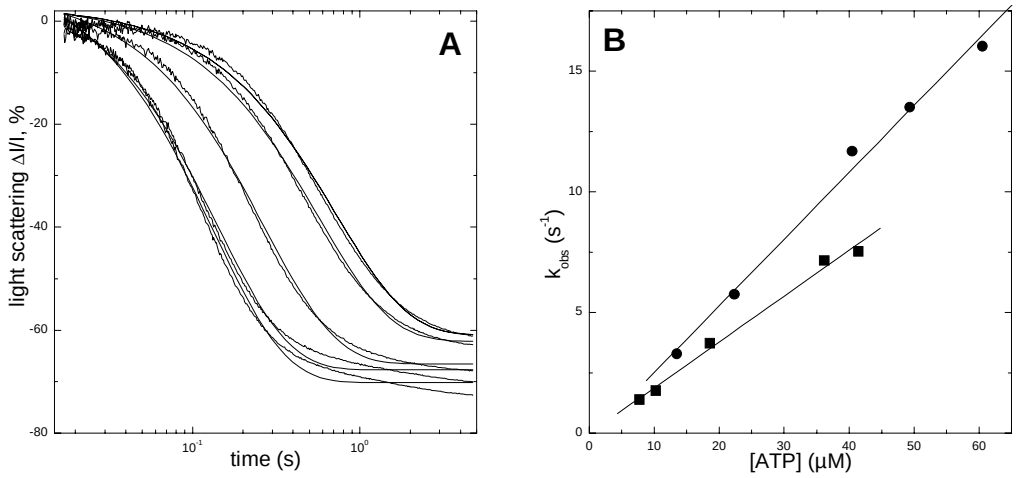


**Figure 6-8:** ATP induced dissociation of human myosin isoforms and actin

A) Light scattering signals from a 20 µl sample containing 0.5 µM actin, approx. 0.15 µM myosin (MHC-I), 0.5 mM cATP and apyrase in a multiple flash experiment. The best fit to a single exponential of the light scattering decrease is shown superimposed. Other conditions: experimental buffer containing 500 mM KCl, 20 mM MOPS, 5 mM $MgCl_2$ and 10 mM fresh DTT at pH 7.0 and 22°C.

B) The apparent rate constants of dissociation $k_{obs}$ for 2 different MHC-isoforms are plotted versus the amount of ATP released. The slope of a linear fit to each set of data from one isoform gives the second order rate constants ($K_1k_{+2}$) (• :MHC-IIA, 0.27 ± 0.01 $\mu M^{-1}s^{-1}$; • :MHC-I, 0.19 ± 0.01 $\mu M^{-1}s^{-1}$)

### 6.4.3 ADP affinity for the acto.myosin complex

The ATP dissociation measurement described in section 6.3.4 for rat isoforms was repeated for the two human isoforms (see Figure 6-9) and gave average values for $K_{AD}$ of 163±11 µM and 237±17 µM for the isoforms MHC-I and MHC-IIA respectively ( see Table 6-1). The averages were calculated from a series of measurements using 4 individual fibres for both myosin isoforms and the difference between the two is statistically significant.

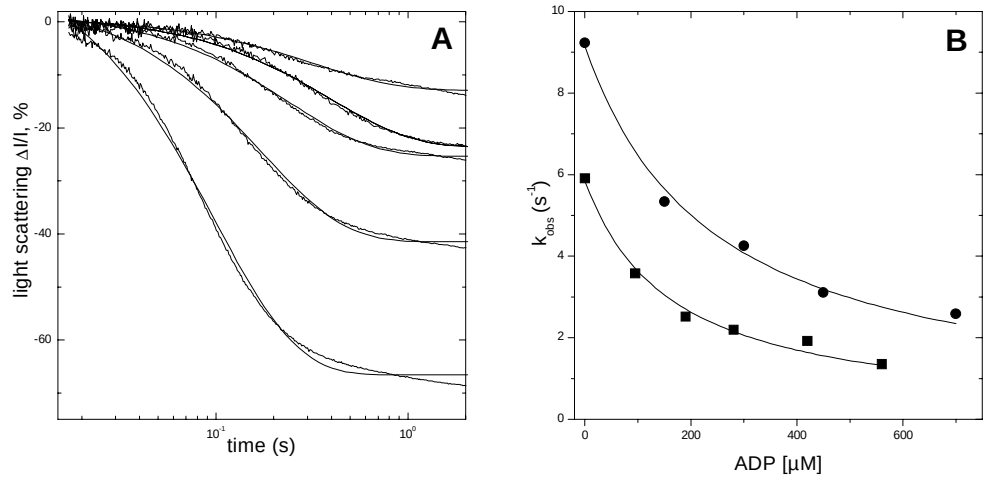


**Figure 6-9:** Determination of ADP affinity for acto.myosin with 2 human myosin MHC isoforms

A) Light scattering signals from a 20 µl sample containing 1 µM actin, approx. 0.75 µM myosin (MHC-IIA), 1 mM cATP, hexakinase, Ap5A and Glucose. During the multiple flash experiment the laser energy was kept constant to ensure a constant release of ATP (ca. 40 µM). A defined amount of ADP as well as a calculated amount of cATP to counteract the loss from the previous flash was added to the sample between flashes. The amplitude of the light scattering changes decreased with increasing ADP concentration. The best fit to a single exponential decay of the light scattering decrease is shown superimposed. Other conditions: experimental buffer containing 500 mM KCl, 20 mM MOPS, 5 mM MgCl2 and 10 mM fresh DTT at pH 7.0 and 22°C.

B) The plot shows the ADP dependence of $k_{obs}$ for each set of data from the 2 different MHC isoforms examined. The data were fitted to the model of Scheme 3-3 and gave values of $K_{AD}$ of 241±19 µM for MHC-IIA (• ) and 163±13 for MHC-I (• ).

## *6.5 The correlations between shortening velocity and kinetic values and the correction of the data for physiological conditions*

Both values $K_1k_{+2}$ and $K_{AD}$ increase in the isoform order MHC-I, MHC-IIA, MHC-IIX, MHC-IIB in rat and also in the isoform order MHC-I, MHC-IIA in human. The only exceptions are the MHC-IIX and IIB values for $K_1k_{+2}$ which do not differ significantly in rat. The values of these constants for rat MHCs increase in the same order as the values for shortening velocity of whole fibres of rat determined previously by Bottinelli *et al.* at 12°C (1994a; see Table 6-1). The values for human fibres are 1.15±0.36 L $s^{-1}$ and 2.37±0.34 L $s^{-1}$ measured at 20°C for MHC-I and MHC-IIA respectively (He et al., 2000). To compare the values the maximum shortening velocities of rat fibres need to be corrected for the difference in temperature. The $Q_{10}$ (factor for the change in shortening velocity for a change in temperature of 10°C) for $V_0$ in rat muscles is approximately 2 (Ranatunga, 1984). This predicts that values will be doubled at 22°C which is the temperature used in the kinetic measurements presented here (corrected $V_0$ values given in Table 6-2). Because of the small difference in temperature the shortening velocities of human fibres were not corrected. Figure 6-10 shows the correlation between $V_0$ and $K_{AD}$ and between $V_0$ and $K_1k_{+2}$.

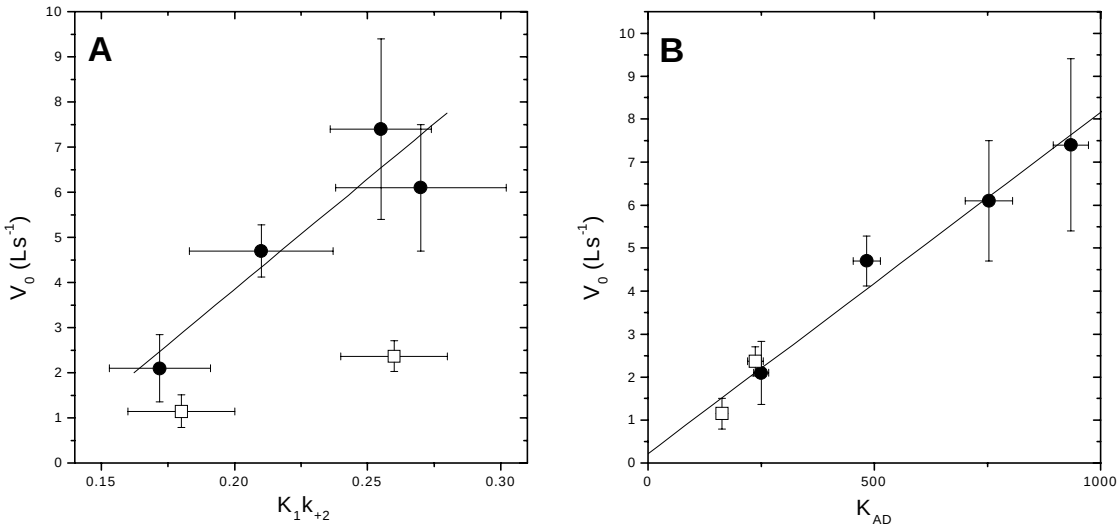


**Figure 6-10:** Correlation between shortening velocity and kinetic values of rat (●) and human (□) isoforms
A) The maximum shortening velocity ($V_0$) is plotted versus the second order rate constant of ATP induced dissociation ($K_1k_{+2}$). A linear fit to the rat values with a slope of 48±12 L μM and an intercept of -6±2.6 L $s^{-1}$ is superimposed.
B) The maximum shortening velocity ($V_0$) is plotted versus the ADP dissociation constant ($K_{AD}$). A linear fit to the rat values with a slope of 0.0074±0.0009 L $s^{-1}$ $\mu M^{-1}$ and an intercept of 0.5±0.6 L $s^{-1}$ is superimposed. The linear fit does not change significantly under inclusion of the human values.
The values for $V_0$ were taken from Bottinelli *et al.* (1994a) for rat fibres measured at 12°C and He *et al.* (2000) for human fibres measured at 20°C. The rat values of $V_0$ at 22°C were calculated from the 12°C data in Table 6-1 (see text). The human $V_0$ values were not further corrected.

It has been proposed that the net rate of detachment of acto.myosin cross bridges after completion of the power stroke limits the shortening velocity in muscle fibres. Of the main steps underlying the net rate of detachment, which are the release of ADP followed by the binding of ATP and subsequent detachment of myosin from actin, the release of ADP has been suggested to be the major determinant for the rate of cross bridge detachment (Siemankowski et al., 1985). The data shows that both the rate of ATP binding ($K_1k_{+2}$) and the affinity of ADP ($K_{AD}$) (which is related to the rate of ADP release) show good correlation with shortening velocity ($V_0$) for rat isoforms. However when the values for human isoforms are included, $K_1k_{+2}$ correlates less well, while $K_{AD}$ is still in good correlation with $V_0$. Although suggestive of an important role of $K_{AD}$ in determining shortening velocity, such a correlation does not establish whether either one of the steps actually determines shortening velocity alone or the relative contribution of each of them. In order to evaluate more carefully the contribution of these events to shortening velocity we must estimate $K_1k_{+2}$ and $K_{AD}$ values under the more physiological conditions used to measure shortening velocities and quantitatively compare them. This will also allow the comparison of $k_{-AD}$ which, as will be

suggested, can limit shortening velocity, with the value of $k_{min}$ (rate of the event limiting shortening velocity) estimated from the maximum shortening velocity of single muscle fibres.

In our experimental set-up, the binding of ADP to and dissociation from acto.myosin can be described as a fast equilibrium with rate constants ($[ADP]\bullet k_{+AD} + k_{-AD}$) more than 10 times faster than the rate of the following ATP induced dissociation of the acto.myosin complex ($[ATP]\bullet K_1k_{+2}$). Under those conditions the net rate of detachment is determined by Equation 3-5, which remains valid for all of our measurements where the ATP concentration is < 100 μM. In the cell the concentration of ATP is much higher and this fast equilibrium assumption for ADP binding may no longer be valid. Estimates of the ATP concentration in intact muscle fibre are in the range 4-8 mM (Kushmerick et al., 1992) and 5 mM was used in the $V_0$ measurements.

The values for $K_1k_{+2}$ and $K_{AD}$ were measured in solution using whole myosin and were therefore made at a concentration of 0.5 M KCl to keep the myosin soluble. Both $K_1k_{+2}$ and $K_{AD}$ values need to be corrected to the ionic strength of 0.14-0.17 M present in the fibre. In principle it would be possible to repeat the measurements with HMM or S1 and to work at physiological ionic strength. However, because of the very small amounts of myosin available, digestion of the protein would lead to unacceptable losses of protein. The corrections necessary can be estimated from a Debye-Hückel-plot for $K_{AD}$ and $K_1k_{+2}$ obtained using bulk preparations of skeletal myosin subfragment 1 (S1). Such measurements have been made for S1 from the back and leg muscle of the rabbit and for S1 isolated from rat soleus and Edl within the group by N. Adamek. The Debye-Hückel-plots (not shown) for $K_{AD}$ show a 3-7-fold decrease from 0.5 M to 0.1 M KCl which corresponds to an overall ionic strength of 0.14 M. For the same change of ionic strength $K_1k_{+2}$ is increased about 3-5 fold (White and Taylor, 1976). The effect of these corrections for $K_1k_{+2}$ at an ATP concentration of 5mM is shown in Table 6-2.

The rate of ADP binding to ($k_{+AD}$) and dissociation from ($k_{-AD}$) acto.myosin are too fast to be measured using the method described here. At the limit we know the sum ($[ADP]\bullet k_{+AD} + k_{-AD}$) is much greater than $[ATP]\bullet K_1k_{+2}$ which has measured values of up to 16 $s^{-1}$ (see Figure 6-8). Siemankowski and White (1984) calculated the binding rate of ADP to acto.myosin, $k_{+AD}$, (from measured values of $K_{AD}$ and $k_{-AD}$) to be $10^7$ $M^{-1}s^{-1}$. This is close to the value expected for a diffusion limited process. If we assume that ADP binding is a diffusion limited process and is therefore similar for all myosins then we can estimate the

dissociation rate constant from $k_{-AD} = K_{AD} \bullet k_{+AD}$. Thus, taking the corrected values of $K_{AD}$ we can calculate the values of $k_{-AD}$ at physiological ionic strength as given in Table 6-2.

Equation 6-1: $k_{min} = V_0 \bullet S_L \bullet d^{-1}$

The minimum value of the rate constant ($k_{min}$) of the event limiting shortening velocity ($V_0$) can be estimated from the half sarcomere length ($S_L$) and the myosin step size (d; Equation 6-1) (Siemankowski et al., 1985). The values of $V_0$ for rat were measured at 12°C and were corrected by a $Q_{10}$ for $V_0$ in rat muscles which is approximately 2 (Ranatunga, 1984) (corrected $V_0$ values given in Table 6-2). Because of the small difference in temperature, the shortening velocities of human fibres which were measured at 20°C were not corrected. The value of the half sarcomere length (1.35 µm) is that of the fibres used in the $V_0$ measurements by Bottinelli *et al*. (1994a) and the step size is assumed to be 5-10 nm. With these values $k_{min}$ can be calculated and the results are shown in Table 6-2. The values of $k_{min}$ and $k_{-AD}$ are similar for all six myosin isoforms, varying less than a factor of 2 in each case.

| | $V_0$ ($L\ s^{-1}$) | $K_1k_{+2}$ [ATP] ($s^{-1}$) | $k_{-AD}$ ($s^{-1}$) | $k_{min}$ ($s^{-1}$) |
|---|---|---|---|---|
| rat MHC-I | 2.1±0.74 | 3400±860 | 600±240 | 420±140 |
| rat MHC-IIA | 4.7±0.58 | 4200±1050 | 1150±460 | 940±310 |
| rat MHC-IIX | 6.1±1.4 | 5200±1300 | 1790±715 | 1240±420 |
| rat MHC-IIB | 7.4±2.0 | 5200±1300 | 2220±885 | 1490±500 |
| human MHC-I | 1.15±0.36 | 3600±900 | 390±155 | 230±77 |
| human MHC-IIA | 2.37±0.34 | 5200±1300 | 565±225 | 474±158 |

**Table 6-2:** Parameters contributing to shortening velocity
The values for $V_0$ were taken from Bottinelli *et al*. (1994ab) for rat fibres measured at 12°C and He *et al*. (2000) for human fibres measured at 20°C. The rat values of $V_0$ at 22°C were calculated from the 12°C data in Table 6-1 (see text). The human $V_0$ values were not further corrected. The rates of dissociation of acto.myosin at physiological salt conditions were calculated from the values of $K_1k_{+2}$ in Table 6-1 and section 6.4.2 and multiplied by a correction factor of 3-5 for the decrease in ionic strength and a concentration of 5 mM ATP as used in $V_0$ measurements. Numbers are quoted as the mean with range of possible values. The rate of ADP release under physiological salt condition was calculated by dividing the experimental values of $K_{AD}$ in Table 6-1 and section 6.4.3 by a correction factor of 3-7 for the decrease in ionic strength. This value was used in the equation $k_{-AD} = K_{AD} \bullet k_{+AD}$ with $k_{+AD} = 10^7\ M^{-1}s^{-1}$. Values are quoted as the mean with range of possible values. $k_{min}$ was calculated from values of $V_0$ at 22°C according to equation 2 with $S_L$ = 1.35 µm and d = 5-10 nm.

### *6.6 Sequence analysis*

The various isoforms of rat and human which were investigated clearly showed significantly different mechanical and kinetic properties. The shortening velocity as well as the rate of ATP induced dissociation and the release of ADP were faster in the order MHC-I, IIA, IIX and IIB in rat and the human isoforms were slower than the corresponding (orthologous) rat isoforms. These differences are to a large extent attributed to the sequence differences of the myosin heavy chains of the isoforms. It is therefore of great interest to analyse the differences between the sequences.

The motor domain is highly conserved for most myosins. There are however highly diverse surface loops connecting the 25 kDa and the 50 kDa domain (loop 1) and the 50 kDa and the 20 kDa (loop 2) domain. These loops vary between the isoforms within a species (parologous) in length, charge and number of proline residues which can make the loop more rigid. Changes in both loops are believed to influence mechanical properties of the myosin (Goodson et al., 1999): loop 1 the speed of actin translation (Spudich, 1994) and loop 2 the ATPase activity (Uyeda et al., 1994).

The human sequences are all known and have been compared by Weiss *et al.* (1999). These show ~90% identity between the three MHC-II sequences and 80% identity comparing MHC-I and II(s). There are, for example, 99 non-conservative changes of which 58 are located in the motor domain found between parologous human isoforms MHC-I and MHC-IIA. This includes changes in both loops which alter the charge and the number of proline residues. In comparison, corresponding orthologous isoforms between species are better conserved. Currently only the MHC-I isoform of rat is in the databases (SWISSPROT; EMBL) and it shows only 14 non-conservative changes compared to human MHC-I of which 11 are located in the motor domain (see Figure 6-11). None of those changes are located in either loop 1 or loop 2. However there are 3 changes in the area of the secondary actin binding loop (loop 3, see section 1.5.3.2). According to Van Dijk *et al*. (1999) changes in this loop can modulate binding of myosin to actin but not ATPase activity. Given the significant difference in mechanical and biochemical properties between these isoforms a further investigation of the 14 changes in sequence becomes interesting (Canepari et al., 2000).

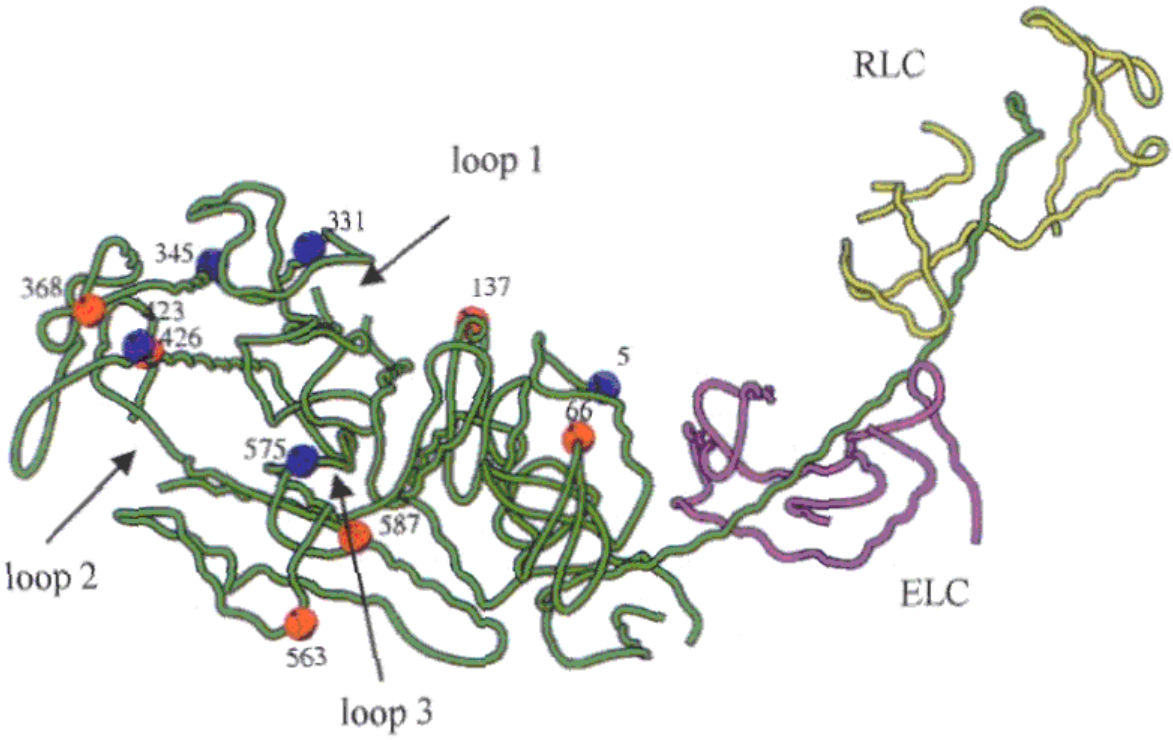


**Figure 6-11:** Localisation of the 11 non-conservative changes between human and rat MHC-I isoform in the motor domain. Non-conservative residues are shown as spheres on the 3D structure of chicken skeletal myosin (Rayment *et al*., 1993). The numbers of the corresponding residues in the figure display their position in chicken skeletal muscle which differs from the numbering in rat muscle. Red spheres indicate substitutions where residues in rat MHC-I are similar to residues in fast type MHCs (Canepari et al., 2000)

The first substitution is at residue 4 at the very beginning of the MHC, the second is located at residue 65 in the SH3 region. The following 3 substitutions (136; 329; 343) are all near the nucleotide binding pocket and might therefore influence ATP binding and ADP release. The next substitution (366) is in a region to which no functional role is attributed. The substitutions at positions 421 and 424 are in an α-helix which connects two functional regions involved in actin binding, the cardiomyopathy surface loop (403-413)(Geisterfer-Lowrance *et al*., 1990, see section 1.5.3.2) and a hydrophobic actin binding domain (527-553). These are followed by the 3 substitutions in the loop 3 area (561; 573; 585). At residue 573, located in loop 3, a glutamine in rat is replaced by a proline in human increasing the rigidity of the loop which might have a strong effect on the actin binding kinetics. Two more substitutions (845; 857) are located in the proximal S2 domain which is believed to modulate the flexibility of the head-tail junction and the last substitution is in the tail region (1275).

| Residue | 4 | 65 | 136 | 329 | 343 | 366 | 421 | 424 | 561 | 573 | 585 | 845 | 857 | 1275 |
|---|---|---|---|---|---|---|---|---|---|---|---|---|---|---|
| MHC-I rat | R | N | A | H | P | Q | A | I | N | Q | T | T | G | R |
| MHC-I human | S | Y | P | L | S | L | I | T | A | P | I | R | T | S |
| MHC-α rat | A | N | A | L | A | Q | Y | I | N | Q | T | T | G | T |
| MHC-α human | A | N | A | L | S | Q | Y | I | N | P | T | T | G | T |
| MHC-IIB human | D | A | P | L | A | Q | Y | V | N | P | T | T | E | A |
| MHC-IIX human | D | A | A | L | S | Q | Y | V | N | P | T | T | E | A |
| MHC-IIA human | D | G | P | L | N | Q | S | V | A | A | V | T | Q | A |

**Table 6-3:** Non-conservative sequence changes between MHC-1 in rat and human (Canepari et al., 2000) The corresponding residues in MHC-α and human skeletal MHC-II isoforms are also listed. Compared sequences were taken from McNally *et al*. (1989) for rat MHC-I and α; Liew *et al*. (1990) for human MHC-I and α and Weiss *et al*. (1999) for human MHC-IIA, IIX and IIB.

As shown in Table 6-3: 8 out of the 14 changes in rat MHC-1 have the same residue as in the faster rat and human cardiac MHC-α and in some positions the faster human skeletal isoforms MHC-II. This makes these substitutions potential candidates to modulate the overall speed.

## *6.7 Discussion*

As shown in the example of rat Edl and soleus, myosins from fast and slow muscle have different kinetic properties. The properties of the muscle types can to a large extent be attributed to the content of myosin heavy chain isoforms which is always mixed in bulk mammalian muscle. In contrast to bulk muscle, single muscle fibres often contain pure MHC isoforms. However the amounts which can be extracted from a single fibre are not sufficient to characterise the myosin by traditional methods such as stopped flow and to date no satisfactory over-expression system exists for mammalian skeletal muscle myosin which might yield higher amounts of protein. Using the flash photolysis method it was possible to measure myosins extracted from single muscle fibres. Separate extractions yielded all four skeletal muscle myosin heavy chain isoforms of adult rat and two major isoforms of human. From these preparations the rate of ATP induced dissociation of and the ADP affinity for the acto.myosin complex could be determined for each isoform.

About 2-3 µg pure myosin isoforms could be obtained from 15 mm single fibres of rat psoas (MHC-IIB, MHC-IIX) and soleus (MHC-I and MHC-IIA) and human vastus lateralus (MHC-I and MHC-IIA) muscles. This amount is sufficient to determine the second order rate constant of ATP induced dissociation with the flash photolysis apparatus while it would be too small an amount to obtain results from traditional stopped flow methods for which an

amount of 10 µg is needed for a single measurement (Kurzawa and Geeves, 1996). High ADP concentrations weaken the affinity of myosin for actin and decrease the dissociation signal. The amount of protein from one fibre is therefore not sufficient to measure the ADP affinity to acto.myosin over a wide range of ADP concentrations. For this experiment a higher myosin concentration is needed. 5 fibres for which the same isoform type had been confirmed by electrophoresis were pooled and the myosin extracted. The total amount of protein used is still far less than would be needed using traditional methods.

Our results for both the rate of ATP induced dissociation of acto.myosin and the ADP affinity for acto.myosin are well defined. The values were highly reproducible, showing both the effectiveness of the flash photolysis method for the measurement with small amounts of acto.myosin, as well as the dependence of these values on the myosin heavy chain isoform. The confidence in this data from single fibre extractions is very high, not only because of the high reproducibility, but also because similar results were obtained from bulk muscle preparations with mixed isoforms in flash photolysis. These results in turn could be confirmed in stopped flow measurements which differ only in the slightly higher observed rate constants generally determined by this method (see section 5.14).

In rat, both values $K_1k_{+2}$ and $K_{AD}$ increase in the isoform order MHC-I, MHC-IIA, MHC-IIX, MHC-IIB. The only exceptions are the MHC-IIX and IIB values for $K_1k_{+2}$ which do not differ significantly. Also in human the values $K_1k_{+2}$ and $K_{AD}$ increase from MHC-I to MHC-IIA.

The values for these constants increase in the same sequence as the values for unloaded shortening velocity and ATPase activity of whole fibres determined previously by Bottinelli *et al.* (1994ab; 1996), Canepari *et al*. (2000) and He *et al.* (2001). Looking at the data from rat muscle alone, both $V_0$ and $K_{AD}$ as well as $V_0$ and $K_1k_{+2}$ seem to correlate (see Figure 6-10). However when the data from human muscle is added, $V_0$ and $K_1k_{+2}$ correlate less well while the plot of $V_0$ versus $K_{AD}$ still shows a good correlation. Whether this correlation indicates a causality between the values needs to be discussed further.

It is believed that the net rate of detachment of acto.myosin cross bridges after completion of the power stroke limits the overall cross bridge cycle and therefore the shortening velocity in muscle fibres. Siemankowski and White (1985) proposed that of the main steps underlying the net rate of detachment which are the release of ADP followed by the binding of ATP and subsequent detachment of myosin from actin the release of ADP is the major determinant for the rate of cross bridge detachment. To prove this hypothesis for a closely related system of fast muscle we needed to correct our data to physiological conditions including a

physiological ionic strength of 0.14 M and an ATP concentration of 5 mM in fibres (Kushmerick et al., 1992). These corrections are discussed in detail in section 6.5. Under these conditions, the binding and dissociation of ADP can no longer be treated as a preceding equilibrium as it was under experimental conditions. In this case ADP has to be released from acto.myosin before ATP can bind and dissociate the complex. The rate of ADP dissociation is too fast to be measured in the experiments for the myosins used, it could however be calculated from $K_{AD}$ under the assumption that the binding of ADP is a diffusion limited process with a rate of $10^7$ $M^{-1}s^{-1}$ and the same for all myosins (Siemankowski and White, 1984).

Siemankowski *et al.* (1985) proposed that the minimum value of the rate constant ($k_{min}$) of the event limiting shortening velocity ($V_0$) can be estimated from the half sarcomere length ($S_L$) and the myosin step size (d; Equation 6-1). To match the conditions of my experiments the rat values for the maximum shortening velocity were corrected for 22°C to calculate $k_{min}$. The corrected values for the maximum shortening velocity ($V_0$), the rate of ATP induced dissociation ($K_1k_{+2}$ • [ATP]), the rate of ADP dissociation from the complex ($k_{-AD}$) and the theoretical rate constant limiting the shortening velocity ($k_{min}$) for 4 MHC isoforms of rat and 2 MHC isoforms of human are shown in Table 6-2. All corrections and calculations leading to these values are described in detail in section 6.5.

Debye-Hückel plots made to correct for the different salt concentrations are not well defined and also seem to vary from muscle type to muscle type and for different species. Likewise slight differences in the Q10 for the temperature corrections of $V_0$ have been observed for different species. Also the value for the ADP binding rate is an estimate based on the assumption that it is a diffusion limited process and therefore should be the same for ADP binding to all fast myosins. Furthermore, the maximum axial cross bridge translation has been described by values of 5-10 nm. These uncertainties are accounted for by large errors on the values in Table 6-2, which should be seen as estimates.

Within the limits of the measurements and corrections made here the agreement between the values of $k_{min}$ and $k_{-AD}$ is remarkably close for all four rat and the two human myosin isoforms, varying by less than a factor of 2 in each case. The results are therefore compatible with the rate of ADP release limiting the shortening velocity for the six muscle fibres as predicted by Siemankowski *et al.* (1985).

Under physiological conditions the concentration of ATP is of the order of 5 mM thus the rates of ATP binding and actin dissociation, $[ATP]•K_1k_{+2}$, are approximated as shown in

Table 6-2. Taking the mid range values of $[ATP]\bullet K_1k_{+2}$, these are approximately 4 fold faster than $k_{min}$ for all MHC-II isoforms and 8 fold faster for MHC-I in rat. In the two human isoforms investigated they are greater than 10-fold faster. Thus it is clear that $[ATP]\bullet K_1k_{+2}$ is unlikely to contribute to $k_{min}$ for the MHC-I isoform of rat and the human isoforms, but the situation is not clear-cut for the faster isoforms of rat. At the lower limits of the estimated range, the ATP binding step could be a significant contributor to $k_{min}$ and is of the same order as $k_{-AD}$. It is of interest to note that differences in $K_1k_{+2}\cdot[ATP]$ and $k_{AD}$ are smallest for the fastest rat MHC-IIB isoform (2.5 fold) and largest for the slow rat MHC-I (5.5 fold) as well as the slow human isoforms (10 fold). Thus, any significant drop in the concentration of ATP (or an increase in the competing free [ADP]) could result in a slowing of acto.myosin dissociation and a decrease of $V_0$ for the fastest isoforms. Interestingly the maximum shortening velocity ($V_0$) of fast fibres has been shown to be more affected by a decrease in the ATP concentration than $V_0$ of slow fibres (Pate et al., 1992). It is possible that a small difference between $K_1k_{+2}\cdot[ATP]$ and $k_{AD}$ is a contributor to fatigue-induced loss of muscle performance, which is more marked in fast muscles.

This result demonstrates that for 6 closely related muscle myosins in which the shortening velocity varies by 6-7 fold, the primary controlling factor is likely to be the rate at which ADP can escape from the cross bridge after completion of the power stroke. This view is also supported by the fact that the human MHC-I isoform, which has a much slower shortening velocity than the rat isoform, has the same value for $K_1k_{+2}$ as the rat isoform, but a significantly lower value for $K_{AD}$. A contribution from ATP dissociation of the cross bridge remains possible for the fastest isoforms. It is of interest to note the ATP induced dissociation varies by less than 2 fold between the 6 myosin types compared to an about 6 fold variation in both $k_{min}$ and $k_{-AD}$. The increase of the ATP induced dissociation rate for the faster myosins has previously been reported for different muscle types of chicken muscle (Marston and Taylor, 1980). It appears that this step must remain faster than the preceding ADP release step but its precise value does not correlate as closely with the shortening velocity.

It may not be surprising that both ATP binding and $K_{AD}$ show a similar (but not identical) dependence on myosin isoform since both nucleotides are binding to the same pocket. Thus, changes in sequence which result in changes of the biochemical environment of the nucleotide binding pocket that lead to a faster ADP release may also produce faster binding of ATP. This is however contradicted by comparison of orthologous rat and human isoforms where human isoforms have a lower $K_{AD}$ but $K_1k_{+2}$ remains unchanged, in the case of MHC-I, or even

increases, in the case of MHC-IIA. This behaviour supports the view that the ADP release step determines the overall speed of shortening rather than the ATP induced dissociation.

Although early studies by Barany (1967) suggested a strong correlation between the shortening velocity and the ATPase activity, the release of ADP from the cross bridge is clearly too fast to limit ATPase activity. Values for the ADP release are at least 30 times higher than the ATPase activity (turnover number) during unloaded shortening. This is because only a fraction of myosin heads undergo a cross bridge cycle at any given time. Only these are contributing to the shortening velocity, which is therefore directly related to the rate limiting step of ADP release while the ATPase is calculated over the total concentration of myosin. A myosin head has to bind actin before it can go through the cross bridge cycle. The binding and dissociation of the myosin.ADP.Pi complex to actin therefore forms a preceding equilibrium to the rest of the cross bridge cycle. Under the experimental conditions, as well as in the fibre during unloaded shortening velocity, this equilibrium is on the dissociated side. The speed of the ATPase can be described by a classical Michaelis-Menten kinetic (see section 3.2.3). The complex kinetic scheme of the cross bridge cycle, including intermediate steps between actin binding and ADP release, makes both the Michaelis-Menten constant and the maximum reaction rate constant, complex constants involving the rates of the intermediate steps for which the rate constants are not determined.

In the overall ATPase cycle the flux (i.e. the steady-state rate of ATP comsumption) through all steps is equal. For a step which can be considered irreversible the flux is given by the forward rate constant multiplied by the concentration of the reactants. Therefore the ATPase activity (i.e. the turnover number, which is the steady-state rate divided by the total concentration of myosin, $[M_{total}]$) is equal to the rate of the step multiplied by the occupancy (i.e. the occupancy being the concentration of the reactants of that step divided by the concentration of the total concentration of myosin, $[M_{total}]$).

**Equation 6-2: ATPase activity = Flux/$[M_{total}]$ = $k_{-AD} \cdot [A.M.ADP]/[M_{total}]$**

The occupancy of the species preceding the ADP release , the complex acto.myosin.ADP, can be calculated according to Equation 6-2 by division of the ATPase activity by the rate of ADP release. In Table 6-4 this ratio has been calculated for the 2 human isoforms. ATPase activity values were taken from a study by He *et al* (2000) and were measured at 20°C. For rat fibres the data on ATPase activity is limited to measurements of shortening velocities below the unloaded maximum shortening velocity, which were perfomed at 12°C. Since a reliable

extrapolation of this data for a temperature of about 22°C and maximum shortening velocity is not possible no attempt at calculating the occupancy of the acto.myosin.ADP complex has been made.

| | ATPase activity ($s^{-1}$) | $k_{-AD}$ ($s^{-1}$) | ATPase/$k_{-AD}$ (%) |
|---|---|---|---|
| human MHC-I | 5.4 | 390 | 1.4 |
| human MHC-IIA | 13.9 | 565 | 2.5 |

**Table 6-4:** Calculation of the ratio of myosin heads undergoing a cross bridge cycle during unloaded shortening velocity. The ATPase activity values were taken from He *et al*. (2000). The values for $k_{-AD}$ were taken from Table 6-2.

If the ADP release rate is rate limiting for the shortening of the fibre as suggested here, the acto.myosin.ADP complex is the predominant tension bearing species. The occupancy of this species is equivalent to the fraction of cross bridges in a strongly attached state at any given time and hence gives the duty cycle ratio. Relating the rate of ADP release to the ATPase activity is therefore an alternative way to calculate the duty cycle ratio. This ratio was previously determined, in shortening velocity/ATPase or in *in vitro* motility/ATPase measurements, by division of the distance travelled per hydrolytic cycle by the distance of the working stroke (He et al., 2000; Reggiani et al., 1997). The values obtained from these measurements are of the same order of magnitude and in both cases a higher duty cycle ratio was calculated for fast isoforms compared to slow isoforms. However, given the large errors on both values, the $k_{-AD}$ and the ATPase activity, the difference of a factor of 2 in the duty cycle ratio between fast and slow isoforms is not significant. For the shortening of fibres bearing a load both the shortening velocity and the ATPase activity decrease while the duty cycle ratio is known to increase significantly (He et al., 2000). Therefore the rate of ADP release must decrease with increasing load.

Several comparisons between myosin isoforms have highlighted Loop1 (on the myosin surface at the entrance to the nucleotide pocket) as responsible for modulating ADP affinity to acto.myosin and velocity seen in either the muscle fibre shortening or in *in vitro* motility assays (Spudich, 1994). These include scallop striated and catch muscle myosin (Kurzawa-Goertz *et al*., 1998) and the phasic and tonic isoforms of smooth muscle myosin (Rovner et al., 1997; Sweeney et al., 1998) in addition to artificial myosin constructs (Uyeda et al., 1994). It is therefore of interest to consider the changes in sequence which produce these changes in the properties of the rat striated muscle myosin isoforms. Unfortunately the sequences of the MHC-II rat isoforms are not currently in the database and only the MHC-I

sequence is known. However, given that the MHC-I sequences are heavily conserved between rat and human a similar conservation maybe expected in the MHC-II sequences. The human sequences are all known and have been compared by Weiss *et al.* (1999). These show ~90% identity between the three MHC-II sequences and 80% identity comparing the MHC-I and II. Surprisingly, although there are changes in sequence in Loop 1 between MHC-I and II, the sequence of Loop I is well conserved among the three MHC-II myosins and it may be necessary to look for more subtle changes in structure to account for the 2 fold changes in $V_0$ and $K_{AD}$ reported here. The comparison between the human and rat MHC-I isoforms gives further evidence that major modulation of mechanical and biochemical properties can not be attributed only to changes in loop 1 or loop 2, since no non-conservative changes can be found in this region. However 3 of 14 non-conservative changes are found in the secondary actin binding loop (loop 3, see section 1.5.3.2) which hints towards an influence of that region on the speed of the isoform. Considering the changes in ADP affinity and the proposed actin binding function of loop 3, it might play an important role in the coupling of ADP and actin affinity and therefore the actin activation of the myosin ATPase function. It is however curious that previous studies in which a mammalian loop 3 was inserted into a *Dictyostelium* myosin proved that loop 3 influences the actin binding affinity, but not the ATPase function, which would have supported the hypothesis suggested here (Van Dijk et al., 1999). On the other hand, changes in other surface loops are known to change the ATPase function and especially the ADP release, along with a change in actin binding properties (De La Cruz *et al*., 2001; Goodson *et al*., 1999; Kurzawa-Goertz *et al*., 1998; Uyeda *et al*., 1994). Like the substitutions in loop 3, several other substitutions in rat MHC-1 have the same residue as in the faster rat and human cardiac MHC-α, and in some positions the faster human skeletal isoforms MHC-II, indicating that they might also be influential. Interestingly, only the ADP affinity or ADP release is modulated but not the ATP induced dissociation as in the 4 isoforms of rat which also have more fundamental changes in sequence. It seems that a correlation of sequence and properties is far more difficult than initially suggested and various substitutions located all over the myosin motor domain might be influential on the properties, instead of just changes in a few specific domains like loop 1 and loop 2. This would also make sense from an evolutionary point of view, as various isoforms were designed for different purposes and then minor changes evolved in the orthologous isoforms to adapt the muscle proteins to a specific species.

To support such speculations, more knowledge of the sequence and functional diversity of mammalian isoforms needs to be obtained. The most direct way to such information would be

the mutational analysis of the differences in isoform sequences by replacing amino acids in question. However since currently no *in vitro* expression system for muscle myosin is available this approach is not possible. Therefore further investigation is limited to either the elucidation of missing sequences of mammalian isoforms or the functional characterisation of isoforms for which the sequence is already known. For this study especially, the sequences of the fast skeletal isoforms of rat (MHC-IIA, IIX and IIB) would be of high interest. The sequences for MHC-I of pig and mouse are known and kinetic experiments with these isoforms as well as the determination of shortening velocity of fibres of that type are planned to continue and complement the work presented in this thesis.

In conclusion we have confirmed the hypothesis proposed by Siemankowski *et al.* (1985) for this closely related set of rat and human MHC isoforms and that ADP release can provide the limiting molecular event which limits shortening velocity. It has been estimated that under physiological conditions the rate of the ATP induced dissociation of A.M remains up to 2-10 fold faster than the preceding step of ADP release from A.M.D. Further information on the sequence differences between the rat MHC isoforms will be required to understand how the ADP release rate is modulated by the myosin structure. The comparison between rat and human isoforms hints towards a few specific changes which strongly influence the properties of an isoform but also suggests a possible different form of modulation between parologous and orthologous isoforms.

### *6.8 Summary*

To understand mammalian skeletal myosin isoform diversity pure myosin isoforms of the four major skeletal muscle myosin types (myosin heavy chains: MHC-I, IIA, IIX and IIB) from single rat muscle fibres and two from human single fibres (MHC-I, IIA ) were extracted. The extracted myosin (~2 μg/ 15 mm length) was sufficient to define the acto.myosin dissociation reaction with the flash photolysis method. The ADP inhibition of the dissociation reaction was also studied to give the ADP affinity for acto.myosin ($K_{AD}$). The apparent second order rate constant of acto.myosin dissociation gets faster ($K_1k_{+2}$ = 0.17 - 0.26 $\mu M^{-1}.s^{-1}$) while the affinity for ADP is weakened (250 - 930 μM ) in the isoform order I, IIA, IIX, IIB in rat. The values of 0.18 and 0.26 $\mu M^{-1}s^{-1}$ for $K_1k_{+2}$ and 163 and 237 μM for $K_{AD}$ of human isoforms MHC-I and IIA increased in the same order. Both sets of $K_{AD}$ values correlate well with the measured maximum shortening velocity ($V_0$) of the parent fibres. If the value of $K_{AD}$ is controlled largely by the rate constant of ADP release ($k_{-AD}$) then the estimated value of $k_{-AD}$ is sufficiently low to limit $V_0$. In contrast $[ATP]\cdot K_1k_{+2}$ at 5 mM ATP would be 2.5-10 times faster than $k_{-AD}$ and would thus only contribute to $V_0$ if the [ATP] drops well below 5 mM. An alignment of the sequences shows that the mechanical and biochemical properties of orthologous isoforms can be influenced by substitutions of a few residues which do not need to be in either loop 1 or loop 2. The more fundamental changes, including in loop 1 and 2, in parologous isoforms, however, point towards a wider variety of changes which might cause modulation of the properties.

# 7 Biochemical characterisation of myosin XIV from *Toxoplasma gondii*

## *7.1 Introduction*

The phylum of *Apicomplexa* mainly consists of medically and economically important pathogens infecting humans and animals. These obligate intracellular parasites actively penetrate host cells in a few seconds by squeezing through a moving junction formed between the host cell and the parasite plasma membrane. Parasite replication then occurs within a parasitophorous vacuole. Gliding motility by *T. gondii* tachyzoites, and *Plasmodium* species sporozoites has proven to be an essential component of the invasion process (Sibley et al., 1998; Sultan et al., 1997). This unusual form of motility is not generated by the action of cilia or flagella but is likely to be driven by the capping of surface adhesin complexes towards the posterior pole of the parasite. These adhesin complexes establish a tight interaction with host cells and via the cytoplasmic tail of their transmembrane subunits a direct or indirect connection with the acto.myosin system of the parasite (Dobrowolski and Sibley, 1996; Kappe et al., 1999). Time-lapse video microscopy of gliding revealed that *T. gondii* moves at a speed of 1-3 μm/s, based on a combination of three major modes of locomotion involving one or more myosin motor(s) (Hakansson et al., 1999). One of these myosin motors, TgMyoA, features highly unusual structural differences compared to all other known classes of myosin and is part of a separate class XIV within the superfamily of myosins. The structural differences include a highly divergent converter domain and an extremely short neck and tail region without clearly identifiable IQ-motifs. Five class XIV myosins have been identified so far in *T. gondii* (TgMyoA to E) (Heintzelman and Schwartzman, 1997; Hettmann et al., 2000; Delbac *et al*., unpublished results) and close homologues are present in the genomes of *Plasmodium* (Heintzelman and Schwartzman, 1997; Hettmann et al., 2000; Pinder et al., 1998), *Eimeria*, and *Theileria* (unpublished observations by D.Soldati) but have not been found in higher organisms. TgMyoA is an essential protein and localises beneath the plasma membrane, making it a prominent candidate to transmit mechanical energy into forward motion, propelling the parasite into the host cell (Hettmann et al., 2000). To power the gliding needed for effective and fast host invasion the motor(s) involved is expected to be a fast motor like skeletal muscle myosin, which is designed for fast motility rather than the production of a large force over a longer time period or keeping tension. However TgMyoA, like all other class XIV myosins described so far, exhibits a very unusual amino acid sequence

that pertinently questions its ability to fulfil such a function. In this study TgMyoA was characterised kinetically and together with results from collaborating laboratories an attempt is made to elucidate the properties which make this unusual myosin work.

## *7.2 Preparation of the myosin XIV TgM-A from Toxoplasma gondii*

Full length TgMyoA and TgMyoAΔtail (a mutant lacking 53 C-terminal residues) were purified from recombinant parasites as described in section 4.4.5. Parasites were grown and the myosin prepared by Angelika Herm in Dr. D. Soldati's lab at the ZMBH Heidelberg. 250 µg TgMyoAΔtail could be purified from $10^{10}$ parasites. The yields for full length TgMyoA were much less (30 µg) due to the low solubility of the full length protein. Native TgMyoA is a monomer, as predicted by the absence of a coiled-coil domain in the tail and confirmed by glycerol gradient centrifugation (data not shown)

## *7.3 Kinetic characterisation*

### 7.3.1 ATP induced dissociation

Binding of ATP causes fast and irreversible dissociation of the acto.myosin complex. The rate constant of the ATP induced dissociation of TgMyoAΔtail from rabbit actin was determined in the stopped flow by mixing 400/200 nM acto.myosin complex with ATP concentrations in the range 5 µM – 50 µM (see Figure 7-1).

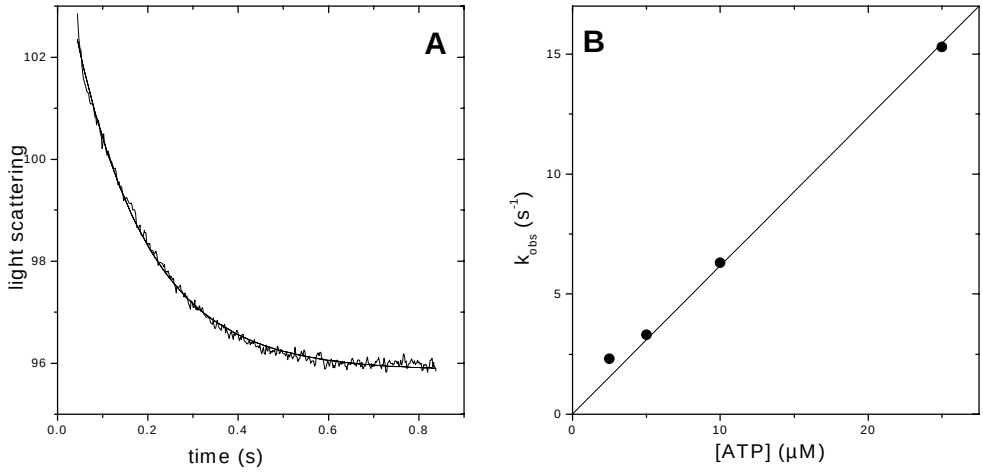


**Figure 7-1:** ATP induced dissociation of the acto.TgMyoAΔtail complex in stopped flow.
A) 400/200 nM TgMyoAΔtail and 400/200 nM actin were mixed with 20/10 µM ATP. The decrease in light scattering monitors the ATP induced dissociation of the acto.myosin complex. A single exponential fit is superimposed and gives an apparent rate constant of $k_{obs}$ of 6.3 $s^{-1}$ for the reaction.
B) The experiment was repeated with a variety of ATP concentrations. The plot of $k_{obs}$ vs. [ATP] is linear and the linear regression results in an apparent second order rate constant of 0.62±0.02 $\mu M^{-1}s^{-1}$.
Other conditions: experimental buffer containing 100 mM KCl, 20 mM MOPS, 5 mM $MgCl_2$ at pH 7.0 and 20°C.

The experiment was performed in experimental buffer containing 100 mM KCl; 20 mM MOPS; 5 mM $MgCl_2$ at pH 7.0 and 20°C. Unlike any other myosin so far examined TgMyoA (and TgMyoAΔtail) did not quench the fluorescence of a pyrene label covalently attached to actin. Therefore, the dissociation of the complex could be analysed only by light scattering (Scheme 3-2) requiring a higher protein concentration than fluorescence measurements in stopped flow. A single exponential could be fitted to the decrease in light scattering for each reaction giving the observed exponential rate constant ($k_{obs}$). A plot of $k_{obs}$ vs. [ATP] was linear over the range of concentrations used and the slope of the linear regression defines the apparent second order rate constant $K_1k_{+2}$ = 0.6 $\mu M^{-1}s^{-1}$ (Equation 3-4).

The measurement of the apparent second order rate constant was repeated in a typical multiflash experiment in the flash photolysis apparatus (see section 5.6). Samples contained 1 µM TgMyoAΔtail, 1 µM phalloidin stabilised actin and 0.5 mM cATP, 10 mM DTT, 10 µg/ml apyrase in 130 mM KCl experimental buffer. A very similar result was obtained by releasing ATP into the pre-mixed sample by flash photolysis of caged ATP. Releasing a range of ATP concentrations (8 µM – 50 µM) the second order rate constant $K_1k_{+2}$ was 0.4 $\mu M^{-1}s^{-1}$.

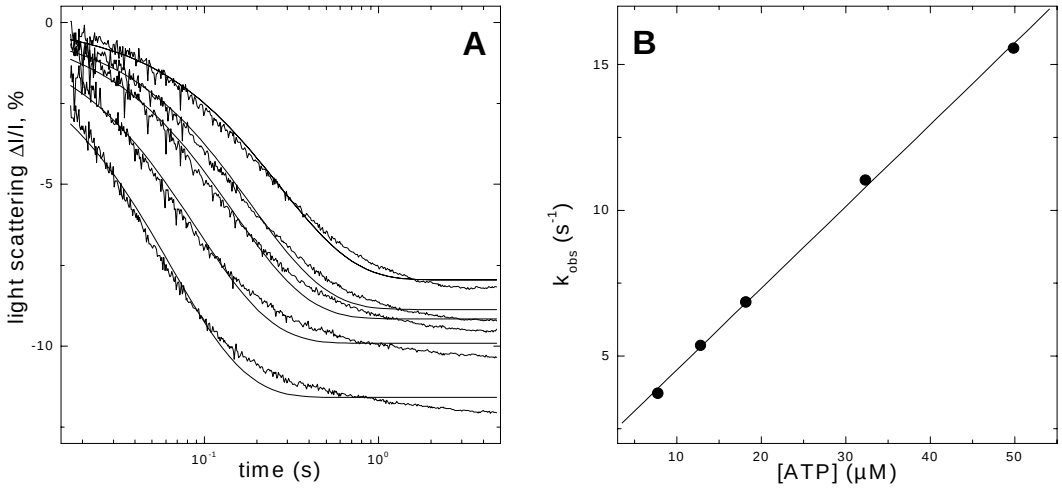


**Figure 7-2:** ATP induced dissociation of actin and full length TgMyoA in flash photolysis
A) Light scattering signals from a 20 µl sample containing 0.5 µM actin, 1 µM TgMyoA, 0.5 mM cATP and apyrase in a multiple flash experiment. The best fit to a single exponential decay of the light scattering decrease is shown superimposed.
B) The observed rate constants of dissociation $k_{obs}$ are plotted versus the concentration of ATP released. The slope of a linear fit to each set of data from one isoform gives a second order rate constant ($K_1k_{+2}$) of 0.28±0.005 $\mu M^{-1}s^{-1}$. The intercept was 0.17±0.2 $s^{-1}$.
Other conditions: experimental buffer containing 130 mM KCl, 20 mM MOPS, 5 mM $MgCl_2$ and 10 mM fresh DTT at pH 7.0 and 22°C.

Too little full length TgMyoA was yielded to define the second order rate constant in stopped flow measurements. The amount was however enough for this value to be determined in a multiflash flash photolysis experiment (see Figure 7-2). Experiments were performed under the same conditions and with the same concentrations as for TgMyoAΔtail. The second order rate constant $K_1k_{+2}$ was 0.28 $\mu M^{-1}s^{-1}$ for the full length TgMyoA. Both TgMyoAΔtail and full length TgMyoA gave smaller light scattering signal amplitudes in flash photolysis than skeletal muscle myosin in comparable amounts. Furthermore deviations of the light scattering transients for a single exponential reaction kinetic suggests a significant error on the values obtained. However the quality of the data is sufficient to give an estimate and to establish that the values for TgMyoAΔtail and full length TgMyoA are of the same order. The clear linear dependency of $k_{obs}$ on the concentration of ATP gives confidence in this estimate while the relatively high intercept, which is expected to be 0, may be an indication of a systematic error in the fitting process. The reason for the stronger deviations from single exponential reaction kinetics compared to skeletal muscle myosins might be due to a more pronounced gelation of proteins in the presence of TgMyoA.

### 7.3.2 ADP affinity for acto.myosin

The stopped flow dissociation experiments were repeated by mixing the solution of a 400/200 nM acto.TgMyoAΔtail complex with solutions containing a constant ATP concentration of 50/25 µM and increasing amounts of ADP (0 µM – 2 mM). $k_{obs}$ decreased as the ADP concentration increased as a result of the competition between ATP and ADP binding to acto.TgMyoA and the data can be described by a hyperbola (see Scheme 3-3 and Equation 3-5). This suggests that ADP is in rapid equilibrium with acto.TgMyoA on the time scale of the measurement and analysis of the hyperbola defines the ADP affinity, $K_{AD}$, as 300 µM.

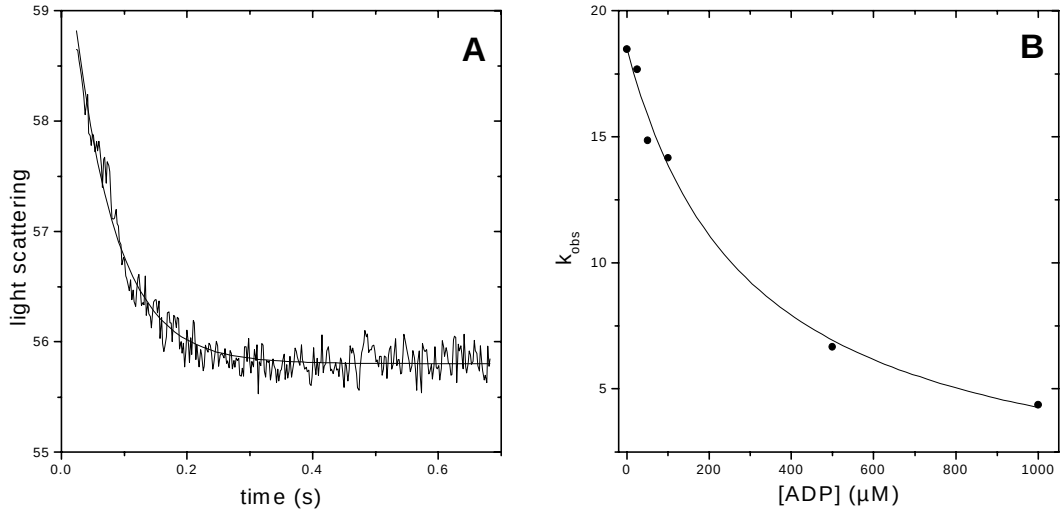


**Figure 7-3:** Determination of the affinity of ADP for the acto.TgMyoAΔtail complex by stopped flow.
A) 400/200 nM TgMyoAΔtail and 400/200 nM actin were mixed with 50/25 µM ATP and 200/100 µM ADP. The decrease in light scattering monitors the ATP induced dissociation of the acto.myosin complex. A single exponential fit is superimposed and gives an apparent rate constant of $k_{obs}$ of 14.2 $s^{-1}$ for the reaction.
B) Using a variety of ADP concentrations at a constant ATP concentration (20 µM) a fit to the hyperbola of the plot of $k_{obs}$ vs. [ADP] gives a $K_{AD}$ of 300 µM.
Other conditions: experimental buffer containing 100 mM KCl, 20 mM MOPS, 5 mM $MgCl_2$ at pH 7.0 and 20°C.

As with experiments defining the second order rate of ATP induced dissociation the amount of the full length TgMyoA was not sufficient to measure the ADP affinity in stopped flow. The affinity was measured for both constructs with the flash photolysis method. Fresh samples of 20 µl were prepared for each experiment containing 1 µM TgMyoAΔtail (or TgMyoA), 1 µM phalloidin stabilised actin and 0.5 mM cATP, 10 mM DTT, 0.03 units/µl Hexakinase, 1 mM Glucose 100 µM Ap5A and a defined concentration of ADP in 100 mM

KCl experimental buffer. Analysis by hyperbolic fits to the plot of $k_{obs}$ versus [ADP] confirmed the low affinity of ADP to the TgMyoA.actin complex by giving a $K_{AD}$ = 775 µM and a $K_{AD}$ = of 880 µM for TgMyoAΔtail and TgMyoA full respectively.

As pointed out in section 7.3.1 flash photolysis measurements of TgMyoA give small signal amplitudes and deviations from single exponential reaction kinetics. Therefore a large error is expected for the values given. This might account for the difference in the $K_{AD}$ values obtained from flash photolysis and stopped flow measurements. The clear hyperbolic dependency of the $k_{obs}$ on the ADP concentration however gives confidence in these estimates showing that for both, TgMyoAΔtail and full length TgMyoA, the acto.myosin complex has similar affinity to ADP.

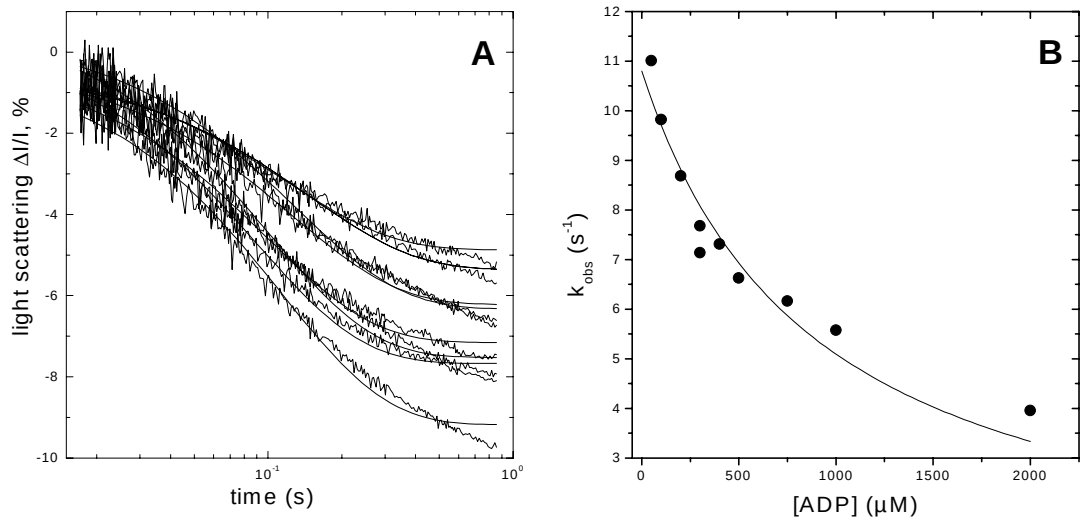


**Figure 7-4:** Determination of ADP-affinity for acto.TgMyoA (full length)

A) Light scattering signals from 7 20 µl samples containing 1 µM actin, 2 µM full length TgMyoA, 1 mM cATP, hexakinase, Ap5A and Glucose. Each sample contained a different amount of ADP and the samples were irradiated with the same laser intensity releasing an identical concentration of 30 µM ATP from cATP. The best fit to a single exponential decay of the light scattering decrease is shown superimposed.

B) The plot shows the ADP dependence of $k_{obs}$. The data were fitted to the model of Scheme 3-3 and gave a $K_{AD}$ of 877±140 µM.

Other conditions: experimental buffer containing 130 mM KCl, 20 mM MOPS, 5 mM MgCl2 and 10 mM fresh DTT at pH 7.0 and 22°C.

### 7.3.3 ATP binding to myosin

The rate of ATP binding to TgMyoAΔtail was determined in stopped flow by measuring the intrinsic tryptophan fluorescence change, which occurs on ATP binding (Scheme 3-1). A solution of 400/200 nM TgMyoAΔtail was mixed with a range of ATP concentrations. A 3% decrease in intrinsic fluorescence was observed compared to the more usual 20% increase in fluorescence upon ATP binding for other myosins. This is probably due to the absence of a tryptophan (W510 in chicken skeletal myosin) involved (Malnasi-Csizmadia *et al*., 2000; Batra *et al*., 1999; see section 3.1.2.1).

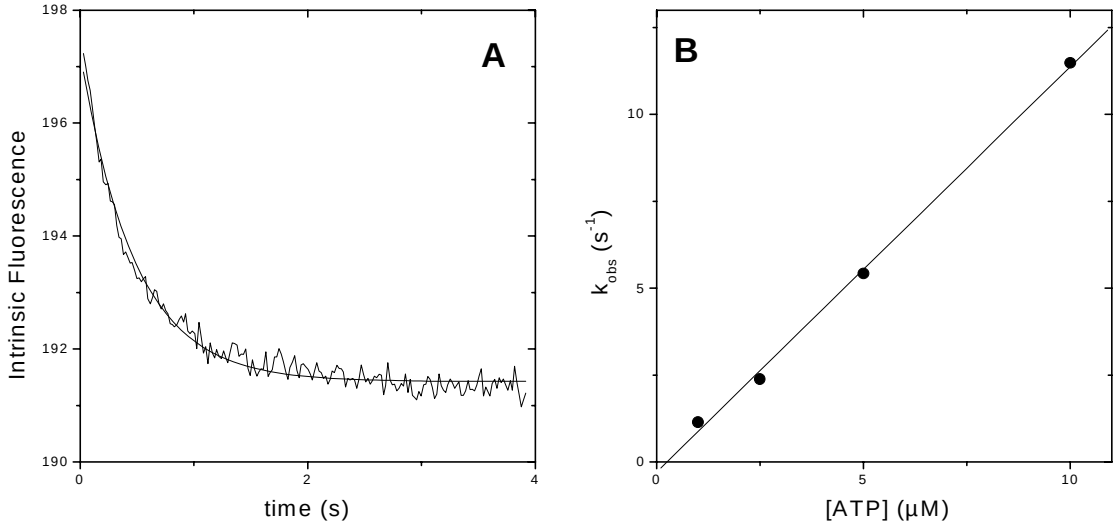


**Figure 7-5:** ATP binding to TgMyoAΔtail.
A) 400 nM TgMyoAΔtail were mixed with 5/2.5 µM ATP. The decrease in intrinsic fluorescence monitors the ATP binding. A single exponential fit is superimposed and gives an observed rate constant of $k_{obs}$ of 2.4±0.1 $s^{-1}$ for the reaction.
B) The experiment was repeated with a variety of ATP concentrations. The plot of $k_{obs}$ vs. [ATP] is linear and the linear regression results in an apparent second order rate constant of 1.16±0.05 $\mu M^{-1}s^{-1}$.
Other conditions: experimental buffer containing 100 mM KCl, 20 mM MOPS, 5 mM $MgCl_2$ at pH 7.0 and 20°C.

A single exponential fit to the signal change gives the observable rate constant $k_{obs}$. The slope of the linear fit to a plot of $k_{obs}$ vs. ATP concentration gives $K_1k_{+2}$ = 1.1·$\mu M^1s^{-1}$ which defines the second order rate constant for ATP binding to myosin.

The measurement was repeated using the fluorescent analogues mantATP instead of ATP and monitoring the signal change of the mant fluorescence. The slope of the linear fit here is $K_1k_{+2}$ = 0.65·$\mu M^1s^{-1}$. The mant fluorescence increased by 8% in an experiment with 1/0.5 µM

TgMyoAΔtail and 10/5 µM mantATP. Therefore if $1/10^{th}$ of the mantATP is bound mant fluorescence increases by 80% for each bound mantATP molecule. This is comparable to the mantATP fluorescence change upon binding skeletal muscle S1 (100%, Cremo and Geeves, 1998)

### 7.3.4 ADP binding to myosin

The experiment described in the previous section 7.3.3 was repeated with mantADP instead of ATP or mantATP. The change in mant fluorescence was monitored and a fit to the fluorescence change gave the observed rate constant $k_{obs}$ which was linearly dependent on the concentration of mantADP. The average slope of the linear fit is $k_{-6}/K_7 = 0.43 \cdot \mu M^{-1}s^{-1}$ and defines the second order rate constant of the binding of ADP to TgMyoAΔtail (see Scheme 3-1). The intercept of that fit gives an estimate of the rate of dissociation of ADP from myosin, $k_{+6}$, of 1.3 $s^{-1}$.

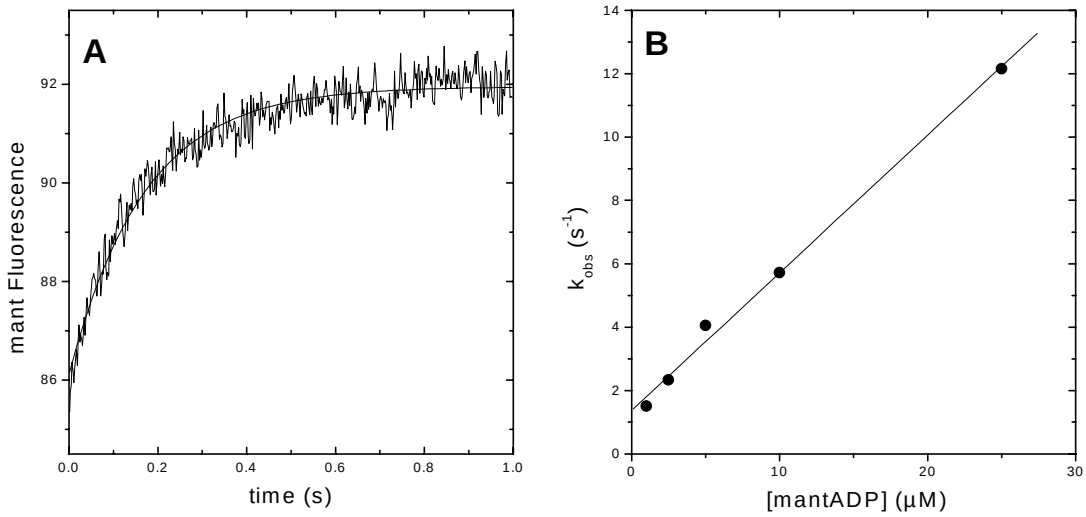


**Figure 7-6:** mantADP binding to TgMyoAΔtail.

A) 1/0.5 µM TgMyoAΔtail were mixed with 20/10 µM mantADP. The increase in mant fluorescence monitors the binding of ADP. A single exponential fit is superimposed and gives an observed rate constant of $k_{obs}$ of 5.7 $s^{-1}$ for the reaction.

B) The experiment was repeated with a variety of mantADP concentrations. The plot of $k_{obs}$ vs. [ATP] is linear and the linear regression results in an apparent second order rate constant of 0.43±0.02 $\mu M^{-1}s^{-1}$. The intercept of that fit gives an estimate of the rate of dissociation of ADP from myosin, $k_{+6}$, of 1.3±0.2 $s^{-1}$.

Other conditions: experimental buffer containing 100 mM KCl, 20 mM MOPS, 5 mM $MgCl_2$ at pH 7.0 and 20°C.

### 7.3.5 Dissociation rate of ADP from myosin

To determine the rate constant of dissociation of ADP from TgMyoAΔtail in stopped flow measurements a solution containing 400/200 µM myosin and 0.5/0.25 µM mantADP was mixed with a solution containing a large excess of ATP (20/10 or 10/5 µM). A single exponential fit to the mant fluorescence gave the rate at which bound mantADP was displaced by ATP and resulted in a value of $k_{+6}$=0.95 $s^{-1}$. $k_{+6}$ was independent of the mantADP or the ATP concentration. The value is in good agreement with the intercept of the previous measurement (see section 7.3.4). With the rate of ADP binding from the previous experiment (see section 7.3.4) the dissociation constant of ADP for myosin $K_D=k_{+6}/(k_{-6}/K_7)$=0.95/0.43=2.2 µM can be detemined (see Scheme 3-1).

### 7.3.6 Affinity of myosin for actin

The affinity of actin for TgMyoAΔtail was measured in a competition experiment with rabbit myosin S1 using 2 mM KCl-Buffer to guarantee tight binding of all actin. First the amplitude of dissociation of an equimolar amount of S1 and pyrene actin (50/25 nM) by 20/10 µM ATP was measured by looking at the pyrene fluorescence of actin. The experiment was repeated by mixing actin in presence of 150/75 nM TgMyoAΔtail which reduced the pyrene fluorescence change to 40% (see Figure 7-7). Because the TgMyoA does not change pyrene fluorescence, it can be assumed that 40% S1 and 60% TgMyoAΔtail were bound. The ratio of the affinities of rabbit S1 and TgMyoAΔtail for actin can be calculated according to Equation 7-1 (with rS1 = rabbit skeletal S1 and myoA = TgMyoAΔtail, the signal amplitude is proportional to the concentration of the rS1.actin complex [rS1.actin], virtually all actin is bound to rS1 or myoA)

**Equation 7-1:** $K_{A(rS1)}/K_{A(myoA)} = ([rS1]\cdot[actin]/[rS1.actin])/([myoA]\cdot[actin]/[myoA.actin])$

Thus under the low salt conditions used TgMyoA had a 2-3 fold lower affinity to actin than S1. Under physiological conditions the dissociation equilibrium constant ($K_A$) of S1 for actin is 30 nM suggesting a value of 60-90 nM for TgMyoA if the ratio of $K_{A(rS1)}/K_{A(myoA)}$ does not change significantly with the salt concentration.

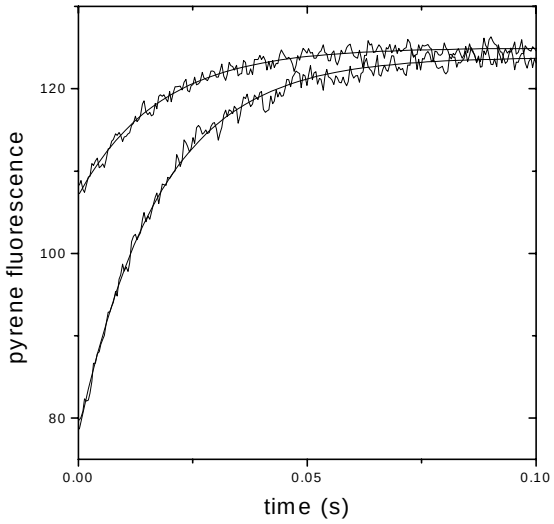


**Figure 7-7:** Determination of the affinity of TgMyoA for actin by competition of actin binding with rabbit S1. The increase of the pyrene fluorescence of pyrene labelled actin (50/25 nM) is monitored upon ATP induced dissociation of an equimolar concentration of S1 in the absence and in the presence of 3 fold the concentration of TgMyoAΔtail (150/75 nM). In the presence of TgMyoAΔtail the amplitude is reduced to 40 %.

### 7.3.7 Table showing the results of the kinetic characterisation of TgMyoA and a comparison with other myosins

| | Rate/Eq constant | Units | TgMyoA Δtail | TgMyoA full length | Dicty $MII^{864}$ | $Ch^{sm}S1$ | $Rb^{st}S1$ |
|---|---|---|---|---|---|---|---|
| Nucleotide binding to acto.M | $K_1 \cdot k_{+2}$ | ($\mu M^{-1}s^{-1}$) | 0.6 | | 0.14 | 0.47 | 2.1 |
| | (FP) $K_1 \cdot k_{+2}$ | ($\mu M^{-1}s^{-1}$) | 0.4 | 0.28 | | | |
| | $K_{AD}$ | ($\mu M$) | 300 | | 94 | 5 | 200 |
| | (FP) $K_{AD}$ | ($\mu M$) | 775 | 880 | | | |
| | $k_{-AD}$ | ($s^{-1}$) | - | | >200 | 22 | >500 |
| mantADP | $k_{-6}/K_7$ | ($\mu M\ s^{-1}$) | 0.43 | | 0.9 | 2 | 2.3 |
| | $k_{+6}$ | ($s^{-1}$) | 0.95 | | 1.5 | 0.13 | 0.23 |
| | $K_D$ | ($\mu M$) | 2.21 | | 1.6 | 0.075 | 0.1 |
| ATP binding | $K_1 \cdot k_{+2}$ | ($\mu M^{-1}s^{-1}$) | 1.1 | | 0.94 | 2.1 | 2.3 |
| | $k_{+3}+k_{-3}$ | ($s^{-1}$) | - | | 24 | 50 | 130 |
| Mant ATP | $K_1 \cdot k_{+2}$ | ($\mu M^{-1}s^{-1}$) | 0.65 | | - | | 3.2 |
| | $K_{AD}/K_D$* | | 148 | | 58.7 | 66 | 2000 |
| Actin binding | $K_A$ | (nM) | 60 - 90 | | | | 30 |

**Table 7-1:** Table showing the results of the kinetic characterisation of TgMyoA and a comparison to other myosins. (FP) in the second column indicates rows where results were obtained with the flash photolysis method. $K_D$ has been calculated from $k_{+6}/(k_{-6}/K_7)$. In the last 3 columns the kinetic results of other myosins are shown for comparison with the TgMyoA results. The myosins used for comparison were the a S1 of a *Dictyostelium* myosin II $MII^{864}$ (Ritchie et al., 1993), chicken smooth muscle S1 (Cremo et al., 1990) and rabbit skeletal muscle S1 (Cremo et al., 1990). (* It has to be pointed out that the value for $K_{AD}/K_D$ for TgMyoA was calculated from a value of $K_{AD}$ determined with ADP and a value of $K_D$ determined with mantADP, which often shows a higher affinity to myosin than ADP.)

## 7.4 ATPase activity (actin activated)

To determine ATP turnover activity 50 nM TgMyoAΔtail were mixed with 50 µM or 200 µM ATP in a 30 mM KCl experimental buffer and quenched with TCA at various time points as described in section 4.6.5.1. Samples were analysed by HPLC and the amount of ATP turned over estimated by looking at the corresponding peak areas of ATP and ADP monitored by UV-light at 254 nm. The plot of [ADP]/([ATP]+[ADP]) ratios of the samples versus the time of quenching gave a straight line. The slope of the linear regression line was multiplied by the initial concentration of ATP and divided by the myosin concentration to give a catalytic ATPase activity, $k_{cat}$, of 0.063±0.003 $s^{-1}$ in the absence and 1.62±0.11 $s^{-1}$ in the presence of 20 µM actin. The basal ATPase is similar to many other myosins and a more than 20-fold activation at 20 µM actin is typical for fast myosins.

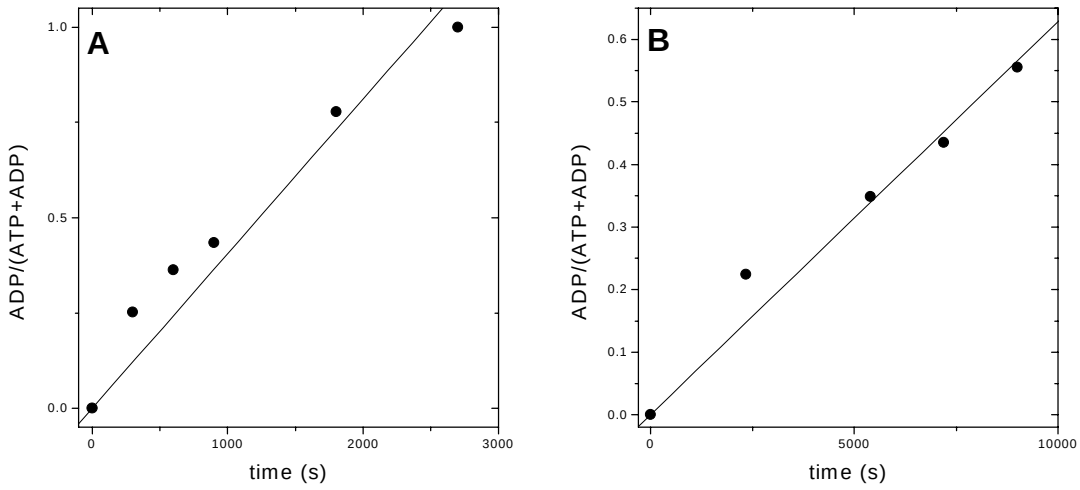


**Figure 7-8:** Determination of the ATPase activity of TgMyoAΔtail by HPLC-analysis
The ratio of [ADP]/([ATP]+[ADP]) was determined from the peak areas of the HPLC-analysis and showed a linear dependency on the time after which the reaction was quenched.

A) 50 nM TgMyoAΔtail and 20 µM actin were mixed with 200 µM ATP. The linear fit through the origin is superimposed and gave a slope of $4.06 \cdot 10^{-4} \pm 2.8 \cdot 10^{-5}\ s^{-1}$.

B) 50 nM TgMyoAΔtail were mixed with 50 µM ATP. The linear fit through the origin is superimposed and gave a slope of $6.3 \cdot 10^{-5} \pm 3 \cdot 10^{-6}\ s^{-1}$.

## 7.5 External results

To complement the transient kinetic data some of the functional properties of this motor were analysed. The sliding velocities of F-actin filaments were measured in a standard *in vitro* motility assay (Kron and Spudich, 1986) in Dr. D. Manstein's lab at the MPI Heidelberg by Dr. S. Fujita-Becker. An average velocity of 5.2 µm/s was measured for TgMyoA.

TgMyoAΔtail showed no motility under the same conditions although the protein displayed ATP-dependent binding to actin. This lack of motility could either be the result of an inappropriate binding of the myosin fragment to the nitrocellulose surface that alters the flexibility of the neck or a functional defect caused by the deletion of the last 53 C-terminal amino acid residues.

The recent finding that myosin VI exhibiting an unusual converter domain is a minus-end directed motor (Wells et al., 1999; Homma et al., 2001b) made the determination of the directionality of TgMyoA interesting. For this purpose the *in vitro* motility assay was conducted with actin filaments that were covalently labelled with Oregon Green at their barbed ends. Additionally, to block actin polymerisation at the plus-end, seeds were generated in the presence of gelsolin. TgMyoA moved these polarisation-marked filaments so that the labelled end was at the back of the moving filament, demonstrating that TgMyoA, like myosin II, moves towards the plus end and away from the minus end of F-actin.

In order to complete the characterisation of this myosin, C. Ruff from the lab of Dr. E. Meyhöfer at the Medical School Hanover employed a combined microneedle-laser trap transducer (Ruff et al., 2001) and directly measured the step displacements generated by single myosin molecules. Using this assay it was observed that, in agreement with the kinetic analysis, TgMyoA transiently interacted with the actin filament. A histogram analysis of a large number of such interactions revealed an average step displacement of about 5.3 nm, comparable to the step size reported for myosin II (Veigel et al., 1999). In addition, these measurements confirmed at the single molecule level that TgMyoA is a non-processive motor.

## 7.6 Sequence analysis

So far, extreme diversity in the myosin superfamily has been restricted to the tail regions, while the motor domain has been remarkably conserved between classes. Even in myosin VI, there is clear structural conservation throughout the catalytic domain and, like for most other myosins, major differences are often restricted to inserts, in particular in surface loops, and to variation in the number of IQ-motifs.

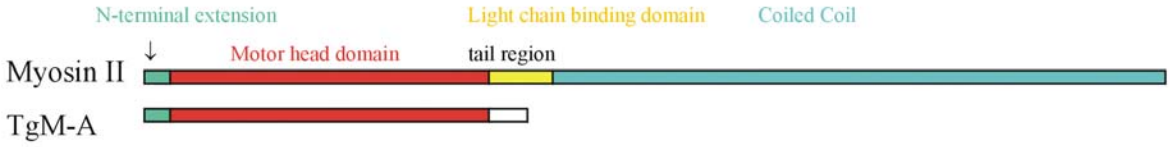


```
                                                          TEDS-site
Sm356   VSSVLQLGNI VFKKERNTDQ ASMPDNTAAQ KVCHLMGINV TDFTRSILTP RIKVGRDVVQ KAQTKEQADF AIEALAKAKF
Sk355   TGAVMHYGNL KFZQZQREEQ AEPDGTEVAD ZAAYLMGLNS AELLKALCYP RVGVGNEAVT ZGETVSQVHN SVGALAZAVY
Dy348   IAGILHLGNI KFEKGAGEGA VLKDKTALNA ASTVFGVNPS VLEKALME.P RILAGRDLVA QHLNVEKSSS SRDALVKALY
Sc352   TASILHMGEM KFKQRPREEQ AESDGTAEAE KVAFLCGINA GDLLKALLKP KVKVGTEMVT KGQNMNQVVN SVGALAKSLY
TgMyoA VSGVLLLGNVEVTATKDGGIDDAAAIEGKNLE VFKKACGLLFLDAERIREELTVKVSYAGNQEI RGRWKQEDGDMLKSSLAKAMY

                                  Hinge
                                    ↓              --------------------Converter Domain----------------------
Sm683   RCIIPNHEKR AGKLDAHLVL EQLRCNGVLE GIRICRQGFP NRIVFQEFRQ RYEILAANAI PKG.FMDGKQ ACILMIKALE LDPNLYRIGQ
Sk673   RCIIPNETZT PGAMEHELVL HQLRCNGVLE GIRICRKGFP SRVLYADFKQ RYRVLNASAI PEGQFMDSKK ASEKLLGGGD VDHTQYAFGH
Dy654   RCIIPNNKQL PAKLEDKVVL DQLRCNGVLE GIRITRKGFP NRIIYADFVK RY.YLLAPNV PRD.AEDSQK ATDAVLKHLN IDPEQYRFGI
Sc669   RCIIPNELKQ PGLVDAELVL HQLQCNGVLE GIRICRKGFP SRLIYSEFKQ RYSILAPNAI PQG-FVDGKT VSEKILAGLQ MDPAEYRLGT
TgMyoA RCIKPNDTKK PLDWVPSKML IQLHALSVLE ALQLRQLGYS YRRPFKEFLF QFKFIDLSAS ENPNLDPKEA ALRLLKSSK  LPSEEYQLGK

       ------------------ →-----Essential LC------------←→------Regulatory LC-----
Sm772   SKIFFRTGVL AHLEEERDLK ITDVIIAFQA QCRGYLARKA FAKRQQQLTA MKVIQRNCAA YLKLRNWQWW RLFTKVKPLL Q
Sk763   TZVFFZAGLL GLLEEMRDDZ LAEIITRTQA RCRGFLMRVE YRRMVERRES IFCIQYNVRS FMNVZHWPWM ZLFFZIKPLL K
Dy742   TKIFFRAGQL ARIEEAREQR ISEIIKAIQA ATRGWIARKV YKQAREHTVA ARIIQQNLRA YIDFKSWPWW KLFSKARPLL K
Sc758   TKVFFKAGVL GNLEEMRDER LSKIISMFQA HIRGYLIRKA YKKLQDQRIG LSVIQRNIRK WLVLRNWQWW KLYSKVKPLL
TgMyoA TMVFLKQTGA KELTQIQREC LSSWEPLVSV LEAYYAGRRH KKQLLKKTPF IIRAQAHIRR HLVDNNVSPA TVQPAF
```

**Figure 7-9:** The sequence of TgMyoA.
On top a schematic comparison between the sequence of conventional myosin and myosin XIV is shown. Beneath parts of the TgMyoA sequence are aligned with sequences from chicken smooth, chicken skeletal, *Dictyostelium* and scallop muscle. Regions aligned include an actin binding loop containing the TEDS-site, the hinge, the converter domain and the neck region.

The sequence of class XIV myosins diverges from that of other myosins starting at a position that corresponds to the 50k/20k-domain junction (loop 2) in conventional myosins (see Figure 7-9). As a result TgMyoA displays no sequence similarity to other types of myosin in regions

that normally form the converter domain and lever arm. As a result a pivot point for the lever arm which is usually a highly conserved glycine (at 699 in chicken skeletal muscle; Kinose et al., 1996) is not identifiable and a serine is where it would be expected. Likewise conventional IQ-domains for the binding of light chains are not identifiable. Recently however a calmodulin like light chain (about 30 kDa) associated with TgMyoA has been discovered, which is highly conserved in *Apicomplexa*. As this putative light chain does bind to full length TgMyoA but not TgMyoAΔtail the binding domain for this light chain is predicted to be in the last 53 amino acids (A. Herm, personal communication).

Furthermore TgMyoA does not obey the TEDS-rule, which proposes that either an acidic or a phosphorylatable residue is found in a position 16 residues upstream the DALAK consensus sequence. It has to be pointed out however that TgMyoA has a negatively charged glutamic acid two residues to the carboxy terminal end from the residue which is believed to correspond to the TEDS-site in other myosins. This residue is located in the cardiomyopathy surface loop (Geisterfer-Lowrance *et al*., 1990) which is involved in actin binding and in TgMyoA a threonine occupies this position. Only a few other myosins are known to be exceptions to this rule (Vargas et al., 1997) and an overall negative charge in this position seems to be essential for the coupling of actin-binding to ATP hydrolysis (Ostap and Pollard, 1996; Bement and Mooseker, 1995). This hypothesis is supported in recent studies of myosin VI, in which a point mutation at this site influenced the release of Pi, the affinity of ADP and the ATPase activity in the presence and absence of actin (De La Cruz et al., 2001).

These differences indicate that sequence elements responsible for the transmission of information between the nucleotide-binding site, the actin binding site and a conformational amplifier with light chain binding domains, are structurally distinct from those in other types of myosin. Additionally, the sequence difference indicates that TgMyoA must have evolved so that the mechanical properties of the converter and lever arm domains are served by a region which most likely adopts a very different structure.

### 7.7 Comparison of myosin A and myosin D

Another myosin XIV from *Toxoplasma gondii*, TgMyoD, is also located beneath the plasma membrane which indicates that it is also involved in the host invasion mechanism. A genetic knock out however shows that, unlike TgMyoA, it is not essential. A brief kinetic characterisation has also been attempted. Preliminary results show a rate of ATP induced dissociation of acto.myosin of $K_1k_{+2} = 1.27 \cdot \mu M^{-1}s^{-1}$, a rate of mantATP binding to myosin of $K_1k_{+2} = 0.59 \cdot \mu M^{-1}s^{-1}$ and an affinity of ADP for acto.myosin with a $K_{AD}$ of 105 µM. The ATPase activity in absence of actin was 0.05 $s^{-1}$.

All values are of the same order as for TgMyoA and it can be speculated that all myosins XIV display roughly similar properties.

### 7.8 Discussion

The transient kinetics of TgMyoAΔtail were analysed by stopped flow and flash photolysis methods, whereas only enough full length TgMyoA could be purified for flash photolysis analysis. The maximum velocity at which the myosin can move over actin is normally limited by the net rate of cross bridge detachment at the end of the power stroke (Siemankowski et al., 1985; see section 6.7). The net detachment rate is limited by the rates of the underlying steps, the release of ADP and the ATP induced dissociation, measurements of which can therefore be diagnostic of the overall speed of the acto.myosin cross bridge cycle. Flash photolysis experiments were essential to prove that both these values are similar for the full length TgMyoA and TgMyoAΔtail, which indicates that the truncation of the tail (53 AA) does not significantly alter the kinetic properties of the myosin XIV. While the quality of the flash photolysis data was sufficient to confirm this, the deviations of the flash photolysis transients from single exponential reaction kinetics are expected to give a large error on the actual values measured. A more complete kinetic characterisation was then performed for TgMyoAΔtail by stopped flow. Another myosin XIV TgMyoD was also partially analysed showing similar properties as TgMyoA. The transient kinetics not only revealed that the myosin XIV, despite the differences in sequence, is a fully functional myosin capable of actin translation, but also shows a high analogy with typical fast myosins like skeletal muscle myosin. TgMyoA dissociates fast from actin upon ATP binding, has a relatively low affinity for actin and the acto.myosin complex has a low affinity for ADP. The similarity to typical fast myosins was further

confirmed by the 20-fold increase of ATPase activity in the presence of actin as well as by the external results of a fast *in vitro* motility and a step-size of about 5 nm. Taken together, the sliding velocity and step size measurements of full length TgMyoA are in perfect agreement with, and thus validate, the kinetic values.

TgMyoA does not follow the TEDS rule (Bement and Mooseker, 1995), the generally conserved glycine residue at the pivot-point (Kinose et al., 1996) is replaced by a serine and the converter domain is highly divergent. Finally the typical lever arm with clearly identifiable IQ motifs is missing (see Figure 7-9). However the discovery of a novel light chain binding to the tail region (C-terminal 53 AA) suggests a potential lever arm function for this area. Despite the structural differences it results in remarkably similar mechanical, biochemical and therefore functional properties as found in typical fast myosins. In the absence of a crystal structure of class XIV myosins, it is difficult to predict the structural elements and the mechanisms that are responsible for the amplification of conformational changes resulting from the turnover of ATP. It can be speculated however that if the light chain binding tail domain acts as a lever arm a possible hinge must be located far further upstream the sequence than in conventional myosins and a mechanism making that possible would be interesting to elucidate. Furthermore, mutational studies with TgMyoA might lead to an understanding of the importance of the TEDS-rule for the coupling of actin-binding and ATPase activity (Ostap and Pollard, 1996; Bement and Mooseker, 1995).

In conclusion, despite its unconventional character, TgMyoA fulfils the biochemical requirements for a fast motor designed for fast motility (Hakansson et al., 1999). Like fast muscle myosins, TgMyoA has a short ”duty cycle”, is thus non-processive and probably operates in the context of large motor arrays which are the predicted properties for a motor powering the gliding motility needed for host invasion. TgMyoA is distributed homogeneously beneath the parasite plasma membrane (Hettmann et al., 2000), ready for a consolidated action. In accordance with the ”capping model” for invasion (Sibley et al., 1998), the directionality of TgMyoA implies that the actin filaments ought to be oriented with the barbed ends towards the posterior pole. Surprisingly, actin filaments have not been detected in the parasites, neither by phalloidin staining nor by sedimentation (Dobrowolski et al., 1997), indicating that they might be either very short, or have a high turnover due to the presence of actin depolymerising factors (Allen et al., 1997) or polymerise only in response to host cell contact during invasion. The elaborate gliding motions of *Apicomplexan* parasites accompanying host cell penetration allow entry significantly faster than via phagocytosis (Morisaki et al., 1995). One might speculate that *Apicomplexa* have

learned to fully exploit the actin cytoskeleton, using a combination of myosin-powered motion together with the force generated directly by actin polymerisation (Theriot, 2000).

## *7.9 Summary*

Many *Apicomplexan* parasites such as *Toxoplasma gondii* depend on their acto.myosin system to actively penetrate host cells. This form of motility called gliding is an adaptive mechanism to power cell invasion at speeds of 1 to 10 μm/s. *T. gondii* myosin A (TgMyoA) is tightly associated with the plasma membrane of the parasite, an ideal position to power gliding motility needed for host invasion. Compared to conventional myosins TgMyoA, like all class XIV myosins, has a highly divergent converter domain and an extremely short neck and tail region without identifiable IQ-motifs. The tail region instead binds a single novel light chain. Despite these structural differences, the kinetic and mechanical properties of TgMyoA show unexpected overall similarity to the fast skeletal muscle myosins. The basal ATPase of TgMyoA was activated more than 20-fold in the presence of actin. Transient kinetic analysis showed that a complex of TgMyoA with actin is rapidly dissociated by ATP and has a very weak affinity for ADP, properties diagnostic of a fast myosin motor. The kinetic characterisation was performed with the C-terminal truncated TgMyoAΔtail and flash photolysis experiments with the full length TgMyoA were essential to validate that the kinetic characterisation of myosin XIV is not significantly influenced by the truncation of the tail region. Motility and microneedle/laser trap assays established that TgMyoA moves in unitary steps of 5.3 nm with a velocity of 5.2 μm/s towards the plus (barbed) end of actin filaments (external results). The properties of a fast myosin like skeletal muscle myosin are in agreement with the requirements for a motor powering gliding motility. However the differences in the sequence suggest that myosins XIV are powered by novel structural and mechanical elements which are yet to be elucidated.

# 8 Summary

This study successfully introduces a novel apparatus for measuring transient kinetics of sub-microgram quantities of acto.myosin, significantly smaller quantities than required by traditional methods like stopped flow. The method is based on the use of flash photolysis of an inert precursor of ATP (cATP) to initiate the dissociation of acto.myosin and the subsequent ATP turnover reaction. The flash photolysis method makes way for a range of experiments which have previously not been possible because the amounts of protein available were too small. Here not only the limits of the flash photolysis system have been explored but the novel method was also used to elucidate biological relevant results which could not have been obtained by traditional methods. This includes a kinetic characterisation of rat and human skeletal muscle myosin isoforms and the collection of transient kinetic data from a full length myosin XIV to confirm stopped flow results of the more readily available truncated form of the protein.

In contrast to other transient kinetic methods such as stopped flow and quenched flow which have been used to elucidate many of the fundamental features of the molecular acto.myosin interactions this method does not require the mixing of solutions and can therefore operate in a very small volume. Using a sample volume of 10 µl a significant amount of information on the transient and steady state kinetics of an acto.myosin system can be obtained, including the determination of the second order rate constant of ATP induced dissociation, the ADP affinity and the catalytic ATPase activity. The results obtained from flash photolysis are highly reproducible, reliable and generally in good agreement with stopped flow data. The sensitivity of the method using a light scattering signal allows measurements with samples containing just 50 nM of acto.myosin or acto.S1 complex in solution. In the presence of an excess of one protein component the measurements require only 250 ng myosin, 62 ng S1 or 25 ng actin. This compares to the 1.5 µg of actin, 2.5 µg of S1 or 10µg of myosin required for a 0.5 ml solution of 30 nM which is the standard stopped flow requirement. Being able to work with such low quantities of protein will have a wide range of uses. Apart from characterisation of myosin isoforms from single muscle fibres and rare myosins of the myosin superfamily, as demonstrated here for rat and human skeletal muscle isoforms and the myosin XIV, TgMyoA, the method will help the investigation of chimeric myosins expressed in low amounts in *in vitro* expression systems or baculo-virus. The method should also allow kinetic characterisation of muscle proteins from micro biopsies allowing diagnostics with small amounts of tissue, thus minimising patient distress. *Drosophila* flight muscle is another

system which is of high interest for mutational studies of myosin. Mutations are easily introduced to *Drosophila* but once again the yields of myosin which can be extracted from *Drosophila* flight muscles are small. First attempts on using the flash photolysis method for the kinetic characterisation of myosins prepared from mutant and wildtype *Drosophila* have successfully been made by Rumika Silva of our lab in collaboration with S. Bernstein's lab (San Diego State University, USA) and J. Sparrow's lab (University of York, UK).

Furthermore the lack of mixing turbulence can make flash photolysis preferable to the stopped flow method for light scattering measurements of the kinesin.microtubule system (see section 5.13). In a collaboration with R. Cross' lab (Marie Curie Institute, Oxted, UK) we used the flash photolysis method for measuring transient kinetics of the non-processive, single headed kinesins, KIF1 and the mutant KIF1D, which helped to elucidate the role of the K-loop for microtubule affinity and ATPase function (Rogers et al., 2001; not part of this thesis). Measuring the transient kinetics of this system was previously less reliable since the stopped flow method introduces large mixing artefacts on light scattering transients, due to the large size of the microtubule filaments. The example of kinesin measurements not only shows that the flash photolysis method is not limited to the acto.myosin system, but also that the range of possible experiments can be extended by using other caged compounds, in this case cADP.

In stopped flow a higher sensitivity for acto.myosin measurements is reached by using the fluorescence signal of actin labelled with pyrene compared to light scattering measurements. The pyrene label however is difficult to use in flash photolysis since the monitoring light at the excitation wavelength releases ATP from cATP prohibiting experiments with the current set-up. Development of a more sophisticated shutter system however might make some experiments using pyrene labelled actin possible. The same problem exists for measuring intrinsic tryptophan fluorescence, but the shorter excitation wavelength releases even more ATP, hence the flash photolysis system is not suitable for experiments of nucleotide binding to myosin. This problem cannot be solved by the use of mant-labelled nucleotides, since these do not exist in caged form. The recently discovered coumarin-labelled nucleotides (Webb and Corrie, 2001) are an exciting possibility for future measurements, in which ADP release could be directly determined. For most myosins however this would also require faster caged compounds. Experiments with the acrylodan label on actin which is excited at a higher wavelength have been proven possible but no increase of sensitivity could be obtained. The lack of an adequate fluorescent label limits the usefulness of the system as not only can the protein amounts not be decreased further but also a range of experiments needing a fluorescent signal are not possible. This includes all experiments which are based on the exact

measurement of the signal amplitude, since these measurements are less reproducible with the light scattering signal.

The parameters which can be measured in the flash photolysis system, however, are major contributors to the myosins overall properties. ATP induced dissociation and the rate of release of ADP from the nucleotide binding site, which is directly related to the ADP affinity, are the two steps involved in the overall detachment of the cross bridge and can therefore limit the rate of the cross bridge cycle. According to Siemankowski and White (1985) the ADP release step is the slower of the two and thus rate limiting. Siemankowski and White based their hypothesis on results from slower and unrelated myosins from different species. In this work their hypothesis was confirmed for a set of very closely related fast myosins.

Pure myosin isoforms of the four major skeletal muscle myosin types (myosin heavy chains: MHC-I, IIA, IIX and IIB) from single rat muscle fibres and two from human single fibres (MHC-I, IIA ) were extracted. The extractions yielded enough myosin (~2 µg/ 15 mm length) to define the second order rate constant of ATP induced dissociation and the ADP affinity (with an extraction of 5 pooled fibres of the same type) with the flash photolysis method, but not for stopped flow analysis. Both the apparent second order rate constant of acto.myosin dissociation ($K_1k_{+2}$) and $K_{AD}$ in both rat and human increased in the order of isoforms I, IIA, IIX, IIB with values of 0.17, 0.21, 0.26, 0.26 $\mu M^{-1}s^{-1}$ for $K_1k_{+2}$ in rat and 250, 480, 750 and 930 µM for $K_{AD}$ in rat respectively. The values for human MHC-I and IIA were 0.18 and 0.26 $\mu M^{-1}s^{-1}$ for $K_1k_{+2}$ and 163 and 237 µM for $K_{AD}$ respectively (all values were measured in a high salt buffer containing 500 mM KCl). Values for the ADP affinity ($K_{AD}$) correlate very well with the maximum unloaded shortening velocity of the fibre. After correction for physiological salt concentrations and under the assumption that ADP binding is a diffusion limited process of the order of $10^7$ $M^{-1}s^{-1}$, the rate of ADP release ($k_{-AD}$) from the nucleotide binding site could be calculated from the ADP affinity. The calculated values for $k_{-AD}$ were for each of the isoforms remarkably close to a theoretical value $k_{min}$, which estimates the rate of a step limiting the speed of the overall cross bridge cycle. It would be interesting to confirm the results for $k_{-AD}$ by directly measuring the ADP release rate with coumarin-labelled ADP in future experiments.

In contrast to the ADP release step, which was sufficiently slow to limit the shortening velocity ($V_0$), $[ATP]\bullet K_1k_{+2}$ at 5 mM ATP would be 2.5-10 times faster than $k_{-AD}$. Hence ATP induced dissociation can only contribute to $V_0$ if the [ATP] drops well below 5 mM and only for the fastest isoforms.

In addition the study of this set of closely related isoforms gave further hints on structure function relations of the myosin heavy chain. Changes in the surface loops 1 and 2, which occur between the different skeletal muscle isoforms within a species (parologous), are known to modulate the properties of a myosin. However a comparison between the orthologous MHC-1 isoforms in rat and human proves that the mechanical and biochemical properties of orthologous isoforms can be influenced by few substitutions of residues which do not need to be in either loop 1 or loop 2. Therefore a wider variety of changes causing modulation of the properties needs to be considered. The results of this study hint towards changes in the secondary actin binding loop to be responsible for a modulation of the rate of ADP release. It can therefore be speculated that this can be a vital area for the actin activation of the ATPase function of skeletal muscle myosin. To gain more confidence with such speculations, however, more information on the sequences of orthologous isoforms needs to be obtained or more measurements of myosins with known sequences should be performed. To continue this work measurements with pig MHC-I for which the sequence is known are currently planned.

A characterisation of TgMyoA, a myosin XIV, of the *Apicomplexan* parasite *Toxoplasma gondii* reveals remarkably similar kinetics to skeletal muscle myosins while it has a very different sequence and structure. TgMyoA is likely to be involved in generating gliding motility at speeds of 1-3 µm/s, which is used by the parasite to actively penetrate host cells.

Gliding motility is generated by “capping” of surface adhesin complexes. Connected to the adhesin complexes by their transmembrane subunits the acto.myosin system moves these complexes towards the posterior pole of the parasite, thereby driving the parasite into the host cell. To power such motility a fast, non-processive myosin motor with a short “duty cycle” is predicted. In agreement with this prediction the transient kinetic analysis showed that a complex of TgMyoA with actin is rapidly dissociated by ATP and has a very weak affinity for ADP. As discussed previously for the example of skeletal muscle isoforms these values are likely to determine the overall speed of the cross bridge cycle and are therefore diagnostic of a fast myosin motor. The activation of the basal ATPase of TgMyoA by more than 20-fold in the presence of actin is also typical for a fast type motor. The kinetic characterisation was performed with the C-terminal truncated TgMyoAΔtail by stopped flow and flash photolysis experiments with the full length TgMyoA were essential to validate that the kinetic characterisation of myosin XIV is not significantly influenced by the truncation of the tail region. External results from motility and microneedle/laser trap assays established that TgMyoA moves in unitary steps of 5.3 nm with a velocity of 5.2 µm/s towards the plus

(barbed) end of actin filaments (external results, see section 7.5). These results also show a high similarity to skeletal muscle myosins and are therefore in good agreement and can confirm the results of the kinetic characterisation. Despite the prediction that the motor powering gliding motility should be a fast myosin, the similarity of TgMyoA to skeletal muscle myosin is very unusual considering its strong differences in protein sequence. TgMyoA, like all class XIV myosins, has a highly divergent converter domain and an extremely short neck and tail region without identifiable IQ-motifs. The tail region instead binds a single novel light chain. Furthermore it does not obey the TEDS rule. These differences in the sequence suggest that myosins XIV are powered by novel structural and mechanical elements. Unfortunately a crystal structure which could help to elucidate the function of these elements is currently not available. From an evolutionary point of view, TgMyoA is the most ancient myosin characterised so far and the conserved catalytic core linked to a structurally unique mechanical element has remarkable outcomes. TgMyoA is one of the smallest myosins and still manages to be as fast as the conventional class II myosin.

In conclusion this work succeeded in introducing a novel apparatus measuring transient kinetics of the acto.myosin system with protein amounts much smaller than previously possible. The usefulness of such a method has been proven for two examples, mammalian skeletal muscle isoforms and a myosin XIV, elucidating or helping to elucidate novel biologically relevant results. The potential uses of the flash photolysis system are much wider still.

# 9 References

Aguirre, R., F. Gonsoulin, and H. C. Cheung. 1986. Interaction of fluorescently labeled myosin subfragment 1 with nucleotides and actin. *Biochemistry.* 25:6827-35.

Allen, M. L., J. M. Dobrowolski, H. Muller, L. D. Sibley, and T. E. Mansour. 1997. Cloning and characterization of actin depolymerizing factor from Toxoplasma gondii. *Mol Biochem Parasitol.* 88:43-52.

Andreeva, A. L., O. A. Andreev, and J. Borejdo. 1993. Structure of the 265-kilodalton complex formed upon EDC cross-linking of subfragment 1 to F-actin. *Biochemistry.* 32:13956-60.

Anson, M. 1992. Temperature dependence and Arrhenius activation energy of F-actin velocity generated in vitro by skeletal myosin. *J Mol Biol.* 224:1029-38.

Anson, M., M. A. Geeves, S. E. Kurzawa, and D. J. Manstein. 1996. Myosin motors with artificial lever arms. *Embo J.* 15:6069-74.

Asai, D. J., and M. P. Koonce. 2001. The dynein heavy chain: structure, mechanics and evolution. *Trends Cell Biol.* 11:196-202.

Bagshaw, C. R. 1982. Muscle Contraction. Chapman and Hall, London.

Bagshaw, C. R., and D. R. Trentham. 1974. The characterization of myosin-product complexes and of product-release steps during the magnesium ion-dependent adenosine triphosphatase reaction. *Biochem J.* 141:331-49.

Barany, M. 1967. ATPase activity of myosin correlated with speed of muscle shortening. *J Gen Physiol.* 50:Suppl:197-218.

Barrow, G. M. 1984. Physikalische Chemie. Springer Verlag, Hamburg.

Batra, R., M. A. Geeves, and D. J. Manstein. 1999. Kinetic analysis of Dictyostelium discoideum myosin motor domains with glycine-to-alanine mutations in the reactive thiol region. *Biochemistry.* 38:6126-34.

Bement, W. M., and M. S. Mooseker. 1995. TEDS rule: a molecular rationale for differential regulation of myosins by phosphorylation of the heavy chain head. *Cell Motil Cytoskeleton.* 31:87-92.

Berg, J. S., B. C. Powell, and R. E. Cheney. 2001. A millennial myosin census. *Mol Biol Cell.* 12:780-94.

Bonafe, N., and P. Chaussepied. 1995. A single myosin head can be cross-linked to the N termini of two adjacent actin monomers. *Biophys J.* 68:35S-43S.

Bottinelli, R., R. Betto, S. Schiaffino, and C. Reggiani. 1994a. Unloaded shortening velocity and myosin heavy chain and alkali light chain isoform composition in rat skeletal muscle fibres. *J Physiol.* 478:341-9.

Bottinelli, R., M. Canepari, C. Reggiani, and G. J. Stienen. 1994b. Myofibrillar ATPase activity during isometric contraction and isomyosin composition in rat single skinned muscle fibres. *J Physiol.* 481:663-75.

Bradford, M. M. 1976. A rapid and sensitive method for the quantitation of microgram quantities of protein utilizing the principle of protein-dye binding. *Anal Biochem.* 72:248-54.

Canepari, M., R. Rossi, M. A. Pellegrino, R. Bottinelli, S. Schiaffino, and C. Reggiani. 2000. Functional diversity between orthologous myosins with minimal sequence diversity. *J Muscle Res Cell Motil.* 21:375-82.

Canepari, M., R. Rossi, M. A. Pellegrino, C. Reggiani, and R. Bottinelli. 1999. Speeds of actin translocation in vitro by myosins extracted from single rat muscle fibres of different types. *Exp Physiol.* 84:803-6.

Cantor, C. R., and P. R. Schimmel. 1980. Biophysical Chemistry. W.H. Freeman & Company, San Francisco.

Chacko, S., M. A. Conti, and R. S. Adelstein. 1977. Effect of phosphorylation of smooth muscle myosin on actin activation and Ca2+ regulation. *Proc Natl Acad Sci U S A.* 74:129-33.

Chizhov, I., D. S. Chernavskii, M. Engelhard, K. H. Mueller, B. V. Zubov, and B. Hess. 1996. Spectrally silent transitions in the bacteriorhodopsin photocycle. *Biophys J.* 71:2329-45.

Coates, J. H., A. H. Criddle, and M. A. Geeves. 1985. Pressure-relaxation studies of pyrene-labelled actin and myosin subfragment 1 from rabbit skeletal muscle. Evidence for two states of acto-subfragment 1. *Biochem J.* 232:351-6.

Coluccio, L. M., and M. A. Geeves. 1999. Transient kinetic analysis of the 130-kDa myosin I (MYR-1 gene product) from rat liver. A myosin I designed for maintenance of tension? *J Biol Chem.* 274:21575-80.

Cope, M. J., J. Whisstock, I. Rayment, and J. Kendrick-Jones. 1996. Conservation within the myosin motor domain: implications for structure and function. *Structure.* 4:969-87.

Corrie, J. E., B. D. Brandmeier, R. E. Ferguson, D. R. Trentham, J. Kendrick-Jones, S. C. Hopkins, U. A. van der Heide, Y. E. Goldman, C. Sabido-David, R. E. Dale, S. Criddle, and M. Irving. 1999. Dynamic measurement of myosin light-chain-domain tilt and twist in muscle contraction. *Nature.* 400:425-30.

Cremo, C. R., and M. A. Geeves. 1998. Interaction of actin and ADP with the head domain of smooth muscle myosin: implications for strain-dependent ADP release in smooth muscle. *Biochemistry.* 37:1969-78.

Cremo, C. R., J. M. Neuron, and R. G. Yount. 1990. Interaction of myosin subfragment 1 with fluorescent ribose-modified nucleotides. A comparison of vanadate trapping and SH1-SH2 cross- linking. *Biochemistry.* 29:3309-19.

Criddle, A. H., M. A. Geeves, and T. Jeffries. 1985. The use of actin labelled with N-(1-pyrenyl)iodoacetamide to study the interaction of actin with myosin subfragments and troponin/tropomyosin. *Biochem J.* 232:343-9.

De La Cruz, E. M., E. M. Ostap, and H. L. Sweeney. 2001. Kinetic mechanism and regulation of myosin VI. *J Biol Chem.* 276:32373-81.

Dobrowolski, J. M., I. R. Niesman, and L. D. Sibley. 1997. Actin in the parasite Toxoplasma gondii is encoded by a single copy gene, ACT1 and exists primarily in a globular form. *Cell Motil Cytoskeleton.* 37:253-62.

Dobrowolski, J. M., and L. D. Sibley. 1996. Toxoplasma invasion of mammalian cells is powered by the actin cytoskeleton of the parasite. *Cell.* 84:933-9.

Dominguez, R., Y. Freyzon, K. M. Trybus, and C. Cohen. 1998. Crystal structure of a vertebrate smooth muscle myosin motor domain and its complex with the essential light chain: visualization of the pre- power stroke state. *Cell.* 94:559-71.

Eccleston, J. F., K. J. Moore, L. Morgan, R. H. Skinner, and P. N. Lowe. 1993. Kinetics of interaction between normal and proline 12 Ras and the GTPase-activating proteins, p120-GAP and neurofibromin. The significance of the intrinsic GTPase rate in determining the transforming ability of ras. *J Biol Chem.* 268:27012-9.

Fisher, A. J., C. A. Smith, J. B. Thoden, R. Smith, K. Sutoh, H. M. Holden, and I. Rayment. 1995. X-ray structures of the myosin motor domain of Dictyostelium discoideum complexed with MgADP.BeFx and MgADP.AlF4. *Biochemistry.* 34:8960-72.

Friefelder, D. M. 1982. Physical Biochemistry. W.H. Freeman & Company, San Francisco.

Furch, M., M. A. Geeves, and D. J. Manstein. 1998. Modulation of actin affinity and actomyosin adenosine triphosphatase by charge changes in the myosin motor domain. *Biochemistry.* 37:6317-26.

Geeves, M. A. 1989. Dynamic interaction between actin and myosin subfragment 1 in the presence of ADP. *Biochemistry.* 28:5864-71.

Geeves, M. A. 1991. The dynamics of actin and myosin association and the crossbridge model of muscle contraction. *Biochem J.* 274:1-14.

Geeves, M. A., R. S. Goody, and H. Gutfreund. 1984. Kinetics of acto-S1 interaction as a guide to a model for the crossbridge cycle. *J Muscle Res Cell Motil.* 5:351-61.

Geeves, M. A., and H. Gutfreund. 1982. The use of pressure perturbations to investigate the interaction of rabbit muscle myosin subfragment 1 with actin in the presence of MgADP. *FEBS Lett.* 140:11-5.

Geeves, M. A., and K. C. Holmes. 1999. Structural mechanism of muscle contraction. *Annu Rev Biochem.* 68:687-728.

Geeves, M. A., and T. E. Jeffries. 1988. The effect of nucleotide upon a specific isomerization of actomyosin subfragment 1. *Biochem J.* 256:41-6.

Geeves, M. A., M. R. Webb, C. F. Midelfort, and D. R. Trentham. 1980. Mechanism of adenosine 5'-triphosphate cleavage by myosin: studies with oxygen-18-labeled adenosine 5'-triphosphate. *Biochemistry.* 19:4748-54.

Geisterfer-Lowrance, A. A., S. Kass, G. Tanigawa, H. P. Vosberg, W. McKenna, C. E. Seidman, and J. G. Seidman. 1990. A molecular basis for familial hypertrophic cardiomyopathy: a beta cardiac myosin heavy chain gene missense mutation. *Cell.* 62:999-1006.

Goodson, H. V., H. M. Warrick, and J. A. Spudich. 1999. Specialized conservation of surface loops of myosin: evidence that loops are involved in determining functional characteristics. *J Mol Biol.* 287:173-85.

Goody, R. S., and K. C. Holmes. 1983. Cross-bridges and the mechanism of muscle contraction. *Biochim Biophys Acta.* 726:13-39.

Gordon, D. J., Y. Z. Yang, and E. D. Korn. 1976. Polymerization of Acanthamoeba actin. Kinetics, thermodynamics, and co- polymerization with muscle actin. *J Biol Chem.* 251:7474-9.

Greaser, M. L., and J. Gergely. 1973. Purification and properties of the components from tropinin. *J Biol Chem.* 248:2125-33.

Greaser, M. L., R. L. Moss, and P. J. Reiser. 1988. Variations in contractile properties of rabbit single muscle fibres in relation to troponin T isoforms and myosin light chains. *J Physiol.* 406:85-98.

Greene, L. E., and E. Eisenberg. 1980. The binding of heavy meromyosin to F-actin. *J Biol Chem.* 255:549-54.

Gulick, A. M., and I. Rayment. 1997. Structural studies on myosin II: communication between distant protein domains. *Bioessays.* 19:561-9.

Hakansson, S., H. Morisaki, J. Heuser, and L. D. Sibley. 1999. Time-lapse video microscopy of gliding motility in Toxoplasma gondii reveals a novel, biphasic mechanism of cell locomotion. *Mol Biol Cell.* 10:3539-47.

Hammer, J. A., 3rd, and G. Jung. 1996. The sequence of the dictyostelium myo J heavy chain gene predicts a novel, dimeric, unconventional myosin with a heavy chain molecular mass of 258 kDa. *J Biol Chem.* 271:7120-7.

He, Z. H., R. Bottinelli, M. A. Pellegrino, M. A. Ferenczi, and C. Reggiani. 2000. ATP consumption and efficiency of human single muscle fibers with different myosin isoform composition. *Biophys J.* 79:945-61.

Heeley, D. H., K. Golosinska, and L. B. Smillie. 1987. The effects of troponin T fragments T1 and T2 on the binding of nonpolymerizable tropomyosin to F-actin in the presence and absence of troponin I and troponin C. *J Biol Chem.* 262:9971-8.

Heintzelman, M. B., and J. D. Schwartzman. 1997. A novel class of unconventional myosins from Toxoplasma gondii. *J Mol Biol.* 271:139-46.

Hettmann, C., A. Herm, A. Geiter, B. Frank, E. Schwarz, T. Soldati, and D. Soldati. 2000. A dibasic motif in the tail of a class XIV apicomplexan myosin is an essential determinant of plasma membrane localization. *Mol Biol Cell.* 11:1385-400.

Hill, T. L., E. Eisenberg, and L. Greene. 1980. Theoretical model for the cooperative equilibrium binding of myosin subfragment 1 to the actin-troponin-tropomyosin complex. *Proc Natl Acad Sci U S A.* 77:3186-90.

Hiratsuka, T. 1983. New ribose-modified fluorescent analogs of adenine and guanine nucleotides available as substrates for various enzymes. *Biochim Biophys Acta.* 742:496-508.

Hirokawa, N. 1998. Kinesin and dynein superfamily proteins and the mechanism of organelle transport. *Science.* 279:519-26.

Hodge, T., and M. J. Cope. 2000. A myosin family tree. *J Cell Sci.* 113 Pt 19:3353-4.

Holmes, K. C., and M. A. Geeves. 2000. The structural basis of muscle contraction. *Philos Trans R Soc Lond B Biol Sci.* 355:419-31.

Holmes, K. C., D. Popp, W. Gebhard, and W. Kabsch. 1990. Atomic model of the actin filament. *Nature.* 347:44-9.

Homma, K., J. Saito, R. Ikebe, and M. Ikebe. 2001a. Motor function and regulation of myosin x. *J Biol Chem.* 276:34348-54.

Homma, K., M. Yoshimura, J. Saito, R. Ikebe, and M. Ikebe. 2001b. The core of the motor domain determines the direction of myosin movement. *Nature.* 412:831-4.

Horowitz, J. A., and J. A. Hammer, 3rd. 1990. A new Acanthamoeba myosin heavy chain. Cloning of the gene and immunological identification of the polypeptide. *J Biol Chem.* 265:20646-52.

Howard, J. 1997. Molecular motors: structural adaptations to cellular functions. *Nature.* 389:561-7.

Huxley, A. F., and R. C. Niedergerke. 1954. Structural changes in muscle during contraction. Interference microscopy of living muscle. *Nature.* 173:971-3.

Huxley, A. F., and R. M. Simmons. 1971. Proposed mechanism of force generation in striated muscle. *Nature.* 233:533-8.

Huxley, H. E., and J. Hanson. 1954. Changes in the crossstriations of muscle during contraction and stretch and their structural interpretation. *Nature.* 173:973-6.

Huxley, H. E., and M. Kress. 1985. Crossbridge behaviour during muscle contraction. *J Muscle Res Cell Motil.* 6:153-61.

Ishii, Y., and S. S. Lehrer. 1991. Two-site attachment of troponin to pyrene-labeled tropomyosin. *J Biol Chem.* 266:6894-903.

Jontes, J. D., and R. A. Milligan. 1997. Brush border myosin-I structure and ADP-dependent conformational changes revealed by cryoelectron microscopy and image analysis. *J Cell Biol.* 139:683-93.

Kabsch, W., H. G. Mannherz, D. Suck, E. F. Pai, and K. C. Holmes. 1990. Atomic structure of the actin:DNase I complex. *Nature.* 347:37-44.

Kappe, S., T. Bruderer, S. Gantt, H. Fujioka, V. Nussenzweig, and R. Menard. 1999. Conservation of a gliding motility and cell invasion machinery in Apicomplexan parasites. *J Cell Biol.* 147:937-44.

Kinose, F., S. X. Wang, U. S. Kidambi, C. L. Moncman, and D. A. Winkelmann. 1996. Glycine 699 is pivotal for the motor activity of skeletal muscle myosin. *J Cell Biol.* 134:895-909.

Kliche, W., S. Fujita-Becker, M. Kollmar, D. J. Manstein, and F. J. Kull. 2001. Structure of a genetically engineered molecular motor. *Embo J.* 20:40-6.

Knight, A. E., and J. Kendrick-Jones. 1993. A myosin-like protein from a higher plant. *J Mol Biol.* 231:148-54.

Konrad, M., and R. S. Goody. 1982. Kinetic and thermodynamic properties of the ternary complex between F- actin, myosin subfragment 1 and adenosine 5'-[beta, gamma-imido]triphosphate. *Eur J Biochem.* 128:547-55.

Kron, S. J., and J. A. Spudich. 1986. Fluorescent actin filaments move on myosin fixed to a glass surface. *Proc Natl Acad Sci U S A.* 83:6272-6.

Kurzawa, S. E., and M. A. Geeves. 1996. A novel stopped-flow method for measuring the affinity of actin for myosin head fragments using microgram quantities of protein. *J Muscle Res Cell Motil.* 17:669-76.

Kurzawa-Goertz, S. E., C. L. Perreault-Micale, K. M. Trybus, A. G. Szent-Gyorgyi, and M. A. Geeves. 1998. Loop I can modulate ADP affinity, ATPase activity, and motility of different scallop myosins. Transient kinetic analysis of S1 isoforms. *Biochemistry.* 37:7517-25.

Kushmerick, M. J., T. S. Moerland, and R. W. Wiseman. 1992. Mammalian skeletal muscle fibers distinguished by contents of phosphocreatine, ATP, and Pi. *Proc Natl Acad Sci U S A.* 89:7521-5.

Laemmli, U. K. 1970. Cleavage of structural proteins during the assembly of the head of bacteriophage T4. *Nature.* 227:680-5.

Lakowicz, J. R. 1983. Principles of Fluorescence Spectroscopy. Plenum Press, New York.

Lehrer, S. S., and M. A. Geeves. 1998. The muscle thin filament as a classical cooperative/allosteric regulatory system. *J Mol Biol.* 277:1081-9.

Lehrer, S. S., and G. Kerwar. 1972. Intrinsic fluorescence of actin. *Biochemistry.* 11:1211-7.

Liew, C. C., M. J. Sole, K. Yamauchi-Takihara, B. Kellam, D. H. Anderson, L. P. Lin, and J. C. Liew. 1990. Complete sequence and organization of the human cardiac beta-myosin heavy chain gene. *Nucleic Acids Res.* 18:3647-51.

Lorenz, M., K. J. Poole, D. Popp, G. Rosenbaum, and K. C. Holmes. 1995. An atomic model of the unregulated thin filament obtained by X-ray fiber diffraction on oriented actin-tropomyosin gels. *J Mol Biol.* 246:108-19.

Lymn, R. W., and E. W. Taylor. 1971. Mechanism of adenosine triphosphate hydrolysis by actomyosin. *Biochemistry.* 10:4617-24.

Ma, Y. Z., and E. W. Taylor. 1997. Kinetic mechanism of a monomeric kinesin construct. *J Biol Chem.* 272:717-23.

Mabuchi, K., and F. A. Sreter. 1980. Actomyosin ATPase. II. Fiber typing by histochemical ATPase reaction. *Muscle Nerve.* 3:233-9.

Malnasi-Csizmadia, A., D. S. Pearson, M. Kovacs, R. J. Woolley, M. A. Geeves, and C. R. Bagshaw. 2001. Kinetic resolution of a conformational transition and the atp hydrolysis step using relaxation methods with a dictyostelium myosin ii mutant containing a single tryptophan residue. *Biochemistry.* 40:12727-37.

Malnasi-Csizmadia, A., R. J. Woolley, and C. R. Bagshaw. 2000. Resolution of conformational states of Dictyostelium myosin II motor domain using tryptophan (W501) mutants: implications for the open- closed transition identified by crystallography. *Biochemistry.* 39:16135-46.

Margossian, S. S., and S. Lowey. 1982. Preparation of myosin and its subfragments from rabbit skeletal muscle. *Methods Enzymol.* 85:55-71.

Marianne-Pepin, T., D. Mornet, R. Bertrand, J. P. Labbe, and R. Kassab. 1985. Interaction of the heavy chain of gizzard myosin heads with skeletal F- actin. *Biochemistry.* 24:3024-9.

Marriott, G., K. Zechel, and T. M. Jovin. 1988. Spectroscopic and functional characterization of an environmentally sensitive fluorescent actin conjugate. *Biochemistry.* 27:6214-20.

Marston, S. B., and E. W. Taylor. 1980. Comparison of the myosin and actomyosin ATPase mechanisms of the four types of vertebrate muscles. *J Mol Biol.* 139:573-600.

Mathews, C. K., K. E. van Holde, and K. G. Ahern. 2000. Biochemistry. Addison Wesley Longman, Inc., San Francisco.

McKillop, D. F., and M. A. Geeves. 1991. Regulation of the acto.myosin subfragment 1 interaction by troponin/tropomyosin. Evidence for control of a specific isomerization between two acto.myosin subfragment 1 states. *Biochem J.* 279:711-8.

McNally, E. M., K. M. Gianola, and L. A. Leinwand. 1989. Complete nucleotide sequence of full length cDNA for rat alpha cardiac myosin heavy chain. *Nucleic Acids Res.* 17:7527-8.

Mehta, A. D., R. S. Rock, M. Rief, J. A. Spudich, M. S. Mooseker, and R. E. Cheney. 1999. Myosin-V is a processive actin-based motor. *Nature.* 400:590-3.

Mermall, V., P. L. Post, and M. S. Mooseker. 1998. Unconventional myosins in cell movement, membrane traffic, and signal transduction. *Science.* 279:527-33.

Millar, N. C., and M. A. Geeves. 1983. The limiting rate of the ATP-mediated dissociation of actin from rabbit skeletal muscle myosin subfragment 1. *FEBS Lett.* 160:141-8.

Montell, C., and G. M. Rubin. 1988. The Drosophila ninaC locus encodes two photoreceptor cell specific proteins with domains homologous to protein kinases and the myosin heavy chain head. *Cell.* 52:757-72.

Morisaki, J. H., J. E. Heuser, and L. D. Sibley. 1995. Invasion of Toxoplasma gondii occurs by active penetration of the host cell. *J Cell Sci.* 108:2457-64.

Mornet, D., P. Pantel, E. Audemard, and R. Kassab. 1979. The limited tryptic cleavage of chymotryptic S-1: an approach to the characterization of the actin site in myosin heads. *Biochem Biophys Res Commun.* 89:925-32.

Morris, E. P., and S. S. Lehrer. 1984. Troponin-tropomyosin interactions. Fluorescence studies of the binding of troponin, troponin T, and chymotryptic troponin T fragments to specifically labeled tropomyosin. *Biochemistry.* 23:2214-20.

Nogales, E., K. H. Downing, L. A. Amos, and J. Lowe. 1998. Tubulin and FtsZ form a distinct family of GTPases. *Nat Struct Biol.* 5:451-8.

Ostap, E. M., and T. D. Pollard. 1996. Biochemical kinetic characterization of the Acanthamoeba myosin-I ATPase. *J Cell Biol.* 132:1053-60.

Pate, E., M. Lin, K. Franks-Skiba, and R. Cooke. 1992. Contraction of glycerinated rabbit slow-twitch muscle fibers as a function of MgATP concentration. *Am J Physiol.* 262:C1039-46.

Pette, D., and R. S. Staron. 1990. Cellular and molecular diversities of mammalian skeletal muscle fibers. *Rev Physiol Biochem Pharmacol.* 116:1-76.

Pinder, J. C., R. E. Fowler, A. R. Dluzewski, L. H. Bannister, F. M. Lavin, G. H. Mitchell, R. J. Wilson, and W. B. Gratzer. 1998. Actomyosin motor in the merozoite of the malaria parasite, Plasmodium falciparum: implications for red cell invasion. *J Cell Sci.* 111:1831-9.

Pollard, T. D., and E. D. Korn. 1973. Acanthamoeba myosin. I. Isolation from Acanthamoeba castellanii of an enzyme similar to muscle myosin. *J Biol Chem.* 248:4682-90.

Prendergast, F. G., M. Meyer, G. L. Carlson, S. Iida, and J. D. Potter. 1983. Synthesis, spectral properties, and use of 6-acryloyl-2- dimethylaminonaphthalene (Acrylodan). A thiol-selective, polarity- sensitive fluorescent probe. *J Biol Chem.* 258:7541-4.

Ranatunga, K. W. 1984. The force-velocity relation of rat fast- and slow-twitch muscles examined at different temperatures. *J Physiol.* 351:517-29.

Rayment, I., H. M. Holden, M. Whittaker, C. B. Yohn, M. Lorenz, K. C. Holmes, and R. A. Milligan. 1993a. Structure of the actin-myosin complex and its implications for muscle contraction. *Science.* 261:58-65.

Rayment, I., W. R. Rypniewski, K. Schmidt-Base, R. Smith, D. R. Tomchick, M. M. Benning, D. A. Winkelmann, G. Wesenberg, and H. M. Holden. 1993b. Three-dimensional structure of myosin subfragment-1: a molecular motor. *Science.* 261:50-8.

Razzaq, A. 1995. The purification and in vitro motility analysis of Drosophila ACT88F mutants. Dphil thesis. University of York, York.

Redowicz, M. J. 1999. Myosins and deafness. *J Muscle Res Cell Motil.* 20:241-8.

Reggiani, C., E. J. Potma, R. Bottinelli, M. Canepari, M. A. Pellegrino, and G. J. Stienen. 1997. Chemo-mechanical energy transduction in relation to myosin isoform composition in skeletal muscle fibres of the rat. *J Physiol.* 502:449-60.

Reinhard, J., A. A. Scheel, D. Diekmann, A. Hall, C. Ruppert, and M. Bahler. 1995. A novel type of myosin implicated in signalling by rho family GTPases. *Embo J.* 14:697-704.

Ritchie, M. D., M. A. Geeves, S. K. Woodward, and D. J. Manstein. 1993. Kinetic characterization of a cytoplasmic myosin motor domain expressed in Dictyostelium discoideum. *Proc Natl Acad Sci U S A.* 90:8619-23.

Rogers, K. R., S. Weiss, I. Crevel, P. J. Brophy, M. Geeves, and R. Cross. 2001. KIF1D is a fast non-processive kinesin that demonstrates novel K-loop- dependent mechanochemistry. *Embo J.* 20:5101-5113.

Rovner, A. S., Y. Freyzon, and K. M. Trybus. 1997. An insert in the motor domain determines the functional properties of expressed smooth muscle myosin isoforms. *J Muscle Res Cell Motil.* 18:103-10.

Rowlerson, A., F. Mascarello, A. Veggetti, and E. Carpene. 1983. The fibre-type composition of the first branchial arch muscles in Carnivora and Primates. *J Muscle Res Cell Motil.* 4:443-72.

Ruff, C., M. Furch, B. Brenner, D. J. Manstein, and E. Meyhofer. 2001. Single-molecule tracking of myosins with genetically engineered amplifier domains. *Nat Struct Biol.* 8:226-9.

Schiaffino, S., and C. Reggiani. 1996. Molecular diversity of myofibrillar proteins: gene regulation and functional significance. *Physiol Rev.* 76:371-423.

Schroder, R. R., D. J. Manstein, W. Jahn, H. Holden, I. Rayment, K. C. Holmes, and J. A. Spudich. 1993. Three-dimensional atomic model of F-actin decorated with Dictyostelium myosin S1. *Nature.* 364:171-4.

Sellers, J. R., H. V. Goodson, and F. Wang. 1996. A myosin family reunion. *J Muscle Res Cell Motil.* 17:7-22.

Sibley, L. D., S. Hakansson, and V. B. Carruthers. 1998. Gliding motility: an efficient mechanism for cell penetration. *Curr Biol.* 8:R12-4.

Siemankowski, R. F., and H. D. White. 1984. Kinetics of the interaction between actin, ADP, and cardiac myosin-S1. *J Biol Chem.* 259:5045-53.

Siemankowski, R. F., M. O. Wiseman, and H. D. White. 1985. ADP dissociation from actomyosin subfragment 1 is sufficiently slow to limit the unloaded shortening velocity in vertebrate muscle. *Proc Natl Acad Sci U S A.* 82:658-62.

Sleep, J., C. Herrmann, T. Barman, and F. Travers. 1994. Inhibition of ATP binding to myofibrils and acto-myosin subfragment 1 by caged ATP. *Biochemistry.* 33:6038-42.

Sleep, J. A., and R. L. Hutton. 1980. Exchange between inorganic phosphate and adenosine 5'-triphosphate in the medium by actomyosin subfragment 1. *Biochemistry.* 19:1276-83.

Smith, C. A., and I. Rayment. 1996. X-ray structure of the magnesium(II).ADP.vanadate complex of the Dictyostelium discoideum myosin motor domain to 1.9 A resolution. *Biochemistry.* 35:5404-17.

Sobieszek, A., and J. V. Small. 1977. Regulation of the actin-myosin interaction in vertebrate smooth muscle: activation via a myosin light-chain kinase and the effect of tropomyosin. *J Mol Biol.* 112:559-76.

Sokolov, V. S., H. J. Apell, J. E. Corrie, and D. R. Trentham. 1998. Fast transient currents in Na,K-ATPase induced by ATP concentration jumps from the P3-[1-(3',5'-dimethoxyphenyl)-2-phenyl-2-oxo]ethyl ester of ATP. *Biophys J.* 74:2285-98.

Spudich, J. A. 1994. How molecular motors work. *Nature.* 372:515-8.

Staron, R. S., and D. Pette. 1987. Nonuniform myosin expression along single fibers of chronically stimulated and contralateral rabbit tibialis anterior muscles. *Pflugers Arch.* 409:67-73.

Stearns, T. 1997. Motoring to the finish: kinesin and dynein work together to orient the yeast mitotic spindle. *J Cell Biol.* 138:957-60.

Stein, L. A., R. P. Schwarz, Jr., P. B. Chock, and E. Eisenberg. 1979. Mechanism of actomyosin adenosine triphosphatase. Evidence that adenosine 5'-triphosphate hydrolysis can occur without dissociation of the actomyosin complex. *Biochemistry.* 18:3895-909.

Sultan, A. A., V. Thathy, U. Frevert, K. J. Robson, A. Crisanti, V. Nussenzweig, R. S. Nussenzweig, and R. Menard. 1997. TRAP is necessary for gliding motility and infectivity of plasmodium sporozoites. *Cell.* 90:511-22.

Swank, D. M., M. L. Bartoo, S. I. Bernstein, J. E. Molloy, and J. C. Sparrow. 1998. In vitro measurements of velocity, step size and attached lifetime of Drosophila myosins. *Biophysical Journal.* 74:A261.

Sweeney, H. L., M. J. Kushmerick, K. Mabuchi, F. A. Sreter, and J. Gergely. 1988. Myosin alkali light chain and heavy chain variations correlate with altered shortening velocity of isolated skeletal muscle fibers. *J Biol Chem.* 263:9034-9.

Sweeney, H. L., S. S. Rosenfeld, F. Brown, L. Faust, J. Smith, J. Xing, L. A. Stein, and J. R. Sellers. 1998. Kinetic tuning of myosin via a flexible loop adjacent to the nucleotide binding pocket. *J Biol Chem.* 273:6262-70.

Talmadge, R. J., and R. R. Roy. 1993. Electrophoretic separation of rat skeletal muscle myosin heavy-chain isoforms. *J Appl Physiol.* 75:2337-40.

Taylor, E. W. 1979. Mechanism of actomyosin ATPase and the problem of muscle contraction. *CRC Crit Rev Biochem.* 6:103-64.

Theriot, J. A. 2000. The polymerization motor. *Traffic.* 1:19-28.

Trentham, D. R., J. F. Eccleston, and C. R. Bagshaw. 1976. Kinetic analysis of ATPase mechanisms. *Q Rev Biophys.* 9:217-81.

Uyeda, T. Q., K. M. Ruppel, and J. A. Spudich. 1994. Enzymatic activities correlate with chimaeric substitutions at the actin-binding face of myosin. *Nature.* 368:567-9.

van den Ent, F., L. A. Amos, and J. Lowe. 2001. Prokaryotic origin of the actin cytoskeleton. *Nature.* 413:39-44.

Van Dijk, J., M. Furch, C. Lafont, D. J. Manstein, and P. Chaussepied. 1999. Functional characterization of the secondary actin binding site of myosin II. *Biochemistry.* 38:15078-85.

Vargas, M., H. Voigt, P. Sansonetti, and N. Guillen. 1997. Molecular characterization of myosin IB from the lower eukaryote Entamoeba histolytica, a human parasite. *Mol Biochem Parasitol.* 86:61-73.

Veigel, C., L. M. Coluccio, J. D. Jontes, J. C. Sparrow, R. A. Milligan, and J. E. Molloy. 1999. The motor protein myosin-I produces its working stroke in two steps. *Nature.* 398:530-3.

Vernos, I., and E. Karsenti. 1996. Motors involved in spindle assembly and chromosome segregation. *Curr Opin Cell Biol.* 8:4-9.

Vibert, P., R. Craig, and W. Lehman. 1997. Steric-model for activation of muscle thin filaments. *J Mol Biol.* 266:8-14.

Voet, D., and J. G. Voet. 1994. Biochemie. VHC Verlagsgesellschaft, Weinheim.

Wagner, P. D. 1981. Formation and characterization of myosin hybrids containing essential light chains and heavy chains from different muscle myosins. *J Biol Chem.* 256:2493-8.

Walker, M. L., S. A. Burgess, J. R. Sellers, F. Wang, J. A. Hammer, 3rd, J. Trinick, and P. J. Knight. 2000. Two-headed binding of a processive myosin to F-actin. *Nature.* 405:804-7.

Webb, M. R., and J. E. Corrie. 2001. Fluorescent coumarin-labeled nucleotides to measure adp release from actomyosin. *Biophys J.* 81:1562-9.

Weber, G., and F. J. Farris. 1979. Synthesis and spectral properties of a hydrophobic fluorescent probe: 6- propionyl-2-(dimethylamino)naphthalene. *Biochemistry.* 18:3075-8.

Weeds, A. G., and R. S. Taylor. 1975. Separation of subfragment-1 isoenzymes from rabbit skeletal muscle myosin. *Nature.* 257:54-6.

Weiss, A., S. Schiaffino, and L. A. Leinwand. 1999. Comparative sequence analysis of the complete human sarcomeric myosin heavy chain family: implications for functional diversity. *J Mol Biol.* 290:61-75.

Wells, A. L., A. W. Lin, L. Q. Chen, D. Safer, S. M. Cain, T. Hasson, B. O. Carragher, R. A. Milligan, and H. L. Sweeney. 1999. Myosin VI is an actin-based motor that moves backwards. *Nature.* 401:505-8.

West, J. J., B. Nagy, and J. Gergely. 1967. Free adenosin diphosphate as an intermediary in the phosphorylation by creatine phosphate of adenosine disphosphate bound to actin. *J. Biol. Chem.* 242:1140-5.

White, H. D., and E. W. Taylor. 1976. Energetics and mechanism of actomyosin adenosine triphosphatase. *Biochemistry.* 15:5818-26.

# 10 Appendix

## *10.1 Abbreviations*

| | |
|---|---|
| [ ] | indicates a concentration |
| A | actin |
| AA | amino acid |
| A.M | actin.myosin complex or actin.S1 complex |
| amp | amplitude |
| ADP, D | adenosine 5’ diphosphate |
| APS | ammoniumperoxodisulfate |
| ATP, T | adenosine 5’ triphosphate |
| ATPase | adenosine 5’ triphosphatase |
| cATP | caged-ATP: Adenosine 5’-triphosphate (1-(2-nitrophenyl)ethyl ester) |
| cADP | caged-ADP: Adenosine 5’-diphosphate (1-(2-nitrophenyl)ethyl ester) |
| caged-ATP | Adenosine 5’-triphosphate (1-(2-nitrophenyl)ethyl ester) |
| $Ch^{sm}S1$ | myosin subfragment 1 from chicken smooth muscle |
| C-terminal | carboxyterminal |
| Dicty MII | myosin II from *Dictyostelium discoideum* |
| *Dictyostelium* | *Dictyostelium discoideum* |
| DMF | dimethylformamide |
| DMSO | dimethylsufoxide |
| DTT | dithiotreitol |
| ELC | essential myosin light chain |
| h | hour |
| HMM | heavy meromyosin |
| HPLC | high performance liquid chromatography |
| IAF | 5-(iodoactamido)fluorescein |

| | |
|---|---|
| $K_1k_{+2}$ | second order rate constant of ATP binding or ATP induced dissociation |
| $k_{-6}/K_7$ | rate constant of binding of ATP to myosin |
| $k_{+6}$ | dissociation rate constant of ADP from myosin |
| $K_A$ | dissociation constant of myosin from actin |
| $K_{AD}$ | dissciation constant of ATP from the acto.myosin complex |
| $k_{-AD}$ | dissociation rate constant ATP from the acto.myosin complex |
| $K_D$ | dissociation constant of ADP from myosin |
| $k_{obs}$ | observed rate constant |
| kDa | kilo Dalton |
| LC | myosin light chain |
| LMM | light meromyosin |
| M.D | myosin ADP complex |
| min | minute |
| M.N | myosin nucleotide complex |
| M.T | myosin ATP complex |
| MT | microtubule |
| mantADP | 2'(3')-O-(N-methylanthraniloyl)ADP |
| mantATP | 2'(3')-O-(N-methylanthraniloyl)ATP |
| MHC | myosin heavy chain |
| MOPS | 4-morpholinopropanesufonic acid |
| N | nucleotide |
| N-terminal | aminoterminal |
| Pi | anorganic phosphate |
| pyrene | N-(1-pyrenyl)iodoacetamide |
| pyrene actin | actin labelled with pyrene at residue Cys374 |
| $Rb^{st}S1$ | myosin subfragment 1 from rabbit skeletal muscle |

| | |
|---|---|
| RLC | regulatory myosin light chain |
| rpm | rotations per minute |
| S1 | myosin subfragment 1 |
| S2 | myosin subfragment 2 |
| SDS-PAGE | Sodiumdocecylsufate polyacrylamide gel electrophoresis |
| TEMED | N',N',N',N'-tetramethylethylendiamine |
| TgMyoA | myosinA from *Toxoplasma gondii* |
| TgMyoAΔtail | myosinA construct from *Toxoplasma gondii* with a truncated tail domain (lacking 53 C-terminal residues) |
| Tm | tropomyosin |
| Tn | troponin complex |
| *T.gondii* | *Toxoplasma gondii* |
| TRIS | 2-amino-2-(hydroxylmethyl)-1,2-propanediol |
| u | unit |
| $V_0$ | maximum unloaded shortening velocity |

Abbreviations for metric units were used accoring to the SI (Systéme International d'Unités)

## *10.2 Software*

MicroMath Scientist model file used for the fitting of flash photolysis transients and the calculation of $k_{obs}$ taking into account the impact of rate of ATPrelease on the rate of ATP induced dissocitation of acto.myosin:

```
// MicroMath Scientist Model File
IndVars: T
DepVars: A, B, C, D,LS
Params:A0,C0, K1, K2,amp,offset
A'=-k1*A
B'=k1*A-k2*B*C
C'=-k2*B*C
D'=k2*B*C
LS=C*amp+offset
//
T=0.0
A=A0
B=0.0
c=c0
D=0.0
0<A<A0
0<C<C0
***
```

Microcal Origin script for the fitting of multiple flash photolysis transmission changes at 405 nm and the calculation of ATP release from caged ATP:

```
win -a Resultsgraph;
lay -s 2;
nlsf.func$=ExpDecay1;
nlsf.cleanupfitdata();
nlsf.pasteToPlot=0;
A1=0.05; t1=0.01; x0=0; y0=0;
nlsf.v1=1; nlsf.v2=0;
loop (ii,1,n1) {
nlsf.fitdata$=fast_a$(ii);
nlsf.fit(20);
ResultsA_ATP[ii]=733*A1*1.76;
ResultsA_k405[ii]=1/t1;
Results1_pulse[ii]=ii;
};
nlsf.end();
nlsf.uninit();
ResultsA_ADP[1]=0.0;
loop (ii,1,n1) {
ResultsA_ADP[ii+1]=ResultsA_ADP[ii]+ResultsA_ATP[ii];
};
Results1_ATP=ResultsA_ATP;
Fits_A=ResultsA_ATP;

lay -s 3;
lay -i Results1_ATP;
lay -a;
nlsf.func$=ExpDecay1;
nlsf.cleanupfitdata();
A1=30; t1=20; x0=0; y0=0;
nlsf.v1=0; nlsf.v2=0;
nlsf.fitdata$=Results1_ATP;
```

```
nlsf.fit(20);
nlsf.end();
nlsf.uninit();
```

Microcal Origin script for the fitting of multiple flash photolysis light scattering or fluorescence transients and the calculation of $k_{obs}$:

```
win -a Resultsgraph;
lay -s 1;
nlsf.pasteToPlot=0;
nlsf.func$=ExpAssoc;
nlsf.cleanupfitdata();
yo=0; A1=amp; t1=hft; A2=0; t2=1;
loop (ii,1,n1) {
nlsf.fitdata$=fast_f$(ii);
nlsf.v1=1; nlsf.v2=1; nlsf.v3=1; nlsf.v4=0; nlsf.v5=0;
nlsf.fit(40);
fast_C$(ii)= y0 + A1*(1 - exp(-fast_time/t1)) + A2*(1 - exp(-fast_time/t2));
fast_B$(ii)= fast_F$(ii) - fast_C$(ii);
ResultsA_Adis[ii]=A1+y0;
ResultsA_kdis[ii]=1/t1;
Fits_B[ii]=1/t1;
ResultsA_k2K1[ii]=1/t1/ResultsA_ATP[ii];
// set fast_f$(ii) -b 120;
};
nlsf.end();
nlsf.uninit();
//lay -i ResultsA_k2K1;
lay -a;
lay -s 4;
lay -i Fits_B;
lay -a;
```

### *10.3 Publications and presentations*

Subject of this thesis:

Weiss, S., I. Chizhov, and M. A. Geeves. 2000. A flash photolysis fluorescence/light scattering apparatus for use with sub microgram quantities of muscle proteins. J Muscle Res Cell Motil. 21:423-32.

Weiss, S., R. Rossi, M. A. Pellegrino, R. Bottinelli, and M. A. Geeves. in press. Differing ADP release rates from myosin heavy chain isoforms define the shortening velocity of skeletal muscle fibers. J Biol Chem.

Herm-Götz, A., S. Weiss, R. Stratmann, S. Fujita-Becker, C. Ruff, E. Meyhöfer, T. Soldati, D. Manstein, M.A. Geeves and D. Soldati. submitted. Toxoplasma gondii myosin A and its light chain: a fast, single headed, plus-end directed motor. Science

Not subject of this thesis:

Rogers, K. R., S. Weiss, I. Crevel, P. J. Brophy, M. Geeves, and R. Cross. 2001. KIF1D is a fast non-processive kinesin that demonstrates novel K-loop- dependent mechanochemistry. Embo J. 20:5101-5113.

Oral presentations:

S. Weiss, R. Rossi, M.A. Pellegrino, M.A. Geeves and R. Bottinelli. 2001. Rates of acto.myosin dissociation and ADP release of myosin isoforms from rat and human skeletal muscle. XXX European Muscle Conference. Pavia, Italy.

Poster Presentations:

S.Weiss, A. Herm, M. A. Geeves and D. Soldati. 1999. Kinetic characterisation of the myosin A from *Toxoplasma gondii*. 44$^{th}$ Annual Meeting of the Biophysical Society. New Orleans, USA.

S. Weiss, I. Chizhov and M. A. Geeves. 1999. Fast kinetic studies of submicrogram quantities of purified muscle proteins by flash photolysis of cagedATP. New Trends in Physics, Chemistry and Biology with Single Molecules. Wiesbaden, Germany.

Stefan Weiss, Christine Berger, Dietmar J. Manstein & Michael A. Geeves. 2001. Mechanical and geometric constraints on the communication between the motor domains of dimeric myosins. 2nd International Symposium on Physics, Chemistry and Biology with Single Molecules. Banz, Germany.

S. Weiss, R. Rossi, M.A. Pellegrino, M.A. Geeves and R. Bottinelli. 2001. Rates of acto.myosin dissociation and ADP release of myosin isoforms from rat and human skeletal muscle. XXX European Muscle Conference. Pavia, Italy.

Die vorliegende Arbeit wurde im Zeitraum vom Mai 1998 bis Oktober 2001 am Max-Planck-Institut für molekulare Physiologie, Dortmund und an der Unversität zu Kent, Canterbury, UK unter der Betreuung von Herrn Prof. Dr. Roger Goody und Herrn Prof. Dr. Michael A. Geeves durchgeführt.

Ich versichere hiermit, daß ich die vorliegende Arbeit selbstständig angefertigt und keine anderen als die angegebenen Hilfsmittel verwendet habe.

(Stefan Weiß)